

A model-based robust control approach for bilateral teleoperation systems

Citation for published version (APA):

Lopez Martinez, C. A. (2015). *A model-based robust control approach for bilateral teleoperation systems*. [Phd Thesis 1 (Research TU/e / Graduation TU/e), Mechanical Engineering]. Technische Universiteit Eindhoven.
<https://doi.org/10.6100/IR784500>

DOI:

[10.6100/IR784500](https://doi.org/10.6100/IR784500)

Document status and date:

Published: 01/01/2015

Document Version:

Publisher's PDF, also known as Version of Record (includes final page, issue and volume numbers)

Please check the document version of this publication:

- A submitted manuscript is the version of the article upon submission and before peer-review. There can be important differences between the submitted version and the official published version of record. People interested in the research are advised to contact the author for the final version of the publication, or visit the DOI to the publisher's website.
- The final author version and the galley proof are versions of the publication after peer review.
- The final published version features the final layout of the paper including the volume, issue and page numbers.

[Link to publication](#)

General rights

Copyright and moral rights for the publications made accessible in the public portal are retained by the authors and/or other copyright owners and it is a condition of accessing publications that users recognise and abide by the legal requirements associated with these rights.

- Users may download and print one copy of any publication from the public portal for the purpose of private study or research.
- You may not further distribute the material or use it for any profit-making activity or commercial gain
- You may freely distribute the URL identifying the publication in the public portal.

If the publication is distributed under the terms of Article 25fa of the Dutch Copyright Act, indicated by the "Taverne" license above, please follow below link for the End User Agreement:

www.tue.nl/taverne

Take down policy

If you believe that this document breaches copyright please contact us at:

openaccess@tue.nl

providing details and we will investigate your claim.

A Model-based Robust Control Approach for Bilateral Teleoperation Systems

César Augusto López Martínez



The research reported in this thesis is part of the research program of the Dutch Institute of Systems and Control (DISC). The author has successfully completed the educational program of the Graduate School DISC.

This research was supported partially by the Percutaneous Instruments TeleOperated Needles (PITON) project funded by Agentschap NL, an agency of the Dutch Ministry of Economy Affairs.

A catalogue record is available from the Eindhoven University of Technology Library. ISBN: 978-90-386-3768-6

Typeset by the author with the pdfL^AT_EX documentation system.
Cover design: César A. López M. and Nina Simons. Background based on image under creative commons license. Pictures by Thijs Meenink.
Reproduction: Ipskamp Drukkers B.V., Enschede, The Netherlands.

Copyright 2015 by César Augusto López Martínez. All rights reserved.

A Model-based Robust Control Approach for Bilateral Teleoperation Systems

PROEFSCHRIFT

ter verkrijging van de graad van doctor aan de
Technische Universiteit Eindhoven, op gezag van de
rector magnificus, prof.dr.ir. C.J. van Duijn, voor een
commissie aangewezen door het College voor
Promoties, in het openbaar te verdedigen
op dinsdag 10 februari 2015 om 16.00 uur

door

César Augusto López Martínez

geboren te Aguachica, Colombia

Dit proefschrift is goedgekeurd door de promotoren en de samenstelling van de promotiecommissie is als volgt:

voorzitter:	prof.dr. L.P.H. de Goey
1 ^e promotor:	prof.dr.ir. M. Steinbuch
2 ^e promotor:	prof.dr. S. Weiland
copromotor:	dr.ir. M.J.G. van Molengraft
leden:	prof.dr. H. Nijmeijer prof.dr.ir. Stefano Stramigioli (Universiteit Twente) dr. D. Constantinescu (University of Victoria)
adviseur:	dr. E. Vander Poorten (Katholieke Universiteit Leuven)

Societal Summary

Bilateral teleoperation systems allow to manipulate and sense a remote or difficult to access environment. Imagine a system that allows a surgeon to command robotic instruments inside your body with high precision, and moreover, that provides the surgeon the feeling of how rigid the surrounding tissue is. This latter characteristic, called force feedback, can help the surgeon not to exert excessive force on delicate tissues, preventing damage. This means that the patients will have less trauma and faster recovery times after surgery, which will also reduce the costs of the healthcare system.

Robotic surgery is already a reality, however, state of the art systems do not provide high quality force feedback to the operator. This is because high quality force feedback always includes a compromise in the stability of the system, and current techniques do not provide a good balance. Control of bilateral teleoperation systems is not a trivial task, on one hand because the operating environment can vary largely and on the other hand because the system directly interacts with the human being. Therefore, the force feedback to the operator needs to be designed in a clever way.

In this PhD thesis I propose a methodology to design and safely implement high quality force feedback in bilateral teleoperation systems. The method involves modelling of the human operator and the use of specific environment models. This research represents a step towards bringing force feedback capabilities in robotic surgery systems, which will have a direct impact in the human healthcare system.

Summary

A Model-based Robust Control Approach for Bilateral Teleoperation Systems

Bilateral teleoperation systems allow an operator to manipulate a remote environment by means of a master and a slave device while using force feedback to obtain a feeling of tele-presence. The system is supposed to deliver high performance in that the operator feels as if he/she is manipulating the environment directly, in a stable fashion. However, there is an inherent trade-off between stability and performance, and it is a challenging problem to design controllers that meet an appropriate balance. Most of the current design tools are based on passivity theory, which guarantees stability but does not provide means to achieve a systematic stability/performance trade-off. Moreover, the dynamics of both environment and operator are inherently time-varying, which aspect is often overlooked. Luckily, in many applications such as minimally invasive surgery (MIS), needle insertion, suturing, etc., the environment properties vary in a bounded set, e.g. the stiffness of tissue inside a patient under surgery. Therefore, the work in this thesis exploits the knowledge on the bounds of variation in both environment and operator for the purpose of control design.

This thesis adopts a model-based robust control design approach. As a first step, we model the teleoperation system, including an appropriate description of its uncertain dynamics. We consider environments in which the stiffness is the dominant phenomenon, e.g. in stiffness palpation tasks present in surgery. For the human operator, we have constructed a parametric model based on identification experiments, in which the operator stiffness appeared as the dominant varying parameter. Both the environment stiffness and the operator stiffness are treated as parametric uncertainties, which are considered to be bounded and time-varying to account for realistic behaviour. Subsequently, controller synthesis is done via robust control techniques based on Linear Matrix Inequalities (LMI). The operator/environment uncertainty is described via a specific class of Integral Quadratic Constraints (IQCs), which allow to represent the parametric uncertainties as ar-

bitrarily fast time-varying.

Based on the above approach, we propose and validate different controller designs. In our first design a single controller for the considered range of stiffness variation is designed, for which simulations and experiments are performed with a one degree-of-freedom (1-DoF) academic bilateral teleoperation setup. The results show that the closed loop system presents robust performance for the bounded set of uncertainty for which it was designed, including sudden changes in the environment stiffness. The result from experiments matches the theoretical stability result, which validates the assumptions made during modelling and control synthesis. Next, we consider an extended the range of stiffness variation to account for hard contacts, e.g. in contact with bones present in surgery. In such case, one controller might not be sufficient to achieve a desired performance. Therefore, in a second design, to improve performance we propose a multi-controller structure, in which we design multiple robust controllers for different regions of environment stiffness, which controllers are scheduled on the basis of an estimate of the environment stiffness. Moreover, all the controllers are designed to share a common lyapunov function to guarantee smooth switching between them. This approach is simulated and experimentally validated in the 1-DoF setup. The results show that a multi-controller structure can provide an improved performance for the same set of uncertainties, compared with a single controller structure. In a third design, the requirement of a common lyapunov function in the multi-controller structure is relaxed via dwell time conditions during the controller synthesis for the purpose of obtaining an improved performance, which is validated in simulations of an 1-DoF setup. In a fourth design, we relax completely the requirement of a common lyapunov function in the multi-controller structure, designing multiple performance-optimized controllers independently and switching between them using an adapted version of the bumpless transfer technique. Simulations and experiments in the 1-DoF setup validate the designed multicontroller controller architecture. Finally, the proposed model-based robust control methodology is implemented on a real-life surgical robot named Sofie, which has non-ideal properties compared to academic setups, for instance the slave device is non-backdrivable, it is heavy and has high levels of friction, moreover, the master device has structural resonances and does not have force sensor. The experimental results show that the proposed methods can be also successfully applied to such type of teleoperators.

Contents

Societal Summary	i
Summary	iii
1 Introduction	1
1.1 Bilateral teleoperation	1
1.1.1 Teleoperation systems and force feedback	1
1.1.2 A definition of stability for bilateral teleoperation systems	4
1.1.3 Bilateral control design	7
1.1.4 Pros and cons of current bilateral control design methods	9
1.2 Problem statement and challenges	13
1.3 Research approach	14
1.4 Contributions	22
1.5 Outline of the thesis	23
2 Robust Bilateral Control under Time-Varying Dynamics	27
2.1 Introduction	27
2.2 Model based robust control	30
2.2.1 LFR model of a teleoperation system	30
2.2.2 Robust control design with guaranteed performance specifications	39
2.2.3 Weighting filter design	46
2.3 Robust control applied to a 1-DoF academic setup	48
2.3.1 Synthesis results	49
2.3.2 Simulation results	54
2.3.3 Experiments	56
2.4 Conclusions	61
3 Switching Robust Control for Bilateral Teleoperation	63
3.1 Introduction	63

3.2	Switching robust control approach	65
3.2.1	LFR model of a teleoperation system	65
3.2.2	Switching robust control design using a common quadratic Lyapunov function	72
3.2.3	Tailor-made solution for bilateral teleoperation	79
3.2.4	Environment estimation	82
3.2.5	Weighting filter design	84
3.3	Switching robust control applied to a 1-DoF academic setup	85
3.3.1	Synthesis results	87
3.3.2	Simulation results	88
3.3.3	Experiments	93
3.4	Conclusions	99
4	Switching Robust Control via Dwell Time Conditions	101
4.1	Introduction	101
4.2	Adding control design flexibility via dwell time conditions	103
4.2.1	Model of the teleoperation system for switching robust control	103
4.2.2	Switching robust control design using multiple quadratic Lyapunov functions	107
4.3	Simulation results	115
4.4	Conclusions	118
5	Bumpless Transfer of Robust Controllers for Teleoperation	119
5.1	Introduction	119
5.2	Bumpless transfer in bilateral teleoperation	121
5.2.1	Linear fractional representation of a teleoperation system	121
5.2.2	Uncertainty region distribution and robust control design	123
5.2.3	Bumpless transfer between robust controllers	125
5.2.4	Environment estimation	126
5.3	Experimental results on a 1-DoF academic setup	128
5.4	Conclusions	132
6	Model-Based Robust Control for a Non-Ideal Teleoperator	133
6.1	Introduction	133
6.2	Model based robust control applied to SOFIE robot	135
6.2.1	Experimental setup	135
6.2.2	Modelling of the teleoperation surgical system for control synthesis	139
6.2.3	Robust control under time-varying uncertainties	146
6.2.4	Switching robust control via bumpless transfer of robust con- trollers	147
6.2.5	Environment estimation	149
6.3	Results of robust control applied on SOFIE robot	150

6.3.1	Controller synthesis results	151
6.3.2	Simulation results	154
6.3.3	Experiments	156
6.3.4	Discussion	160
6.4	Conclusions	161
7	Conclusions and Recommendations	163
7.1	Conclusions	163
7.2	Recommendations for future research	168
	References	171
A	1-DoF Academic Setup	179
B	Controller-Multiplier Synthesis Procedure	181
B.1	Definitions of variables and set of LMIs	181
B.1.1	Definitions common to all control synthesis methods	182
B.1.2	Definitions for the synthesis method using a common Lya- punov function and for the bumpless transfer method . . .	183
B.1.3	Definitions for the synthesis method using dwell time condi- tions	185
B.2	Synthesis procedure: version I	188
B.3	Synthesis procedure: version II	190
	Acknowledgments / Dankwoord / Agradecimientos	193
	Curriculum Vitae	197

Chapter 1

Introduction

IN this chapter we introduce bilateral teleoperation systems. An overview of the current literature on control design for teleoperation systems is given in order to point out the unsolved challenges. Finally, the proposed methods and the contributions of this thesis are discussed.

1.1 Bilateral teleoperation

1.1.1 Teleoperation systems and force feedback

The word *teleoperation* means “operation at a distance”, thus, a teleoperation system allows the human to interact with environments that for instance: are located remotely, or environments are not of easy access, or that can be hazardous for the human health. Examples of applications are illustrated in Fig. 1.1. For instance, a mobile robot can be driven from a distance to explore disaster areas. In this scenario the robot might be equipped with special sensors to detect movement and heat to spot potential victims. Another application is a nuclear fusion reactor in which the level of radioactivity is dangerous for the operators. Therefore it is desirable to do the maintenance of the reactor using a robotic arm which is placed inside the reactor. The operator will be in another room sending commands through a mechanical device and inspecting the process via cameras. Force feedback can be provided to the operator, which can help him to move objects faster. In other types of applications, such as in robotically assisted minimally invasive surgery, a robotic arm or needle can be inserted in the human body through small incisions to reach internal organs. The surgeon can be situated right next to the

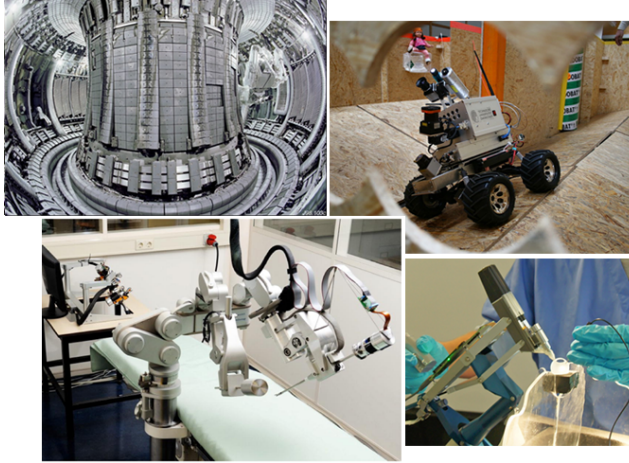


Figure 1.1: Different applications of teleoperation systems. From top-left to bottom-right: Maintenance in the Joint European Torus (JET) nuclear fusion reactor (picture by EFDA, visit www.efda.org); exploration of disaster areas using the RoboCup Rescue robot Hector from Darmstadt at 2010 German Open (picture by Mike1024/Wikimedia Commons); robotic assisted surgery with the SOFIE robot by van den Bedem et al. (2010)(picture by Bart van Overbeeke/Bart van Overbeeke Fotografie); robotic assisted eye surgery (Courtesy of PRECEYES ©).

patient interacting with a master device to drive the movements of the surgical instrument. It is desirable that, via the master device, the teleoperation system provides to the operator the kinaesthetic feeling of a stiffness similar to that of the environment, helping the surgeon to differentiate different types of tissues by means of palpation.

The mentioned applications have one thing in common: the fact that the operator is sending commands that are executed by a robotic device, for instance to perform a specific movement. However, only in some of the mentioned applications, force-feedback is provided from the environment to the operator. When such force feedback is present, the system is said to be *bilaterally teleoperated*. The type of force feedback provided to the operator can vary significantly from one application to the other. For instance, in the reactor maintenance case, the environment consists mainly of rigid objects which have to be moved to a desired position. One can provide haptic information to the operator about when there is contact with an object. This might already help him/her to improve the task performance. On the other hand, in the robotic surgery application, it would be desirable for the surgeon to distinguish the different types of tissues, such that he/she can feel through the master device a similar stiffness as that of the environment.

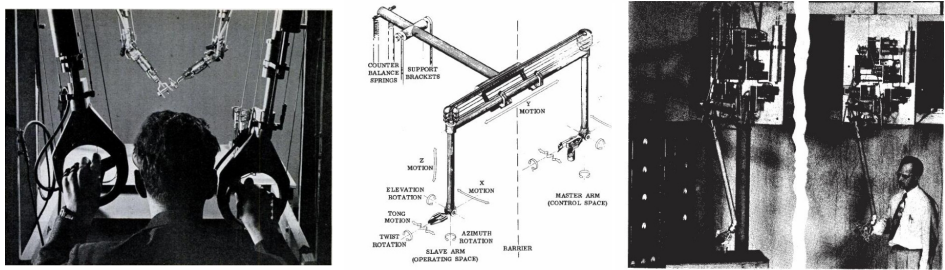


Figure 1.2: Early bilateral teleoperators: first mechanical master-slave manipulators designed by John Payne (left) and Goertz (center), first electric master-slave manipulator designed by Goertz and Thompson (right). Images are taken from Cyberneticzoo (2010)

Force-feedback can improve the task performance significantly, however, when forces are reflected to the operator they cause a reaction on his/her movements. These are passed again to the slave device, which again might result in a different force reflected to the operator. Such loops may cause instability during task execution, and it is more likely to happen if communication delays between the master and the slave sides are present. Hence, determining what kind of feedback is needed for a certain application or task is not a trivial problem, let alone its safe implementation. In fact, during the last six decades, researchers have been working in studying bilateral teleoperation systems. Specifically on the interactions between the operator and the environment, and how to couple them in an efficient way by means of a master-slave system.

The first bilateral teleoperation systems appeared in the late 1940s and the early 1950s. They were used mainly for the remote handling of hazardous materials. Example of these teleoperators are the systems designed by Payne (1949) (Patent filed in 1948) and by Goertz (1953) (Patent filed in 1949), see Fig. 1.2. In these devices the master and slave were mechanically coupled. Later, the first electrically controlled teleoperator was presented in Goertz and Thompson (1954), see Fig. 1.2. After that and until the late 1980s, there was an increased interest in telemanipulation, which encompassed with the increasing computational power and popularity of virtual reality. In that period researchers also started studying the effects of delays in teleoperation systems, and developed the initial control strategies for bilateral teleoperation based on supervisory control. It was then until the mid 1980s, when control theory started to develop, that more systematic approaches towards analysis and control design started to appear. Especially network theory came into play in teleoperation (see, e.g., Raju et al. (1989)), opening the path to techniques like passivity, scattering theory and wave variables, see, e.g., Niemeyer and Slotine (1991); Anderson and Spong (1989). Those theories were in particular motivated

to find solutions due to instability caused by delays in bilateral teleoperation systems. Since then, variations of those theories have been and are still applied in analysis and control design. Also, in the last two decades, techniques based on robust control and \mathcal{H}_∞ have been applied widely to the teleoperation problem. Since then only few deep changes on the control methodologies have been proposed but rather variations on them, with the exception of some techniques such as model mediated control, in which a model of the environment is obtained online and reflected to the operator (see, e.g., Mitra and Niemeyer (2008)), and shared control, in which the force feedback design is centered around the task itself (see, e.g., Abbink et al. (2012)). The reader is referred to the surveys in Hokayem and Spong (2006); Passenberg et al. (2010) for a more detailed overview on the different developments in the history of bilateral teleoperation.

After this brief overview of bilateral teleoperation systems, in the next section we will focus on the most relevant developments on modelling and control design concerning the research presented in this thesis.

1.1.2 A definition of stability for bilateral teleoperation systems

Before addressing the control design problem, we would like to discuss in more depth what stability means for teleoperation systems. To illustrate the concept of stability that is proposed here, consider a very simple teleoperation system: a person cutting a piece from a cake with a knife, as illustrated in the right part of Fig. 1.3. In this case, the knife is considered as the *teleoperator*, i.e. the instrument or tool that serves as a link between the operator and the environment. Moreover, the hand represents the operator and the cake represents the environment. The human hand, the environment, the knife, the interaction between the hand and



Figure 1.3: A simple teleoperation system: a person that cuts a piece of cake. The hand represents the operator, the knife the teleoperator, and the cake the environment.

the knife and the interaction between the knife and the cake constitute a bilateral teleoperation system.

Firstly, consider the knife, i.e. the teleoperator, as shown in the left part of Fig. 1.3. This system is fully defined in the sense that its motion dynamics can be represented by

$$\dot{x} = f(x, t), \quad (1.1)$$

in which x represents the state of the motion dynamics of the knife, $f(x, t)$ is a possibly nonlinear function and t is the time variable. Intuitively, one can say that a knife lying on a table (not shown in Fig. 1.3) is a “stable” system. More formally, the motion dynamics of the knife define an asymptotically stable system in the sense that small perturbations result in movements that will vanish over time and a new equilibrium is reached. At this point we have to consider the interaction between the knife and the table due to gravity as part of the teleoperator as well. For instance, the friction between the table and the knife makes the knife movements to reach equilibrium.

Next, consider the case when the knife is dropped and it buries into the cake. This situation is shown in the center part of Fig. 1.3. There is a difference with the previous case: the resulting system is not fully defined, i.e. it cannot be represented with dynamics of the form in Eq. (1.1). This is because we do not know exactly the consistency of the cake, i.e. its dynamics. However, one can use a system with uncertainty Δ_e to describe the set of dynamics of different cakes. Therefore, the knife-cake system can be considered as an uncertain system, the dynamics of which can be described by the following system

$$\dot{x} = g(x, \Delta_e, t),$$

in which x now also includes the state of the motion dynamics of the cake and $g(x, \Delta_e, t)$ is a possibly nonlinear function. Again, one can say intuitively that the knife-cake system is “stable” in the sense that the knife will be at rest at a certain location in the cake. In a more formal framework, the stability of the knife-cake system has the following meaning: the knife can enter the cake (which has uncertain dynamics) in different ways (that is, different initial conditions), and the knife’s movement will end up in an equilibrium point depending on the cake’s consistency, described by the uncertainty Δ_e . If for all predefined consistency levels $\Delta_e \in \Delta_e$ the knife reaches an equilibrium point, we call the knife-cake system robustly stable with respect to the uncertainty level Δ_e .

Finally, consider the situation in which a person grabs the knife and cuts the cake as shown in the right part of Fig. 1.3. Additional to the uncertainty Δ_e of the cake, the hand also exhibits uncertain dynamics. For instance, the operator can grab the knife with a light or a tight grip. In both of these cases the hand will

have different dynamics. Thus, the hand behavior while interacting with the knife could be described with a system with dynamic uncertainty Δ_h . Moreover, the hand exerts an input u to the system. This input allows to command the knife's movements. Such type of system could be described by the following equation

$$\dot{x} = h(x, u, \Delta_h, \Delta_e, t), \quad (1.2)$$

which is an “open” system because of the presence of the “free will” of the human to exert a certain force with his/her hand. $h(x, u, \Delta_h, \Delta_e, t)$ is a possibly nonlinear function. Once again, one can assume that the hand-knife-cake system is “stable” in the sense that we can perform the desired task of cutting a piece from the cake in a safe way. More formally, there is a main difference with the other two cases: during the execution of the task, there will not always be an equilibrium point of the knife's movements. Rather, we can say that the movements of the knife remain bounded, provided that the input u exerted by the hand remains also bounded, under the presence of the uncertainties Δ_h and Δ_e . Thus, it is said that this system presents robust bounded input to bounded state stability. This concept is also known as Input to State Stability (ISS) and it is illustrated in detail in the work of Sontag (2008). Precisely, the ISS concept of robust stability will be adopted for bilateral teleoperation systems in the rest of this thesis, and it is hereafter simply referred to as the stability of the bilateral teleoperation system.

Up to this point, it is assumed that the system with uncertainty in Eq. (1.2) covers exactly the uncertain dynamics of the true bilateral teleoperation system. In practice, the mathematical function $h(x, u, \Delta_h, \Delta_e, t)$ and the uncertainties Δ_h and Δ_e are approximate models. Thus, hereafter we assume that Eq. (1.2) and its components represent a model, which not necessarily covers exactly the uncertain dynamics of the real system. Hence, the stability analysis of a bilateral teleoperation system depends on the type of uncertainties $\Delta_h \in \mathbf{\Delta}_h$ and $\Delta_e \in \mathbf{\Delta}_e$ that are used in the model. Moreover, those uncertainties can be defined to describe specific dynamics present in a certain application of the bilateral teleoperation system.

We also illustrate the concept of conservatism in the stability analysis of bilateral teleoperation systems. Define two pairs of set of uncertainties of the operator and the environment dynamics: (Δ'_h, Δ'_e) and (Δ''_h, Δ''_e) . Hence, if $\Delta''_h \subset \Delta'_h$ and/or $\Delta''_e \subset \Delta'_e$, then achieving robust stability of the system in Eq. (1.2) could be easier for the pair (Δ''_h, Δ''_e) than for the pair (Δ'_h, Δ'_e) . Therefore, the latter set is said to introduce conservatism in the robust stability test, assuming that both the considered sets cover at least the set of uncertainties present in the real system for a specific application.

To illustrate this concept, imagine that we replace the common knife by an electric knife. Most probably, one cannot say that the electric knife itself is “stable” when it

is ‘on’ and it has no human control. For instance, throwing the electrical knife into the cake will have very undesired results in the sense that the vibrations could make the knife move uncontrollably inside the cake. In the previous intuitive stability test, Δ'_h can be considered to include the case of the electric knife inserted in the cake without an operator’s control, in which case the stability test on the basis of the uncertain model is likely to be conservative. This because the test covers cases that are not present in the application, which is cutting a piece from the cake. However, we can define another set of uncertainties Δ''_h to cover only the case of the operator holding the electric knife while it is ‘on’. In such a case, we can reasonably say that the system is stable.

Finally, one can see the electric knife has problematic dynamics not present in a purely mechanical knife. Therefore, the human operator needs to provide control and stabilization to now maintain the (robust) stability of this teleoperation system. Under a proper human control action, one may improve the performance of the system, which in this case means cutting the cake in a faster way and with less required effort. Thus, in such case we say that robust stability has been “traded-off” to achieve a better performance.

Now that the concept of stability of bilateral teleoperation systems is defined, we are ready to move forward to consider the bilateral control design problem.

1.1.3 Bilateral control design

Consider a realistic application of teleoperation systems, for instance in robotically assisted Minimally Invasive Surgery (MIS). A block diagram representation of such an application with the different components of the bilateral teleoperation system is depicted in Fig. 1.4.

The ultimate goal of the bilateral control design is to develop a control strategy or algorithm that serves as a link between the operator/master and the slave/environment side, generating the necessary actuation signals for the master and slave devices, such that a desired task by the operator is accomplished satisfactorily under certain performance criteria. At this point, we make the remark that it is not clear which performance criterion for controller design translates directly into better task performance for every application. The difficulty to quantify performance is caused by the fact that different tasks can have very different task performance criteria. This can be for instance, time completion, less possible stress for the operator, etc., and thus a single controller design criterion might not be the most efficient for all tasks. However, for control design purposes, the tendency has been on defining standard criteria. Among the most popular criteria proposed in the literature are:

- *transparency* (see Lawrence (1993a)). It is based on the principle that perfect transparency is obtained by a perfect match between forces and positions between the operator and environment sides.
- *z-width* (see Colgate and Brown (1994)). It evaluates the range of impedances that can be reflected to the operator. The impedances reflected to the operator in two extreme cases are calculated: when no environment is present and when the environment is infinitely rigid. The difference between those impedances is the z-width.
- *fidelity* (see Cavusoglu et al. (2002)). It represents how changes in the environment are reflected to the human operator. Thus, fidelity focuses more on how the operator perceives changes in the environment rather than the environment impedance itself.

Transparency is the most intuitive in the sense that perfect force and position tracking would give an operator a perfect kinaesthetic feeling as if he/she is interacting directly with the environment. Reaching perfect transparency is a very difficult task because there is an inherent trade-off between transparency and stability (see Lawrence (1993a)). Hence, when transparency is taken as performance criterion, the control design becomes a challenging task. Nevertheless, it is desirable to achieve certain force and position tracking performance that will give the operator at least a very similar perception of the real environment. For the rest of this thesis, when we refer to the performance of the teleoperation system, we refer to the performance with respect to force and position tracking between the master/operator and slave/environment sides.

Before addressing in more detail the pros and cons of the control design pre-

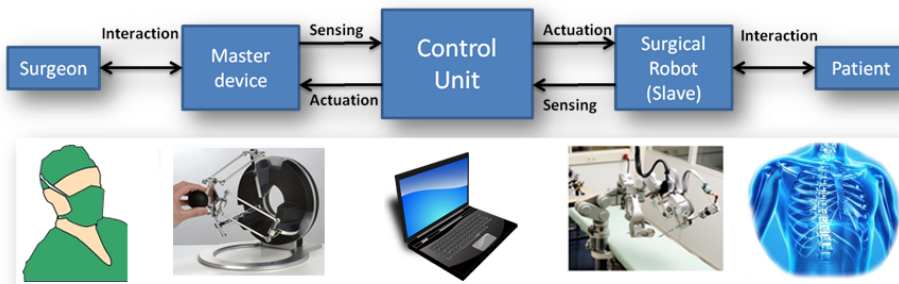


Figure 1.4: Block diagram representation of a bilateral teleoperation system for an application in Minimally Invasive Surgery. The master device shown is an Omega 3 device by dimension (2010). The slave device shown is the surgery robot SOFIE by van den Bedem et al. (2010)

sented in the literature, notice that in our block diagram representation in Fig. 1.4 time delays are not included. Delays will always degrade the achievable performance of a system. In fact, already without delays obtaining high performance and stability for a bilateral teleoperation system is a challenging problem. In this thesis the research focus is on providing solutions towards closing the gap between performance and stability of bilateral teleoperation systems. Hence, time delays are deliberately not covered. Nevertheless, the reader can refer to Polat (2011), in which a similar framework as the one utilized in this thesis, is used to include time delays in the control design.

1.1.4 Pros and cons of current bilateral control design methods

Passivity approaches

Passivity based methods are still widely used. A system is said to be passive if it does not generate energy. In particular, passive systems are asymptotically stable. Moreover, if connected with other passive systems, the resulting system will also not generate energy and thus will be passive as well. This modular property of passive systems has been exploited to generate the stability of teleoperation systems. Indeed, if the operator and the environment are modelled as passive systems, the interconnection with a passive teleoperator will result in a passive teleoperation system. At this point there are two aspects which we would like to discuss. Firstly, in the sense of the stability concept adopted here, a system can temporarily generate energy. In itself, this does not mean that the system becomes unstable, provided that the states of the system remain bounded for bounded inputs. Thus, passivity is a property that can be used as a method to obtain stability of the system even if energy is supplied to the system. Secondly, there is an ongoing discussion on the passivity assumption of the operator, and recent works suggest that the operator cannot be modelled as a passive system for all types of tasks (see, e.g., Polushin et al. (2012); Dyck et al. (2013); Polat (2014)). The operator can show passive behaviour while performing specific tasks, but shows non-passive behavior in performing others. For instance, the operator can choose to inject energy to the master device in order to perform his/her desired movements. Moreover, even if the operator would only show passive behaviour, modelling him/her as a passive system may add excessive conservatism. The set of dynamics covered by a passive system is much larger than the set of dynamics that an operator can show. For instance, an operator can not show the stiffness of a piece of metal, which can be considered as a passive system. Nevertheless, passivity based methods can guarantee stability, but it does not take performance explicitly into account. Therefore, it does not provide the obvious mean to achieve a systematic stability/performance trade-off. However, passivity can still be com-

bined with control design guidelines for performance. For instance, in Willaert et al. (2014) the authors have proposed methodologies that do take both performance and passivity requirements into account. They give guidelines to achieve transparency and passivity, at least in steady state, however the technique is limited to master and slave devices with mass-damper-spring dynamics with identical mechanical properties in both devices. They overcome this restriction by using the controller to also add dynamics on one of the devices, which will limit its application if one of the devices has high damping or high mass. Moreover, in real-life applications master and slave devices can have very different mechanical properties, which makes the technique limited in practice.

One important property of the operator and the environment, which is often overlooked, is that they are inherently time-varying. However, some of the control design tools based on passivity are valid only for Linear Time Invariant (LTI) passive systems, meaning that the operator and/or environment are additionally assumed to be LTI. In fact, in many applications such as minimally invasive surgery (MIS), needle insertion, suturing etc., the environment varies over time in a certain bounded set, say in terms of varying stiffness properties. Moreover, many studies on the human arm dynamics have already shown that the human arm dynamics exhibits behaviour that can be covered by a model describing a bounded set of dynamics, see, e.g., Tee et al. (2004); Speich et al. (2005); Fu and Cavusoglu (2012). Therefore, the bilateral system interacts with a bounded environment and a bounded operator dynamics and the information of those bounds have not yet been fully exploited in the control design for teleoperation systems.

Researchers have proposed different methodologies to reduce the conservatism in stability analysis and control design for bilateral teleoperation systems. Current methods based on the passivity approach do not allow to incorporate uncertainty bounds, other than passive ones, for environment and operator in order to assess the teleoperated system stability. This leads to a conservative methodology for bilateral control design. Indeed, previous works have presented absolute stability tests for a bounded uncertain environment based on passivity consideration, see, e.g., Willaert et al. (2009), Haddadi and Hashtrudi-Zaad (2010). In these tests conservatism is introduced via the operator model, which is taken to be passive. Additionally, the applicability of such stability criteria is limited since LTI environment uncertainties are assumed, which do not match the time-varying nature of the environment and operator dynamics.

Passivity in time

Some studies handle the passivity requirement in time-domain, see, e.g., Hannaford (2002), Ryu et al. (2004) and Franken et al. (2009). These works do take into account the time-varying nature of the bilateral teleoperation system. In those

studies, the main method consists of calculating the energy flow of the system to detect when there is an energy build-up, and then apply the necessary forces to ensure passivity. However, temporal generation of energy does not directly mean instability of the system. According to the authors in Franken et al. (2009), there is a separation in the control design for performance and stability. Nevertheless, the underlying controller could show active behaviour in order to achieve performance. Thus, the forces that would need to be applied to ensure passivity will have an unknown effect on the performance. Moreover, in order to make a correct computation of the energy balance of the system, accurate models of friction forces are needed, which in many real-life applications can be very difficult to obtain.

Robust control approaches

Other researchers have followed a different methodology based on robust control. For instance, Hu et al. (1995); Namerikawa et al. (2005), and Kim and Çavusoglu (2007), have addressed the robust performance control design using a structured singular value based approach. The environment/operator dynamics and uncertainties are considered as LTI systems, which approach will still not capture the time-variations in a real physical setup. In Vander Poorten (2007), a scaled \mathcal{H}_∞ norm method with constant scalings is utilized to handle the time-variations. However, the authors already state themselves that “the fact that the usage of constant scaled \mathcal{H}_∞ guarantees robust interaction with any possible nonlinear and time-varying system, might introduce a certain amount of conservatism”. Additionally, virtual shunt dynamics are considered in order to obtain some bound on the maximum operator impedance. However, bounds on the environment are not exploited, which can limit the achievable performance due to the large size of the uncertainty set. Alternatively, in Khan et al. (2009); Hacıoğlu et al. (2011), sliding mode control is used to guarantee robustness, however, explicit information about the bounded environment is not exploited and the performance is prone to typical artifacts such as chattering behavior which degrades the operator’s feeling of the environment.

Approaches with adaptation to environment stiffness

Next, considering more realistic situations, there might be cases in which stiff environments can be present. For instance, when performing an operation in MIS, there might be contact with bones, or it can be a collision between instruments. Thus, it is desirable to obtain high performance and stability in those cases as well. There is no guarantee that a single LTI controller exists that ensures both performance and stability for a large range of time-varying environment stiffness values.

To cover a large range of environment stiffness values, one can add flexibility in the control design, for instance by means of estimating the actual environment stiffness and use such estimate to design a controller that adapts accordingly. This idea is not new and some works, e.g. by Hashtrudi-Zaad and Salcudean (1996); Love and Book (2004); Willaert et al. (2010); Cho et al. (2013), design controllers that depend on the estimate of the environment stiffness. However, either they do not guarantee robust performance, or the achieved range of operation is limited to low values of environment stiffness. Moreover, all of these works rely on accurate, unbiased, low noise and/or fast convergence of the estimated environment stiffness, requirements which in practice are difficult to meet simultaneously. Therefore, it is desirable that the limited performance of environment estimators is taken into account during controller design. One approach that can be promising in providing adaptation to the environment and does not rely on accurate estimates of the environment, is the use of switching control. For instance, multiple model adaptive control has been used in teleoperation in Shahdi and Sirouspour (2005). The main underlying idea is to use different controllers under different kind of environment stiffness, i.e. one controller for soft environments and another for stiff environments. The main issue in the implementation of the work presented in Shahdi and Sirouspour (2005) is that at the moment of switching they obtain non-smooth responses that can compromise the stability of the system. Moreover, in the controller design, uncertainty in the operator is not taken into account.

Applicability in real-life systems

Next, considering more practical aspects, most of the control approaches for bilateral teleoperation have been tested either only on academic setups, or in teleoperators with low masses and/or low friction. In practice, the force feedback implementation in teleoperators can be very challenging. The main reason is that the master and slave devices must meet specifications on, for instance, dimensions, degrees of freedom (DoFs), resistance and costs among others. This results in a number of mechanical limitations, e.g. high friction levels, heavy devices, structural resonances and lack of force sensors, limitations that in general are not present in academic setups that are commonly used in the literature to test bilateral controllers. Therefore, commercially available surgical systems do not have force feedback, e.g. the Da Vinci system (Guthart and Salisbury Jr (2000)), for which achieving force feedback is difficult due to the high masses involved (Shimachi et al. (2008)). It is typical that these type of systems have a slave device with large mass, and a master device with low mass and without force sensors. Only few methods have been implemented and tested in such type of devices due to the challenges involved (see, e.g., Beelen et al. (2013)). Thus, a systematic and practically feasible methodology is needed.

This short literature survey covered the main control methodologies of interest based on linear techniques, because the methods that will be presented here are also based on linear techniques. However, we would like to mention that non-linear techniques have similar issues as the linear techniques in what concerns mainly to operator modelling. Most of the non-linear control techniques are based on passivity, thus assuming passive operators and environments. Moreover, they focus mainly on the stability of the system, see, e.g., Nuño et al. (2011). Some authors have extended control methodologies to include also non-passive behaviour, see, e.g., Polushin et al. (2012). Thus, due to the large class of dynamics covered, these techniques based on passivity deliver results that can add excessive conservatism. Therefore, most of the motivation for the need of new modelling and control approaches also holds for the non-linear case.

As a final remark, we would like to mention that the survey hereby provided, is by far not complete, and many other areas of bilateral teleoperation have been left out in order to focus on the problem that is treated here. For instance, there are a large volume of active research focused on delayed teleoperation, on teleoperation via the network, on multi-user teleoperation, etc.

1.2 Problem statement and challenges

After we reviewed the main control methodologies proposed in the literature, one can conclude that there is still a number of challenges that demand research attention. Therefore, an alternative approach towards bilateral control design is needed. In particular, there is a need to develop an approach that:

- *takes explicitly into account the time-varying nature of operator and environment dynamics.* A better characterization of those dynamics will help to guarantee that experimental results match better with the theory, improving our understanding of bilateral teleoperation systems,
- *allows for including information on the bounds of model parameters of the operator and environment.* This will narrow the set of dynamics for which the teleoperation system needs to have robust performance, thus less conservative results could be obtained,
- *provides means to address performance and stability systematically.* This will allow to specify a-priori the desired performance and stability properties of the teleoperation system and then design a controller that aims to achieve both simultaneously,
- *is suitable for master and slave devices with structural resonances and different mechanical properties.* Thus the technique can be applied in real-life

applications in which the master and slave devices are designed under a number of specifications that results in limitations in their mechanical properties.

Moreover, in order to improve the performance in bilateral teleoperation systems, it is desirable to have a control structure that additionally:

- *provides adaptation to the environment dynamics when properly dealt with.* This allows to increase the performance of the system,
- *takes into account that environment estimators have limitations in accuracy and/or estimation noise and/or convergence speed.* There is an inherent trade-off between high accuracy, low noise and fast convergence in environment estimators. Thus, the controller should be designed to take this trade-off into account.

1.3 Research approach

In order to provide a solution for the challenges previously mentioned, we adopt a model-based robust control design approach. We will use a parametric model of the teleoperation system that captures the bounded dynamics present during normal operation. To this end, for the human operator, we derive a parametric model based on identification experiments, thus characterizing a bounded set of dynamics inspired by the mechanical properties of the operator's arm. The environment can be modelled according to the application of the bilateral teleoperation system. For instance, we consider environments in which stiffness is the dominant phenomenon, e.g. in stiffness palpation tasks present in surgery. In that case, the environment stiffness is considered a parameter of the environment model. Subsequently, the parameters of both the environment and the operator models can be treated as parametric uncertainties. To account for realistic behaviour, those parametric uncertainties are considered to be bounded and time-varying. On the other hand, models for the master and slave devices can be identified using existing system identification techniques. Hence, the models of the components of the bilateral teleoperation system can then be incorporated into a model-based control design framework as depicted in Fig. 1.5, in which the uncertainty parameters can be isolated in a separate block Δ .

Closed loop system

In the representation of Fig. 1.5 we distinguish the following vector valued signals:

- q and p : define the signals through which model uncertainty is represented.

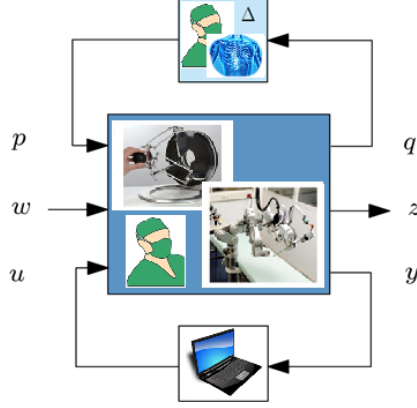


Figure 1.5: Representation of a generalized plant model for an application in Minimally Invasive Surgery

- y : contains the measured signals. For instance, position and force signals.
- w : defines all disturbances and noises that influence the system's performance. For instance, w contains sensor noise signals. We also include in w the signals representing the active forces from the environment and the operator that act on the system. These signals perturb the position and the force tracking of the system.
- u : defines the actuation signals of the system such as the actuation signals of the master and the slave devices.
- z : defines the performance signals, e.g. position and force tracking errors.

Uncertainty specification

We aim to achieve robust stability of the system against the operator and the environment model uncertainties. We will use a specific class of Integral Quadratic Constraints (IQCs) (see Megretski and Rantzer (1997)) to model uncertainties $\Delta \in \mathbf{\Delta}$. They allow to easily incorporate bounds and time-varying properties on the uncertainty for control design. To this end, the class of dynamics $\mathbf{\Delta}$ of the uncertainty block Δ can be represented by the IQC:

$$\int_0^{T_0} \begin{pmatrix} \Delta(\delta)q(t) \\ q(t) \end{pmatrix}^T P \begin{pmatrix} \Delta(\delta)q(t) \\ q(t) \end{pmatrix} dt \geq 0 \quad (1.3)$$

Specifically, let $P = P^T$ be a symmetric matrix of dimension $[\dim(p) + \dim(q)] \times [\dim(p) + \dim(q)]$ and suppose that $p(t) = \Delta(\delta)q(t)$ in Fig. 1.5 where Δ is an operator $\Delta : \mathcal{L}_2 \rightarrow \Delta\mathcal{L}_2$ that has the property that Eq. (1.3) holds for all $q \in \mathcal{L}_2[0, T_0]$, $T_0 \in \mathbb{R}_+$.

The matrix P is a so called *multiplier*. Eq. (1.3) provides a generic way to represent uncertainties. However, by itself it does not provide a means to find a specific class of matrices P that describes specific properties of the uncertainty Δ . Therefore, in order to use Eq. (1.3), P needs to be classified or specified. There exists already a number of multipliers that describe certain classes of uncertainties. To give some common examples, let us assume LTI uncertainties Δ . Then Eq. (1.3) is *equivalent to*:

$$\int_0^\infty \begin{pmatrix} \Delta(i\omega) \\ I \end{pmatrix}^* P \begin{pmatrix} \Delta(i\omega) \\ I \end{pmatrix} d\omega \geq 0 \quad (1.4)$$

Next, consider for instance the following multiplier

$$P = \begin{pmatrix} 0 & I \\ I & 0 \end{pmatrix}.$$

Then we have that

$$\begin{aligned} \begin{pmatrix} \Delta(i\omega) \\ I \end{pmatrix}^* \begin{pmatrix} 0 & I \\ I & 0 \end{pmatrix} \begin{pmatrix} \Delta(i\omega) \\ I \end{pmatrix} &\succeq 0 & \forall \omega \in \mathbb{R} \\ \Delta(i\omega)^* + \Delta(i\omega) &\succeq 0 & \forall \omega \in \mathbb{R} \end{aligned}$$

which is equivalent to the positive realness of the uncertain system Δ , i.e. same property as in passivity. In turn, this means that the uncertainty is modeled as a passive LTI system. Consider also

$$P = \begin{pmatrix} -I & 0 \\ 0 & I \end{pmatrix}.$$

With such a multiplier we have that (1.4) is equivalent to:

$$\Delta(i\omega)^* \Delta(i\omega) \preceq I \quad \forall \omega \in \mathbb{R}$$

which means bounded gain of the uncertain system, which can be used in combination with the small gain theorem in a robust control framework. The multiplier P can describe mathematical properties of the uncertainties Δ . In our particular case, we focus on a certain class of frequency independent multipliers that allow to characterize arbitrarily fast time-varying parametric uncertainties. This type of characterization accounts for sudden changes of the environment and of the operator dynamics.

To illustrate how to find a proper matrix P that describes parametric uncertainties, consider the example in which we have a vector δ containing parametric uncertainties such that they are contained in a certain set δ . To not introduce conservatism in the uncertainty description via the IQC (1.3), *ideally* we need to find matrices P such that (1.3) holds *only* for $\delta \in \delta$. In practice, this can not always be achieved, thus approximations are used. For the case of bounded parametric uncertainties, we use the following procedure:

Consider the case when each of the N_p uncertain parameters δ_i is time-varying and bounded in the sense that $\delta_i : \mathbb{R}_+ \rightarrow [\underline{\delta}_i, \bar{\delta}_i]$, for $i = 1, \dots, N_p$. Then, the class $\delta = \prod_{i=1}^{N_p} [\underline{\delta}_i, \bar{\delta}_i]$ is the uncertainty ‘cube’ in \mathbb{R}^{N_p} which can actually be written as the convex hull of $M = 2^{N_p}$ corner points $\delta^1, \dots, \delta^M \in \mathbb{R}^{N_p}$. That is, $\delta = \text{co}\{\delta^1, \dots, \delta^j, \dots, \delta^M\}$. For instance, if $N_p = 2$ we will have that $\delta^1 = \text{col}(\underline{\delta}_1, \underline{\delta}_2)$, $\delta^2 = \text{col}(\underline{\delta}_1, \bar{\delta}_2)$, $\delta^3 = \text{col}(\bar{\delta}_1, \underline{\delta}_2)$ and $\delta^4 = \text{col}(\bar{\delta}_1, \bar{\delta}_2)$. Next, we assume that the uncertain parameters δ_i of the system can be included in the Δ block of Fig. 1.5 such that $\Delta(\delta) = \text{diag}(\delta_1, \dots, \delta_{N_p})$.

Now, if both q and T_0 are arbitrary in Eq. (1.3), it is then equivalent to:

$$\begin{pmatrix} \Delta(\delta) \\ I \end{pmatrix}^T P \begin{pmatrix} \Delta(\delta) \\ I \end{pmatrix} \succeq 0 \quad \forall \delta \in \delta \quad (1.5)$$

One way to find a set \mathbf{P} of symmetric matrices P that describes δ and satisfies (1.5) is the following: because of the convexity property of δ , it suffices to force concavity in the left hand side of (1.5) and evaluate (1.5) on the corner points $\delta^j, j = 1, \dots, M$ that generate δ . Thus, we classify \mathbf{P} by the matrices P such that

$$\begin{pmatrix} \Delta(\delta^j) \\ I \end{pmatrix}^T P \begin{pmatrix} \Delta(\delta^j) \\ I \end{pmatrix} \succeq 0, \quad j = 1, \dots, M. \quad (1.6)$$

and

$$\begin{pmatrix} I \\ 0 \end{pmatrix}^T P \begin{pmatrix} I \\ 0 \end{pmatrix} \preceq 0. \quad (1.7)$$

These equations are the conditions that will allow to find a proper symmetric matrix P that will describe the class of bounded parametric uncertainties considered in this thesis. For other ways to describe bounded parametric uncertainties, see, e.g., Megretski and Rantzer (1997); Scherer and Weiland (2000); Polat (2011).

Performance specification

The system’s representation in Fig. 1.5 allows to systematically incorporate performance and (robust) stability in the control design. The performance of the

system is quantified via a quadratic performance criterion from the disturbance signals w to the performance signals z . Specifically, let $P_p = P_p^T$ be a symmetric matrix of dimension $[\dim(w) + \dim(z)] \times [\dim(w) + \dim(z)]$ and consider the uncertain controlled system of Fig. 1.5. Suppose that z is uniquely defined by w for all possible uncertainties $\Delta \in \mathbf{\Delta}$. Then we will say that the controlled system achieves robust performance (or robust performance) if (1.8) holds for all $w \in \mathcal{L}_2$ and for all $\Delta \in \mathbf{\Delta}$.

$$\int_0^\infty \begin{pmatrix} w(t) \\ z(t) \end{pmatrix}^T P_p \begin{pmatrix} w(t) \\ z(t) \end{pmatrix} dt < 0 \quad \forall w \neq 0, \quad (1.8)$$

Hence P_p describes a specific quadratic performance criterion. For instance, one could state that passivity can be seen as a performance criterion for a certain system. Then, for the case that w and z are vector signals with one element, replacing

$$P_p = \begin{pmatrix} 0 & -I \\ -I & 0 \end{pmatrix}$$

in (1.8) results in

$$\int_0^\infty w(t)^T z(t) dt > 0 \quad \forall w \neq 0. \quad (1.9)$$

When $w(t)$ and $z(t)$ are defined such that they represent effort and flow variables respectively, (1.9) is equivalent to require that the total energy flow of the system through the ports defined by $w(t)$ and $z(t)$ is positive, i.e. the same property as in passivity (see Llewellyn (1952)).

Another example is the \mathcal{L}_2 gain of the mapping from disturbance signals to the performance signals. Indeed, if we set

$$P_p = \begin{pmatrix} -\gamma^2 I & 0 \\ 0 & I \end{pmatrix}$$

then (1.8) becomes $\|z\|_2^2 < \gamma^2 \|w\|_2^2$ for all $w \in \mathcal{L}_2$. This performance criterion is equivalent to saying that

$$\sup_w \frac{\|z\|_2}{\|w\|_2} < \gamma, \quad (1.10)$$

which for an LTI system it is equivalent to a bounded \mathcal{H}_∞ . In Eq. (1.10), γ can be interpreted as a worst-case gain from the disturbances to the performance signals. Therefore, instantaneous responses that can be felt by the operator have a direct effect on the performance criterion. This makes the \mathcal{L}_2 gain a suitable performance criterion for teleoperation systems and it will be used as the performance criterion in this thesis.

One can see that other performance criteria can be also incorporated in the design by defining properly the matrix P_p , see, e.g., Scherer and Weiland (2000). Such

flexibility in defining performance is one of the advantages of the framework utilized in this thesis.

Robust stability and robust performance

The robust stability of the system is achieved if we obtain Input to State Stability (ISS) of the bilateral teleoperation system, as previously mentioned. The ISS concept is based on the principle that for any initial condition x_0 of the state vector x , and any bounded input u , there should exist some functions $\beta \in \mathcal{KL}$ and $\alpha \in \mathcal{K}_\infty$ such that

$$|x(t)| \in \beta(|x_0|, t) + \alpha(\|u\|_\infty) \quad (1.11)$$

for all solutions $x(t)$ of the system and for all $t > 0$. The classes \mathcal{KL} and \mathcal{K}_∞ are basically unbounded strictly increasing functions, the reader is referred to the work of Sontag (2008) for details. ISS is closely related to the concept of stability of dissipative dynamical systems. Here we present a brief conceptual description on how such theory can be used to incorporate robust performance and stability. Let X be the state space of the state vector x of the system in Fig. 1.5. Let W and Z be the disturbance vector space and the performance vector space respectively. Let $s : W \times Z \rightarrow \mathbb{R}$ be a mapping (referred as the supply function) acting on all pairs (w, z) of the system. Then, the system with supply function s is said to be robustly dissipative against time-varying uncertainties $\Delta \in \mathbf{\Delta}$ if there exists a function $V : X \times \mathbf{\Delta} \rightarrow \mathbb{R}$ such that

$$V(x(t_1), \Delta(t_1)) \leq V(x(t_0), \Delta(t_0)) + \int_{t_0}^{t_1} s(w(t), z(t)) dt \quad (1.12)$$

for all $t_0 \leq t_1$ and all signals (x, w, z, Δ) that satisfy the system's dynamics and all $\Delta \in \mathbf{\Delta}$. We call the function V a robust storage function. It expresses the amount of internal energy in the system when it finds itself in the state $x \in X$ and with uncertainty $\Delta \in \mathbf{\Delta}$. As a remark, the storage function V in (1.12) is not required to be non-negative. However, for control design purposes, later we will restrict ourselves to quadratic storage functions which are also non-negative in order to guarantee the system's stability.

The concept in Eq. (1.12) can be interpreted as the requirement that a system dissipates “energy” at a faster rate than the rate $s(w, z)$ at which this “energy” is being supplied to it. In practice the “energy” quantity does not need to be literally the energy of the system. For instance, in the performance specification section, different performance criteria were illustrated, which are directly related to the supply function $s(w, z)$. The quadratic performance specified by P_p describes the supply function s . Thus, P_p will determine the corresponding type of “power” that is used.

It is beyond the scope of this thesis to enter into the details of the derivation of the corresponding theory to get from the dissipation concept to tractable equations useful for control design. We will give a brief example on how this could be achieved. We restrict ourselves to Lyapunov functions of the form

$$V(x, \Delta) = x^T \mathcal{X} x,$$

i.e. V independent of Δ , and Lyapunov functions of the form

$$V(x, \Delta) = x^T \mathcal{X}(\Delta) x$$

with $\mathcal{X} = \mathcal{X}^T$ and $\mathcal{X}(\Delta) = \mathcal{X}(\Delta)^T$ being positive definite matrices. Consider we have a system of the form:

$$\begin{aligned} \dot{x} &= A(\Delta)x + B(\Delta)w \\ z &= Cx + Dw. \end{aligned}$$

Then for $t_1 \rightarrow t_0$ (1.12) is equivalent to :

$$\frac{\partial V}{\partial x} \dot{x} \leq s \quad (1.13)$$

Considering also the supply function of the form $s(w, z) = -[w \ z]^T P_p [w \ z]$. Then (1.13) is equivalent to each of the following inequalities

$$\begin{aligned} 2x^T \mathcal{X}(\Delta)(A(\Delta)x + B(\Delta)w) &\leq - \begin{pmatrix} w \\ z \end{pmatrix}^T P_p \begin{pmatrix} w \\ z \end{pmatrix} \\ \begin{pmatrix} x \\ A(\Delta)x + B(\Delta)w \end{pmatrix}^T \begin{pmatrix} 0 & \mathcal{X}(\Delta) \\ \mathcal{X}(\Delta) & 0 \end{pmatrix} \begin{pmatrix} x \\ A(\Delta)x + B(\Delta)w \end{pmatrix} &\leq \\ - \begin{pmatrix} w \\ Cx + Dw \end{pmatrix}^T P_p \begin{pmatrix} w \\ Cx + Dw \end{pmatrix} \\ \begin{pmatrix} x \\ w \end{pmatrix}^T \begin{pmatrix} I & 0 \\ A(\Delta) & B(\Delta) \end{pmatrix}^T \begin{pmatrix} 0 & \mathcal{X}(\Delta) \\ \mathcal{X}(\Delta) & 0 \end{pmatrix} \begin{pmatrix} I & 0 \\ A(\Delta) & B(\Delta) \end{pmatrix} \begin{pmatrix} x \\ w \end{pmatrix} &\leq \\ - \begin{pmatrix} x \\ w \end{pmatrix}^T \begin{pmatrix} 0 & I \\ C & D \end{pmatrix}^T P_p \begin{pmatrix} 0 & I \\ C & D \end{pmatrix} \begin{pmatrix} x \\ w \end{pmatrix} \end{aligned}$$

which for arbitrary $x \in X$ and $w \in W$ is equivalent to:

$$\begin{aligned} \begin{pmatrix} I & 0 \\ A(\Delta) & B(\Delta) \end{pmatrix}^T \begin{pmatrix} 0 & \mathcal{X}(\Delta) \\ \mathcal{X}(\Delta) & 0 \end{pmatrix} \begin{pmatrix} I & 0 \\ A(\Delta) & B(\Delta) \end{pmatrix} \\ + \begin{pmatrix} 0 & I \\ C & D \end{pmatrix}^T P_p \begin{pmatrix} 0 & I \\ C & D \end{pmatrix} \preceq 0 \end{aligned} \quad (1.14)$$

which is already a *matrix inequality*. Moreover, for specific cases of the dependency on the uncertainty Δ , the inequality (1.14) can be expressed as a *linear matrix inequality* (LMI). In fact, for the trivial case that there is no dependency on the uncertainty Δ , (1.14) is already linear with respect to \mathcal{X} . Hence, in that case it is said that (1.14) is an LMI. Therefore, it is possible to incorporate the performance and uncertainty specifications (which were already introduced as tractable mathematical conditions) in a series of linear matrix inequalities.

In fact, in the next chapters of this thesis, we will use the results from robust control theory based on Linear Matrix Inequalities (LMIs) (see Scherer and Weiland (2000)). These techniques are introduced and applied to the control design problem.

Switching Control

Finally, to include adaptation to the environment properties, we propose the use of a multi-controller structure, in which we divide the environment dynamics in subregions, such that one controller covers each subregion. In this way, we do not rely on accurate estimates of the environment but only on a correct estimation of the subregion to which the environment currently belongs to.

Then for each subregion, we will design a LTI controller which presents robust performance. The main challenge in such a multi-controller structure is to achieve robust stability of the overall system including the switching between its different LTI controllers. We propose the use of three different switching techniques:

- *based on the existence of a common Lyapunov function*: It is known from the switching systems theory (see Liberzon (2003)) that if different closed loop systems have a common Lyapunov function, then arbitrary fast switching among those closed loop systems will result in a stable system. This idea is intuitive in the sense that the system will respect always the dissipation inequality in (1.12).
- *based on average dwell time switching*: In this concept, switching among different closed loop systems is restricted to a minimum average dwell time τ (see Hespanha and Morse (1999)). This allows to use different Lyapunov functions for different closed loop systems, provided that the discrepancy of the different lyapunov functions is conditioned to a relation depending on the average dwell time τ . In view of Eq. (1.12), in this case the times t_0 and t_1 are restricted with respect to τ and the overall Lyapunov function is then allowed to increase temporarily.

- *based on bumpless transfer*: This concept was proposed by Zaccarian and Teel (2005) in order to activate a controller in a safe way. The main idea is to reduce the transient behavior at the moment that a certain controller is put ‘on-line’ with a plant. This is achieved by virtually putting the controller ‘on-line’ before it is actually activated. To this end, the controller is simulated in a virtual loop and perturbed using signals measured from the real system. In this thesis we will adapt the bumpless transfer concept to perform switching among different robust controllers.

1.4 Contributions

Using the research approach previously described, in this thesis we present methods and results that lead to contributions in the following areas:

Contribution 1. *A systematic modelling and control design approach for bilateral teleoperation systems.*

The proposed approach uses an experimentally identified parametric model for the operator and a pre-defined parametric model of the environment. The combination of both models lead to a Linear Fractional Representation of the bilateral teleoperation system. Then the parameters of the system are described explicitly as time-varying to account for realistic behaviour. Moreover, we describe how to use robust control synthesis techniques to design controllers with robust performance under time-varying dynamics in the operator and environment of the teleoperated system. We provide guidelines on how to implement successfully such type of controllers. This type of approach leads to a consistent theory, simulations and experiment results.

Contribution 2. *A gain-scheduling multi-controller structure with switching based on Lyapunov Function Conditions.*

This controller structure allows for different LTI controllers. Each controller is designed for a different range of environment stiffness, which leads to an improved overall performance of the teleoperated system. This structure is particularly useful when the environment stiffness varies within a wide range including soft and stiff environments. The main challenge is how to design the controllers to achieve a smooth switching among them.

Contribution 2.a. *A gain-scheduling multi-controller structure with switching based on the existence of a common Lyapunov Function.*

The proposed method ensures smooth switching among controllers and improves the performance of the teleoperated system in comparison when a single LTI controller is used. The controller structure is also tested experimentally.

Contribution 2.b. *A gain-scheduling multi-controller structure with switching*

based on dwell time conditions.

The proposed method presents stable switching among controllers under the assumption that the operator drives the system such that fast switching among controllers is avoided. Simulation showed that the overall performance can be improved with respect to the structure in contribution 2.a.

Contribution 3. *A gain-scheduling multi-controller structure with switching based on Bumpless Transfer of Robust Controllers.*

The proposed structure allows for designing controllers independently for different regions of environment stiffness. Stable switching is achieved by means of bumpless transfer. The structure is experimentally validated under regular operating conditions.

Contribution 4. *A controller design and implementation approach for a non-ideal teleoperator.*

We show how the model-based robust control techniques can be applied to teleoperators with non ideal properties, e.g. high difference in dynamics of master and slave device, no force sensor or with structural resonances in the master device.

1.5 Outline of the thesis

This thesis is the compilation of several research works. The chapters are based on journal or conference articles, which are either published or currently under review. Because of this, there is partial overlap between the chapters.

Chapter 2

This chapter addresses Contribution 1. It is based on the paper:

- López Martínez, C. A., Polat, İ., Molengraft, R. v. d., and Steinbuch, M. (2014e). Robust high performance bilateral teleoperation under bounded time-varying dynamics. *IEEE Transactions on Control Systems Technology*. *Accepted for journal publication*

In this chapter, we propose a methodology in which we develop a parametric model of the teleoperation system. Subsequently, we exploit robust control techniques to design controllers that aim to achieve a predefined performance, and are robust to bounded but arbitrarily fast-time-varying parametric uncertainties. Analysis, simulation and experimental results shows the effectiveness of the method to trade-off perfect transparency and stability.

Chapter 3

This chapter addresses Contribution 2.a. It is based on the paper:

- López Martínez, C. A., Molengraft, R. v. d., and Steinbuch, M. (2014c).

Switching robust control for bilateral teleoperation. *Under review for journal publication*

In this chapter we propose the synthesis of a switching robust controller that allows to design multiple robust controllers suitable for different ranges of environment stiffness, so that an overall better performance among a wide range of environment stiffness is achieved. The controllers are scheduled using an estimate of the environment stiffness. We present synthesis, simulation and experimental results of the proposed approach, thus showing the effectiveness of the method to improve the robust performance of the teleoperated system.

Chapter 4

This chapter addresses Contribution 2.b. It is based on the paper:

- López Martínez, C. A., Molengraft, R. v. d., and Steinbuch, M. (2014d). Switching robust control synthesis for teleoperation via dwell time conditions. In *9th International Conference, EuroHaptics 2014*, Versailles, France. Springer. *To appear online*

In this chapter, we propose a method to further reduce conservatism in the achievable performance of switching robust control synthesis for teleoperation systems. In this approach multiple Lyapunov functions with a special structure are introduced, linked by conditions of minimum average dwell time switching among controllers. We show the advantage of the proposed method by means of control synthesis and simulation for an 1-DoF teleoperation system.

Chapter 5

This chapter addresses Contributions 3. It is based on the paper:

- López Martínez, C. A., Molengraft, R. v. d., and Steinbuch, M. (2014a). High performance teleoperation by bumpless transfer of robust controllers. In *IEEE Haptics Symposium 2014*, pages 209–214, Houston, TX, U.S.A

In this chapter we propose a controller scheme with multiple robust controllers in which every controller is performance-optimized separately. The switching among them is based on bumpless transfer and they are scheduled using an environment stiffness estimator. Limited accuracy and noise of such estimator is also taken into account during control design. We show the applicability of the approach by experiments on a 1-DOF teleoperated system.

Chapter 6

This chapter addresses Contribution 4. It is based on the paper:

- López Martínez, C. A., Molengraft, R. v. d., and Steinbuch, M. (2014b). Model based robust control for bilateral teleoperation: Applied to a non-ideal teleoperator. *In preparation for journal publication*

Design specifications in real-life applications of bilateral teleoperation, e.g. minimally invasive surgery, can impose a series of limitations on the master and slave devices, e.g. lack of force sensors among others, resulting in non-ideal teleoper-

ators, making the design and implementation of a bilateral controller very challenging. In this chapter, we show how to implement model-based robust control techniques in a surgical setup designed for robotic assisted surgery. The experimental results demonstrate that using a model based robust control methodology, high performance is achieved despite the limitations of the system.

Chapter 7

In this chapter we draw the conclusions obtained from this thesis and recommendations for future works are given.

Chapter 2

Robust Bilateral Control under Time-Varying Dynamics

IN *THIS* chapter, we propose a methodology in which we develop a parametric model of the teleoperation system. Subsequently, we exploit robust control techniques based on Linear Matrix Inequalities to design controllers that aim to achieve a predefined performance, and are robust to bounded but arbitrarily fast-time-varying parametric uncertainties. We present analysis, simulation and experimental results of the designed controller, thus showing that the assumptions made during modeling are appropriate and the effectiveness of the method to trade-off perfect transparency and stability.

2.1 Introduction

Bilateral teleoperation systems allow an operator to manipulate a remote environment by means of a master and a slave device with which a feeling of tele-presence using force feedback is obtained. The system is supposed to present high performance, e.g. the operator feels as if he/she is manipulating the environment directly, in a stable fashion. However, there is an inherent trade-off between (robust) stability and performance, see, e.g., Hannaford (1989); Lawrence (1993b),

This chapter is based on the following manuscript: López Martínez, C. A., Polat, İ., Molengraft, R. v. d., and Steinbuch, M. (2014e). Robust high performance bilateral teleoperation under bounded time-varying dynamics. *IEEE Transactions on Control Systems Technology*. Accepted for journal publication

and it is a challenging problem to design controllers that meet an appropriate balance, see, e.g. Hokayem and Spong (2006), Passenberg et al. (2010). Most of the current design tools are based on passivity theory (Niemeyer and Slotine (1991)), which guarantees stability but does not provide a means to achieve systematic robust stability/performance trade-off. Moreover, the dynamics of the environment and the operator are inherently time-varying, which is a property that is often overlooked, see Chapter 1 Section 1.1.4. Also, in many applications such as minimally invasive surgery (MIS), needle insertion, suturing etc., the environment varies in a certain range, say in terms of stiffness properties, e.g., 83 N/m for fat, up to 2483 N/m and so on (Gerovich et al. (2004)). Therefore, the bilateral system interacts with a bounded environment and bounded operator dynamics and the information of those bounds have not yet been fully exploited in the control design for teleoperation systems. In principle, this can lead to improve the system's performance. Current methods based on the passivity approach require that the uncertain dynamics are passive for at least one of both the environment or the operator in order to assess the teleoperated system stability. Therefore, an alternative approach towards bilateral control design is needed, which allows us to incorporate bounds on the uncertainty of environment and operator dynamics. This will allow to reduce the conservatism for guaranteeing stability while meeting the performance requirements, and at the same time, to take the time-varying nature of teleoperation systems into account.

Researchers have proposed different methodologies to reduce the conservatism in stability analysis and control design for bilateral teleoperation systems. Previous works have presented absolute stability tests for a bounded environment, see, e.g., Willaert et al. (2009), Haddadi and Hashtrudi-Zaad (2010). Such tests are non-conservative in terms of stability characterization based on Llewellyn's absolute stability criteria (Llewellyn (1952)), however the modeling still introduces conservatism due to the passivity assumption. Additionally, the applicability of the stability criteria in Willaert et al. (2009) and Haddadi and Hashtrudi-Zaad (2010) is limited since we have to assume that the uncertainties of the environment are Linear Time Invariant (LTI), which does not match the time-varying nature of the environment and operator dynamics. Some studies handle the passivity requirement in the time-domain, see, e.g., Hannaford (2002), Ryu et al. (2004) and Franken et al. (2009). In these studies, the authors ensure the stability of the bilateral system by forcing the involved model(s) of the teleoperation system to be passive by explicitly monitoring the external behavior. The underlying controller that is design for performance may show non-passive behavior. Thus, the forces that are necessary to ensure passivity will have an unknown effect on the performance. Other works such as those by Hu et al. (1995); Namerikawa et al. (2005), and Kim and Çavusoglu (2007), have addressed the robust performance control design using a structured singular value (SSV) based approach. The environment/operator dynamics and uncertainties are considered as LTI systems. This approach cannot

capture the time-variations in the physical setup. In Vander Poorten (2007), a scaled \mathcal{H}_∞ method with constant scalings is utilized to handle the time-variations. However, the authors point out that “the fact that the usage of constant scaled \mathcal{H}_∞ guarantees robust interaction with any possible nonlinear and time-varying system, might introduce a certain amount of conservatism”. Additionally, virtual shunt dynamics are considered in order to obtain some bound on the maximum operator impedance. But again, bounds on uncertainty of the environment are not exploited, which can limit the achievable performance due to the large size of the uncertainty set. Alternatively, in Khan et al. (2009); Hace et al. (2011), sliding mode control is used to guarantee robustness, however, explicit information about the bounded environment is not exploited and the performance is prone to typical artifacts such as chattering behavior. This degrades the operator’s feeling of the environment.

We use a model-based robust control approach to controller design. We utilize mass-damper-spring models for the master and slave devices. For most applications in bilateral teleoperation, such models are appropriate for describing the environment. For the human operator, we have constructed a parametric model based on identification experiments. Having a parametric structure for operator and environment models, we can, then, extract the uncertain parameters to obtain a Linear Fractional Representation (LFR) of the teleoperation system. This representation allows to treat the uncertain parameters independently with separate bounds with ease (cf. Vander Poorten (2007)). Moreover, stability and performance specifications are addressed simultaneously via Linear Matrix Inequalities (LMIs). We describe the operator/environment uncertainty via a specific class of Integral Quadratic Constraints (IQCs) as in Megretski and Rantzer (1997). Such IQCs allow to represent several types of uncertainty, including time-varying parametric uncertainty, arbitrary fast or bounded rate uncertainty among others. They have been previously used for stability analysis of teleoperation systems in Polat and Scherer (2012). Thus, in view of future works, IQCs offer great flexibility in uncertainty descriptions.

In this chapter, the synthesis of controllers that guarantee both performance and stability for a bounded range of time-varying environment and operator dynamics is presented. To illustrate the design method, we consider environments in which the stiffness is the dominant phenomenon, e.g. in stiffness palpation tasks present in surgery. Therefore, we assume an environment in which the stiffness is modeled to be bounded and time-varying at an arbitrarily fast rate. The latter aspect models the possibility of sudden changes in the environment stiffness, whereas the mass and damping coefficients are fixed. For the operator dynamics, we use a model that is based on a low-frequency approximation in which the stiffness is again considered to be time-varying.

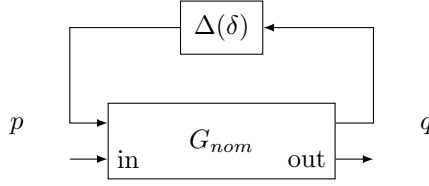


Figure 2.1: Linear Fractional Representation of a System.

In Section 2.2.1 the LFR model of the system is obtained and the general control design framework is presented. The LMI conditions for control design are presented in Section 2.2.2. The experimental setup is described in Appendix A. The synthesis, simulations and experimental results are shown in Sections 2.3.1, 2.3.2 and 2.3.3 respectively followed by the discussion of the results. Finally, in Section 2.4, the conclusions are given.

2.2 Model based robust control

2.2.1 LFR model of a teleoperation system

Deriving the Linear Fractional Representation of a system amounts to isolating the uncertain parameters such that an interconnection structure as depicted in Fig. 2.1 is obtained. Let $\delta_i = [\underline{\delta}_i, \bar{\delta}_i] \in \mathbb{R}_+, i = 1, \dots, n_p$ be families of bounded parametric uncertainties with possibly different lower and upper bounds. Let $\delta_i(t) \in \delta_i, i = 1, \dots, n_p$ be parametric uncertainties and define the vector δ as the

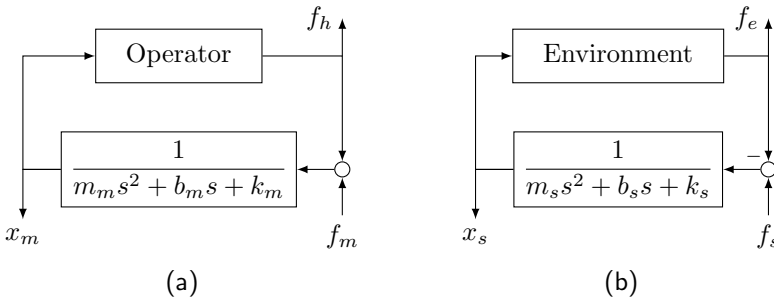


Figure 2.2: Diagram of (a) operator/master device and (b) environment/slave device.

vector of all n_p parametric uncertainties, that is, $\delta = \text{col}(\delta_1, \dots, \delta_{n_p}) \in \mathbb{R}^{n_p}$. $\Delta(\delta)$ is the block diagonal mapping that acts on δ , i.e. $\Delta(\delta) = \text{diag}(\delta_1, \dots, \delta_{n_p})$. q and p are the signals interfacing with the uncertainty block in the sense that $p = \Delta(\delta)q$. In particular, at any time instant t this means that $p(t) = \Delta(\delta(t))q(t)$ is an ordinary matrix multiplication. To derive the LFR model of the teleoperation system, the uncertainty parameters δ are defined and then isolated and collected into the uncertainty block $\Delta(\delta)$. To this end, we first define the models of the different components of a teleoperation system. We focus on the particular mass-damper-spring models for master and slave devices, which interact with the operator and environment respectively as depicted in Fig. 2.2, where $m_m > 0$, $b_m \geq 0$, $k_m \geq 0$ are the fixed parameters of the master device representing its mass, damping and stiffness coefficients respectively; similarly, $m_s > 0$, $b_s \geq 0$, $k_s \geq 0$ are the fixed parameters of the slave device representing its mass, damping and stiffness coefficients respectively; f_m , f_s are the actuation forces to the master and slave devices respectively; f_h , f_e represent the total force exerted by the operator and environment respectively; and x_m , x_s are the positions of the master and slave devices respectively. By definition they also represent the positions of the operator and environment respectively.

Environment model

We consider environments with mass-damper-spring dynamics:

$$f_e = f_e^* + (m_e \ddot{x}_s + b_e \dot{x}_s + k_e x_s), \quad (2.1)$$

which models a significant class of applications of interest. Here, $m_e \geq 0$, $b_e \geq 0$ and $k_e \geq 0$ are the mass, damping and stiffness coefficients of the environment respectively, and f_e^* is the active force from the environment, if present. We focus on the environment stiffness k_e as the main cause of the dynamic variation, hence m_e and b_e are assumed fixed and k_e is assumed to be bounded and in addition time-varying. That is $0 \leq \underline{k}_e \leq k_e(t) \leq \bar{k}_e$ for constants \underline{k}_e and \bar{k}_e . This choice is suitable for applications in which the effect of k_e on f_e is dominant, e.g. in stiffness discrimination tasks like those in surgery. For other environment types, Eq. (2.1), the uncertainty structure and parameters can be redefined. One should keep in mind that because of the intrinsic robust stability/performance trade-off, it is expected that the greater the uncertainty set, the lower the achievable performance. Finally, the coupled environment/slave-device system in Fig. 2.2b can be represented as in Fig. 2.3, where the uncertainty block in this model is given, then, by $\Delta_e = k_e$.

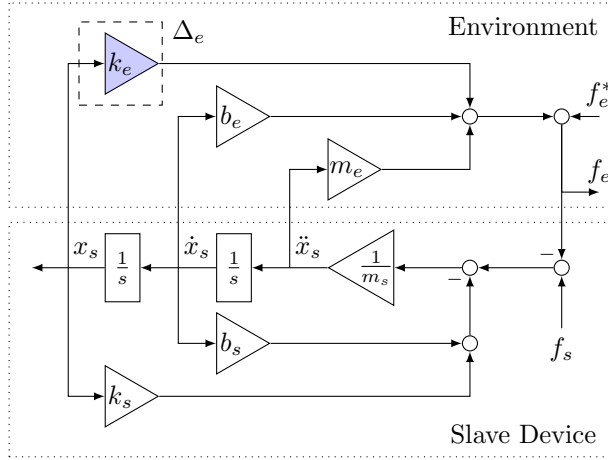


Figure 2.3: Block diagram representation of the environment/slave device pair.

Operator model

Next, in order to construct a realistic model for the operator, we identified experimentally the arm-hand dynamics of an operator while the operator manipulated the master-device of our experimental setup described in Appendix A, which has built-in force and position sensors. The operator dynamics are inherently time-varying and to obtain a time-varying model can be a difficult task. Instead, we simply identify several LTI models and then we combine them into a time-varying model. This works under the assumption that the operator can behave as an LTI system if he/she tries to remain static. We presented seven virtual springs to the operator with stiffness values $k_e^V \in [0, 5000]$ N/m such that $f_m = -k_e^V x_m + f_m^{ID}$, in which f_m^{ID} will be used as a disturbance signal for system identification. In particular, we used a system's sampling rate of 2000 Hz and a frequency range of $[1, 30]$ Hz for the multi-sine. The block diagram used for the experiment is shown in Fig. 2.4. Initially we set $f_m^{ID} = 0$ N and then the operator was asked to move the master device in order to feel the virtual spring. Subsequently, the operator was asked to stop in a position of his/her choice where he/she could still feel the virtual spring. The idea is that the operator exerts a force level such that he/she could feel that he/she has a correct haptic perception of the virtual environment. This is clearly subjective to the operator. Nevertheless, the aim of the experiment is that the operator changes intuitively his/her exerted force and grip for different virtual springs. Afterwards, a multi-sine signal was applied to the master device via f_m^{ID} while the operator tried to keep his/her hand-arm remain static. Forces $f_h(t)$ and positions $x_m(t)$ were measured and then the corresponding Fourier trans-

form $F_h^{\text{meas}}(j\omega) = \mathcal{F}(f_h(t))(j\omega)$ and $X_m^{\text{meas}}(j\omega) = \mathcal{F}(x_m(t))(j\omega)$ were computed. Next, we obtained the frequency response measurements of the static operator's arm-hand dynamics as

$$Z_h^{\text{meas}}(j\omega) = \frac{F_h^{\text{meas}}(j\omega)}{X_m^{\text{meas}}(j\omega)}$$

for each virtual spring. All the resulting Frequency Response Measurements (FRFs) are depicted in Fig. 2.5. Based on the shape of those frequency domain measurements, for the static arm-hand dynamics $Z_h(s)$ we selected the model structure given in (2.2), where m_h , b_h , k_h , are the mass, damping and stiffness of the human arm-hand, ω_{zh} , z_{ph} and ω_{ph} are the parameters of the filter $Q_h(s)$ in Eq. (2.3) which characterizes the operator dynamics above 10 Hz.

$$Z_h(s) = \frac{F_h(s)}{X_m(s)} = (m_h s^2 + b_h s + k_h)Q_h(s), \quad (2.2)$$

where

$$Q_h(s) = \frac{\frac{s}{\omega_{zh}} + 1}{\frac{s^2}{\omega_{ph}^2} + 2z_{ph}\frac{s}{\omega_{ph}} + 1} \quad (2.3)$$

Then, we optimized the variables m_h , b_h , k_h , ω_{zh} , z_{ph} and ω_{ph} to fit each measurement to the model minimizing the cost function $W_{Z_h}(i\omega) = \|Z_h(i\omega) - Z_h^{\text{meas}}(i\omega)\|_2$ for $\omega \in 2\pi[1, 30]$ rad/s. The optimization is done using a constrained nonlinear optimization method provided by the command `fmincon` in Matlab®. In practice the optimization problem has several local minima, thus initial conditions and interval constraints must be provided to the solver. Those initial conditions and their respective constraints are estimated based on the measurements and are adjusted until a satisfactory match between $Z_h(i\omega)$ and $Z_h^{\text{meas}}(i\omega)$ is obtained. The resulting parameters were found to be within the following ranges; $m_h \in [0.39, 0.67]$ kg, $b_h \in [7.50, 9.66]$ N s/m, $k_h \in [649.54, 903.82]$ N/m, $\omega_{zh} \in [62.85, 134.55]$ rad/s, $z_{ph} \in [0.38, 0.59]$ and $\omega_{ph} \in [80.03, 94.59]$ rad/s. To reduce complexity of the

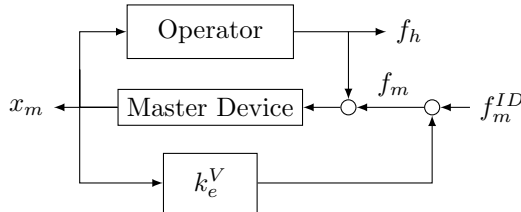


Figure 2.4: Diagram for arm-hand dynamics identification.

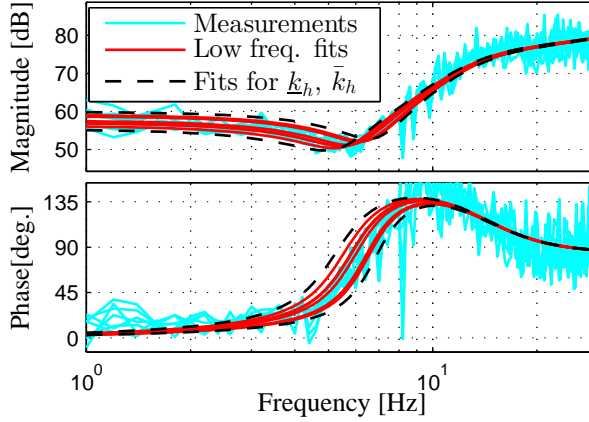


Figure 2.5: Arm-hand frequency response measurements and low-frequency approximations.

model, we have used a low-frequency approximation by allowing variation only on k_h and by fixing all other parameters to their centered values in the corresponding intervals, $m_h = 0.53$ kg, $b_h = 8.58$ N s/m, $\omega_{zh} = 98.7$ rad/s, $z_{ph} = 0.49$ and $\omega_{ph} = 87.31$ rad/s. The corresponding fits are depicted in solid red lines in Fig. 2.5. Finally, to include extra variation in k_h , we enlarge the range of values of k_h by 20%, and we use $k_h \in [584.55, 994.20]$ N/m. Thus the minimum and maximum human arm-hand stiffness we consider are $\underline{k}_h = 584.55$ N/m and $\bar{k}_h = 994.2$ N/m respectively. The resulting $Z_h(s)$ fits for \underline{k}_h and \bar{k}_h are depicted with dashed lines in Fig. 2.5. One can see that the approximation works well for low frequencies and, moreover, allows to reduce the number of uncertain parameters in the operator model. It also has the implications that the system's performance could decrease for users with dynamic properties that differ largely from those here considered. It is possible to extend the operator uncertainty structure at the cost of increasing the numerical complexity of the synthesis procedure.

As previously mentioned, the LTI identification techniques were used to find a structure on the operator's arm-hand dynamics. In what follows next, we assume that during operation k_h is time-varying within the identified range $k_h(t) \in [\underline{k}_h, \bar{k}_h]$ for all $t > 0$. Finally, combining the master device and operator models, we arrive at the model diagram for the operator/master device depicted in Fig. 2.6, where f_h^* is the active force generated by the operator and $\Delta_h = k_h$ defines the time-varying, bounded and uncertain parameter of the human arm-hand dynamics model. This modeling strategy allowed us to reduce the size of the uncertainty, which in turn reduces conservatism in the achievable performance during the control synthesis.

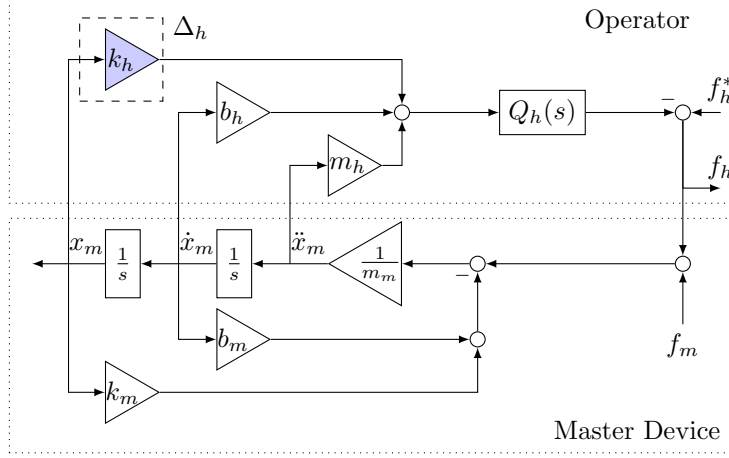


Figure 2.6: Block diagram representation of the operator/master device pair.

Generalized plant

Notice that both for the operator as well as for the environment we could add uncertainty models which are non parametric yet time-varying, so as to account for unmodeled dynamics, e.g. in the master/slave devices models. This will not change the application of the method except the utilized multiplier structure, but for simplicity, we restrict our analysis and synthesis to the parametric uncertainty case. Moreover, as shown by the experiments later, with the selected uncertainty description the teleoperated system presents satisfactory performance.

Having the models of the environment/slave-device and operator/master-device, we set up an LFR model of the teleoperation system as a generalized plant G as in Fig. 2.7.

The different components of the illustrated diagram are defined as follows:

- From the previous modeling, the vector of uncertain parameters is given by: $\delta_1 = k_h$, $\delta_2 = k_e$, thus $\delta = \text{col}(k_h, k_e)$. The uncertainty block is then defined as:

$$\Delta(\delta(t)) = \begin{bmatrix} k_h(t) & 0 \\ 0 & k_e(t) \end{bmatrix}, \quad \Delta \in \mathbf{\Delta},$$

where

$$\mathbf{\Delta} = \left\{ \begin{bmatrix} k_h & 0 \\ 0 & k_e \end{bmatrix} : k_h \in [\underline{k}_h, \bar{k}_h], k_e \in [\underline{k}_e, \bar{k}_e] \right\}$$

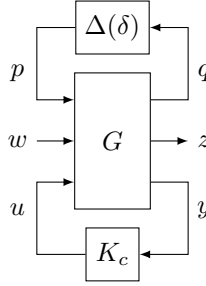


Figure 2.7: Generalized plant.

- The vector q and p contain the signals interfacing the uncertainty, thus from Fig. 2.3 and Fig. 2.6, we can infer that

$$q = \text{col}(x_m, x_s), p(t) = \Delta(\delta(t))q(t)$$

One can see that the model can be easily adapted to the cases in which other parameters might also be assumed to be uncertain.

- The measured signals are collected in the vector y . A control technique will be applied to an experimental academic setup that is equipped with force and position sensors in both the master and the slave devices. We will use all available sensors of the setup for two reasons: first, to show that our method can easily deal with a complex structure in the controller, and second, for not limiting the available information to improve the system's performance. Therefore, we have that

$$y = \text{col}(f_h, f_e, x_m, x_s) + y_n,$$

where

$$y_n = \text{col}(f_{hn}, f_{en}, x_{mn}, x_{sn}).$$

represents the noise in the measurements.

- The disturbance signals of the system are represented by the vector w . We treat the active forces from the operator and environment as disturbance signals. Including the noise channels y_n as disturbances explicitly increases the robustness properties that would help to obtain a controller more suitable for the actual implementation. Thus, we define

$$w = \text{col}(f_h^*, f_e^*, f_{hn}, f_{en}, x_{mn}, x_{sn}).$$

- Additionally, the actuation signal vector u contains the forces actuated from

the motors of the master and the slave devices. Thus,

$$u = \text{col}(f_m, f_s)$$

- The performance vector z is defined as

$$z = \text{col}(f_h - f_e, x_m - x_s, f_m, f_s)$$

Via the component, $f_h - f_e$, we enforce that the human operator should feel the same force applied by the environment. The second component, $x_m - x_s$, is the position error to obtain tracking between master and slave. The actuation variables are also included as channels to be penalized to avoid controllers with high gains.

- G is the model that contains all the fixed model dynamics of the different components of the bilateral teleoperation system: the master device, the slave device, the fixed operator dynamics and the fixed environment dynamics if present. One can obtain a numerical model of G from the model diagrams presented in Figures 2.3 and 2.6 by making a partition as follows:

$$\begin{pmatrix} q \\ z \\ y \end{pmatrix} = G \begin{pmatrix} p \\ w \\ u \end{pmatrix}$$

where G is assumed to be LTI.

- K_c is the to-be-designed controller that maps the measured signals y to the actuation signals u .

The control design problem is then to find a controller K_c that achieves robust stability and robust performance for all $\Delta \in \mathbf{\Delta}$. At this point we still need to define what structure the controller K_c will have and the type of performance that is required from the system. This will be the subject of the coming sections.

Augmented generalized plant model for control design

The model presented in Fig. 2.7 is not suitable in its actual form for control design. Therefore, we augment the model such that the model that will be used for control design is illustrated in Fig. 2.8. The different components of the augmented plant are described as follows:

- V and W are weighting filters described with stable LTI systems. They allow to shape in frequency domain the desired system performance. These filters

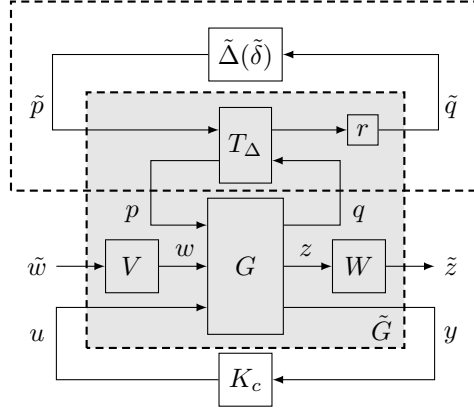


Figure 2.8: Generalized plant with weighting filters, uncertainty transformation and scaling. The dashed block in the upper part equals $\Delta(\delta)$ provided $r = 1$.

will be defined in detail in Section 2.2.3. Meanwhile they are assumed to be known.

- \tilde{w} and \tilde{z} are weighted copies of w and z via predefined filters V and W respectively. That is $w = V\tilde{w}$ and $\tilde{z} = Wz$.
- $\tilde{\delta}$ is the vector of the transformed uncertain parameters $\tilde{\delta}_i \in \tilde{\delta}_i, i = 1, \dots, n_p$ such that $\tilde{\delta}_i = [\underline{\tilde{\delta}}_i, \bar{\tilde{\delta}}_i] \in \mathbb{R}_+$ and $0 \in \tilde{\delta}_i$. Specifically, $\tilde{\delta} = \text{col}(\tilde{\delta}_1, \tilde{\delta}_2) = \text{col}(\tilde{k}_h, \tilde{k}_e)$, where \tilde{k}_h, \tilde{k}_e are the transformed parameters corresponding to k_h and k_e respectively. In particular, we will use the following specific transformation functions to the parameters: In order to apply this procedure to our design case, we modify the loop such that the scaling $r = 0$ corresponds to the nominal case. We apply a transformation to the uncertainty parameters such that $\delta_i \in [\underline{\delta}_i, \bar{\delta}_i]$ are mapped to the uncertain parameters $\tilde{\delta}_i \in [0, 1]$, $i = 1, \dots, n_p$. This is achieved via the following transformations:

$$\tilde{\delta}_i = \frac{\delta_i - \underline{\delta}_i}{\bar{\delta}_i - \underline{\delta}_i}, \quad i = 1, \dots, n_p \quad (2.4)$$

- $\tilde{\Delta}(\tilde{\delta})$ is the block diagonal concatenation of the parameters in $\tilde{\delta}$.

$$\tilde{\Delta}(\tilde{\delta}(t)) = \begin{bmatrix} \tilde{k}_h(t) & 0 \\ 0 & \tilde{k}_e(t) \end{bmatrix}, \quad \tilde{\Delta} \in \tilde{\Delta},$$

where

$$\tilde{\Delta} = \left\{ \begin{bmatrix} \tilde{k}_h & 0 \\ 0 & \tilde{k}_e \end{bmatrix} : \tilde{k}_h \in [\underline{\tilde{\delta}}_1, \bar{\tilde{\delta}}_1], \tilde{k}_e \in [\underline{\tilde{\delta}}_2, \bar{\tilde{\delta}}_2] \right\}$$

- The vector \tilde{q} and \tilde{p} contain the signals interfacing the new uncertainty block $\tilde{\Delta}$. Thus $\tilde{p}(t) = \tilde{\Delta}(\tilde{\delta}(t))\tilde{q}(t)$.
- $r \in [0, 1]$: is a scaling factor that allows to scale down the uncertainty block $\tilde{\Delta}$. This allows to perform an iterative process during the control design in which one starts with the nominal case $r = 0$, i.e. no uncertainty, and finalizes with an unscaled uncertainty set for $r = 1$. We will refer to a nominal plant if $r = 0$. If $r = 1$ we have that $\Delta(\delta)$ equals the dashed block in the upper part of Fig. 2.8.
- $T_{\Delta} : \mathbb{R}^{2n_p \times 2n_p}$ is a constant matrix such that :

$$\begin{pmatrix} \tilde{q} \\ p \end{pmatrix} = \begin{pmatrix} r & 0 \\ 0 & 1 \end{pmatrix} T_{\Delta} \begin{pmatrix} \tilde{p} \\ q \end{pmatrix}$$

T_{Δ} is used to map one to one the uncertain parameter set Δ to the transformed uncertain parameter set $\tilde{\Delta}$. The transformation T_{Δ} allows to obtain a nominal value of $\Delta(\delta^{\text{Nom}}) \in \Delta$ for $r = 0$. The transformations applied to the parameters in Eq. (2.4) can be achieved with the following transformation matrix

$$T_{\Delta} = \begin{pmatrix} 0 & \text{diag}(\bar{\delta}_1 - \underline{\delta}_1, \dots, \bar{\delta}_{n_p} - \underline{\delta}_{n_p}) \\ I & \text{diag}(\underline{\delta}_1, \dots, \underline{\delta}_{n_p}) \end{pmatrix}$$

One can construct a model of the generalized plant \tilde{G} by making the interconnection of blocks depicted in Fig. 2.8. The generality of the modeling procedure allows for adaptation to more complex linear dynamics of master and slave devices, other types of operator/environment models and other combinations of measured variables. Finally, we denote the state space representation of \tilde{G} by the following equation:

$$\begin{pmatrix} \dot{x} \\ \tilde{q} \\ \tilde{z} \\ y \end{pmatrix} = \begin{pmatrix} A & B_1 & B_2 & B \\ rC_1 & rD_{11} & rD_{12} & rE_1 \\ C_2 & D_{21} & D_{22} & E_2 \\ C & F_1 & F_2 & 0 \end{pmatrix} \begin{pmatrix} x \\ \tilde{p} \\ \tilde{w} \\ u \end{pmatrix}$$

2.2.2 Robust control design with guaranteed performance specifications

The common method for designing robust controllers is the use of *multipliers* to characterize the uncertainty and the performance specifications. It is also well-known that the overall robust control design is non-convex and, if exists, a convexifying procedure is not yet known. In the now-classic μ -synthesis framework

Skogestad and Postlethwaite (2005), it has been observed that an upper bound computation with an iterative algorithm is possible and tested extensively in practice to conclude its validity. It is remarked that the resulting non-convex conditions of the μ -synthesis framework can be shown to be bilinear in the unknowns and fixing a subset of unknowns renders the problem convex in the remaining ones. In this fashion the multipliers and the to-be-designed controller are alternately fixed and at each step the uncertainty size is enlarged incrementally. This iterative scheme has originated from the μ -synthesis problem and since it deals exclusively with a norm bounded uncertainty type, the multiplier is typically denoted by D hence the name D - K iteration. Along similar lines, μ -tools are extended to more general cases and classes of multipliers have been reported in the literature Megretski and Rantzer (1997), Polat (2011). In line with our experimental setup, we focus on a particular uncertainty class, namely, the class of arbitrarily fast time-varying real parametric uncertainties.

Uncertainty description

We will use a specific class of Integral Quadratic Constraints (IQCs) (see Megretski and Rantzer (1997)) to model uncertainties $\tilde{\Delta} \in \tilde{\mathbf{\Delta}}$. Then consider \mathbf{P} as a set of symmetric matrices $P \in \mathbb{R}^{2n_p \times 2n_p}$ that satisfy the following IQC

$$\int_0^{T_0} \begin{pmatrix} \tilde{\Delta}(\tilde{\delta})\tilde{q}(t) \\ \tilde{q}(t) \end{pmatrix}^T P \begin{pmatrix} \tilde{\Delta}(\tilde{\delta})\tilde{q}(t) \\ \tilde{q}(t) \end{pmatrix} dt \geq 0 \quad (2.5)$$

for all $q \in \mathcal{L}_2[0, T_0]$, $T_0 \in \mathbb{R}_+$ and $\tilde{\Delta} \in \tilde{\mathbf{\Delta}}$.

The matrix P is a so called *multiplier*. It allows to describe mathematical properties of the uncertainty block $\tilde{\Delta}$. The set \mathbf{P} needs to be further classified in order to describe specific type of uncertainties. Thus Eq. (2.5) as such cannot be used for control design because we need first to formalize the relation between $\tilde{\mathbf{\Delta}}$ and \mathbf{P} . If both q and T_0 are arbitrary, condition in Eq. (2.5) is equivalent to

$$\begin{pmatrix} \tilde{\Delta}(\tilde{\delta}) \\ I \end{pmatrix}^T P \begin{pmatrix} \tilde{\Delta}(\tilde{\delta}) \\ I \end{pmatrix} \succeq 0 \quad \forall \tilde{\Delta} \in \tilde{\mathbf{\Delta}} \quad (2.6)$$

Next, if the class $\tilde{\mathbf{\Delta}}$ is convex, it can be expressed as a convex combination of generators $\tilde{\delta}^i, i = 1, \dots, 2^{n_p}$. In our specific case we have only four generators: $\tilde{\delta}^1 = \text{col}(\tilde{\underline{\delta}}_1, \tilde{\underline{\delta}}_2)$, $\tilde{\delta}^2 = \text{col}(\tilde{\underline{\delta}}_1, \tilde{\underline{\delta}}_2)$, $\tilde{\delta}^3 = \text{col}(\tilde{\underline{\delta}}_1, \tilde{\underline{\delta}}_2)$ and $\tilde{\delta}^4 = \text{col}(\tilde{\underline{\delta}}_1, \tilde{\underline{\delta}}_2)$. One way to find a set \mathbf{P} of symmetric matrices P that describes $\tilde{\mathbf{\Delta}}$ and satisfies (2.6) is the following: because of the convexity property of $\tilde{\mathbf{\Delta}}$, it suffices to force concavity in the left hand side of (2.6) and evaluate (2.6) only at the corner points $\tilde{\delta}^j, j =$

$1, \dots, 2^{n_p}$ that generate $\tilde{\Delta}$. Therefore, the convex class $\tilde{\Delta}$ can be described by the next finite number of inequality conditions:

$$\begin{pmatrix} I \\ 0 \end{pmatrix}^T P \begin{pmatrix} I \\ 0 \end{pmatrix} \preceq 0 \quad (2.7)$$

$$\begin{pmatrix} \tilde{\Delta}(\tilde{\delta}^j) \\ I \end{pmatrix}^T P \begin{pmatrix} \tilde{\Delta}(\tilde{\delta}^j) \\ I \end{pmatrix} \succeq 0, \quad j = 1, \dots, 2^{n_p} \quad (2.8)$$

where condition in Eq. (2.7) ensures concavity of the left hand side of condition in Eq. (2.6). Therefore, the resulting P matrices classified by Eq. (2.7) and Eq. (2.8) imply that Eq. (2.6) holds.

In this case, P is then a constant full block multiplier describing bounded and time-varying real parametric uncertainties. This is an important distinction of the methods in this thesis with those in Vander Poorten (2007), in which a more wider class of uncertainty is taken into account, which might add conservatism in the achievable performance. Also notice that imposing structure and dynamics in the matrix P , other types of uncertainty can be described as shown in Polat and Scherer (2012), which can be exploited in future works.

Performance description

We have chosen the performance criterion based upon the \mathcal{L}_2 gain of the mapping from disturbance channels \tilde{w} to the performance channels \tilde{z} as is customary in model-based \mathcal{H}_∞ control, e.g., see Skogestad and Postlethwaite (2005). The \mathcal{L}_2 gain from \tilde{w} to \tilde{z} can be expressed as:

$$\sup_{0 \neq \tilde{w} \in \mathcal{L}_2} \frac{\|\tilde{z}\|_2}{\|\tilde{w}\|_2} < \gamma, \quad (2.9)$$

in which γ can be interpreted as a worst-case gain from the disturbances \tilde{w} to the performance signals \tilde{z} . Therefore, instantaneous responses that can be felt by the operator have a direct effect on the performance criterion. This makes the \mathcal{L}_2 gain a suitable performance criterion for teleoperation systems.

The \mathcal{L}_2 gain can be expressed as a quadratic performance criterion: (2.9) is equivalent to each of the following conditions:

$$\begin{aligned} \|\tilde{z}\|_2^2 &< \gamma^2 \|\tilde{w}\|_2^2 && \text{for all } 0 \neq \tilde{w} \in \mathcal{L}_2 \\ \int_0^\infty \begin{pmatrix} \tilde{w}(t) \\ \tilde{z}(t) \end{pmatrix}^T P_p \begin{pmatrix} \tilde{w}(t) \\ \tilde{z}(t) \end{pmatrix} dt &< 0 && \text{for all } 0 \neq \tilde{w} \in \mathcal{L}_2, \end{aligned} \quad (2.10)$$

with

$$P_p = \begin{pmatrix} -\gamma^2 I & 0 \\ 0 & I \end{pmatrix}$$

In fact, it is possible to use other quadratic performance criteria, see, e.g., Section 1.3 and Scherer and Weiland (2000). To keep the generality of the theory used here, we will use the symbol P_p to describe our performance criterion.

We proceed with the LMI-based robust controller design such that the closed loop is robustly stable and satisfies the performance specifications.

Robust Control Synthesis

We make use of an LTI controller $K_c(s) = C_c(Is - A_c)^{-1}B_c + D_c$, which we will identify with its state space description:

$$\begin{aligned} \dot{x}_c &= A_c x + B_c y \\ u &= C_c x + D_c y \end{aligned}.$$

by writing

$$K_c(s) = \left[\begin{array}{c|c} A_c & B_c \\ \hline C_c & D_c \end{array} \right].$$

We also introduce the shorthand notation for the closed loop matrices

$$\begin{aligned} \tilde{G}(s) \star K_c(s) &= \left[\begin{array}{c|cc} \mathcal{A} & \mathcal{B}_1 & \mathcal{B}_2 \\ \hline \mathcal{C}_1 & \mathcal{D}_{11} & \mathcal{D}_{12} \\ \mathcal{C}_2 & \mathcal{D}_{21} & \mathcal{D}_{22} \end{array} \right] \\ &= \left[\begin{array}{cc|cc} A + BD_c C & BC_c & B_1 + BD_c F_1 & B_2 + BD_c F_2 \\ B_c C & A_c & B_c F_1 & B_c F_2 \\ \hline r(C_1 + E_1 D_c) & rE_1 C_c & r(D_{11} + E_1 D_c F_1) & r(D_{12} + E_1 D_c F_2) \\ C_2 + E_2 D_c & E_2 C_c & D_{21} + E_2 D_c F_1 & D_{22} + E_2 D_c F_2 \end{array} \right] \end{aligned}$$

obtained via closing the loop in Fig. 2.8 with the controller $K_c(s)$.

We will utilize the following controller-multiplier iteration method: Let \mathbf{P} be the set of symmetric matrices P that satisfy conditions (2.7) and (2.8) and assume we have a controller $K_c(s)$ that achieves nominal stability;

Theorem 2.1. *The closed loop system $\tilde{G}(s) \star K_c(s)$ with $r \in (0, 1]$ shown in Fig. 2.8 is robustly stable for all $\tilde{\Delta} \in r\tilde{\Delta}$ with a guaranteed performance characterized by P_p if there exist a symmetric matrix \mathcal{X} and $P \in \mathbf{P}$ such that*

$$\mathcal{X} \succ 0 \tag{2.11}$$

and

$$\begin{pmatrix} \star \end{pmatrix}^T \left(\begin{array}{cc|cc} 0 & \mathcal{X} & 0 & 0 \\ \mathcal{X} & 0 & 0 & 0 \\ \hline 0 & 0 & P & 0 \\ 0 & 0 & 0 & P_p \end{array} \right) \begin{pmatrix} I & 0 & 0 \\ \mathcal{A} & \mathcal{B}_1 & \mathcal{B}_2 \\ \hline 0 & I & 0 \\ \mathcal{C}_1 & \mathcal{D}_1 & \mathcal{D}_{12} \\ \hline 0 & 0 & I \\ \mathcal{C}_2 & \mathcal{D}_{21} & \mathcal{D}_2 \end{pmatrix} \prec 0 \quad (2.12)$$

holds.

For notational convenience we also introduce the partitions

$$P = \begin{pmatrix} Q & S \\ S^T & R \end{pmatrix}, \quad P_p = \begin{pmatrix} Q_p & S_p \\ S_p^T & R_p \end{pmatrix}.$$

where $Q, R, S \in \mathbb{R}^{n_p \times n_p}$, $Q_p \in \mathbb{R}^{\dim(w) \times \dim(w)}$, $S_p \in \mathbb{R}^{\dim(w) \times \dim(z)}$ and $R_p \in \mathbb{R}^{\dim(z) \times \dim(z)}$.

Remark 2.2. Theorem 2.1 allows to do analysis of robust performance of the system given a controller $K_c(s)$. Then all the involved conditions are LMIs. However, in the case of controller synthesis, there is an issue. In (2.12), the outer factors involving the state-space matrices of $K_c(s)$ multiply the blocks of the multiplier involving unknown variables rendering the constraint a Bilinear Matrix inequality (BMI). Nevertheless, by means of the transformations that have been given in Scherer and Weiland (2000); Masubuchi et al. (1998); Scherer et al. (1997), it is possible to make (2.12) an LMI when P is fixed. Moreover, A_c, B_c, C_c, D_c matrices also multiply each other, hence a linearization is needed. Fortunately, this can be avoided with a Schur complement argument.

Initially, we have neither a controller nor a multiplier by which the constraints are satisfied. Hence one typically starts with the nominal system $\tilde{G}_{nom} = \mathbf{0}_{pq} \star \tilde{G}$ (which is an upper LFT and equivalent to removing the uncertainty channels). Then it is well-known how to design a nominally stabilizing controller (i.e. $r = 0$) with certain performance level. This makes it possible to search for a feasible multiplier via Theorem 2.1. Obviously, we can not expect a robust stability certificate from the initial controller K_{nom} since there is no constraint enforcing it. Thus, we need to first scale down uncertainty size to the level that K_{nom} robustly stabilizes the system. This scaling (often simply a gain) can be subsumed into the uncertainty channels of the closed loop plant. Then by a line search over the feasible uncertainty size denoted by $r \in (0, 1]$, we obtain feasible stability multipliers. Then, we switch to the controller step of the iteration.

As we pointed out in Remark 2.2, there exists a transformation such that the conditions in Theorem 2.1 are converted into LMIs, such transformation is briefly replicated here for completeness. The main difficulty with the bilinear terms in

(2.12) is resolved by changing the search over the variables from $\mathcal{X}, A_c, B_c, C_c, D_c$ to another derived set of variables $v = \{X, Y, K, L, M, N\}$ where X is the left upper block of \mathcal{X} , Y is the left upper block of \mathcal{X}^{-1} and

$$\begin{pmatrix} K & L \\ M & N \end{pmatrix} = \begin{pmatrix} U & XB \\ 0 & I \end{pmatrix} \begin{pmatrix} A_c & B_c \\ C_c & D_c \end{pmatrix} \begin{pmatrix} V^T & 0 \\ CY & I \end{pmatrix} + \begin{pmatrix} XAY & 0 \\ 0 & 0 \end{pmatrix} \quad (2.13)$$

which results from a congruence transformation which is omitted here but detailed in Scherer and Weiland (2000). Hence the closed loop state-space matrices become

$$\begin{pmatrix} \mathbf{A}(v) & \mathbf{B}_j(v) \\ \mathbf{C}_i(r, v) & \mathbf{D}_{ij}(r, v) \end{pmatrix} = \left(\begin{array}{cc|c} AY + BM & A + BNC & B_j + BNF_j \\ K & AX + LC & XB_j + LF_j \\ \hline r_i(C_iY + E_iM) & r_i(C_i + E_iNC) & r_i(D_{ij} + E_iNF_j) \end{array} \right) \quad (2.14)$$

for $i, j = 1, 2$ with $r_1 = r$ and $r_2 = 1$. Finally, the positivity constraint on $\mathcal{X} \succ 0$ becomes

$$\mathbf{X}(v) = \begin{pmatrix} Y & I \\ I & X \end{pmatrix} \succ 0 \quad (2.15)$$

In summary, following result gives the conditions for a stabilizing controller with guaranteed performance levels. Note that it boils down to verifying (2.12) in a different set of variables. For convenience we will omit the v and r dependence from the boldface variables.

Theorem 2.3. *There exists a controller $K_c(s)$ and a Lyapunov certificate \mathcal{X} such that the closed loop is robustly stable against all $\tilde{\Delta} \in r\tilde{\Delta}$ with $r \in (0, 1]$ with P_p performance if and only if there exist variables v such that $\mathbf{X} \succ 0$ and*

$$\begin{pmatrix} \star \end{pmatrix}^T \left(\begin{array}{ccc|ccc} 0 & 0 & 0 & I & 0 & 0 \\ 0 & Q & 0 & 0 & S & 0 \\ 0 & 0 & Q_p & 0 & 0 & S_p \\ \hline I & 0 & 0 & 0 & 0 & 0 \\ 0 & S^T & 0 & 0 & R & 0 \\ 0 & 0 & S_p^T & 0 & 0 & R_p \end{array} \right) \begin{pmatrix} I & 0 & 0 \\ 0 & I & 0 \\ 0 & 0 & I \\ \hline \mathbf{A} & \mathbf{B}_1 & \mathbf{B}_2 \\ \mathbf{C}_1 & \mathbf{D}_1 & \mathbf{D}_{12} \\ \mathbf{C}_2 & \mathbf{D}_{21} & \mathbf{D}_2 \end{pmatrix} \prec 0 \quad (2.16)$$

hold.

At this point, (2.16) is not still an LMI since boldface variables enter quadratically, however it suffices to apply the Linearization Lemma described in Scherer and Weiland (2000) to render it as an LMI; having zero in the parameter intervals

implies $R, R_p \succeq 0$ and hence we can find a factorization T_l such that

$$\begin{pmatrix} Q_l + S_l B_l(v) + B_l(v)^T S_l^T & B_l(v)^T T_l \\ T_l^T B_l(v) & -U_l \end{pmatrix} \prec 0 \quad (2.17)$$

where

$$\begin{aligned} B_l(v) &= \begin{pmatrix} \mathbf{A}(v) & \mathbf{B}_1(v) & \mathbf{B}_2(v) \\ \mathbf{C}_1(v) & \mathbf{D}_1(v) & \mathbf{D}_{12}(v) \\ \mathbf{C}_2(v) & \mathbf{D}_{21}(v) & \mathbf{D}_2(v) \end{pmatrix} \\ Q_l &= \text{diag}(0, Q, Q_p) \\ S_l &= \text{diag}(I, S, S_p) \\ U_l &= \text{diag}(I, R^{-1}, R_p^{-1}) \\ T_l &= \text{diag}(0, I, I) \end{aligned}$$

Constraint (2.17) is now affine in the variables v . After solving for v , the controller parameters can be recovered by solving (2.13) for the original variables

$$\begin{aligned} &\begin{pmatrix} A_c & B_c \\ C_c & D_c \end{pmatrix} \\ &= \begin{pmatrix} U & XB \\ 0 & I \end{pmatrix}^{-1} \begin{pmatrix} K - XAY & L \\ M & N \end{pmatrix} \begin{pmatrix} V^T & 0 \\ CY & I \end{pmatrix}^{-1} \end{aligned}$$

where U and V are arbitrary invertible matrices satisfying $I - XY = UV^T$. In our case we have selected $U = X$ and $V = X^{-1} - Y$. Clearly we assume the existence of a nominal controller that provides an initial condition for the first iteration that will not lead to a local minimum very close to $r = 0$, which in practice is actually the case. To summarize, we start with the design of a nominal controller designed for $r = 0$. Then, we iterate the following two steps:

- for a fixed controller $K_c(s)$, maximize r using the bisection algorithm and get the multiplier P , while optimizing for the P_p .
- for a fixed P matrix, maximize r using the bisection algorithm and get the controller $K_c(s)$ while optimizing for the P_p .

The procedure is stopped when either, no further progress on increasing $r < 1$, or when r approaches 1 with the desired accuracy. Details on the iterative procedure are given in Appendix B, from which we have used the version I of the iterative procedure.

In the next section we describe how to translate the performance specifications via weighting filters W and V .

2.2.3 Weighting filter design

In robust control design it is customary to implement frequency dependent weights on the performance channels (Fig. 2.7). The filters V and W are block diagonal transfer matrices emphasizing the frequency band in which we want the particular channel to be penalized. Thus $V = \text{diag}(V_{f_h^*}, V_{f_e^*}, V_{f_{hm}}, V_{f_{en}}, V_{x_{mn}}, V_{x_{sn}})$ and $W = \text{diag}(W_{f_h-f_e}, W_{x_m-x_s}, W_{f_m}, W_{f_s})$. Ideally, one wants to have $f_h - f_e = 0$ and $x_m - x_s = 0$. In this case we would get perfect transparency, but as is known, this type of design is unrealistic and has poor stability properties. Instead, it is desirable to relax such a strict requirement by appropriate choices of V and W .

Instead we are interested in forcing the force and position tracking errors such that in frequency domain $|F_h(\omega) - F_e(\omega)| < \gamma |F_w(\omega)|$ and $|X_m(\omega) - X_s(\omega)| < \gamma |X_w(\omega)|$, where $F_h(\omega), F_e(\omega), X_m(\omega), X_s(\omega)$ are the Fourier transform of f_h, f_e, x_m, x_s respectively, $F_w(\omega)$ and $X_w(\omega)$ represent the desired level of force and position tracking in the frequency band of interest and $\gamma > 0$ is as small as possible. We assume $|F_w(\omega)| > 0$ and $|X_w(\omega)| > 0$ sufficiently small at low frequencies to achieve force and position tracking for sufficiently slow varying forces and positions. This will lead to a desired level of performance in the frequency range in which the human operator performs movements. On the other hand, we need to have feasible control action with magnitude bounded forces f_m, f_s and a reduced amplification of disturbance w to z at high frequencies. This to avoid saturation and the excitation of high frequency dynamics. These requirements are translated into the filters W and V which are shaped accordingly. To illustrate how to achieve this, consider the design of a controller K_c for the nominal plant. Suppose that, for given V, W this leads to:

$$\sup_{\tilde{w}} \frac{\|W(s)(G(s) \star K_c(s))V(s)\tilde{w}\|_2}{\|\tilde{w}\|_2} < \gamma.$$

for some, preferably small, value of $\gamma > 0$. In the LTI case then we have that

$$\|W(s)(G(s) \star K_c(s))V(s)\|_\infty < \gamma,$$

where $\|\cdot\|_\infty$ denotes the \mathcal{H}_∞ norm. In particular, this implies that the (m, n) th entry of $W(s)(G(s) \star K(s))V(s)$ satisfies

$$|W_n(i\omega)(G(i\omega) \star K(i\omega))_{mn}V_m(i\omega)| < \gamma,$$

for which non-zero W, V implies that

$$|(G(i\omega) \star K(i\omega))_{mn}| < \frac{\gamma}{|W_n(i\omega)V_m(i\omega)|}.$$

Hence, with $\gamma > 0$ fixed, frequencies at which V and W have higher magnitude, will result in frequencies at which $G(s) \star K_c(s)$ has smaller magnitude and therefore

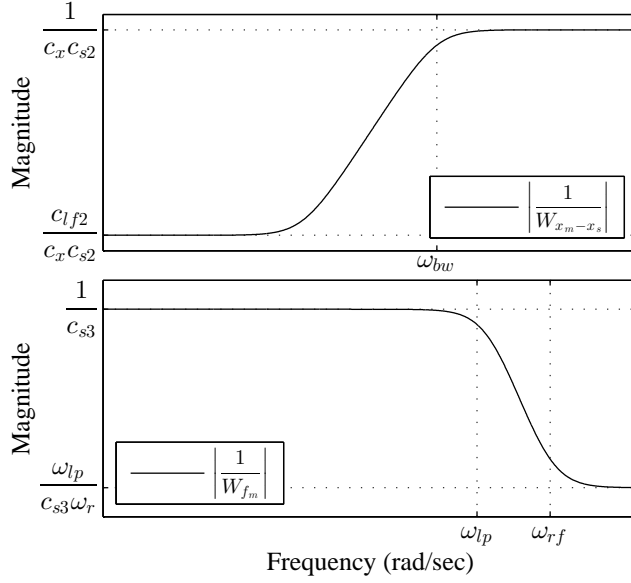


Figure 2.9: Magnitude bode plot of $1/W_{x_m-x_s}$ and $1/W_{f_m}$.

less amplification from w to z . This property can actually be employed to define the filters V and W per frequency of interest.

We translate the performance specifications by defining the following filters:

$$W_{f_h-f_e}(s) = \left(\frac{\frac{s}{\omega_{bw}} + 1}{c_{s1} \frac{\omega_{bw}}{s} + c_{lf1}} \right)^2$$

$$W_{x_m-x_s}(s) = c_{xs} c_{s2} \frac{\frac{s}{\omega_{bw}} + 1}{\frac{\omega_{bw}}{s} + c_{lf2}}$$

$$W_{f_m}(s) = W_{f_s}(s) = c_{s3} \frac{\frac{s}{\omega_{lp}} + 1}{\frac{\omega_{lp}}{s} + 1}$$

$$V_{f_h^*} = V_{f_e^*} = c_{s4}$$

$$V_{f_{hn}} = V_{f_{en}} = c_{s5}$$

$$V_{x_{mn}} = V_{x_{sn}} = \frac{c_{s6}}{c_{xs}}$$

Typical shapes of the magnitude-bode plots $|1/W_{x_m-x_s}(i\omega)|$ (which has a similar shape as $|1/W_{f_h-f_e}(i\omega)|$) and $|1/W_{f_m}(i\omega)|$ (which has the same shape as $|1/W_{f_s}(i\omega)|$) are shown in Fig. 2.9.

ω_{bw} defines the desired closed-loop bandwidth, ω_{lp} defines the desired bandwidth of the actuation force signals. With the values c_{lf1} , c_{lf2} we put a limit to $W_{f_h-f_e}$ and $W_{x_m-x_s}$ at low frequencies. This also ensures the filters $W_{f_h-f_e}$ and $W_{x_m-x_s}$ to be stable. Stability of all filters is necessary to ensure that a stabilizing controller K_c exists for the guaranteed plant. A second order filter was selected for $W_{f_h-f_e}$ to increase the tracking performance obtained in practice. On the other hand for $W_{x_m-x_s}$ a first order filter was sufficient. To avoid non-causal W_{f_m} and W_{f_s} , we inserted high frequency poles at ω_r . Moreover, c_{xs} is used to scale penalties on positions with respect to penalties on forces. This makes the magnitude of positions and forces numerically comparable. To keep the tuning more intuitively, c_{xs} is tuned independently and it is not integrated into the scaling c_{s2} in $W_{x_m-x_s}$. Finally, c_{s1}, \dots, c_{s6} are scaling constants that are used for further tuning.

The structure of the weighting filters was designed to achieve position and force tracking. However, other choices may be explored. For instance, one can add an intermediate impedance between the positions and forces of environment and operator to mimic a “mechanical tool” as described in Vander Poorten (2007) in which again perfect transparency is avoided. This can be achieved by adapting V and W .

2.3 Robust control applied to a 1-DoF academic setup

The potential of the synthesis method described above is demonstrated by applying it to the experimental setup described in Appendix A. We demonstrate the robust performance properties of the Robust Controller (hereafter referred to as RC) by means of simulations and experiments under operating conditions of permanent contact with springs and sudden changes of environment stiffness.

Using frequency response measurements, the parameters of second order models for the devices of the 1-DoF setup are identified. The parameters are listed in Table 2.1. In the same table we show the parameters of the operator and the environment dynamics that are computed at the end-effector. We have selected $k_e \in [80, 3000]$ N/m because we aim to guarantee performance and stability for environment stiffness values in the range of soft tissue environments.

2.3.1 Synthesis results

The numerical parameters of the weighting filters are selected as follows. We have selected $\omega_{bw} = 2\pi \times 10$ rad/s as the desired closed loop bandwidth. The actuation forces f_m, f_s were penalized from 60 Hz and beyond, hence $\omega_{lp} = 2\pi \times 60$ rad/s. c_{lf1} and c_{lf2} are selected to be small shifts to the poles at the origin to render the corresponding filters stable, i.e., $c_{lf1} = c_{lf2} = 10^{-2}$ and $\omega_r = 2\pi \times 500$ rad/s. We assume that the bandwidth of the actuators and sensors is higher than ω_{lp} , so that stability is not compromised. In fact this assumption is validated by the experiments. Next, the scaling c_{xs} corresponds to the scaling between the forces in the disturbance channels and the positions in the performance channels. Now, to estimate the order of such scaling, assume that we indeed achieve perfect force and position tracking, therefore we can assume that the scaling between f_h and positions is equivalent to the environment stiffness. Because the force due to the arm-hand dynamics opposes to the force f_h^* (Fig. 2.6), c_{xs} is expected to be bigger than the environment stiffness. Therefore the \bar{k}_e can be used as a lower bound for $c_{xs} > 3000(0.075)^2 = 16.9$. Note that the end-effector length is included since the internal parameters are computed at the rotational axis. We have further tuned experimentally by increasing it until satisfactory results were obtained, which led us to the value $c_{xs} = 31.6$.

The scaling parameters c_{s1}, \dots, c_{s6} are tuned iteratively with the design process. We start with all values at 1, i.e. no scaling. The synthesis process is run and if no controller is found or the results are not satisfactory, e.g. factor r is too small, we relax the penalization on the actuation variables by decreasing c_{s3} . In case we still do not make progress, then we start relaxing the penalization on one (or more) performance variable(s) by decreasing the respective scaling parameter(s), depending on where we want to sacrifice performance, for instance by decreasing c_{s6} we allow for more position-sensor noise amplification. We iterate on the previous steps to obtain finally the values $c_{s1} = 0.56$, $c_{s2} = 0.5$, $c_{s3} = 0.4$, $c_{s4} = 1$, $c_{s5} = 0.5$ and $c_{s6} = 0.25$. We have included low-pass filters with a bandwidth of

Table 2.1: Numerical parameters

$m'_m = 1.36 \times 10^{-3}$	$m'_s = 1.29 \times 10^{-3}$	kg m ² /rad
$b'_m = 1.01 \times 10^{-1}$	$b'_s = 6.02 \times 10^{-2}$	N m s/rad
$k'_m = 1.75$	$k'_s = 0.46$	N m/rad
$m_h = 0.53$	$m_e = 0$	kg
$b_h = 8.58$	$b_e = 0$	N s/m
$k_h \in [584.6, 994.2]$	$k_e \in [80, 3000]$	N/m
$\omega_{ph} = 87.31$	$\omega_{zh} = 98.7$	rad/s
$z_{ph} = 0.49$		—

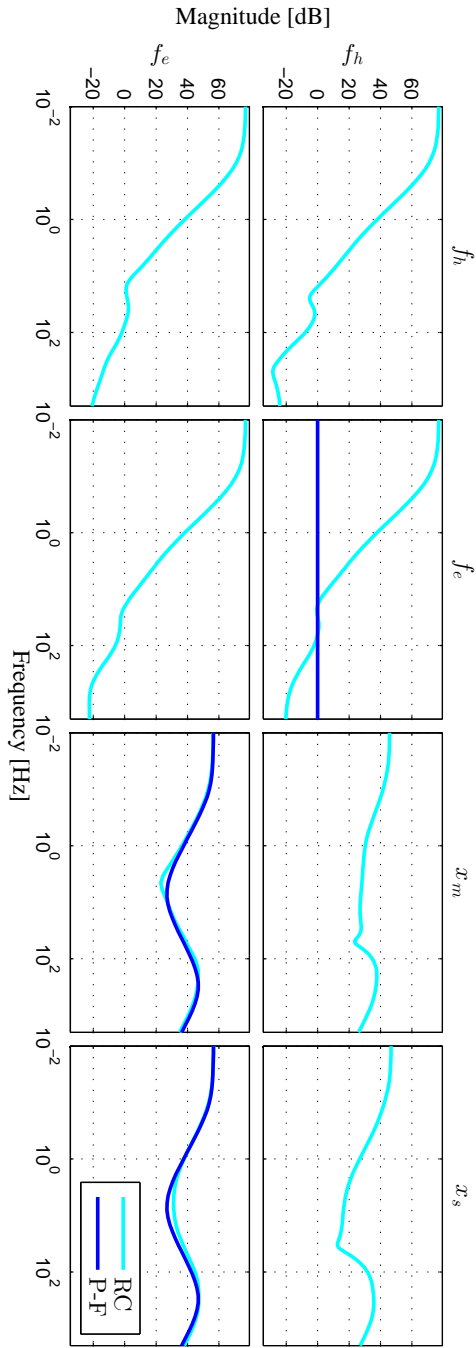


Figure 2.10: Magnitude Bode diagrams of Robust Controller and Position-Force Architecture Controller.

200 Hz to the output signals y which are implemented in the experimental setup.

We limit our focus to the case when the operator is grasping the device, however, this leaves out the case when the user releases the master device, for which only stability is relevant. Roughly speaking, when the operator releases the device, the total mass of the system decreases, increasing the open-loop gain and possibly compromising stability. Instead of increasing the number of uncertain parameters to cover the release case in a conservative fashion, we utilize an alternative pragmatic approach. It consists in making the design using a reduced but fixed value of $m_h = \alpha m_h^N$ for $1 > \alpha \geq 0$ such that the system is stable in free air. Under the previous assumptions, the synthesis algorithm was performed. The LMI's for controller synthesis were solved using the solver SeDuMi Sturm (1999). We started from $\alpha = 0$ and we increased it by steps of 0.1. For each tested α , the desired scaling value $r = 1$ was achieved using the algorithm described in Appendix B.2. We stopped increasing α when stability of the system in free air was not satisfied, which was verified analytically and also experimentally. In this fashion, we took the penultimate tested α . Therefore we finally used $m_h = 0.4m_h^N$. The gamma values and scalings obtained at each controller/multiplier iterations for the final design are shown in Table 2.2. As a remark, the order of the controller is the order of the generalized plant G , which already includes the weighting filters. In our case, the controller is of order 15, the respective magnitude Bode diagram of the RC is shown in Fig 2.10.

In Table 2.2, one can see that during the synthesis process, a minimal \mathcal{L}_2 -gain performance $\gamma = 4.86$ is achieved for the desired ranges of environment and operator parameters. That is, feasibility of the synthesis LMIs for $(\alpha, r, \gamma) = (0.4, 1, 4.851)$. This design was made for $\alpha = 0.4$, however the performance can be different for the more realistic mass value $\alpha = 1$. To illustrate the performance decrease, we also analyze the performance using the obtained generalized plant (including the weighting filters) in closed loop with the designed controller. Such analysis can be done by minimizing γ while solving the LMI's of Theorem 2.1. We did two

Table 2.2: γ and r during iterations of the final design

Iter.	r	γ	K_c/P
1	0	2.391	K_c
2	0.141	3.443	P
3	0.382	3.966	K_c
4	0.556	3.808	P
5	0.792	4.386	K_c
6	0.883	4.211	P
7	1.0000	4.851	K_c

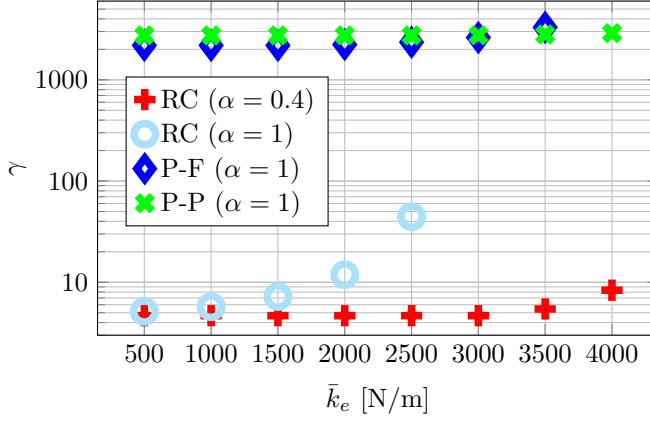


Figure 2.11: Weighted \mathcal{L}_2 -gain performance analysis with different controllers for increasing maximum environment stiffness \bar{k}_e

performance analysis of the obtained RC, one for $\alpha = 0.4$ used during synthesis, and another for $\alpha = 1$. The resulting γ values as a function of \bar{k}_e are given in Fig. 2.11.

When $\alpha = 0.4$, one can see that we obtain $\gamma \approx 5$ for $\bar{k}_e \leq 3000$ N/m as already expected from Table 2.2. On the other hand, when the analysis is done for $\alpha = 1$, which better describes the real system behavior during normal operation, γ increases for increasing values of \bar{k}_e , i.e. there is a bigger influence of the disturbance signals on the performance channels hence a degradation of the overall performance. Notice that unfortunately, there is no one to one correspondence between the γ values and the resulting performance. This is because γ is the worst-case L_2 gain from the weighted inputs to the weighted outputs. Therefore γ is a relative and not absolute measurement.

For $\alpha = 1$ and $0 < \bar{k}_e > 2500$ N/m no feasible γ was found. Since our test is only sufficient, and it accounts for arbitrarily fast time-varying uncertainty, infeasibility for all values of γ in this analysis results means that there might exist a series of driving signals and time-varying change in environment that can destabilize the system. However, we were not able to destabilize the system when tested with environment stiffness values up to $\bar{k}_e \approx 3000$ N/m, as shown in the simulations and experimental results.

Finally, we performed a similar performance analysis with $\alpha = 1$ to other well-known architectures for bilateral teleoperation: “position-position” (P-P) architecture, “position-force” (P-F) architecture and “transparent four-channel” (T4C)

architecture. The control laws are given by; for the “position-position” controller,

$$\begin{aligned} f_m &= g_{md}C_{pt}(s, \omega_{olc})(x_s - x_m) \\ f_s &= g_{sd}C_{pt}(s, \omega_{olc})(x_m - x_s) \end{aligned}$$

for the “position-force” controller,

$$\begin{aligned} f_m &= -L(s, \omega_{lpc})f_e \\ f_s &= g_{sd}C_{pt}(s, \omega_{olc})(x_m - x_s) \end{aligned}$$

and for the “transparent four-channel” controller,

$$\begin{aligned} f_m &= g_{md}C_{pt}(s, \omega_{olc})(x_s - x_m) - L(s, \omega_{lpc})f_e \\ f_s &= g_{sd}C_{pt}(s, \omega_{olc})(x_m - x_s) + L(s, \omega_{lpc})f_h \end{aligned}$$

where

$$C_{pt}(s, \omega_{olc}) = \left(\frac{\frac{s}{\omega_{olc}/6} + 1}{\frac{s}{\omega_{olc}/6} + c_{lfc}} \right) \left(\frac{s}{\omega_{olc}/3} + 1 \right) L(s, \omega_{lpc})$$

is a standard position tracking controller based on a weak integrator (i.e. with limited gain for low frequencies) and a lead filter, $L(s, \omega_{lpc})$ is a second order low pass filter at ω_{lpc} , g_{md} and g_{sd} are gains to guarantee a 0dB open loop-gain at the desired bandwidth ω_{olc} on the master and slave devices respectively. To make in some extent a fair design of the classical controllers with respect to the RC, the parameters were manually tuned such that the controller frequency response approximates that of the controller elements from x_m and x_s to f_s of the RC. This is illustrated in Fig 2.10 where the magnitude bode diagram of the P-F controller is compared to that of the RC. Therefore we used $c_{lfc} = 2.2 \times 10^{-2}$, $\omega_{lpc} = 2\pi \times 300$ rad/s, $g_{md} = 15.84$, $g_{sd} = 14.72$ and $\omega_{olc} = 2\pi \times 30$ rad/s

The performance analysis results by minimizing γ using Theorem 2.1 and the generalized plant with the classical controller architectures are shown in Fig. 2.11. During the analysis no γ values were found for the “transparent four-channel” architecture, which was expected because of its poor stability properties (See Lawrence (1993b)). Moreover, for $\bar{k}_e < 2500$ N/m the RC has higher performance than the other conventional architectures in the sense that γ is smaller. Similarly, for $\bar{k}_e < 3000$ N/m, the “position-force” controller presents a better performance than the “position-position”. However, in our analysis, no γ value was found for the “position-force” controller for $\bar{k}_e > 3500$ N/m. This is in accordance with the known fact (see, e.g., Aliaga et al. (2004)) that the “position-force” controller has poorer stability properties than the “position-position” controller. Especially, it is

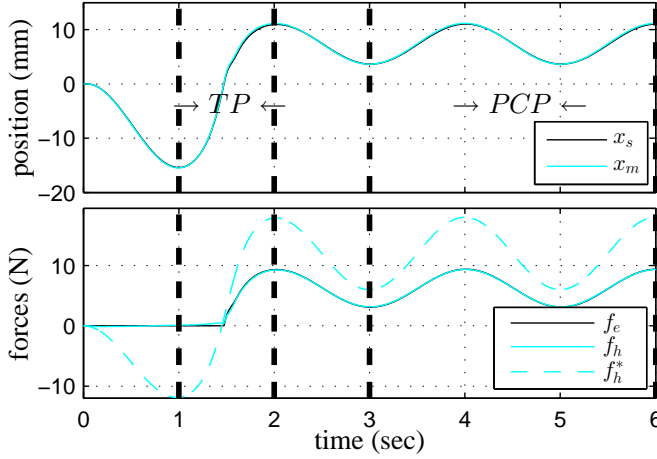


Figure 2.12: Operating conditions for testing the RC: Transient Part (TP) and Permanent Contact Part (PCP)

known that the “position-force” architecture presents stability issues for stiff environments. From the analysis results, we can see that with the RC the performance has been increased at the price of reducing the maximal environment stiffness for which stability is guaranteed.

2.3.2 Simulation results

The RC was discretized using a Tustin approximation with a sample rate of 2000Hz which is also the case for the experiments. In order to test the controller, we simulate a scenario in which an operator manipulates the system with the slave device in free-air and then gets in contact with a spring located at $x_s > 0$. As an example of such situation consider Fig. 2.12, where we used $f_h^* = 9(1 + \tanh((t - 1.5)/0.2)) + 6(\cos(\pi t) - 1)$ N and $k_h = 776.7$ N/m for the operator. The Transient Part (TP) corresponds to a time slot where there is a transition between free air and contact with the spring. The Permanent Contact Part (PCP) is a time slot after the TP has passed and periodic movements are performed while being in permanent contact with the spring.

We performed simulations of the RC for three different springs $k_e = 850$ N/m, $k_e = 2300$ N/m and $k_e = 3500$ N/m. The first two springs are within the range in which robust stability is guaranteed according to Fig. 2.11. The third spring is used to evaluate the system’s behavior outside such range. The time domain

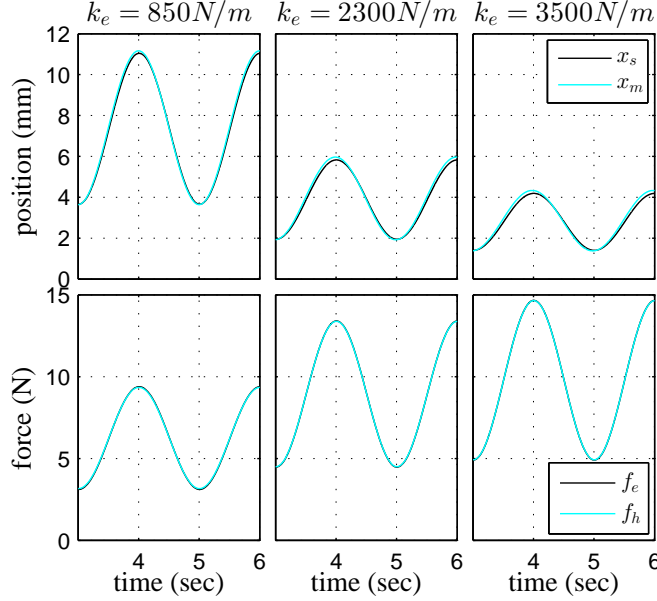


Figure 2.13: Time domain responses from simulations of interaction with different springs during the PCP.

signals of positions and forces for the PCP are presented in Fig. 2.13.

One can see that for all spring values, position and force tracking is achieved. The position tracking is slightly degraded for increasing values of environment stiffness. Such tendency of performance degradation was already observed in Fig. 2.11. The system is still stable for $k_e = 3500 \text{ N/m}$ though the robust analysis test performed in the previous section does not guarantee robust stability. We further analyze the performance of the RC via force vs. position plots. Because such plots are a good indication of the system's performance for fixed environments, they were also obtained for the controllers based on the P-P and P-F architectures when interacting with the soft spring with $k_e = 850 \text{ N/m}$.

The forces f_h and f_e are displayed against the positions x_m and x_s in Fig. 2.14. For illustrative purposes, the forces and positions plots are shifted such that all the plots at the environment side have the $(0,0)$ point in common. The slope of the f_e vs. x_s plots represent the stiffness of environment and the slope of the f_h vs. x_m plots represent the stiffness being felt by the operator. For all test springs using the RC, the slopes of the plots of the operator and environment sides are similar, thus the operator feels a realistic spring in all cases and a high performance is

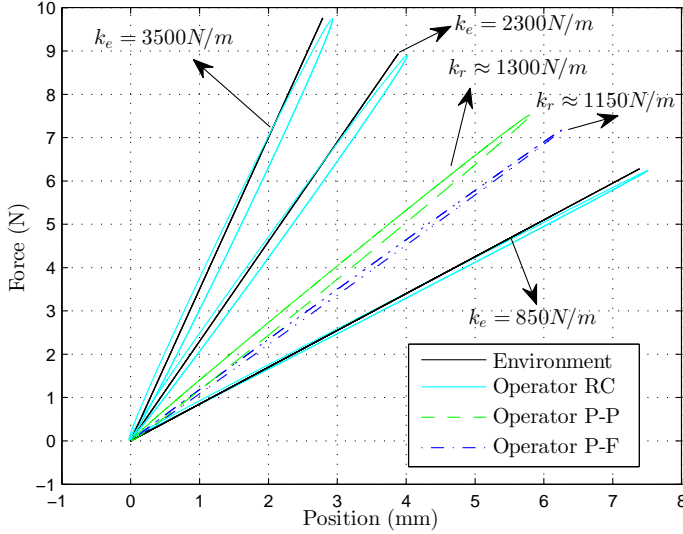


Figure 2.14: Force vs Position plots from simulations of interaction with different springs during the PCP. Controllers P-P and P-F are tested for $k_e = 850 \text{ N/m}$.

indeed achieved. As already observed from the time domain plots, the performance slightly decreases for increasing environment stiffness values. Next, Fig. 2.14 shows that for soft environments, the P-P and P-F architectures have lower performance compared to the RC. The reflected stiffness k_r to the operator is bigger than the environment stiffness of $k_e = 850 \text{ N/m}$. The operator feels a stiffer environment with the classical architectures, being more noticeable for the P-P controller. These results confirm the theoretical analysis previously performed.

Regarding the TP behavior, the corresponding time domain signals to the RC are shown in Fig. 2.15. Especially for $k_e = 850 \text{ N/m}$ and $k_e = 2300 \text{ N/m}$, a smooth transition is made despite the sudden change in environment stiffness, validating the robust performance properties of the proposed RC. For the third spring, which is larger than \bar{k}_e with guaranteed performance, one can observe a small overshoot at the transition instance and tracking performance worsens.

2.3.3 Experiments

In this section, we validate the promising simulation results with experiments on a physical setup. We test three springs with stiffness values $k_e \approx 850 \text{ N/m}$, $k_e \approx 2300 \text{ N/m}$ and $k_e \approx 3500 \text{ N/m}$ respectively. They were placed below the end-

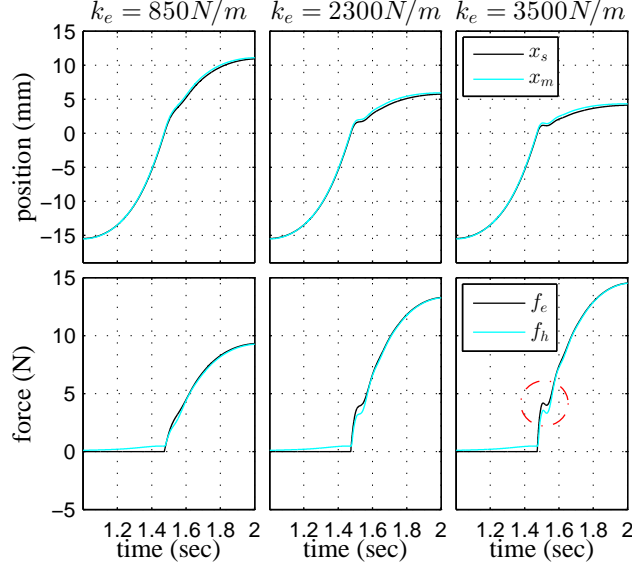


Figure 2.15: Time domain responses from simulations of interaction with different springs during the TP.

effector of the slave device as shown in Fig. A.1. We drove the system under similar operating conditions as to the simulation part, i.e. Transient Part and Permanent Contact Part.

The time domain response of the signals x_m , x_s , f_h and f_e for the PCP are shown in Fig. 2.16. Results are very similar to those of simulations. In all three cases, position and force tracking is achieved with slight decrease of position tracking performance as the environment stiffness increases. Now, In Fig. 2.17 we plot the forces versus the positions at both master and slave sides with the same plot shifts are used for a better visual comparison. One can see that, with all test springs, the stiffness the human feels is very close to the real environment stiffness. This shows that the performance criteria used during the design step of the RC were successful in meeting the requirements of transparency in the time domain, not only in simulation, but also experimentally.

The time domain response of the signals x_m , x_s , f_h and f_e for TP are also shown in Fig. 2.18. This time, the position signals were shifted such that all spring positions coincided at $x_s > 0$. As expected, the transition with $k_e < 2500$ N/m was made in a smooth fashion, validating experimentally the performance achieved by the proposed controller. For the transition with $k_e \approx 3500$ N/m, an overshoot can be

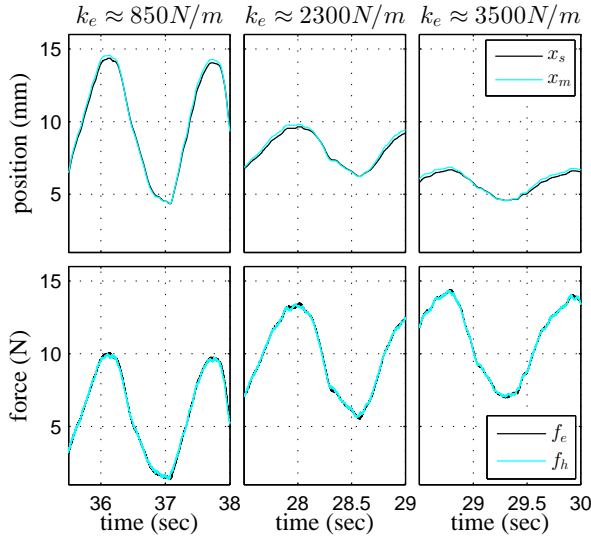


Figure 2.16: Time domain responses from experiments of interaction with different springs during the PCP.

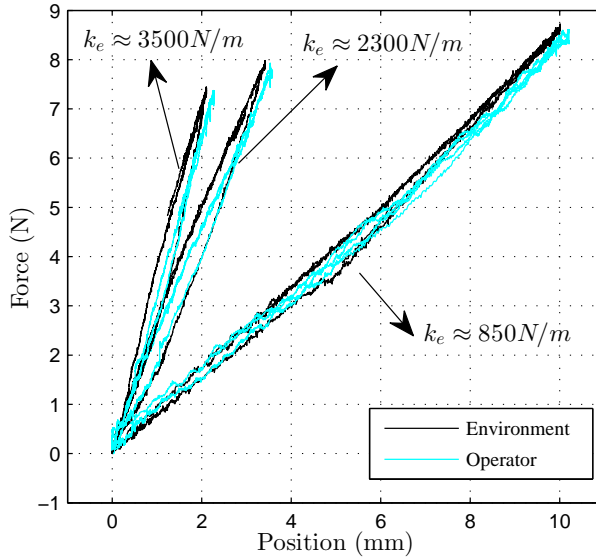


Figure 2.17: Force vs. Position plot from experiments of interactions with different springs during the PCP.

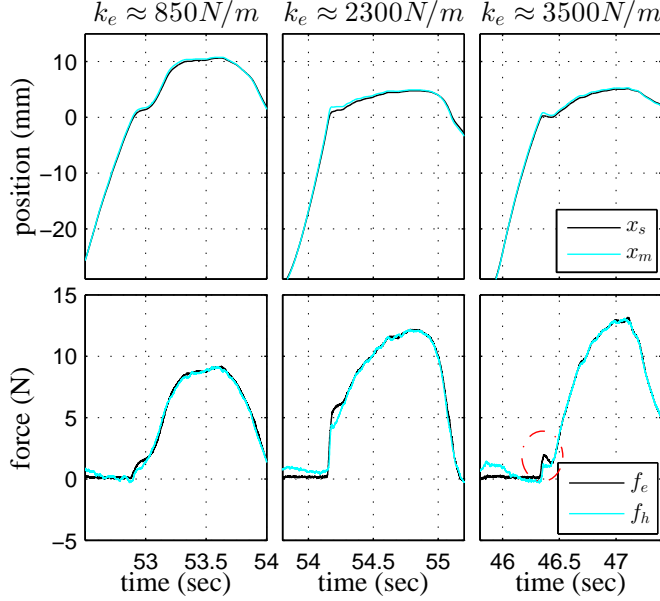


Figure 2.18: Time domain responses from experiments during the TP of a transition from free air to different springs at $x_s > 0$

observed especially in the force signals. According to our robust performance analysis from Fig. 2.11 stability is not guaranteed. In practice, we only experienced the overshoot but we could not destabilize the system. However, such overshoot can degrade the subjective haptic perception of the environment. Though the analysis can introduce conservatism, it still ensures a safe and high performance operation of the system under realistic conditions in which the human and environment dynamics vary with time.

Finally, the TP time slot is further analyzed and the corresponding power spectral density plots are shown in Fig. 2.19. For all cases, the system presented position tracking up to 10 Hz and force tracking up to 4 Hz for the time-varying stiffness. Thus, practically high-performance is achieved up to 4 Hz. One can see that for the third stiffness the overshoot can be also noticed in frequency-domain by an increase of the power concentration of the environment forces between [4,10] Hz, which might not be safe for the environment, for instance when the environment is, say a soft tissue. Therefore, it is validated that Fig. 2.11 can give a good indication for the safe region of operation of the bilateral system, which shows that the model and the assumptions we made are sufficiently realistic.

As final remarks, we have assumed that the human arm-hand stiffness can vary in-

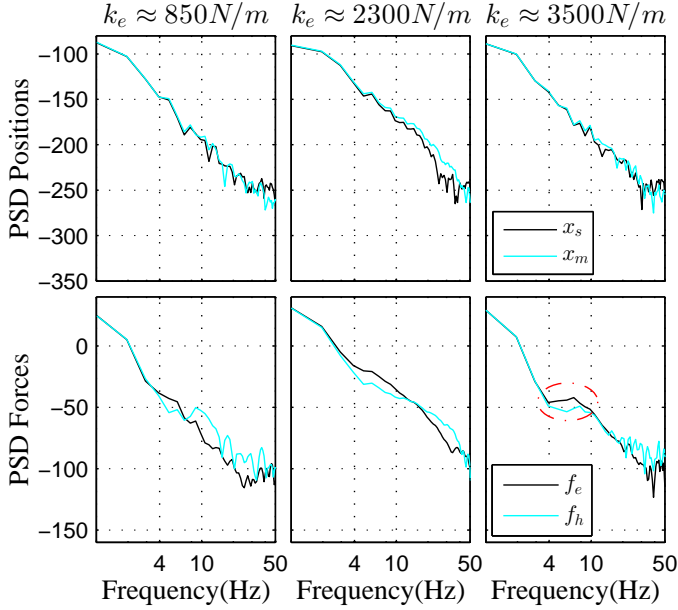


Figure 2.19: Power Spectral plots of responses from experiments after transition from free air to different springs at $x_s > 0$.

finitely fast. However, in reality the operator can only change the mechanical properties of his/her arm-hand only with a bounded rate of variation. Including such information in the control design could further reduce the conservatism. Methodologically, the conservatism reduction is made possible via frequency-dependent, i.e., dynamic multipliers Megretski and Rantzer (1997) as opposed to the constant multipliers utilized here. Moreover, we did not consider delays, and thus, no conclusions can be drawn on how it would worsen the performance and stability properties of the system. However, we emphasize that it boils down to rewriting the interconnection such that delays are also collected in the uncertainty block. Via the use of dynamic multipliers, which are a class of IQCs, this case can be analyzed applying the tests given in Polat and Scherer (2012). Finally, we considered here devices that can be modeled via LTI models, thus for devices with strong non-linear behavior, existing techniques like feedback linearization could be applied before the techniques here described.

2.4 Conclusions

In this chapter, we have presented a systematic approach towards control design for bilateral teleoperation. Such approach uses a parametric model of a bilateral teleoperation system, this allowed us to handle the uncertain parameters of the bilateral system systematically. Operator and environment with bounded and time-varying stiffness were considered. The experimental results demonstrated that such uncertainty description allowed to obtain high performance and stability simultaneously in the range of soft environments, not only for continued contact with the environment, but also for sudden changes in it. Moreover, the analysis, simulation and experimental results of the controlled system were consistent with each other, showing that the assumptions we made during modeling and synthesis were appropriate, thus demonstrating the potential of the design methodology here presented.

In the next chapter, dependency on the environment properties are included during control design, allowing for different controller for soft and hard environments.

Chapter 3

Switching Robust Control for Bilateral Teleoperation

WHEN the environment of the teleoperation system varies within a large range, a single controller might not be sufficient to achieve both stability and high performance. In this chapter we propose the synthesis of a switching robust controller that allows to design multiple robust controllers suitable for different ranges of environment stiffness, so that an overall better performance is achieved. The controllers are scheduled using an estimate of the environment stiffness. During the design we account for smooth switching among controllers and for the fact that environment estimators will have limited accuracy and uncertainty. We present synthesis, simulation and experimental results of the proposed approach, thus showing the effectiveness of the method to improve the robust performance of the teleoperated system.

3.1 Introduction

Teleoperation systems can provide a feeling of tele-presence using force feedback while an operator manipulates a remote environment by means of a master and a slave device. It is desirable that the system has high performance, e.g. the operator feels as if he/she is manipulating the environment directly, in a stable fashion.

This chapter is based on the following manuscript: López Martínez, C. A., Molengraft, R. v. d., and Steinbuch, M. (2014c). Switching robust control for bilateral teleoperation. *Under review for journal publication*

However, there is an inherent trade-off between (robust) stability and performance, see, e.g., Hannaford (1989); Lawrence (1993b), and it is a challenging problem to design controllers that meet an appropriate balance, see, e.g., Hokayem and Spong (2006), Passenberg et al. (2010). Control design tools based on Passivity theory, see, e.g., Niemeyer and Slotine (1991), Ryu (2007), have been widely used. They mainly focus on stability but the stability/performance trade-off is not taken into account systematically. More recent works by, e.g. Kim et al. (2013), Willaert et al. (2014) consider performance in the design, but either neglect the fact that both operator and environment dynamics are inherently time-varying, or the applicability is limited to master and slave devices with identical mass-damper-spring dynamics.

Additionally, in many applications environment parameters such as mass, damping and stiffness are bounded. In Chapter 2, we included this boundedness into the control design process to balance performance and stability. We also experimentally validated the design of a robust Linear Time Invariant (LTI) controller, which yields a high performance for time-varying environment stiffness in the range of those encountered in soft tissues in applications such as minimally invasive surgery, needle insertion, etc. However, in the same sort of applications there are other tissues with larger stiffness coefficients, for example up to around $7000N/m$ for the ribcage (Bankman et al. (1990)) and there might even be rigid contacts, e.g. in the collision of two robotic arms. Therefore, it is desirable to increase the range in which performance and stability is achieved in order to get closer to the requirements of real-life surgical conditions.

On the other hand, there is no guarantee that a single LTI controller exists that ensures both performance and stability for a large range of time-varying environment stiffness values. To cover a large region of environment stiffness, one can add flexibility in the control design, for instance by means of estimating the environment stiffness and use such estimation to design a controller that adapts accordingly. Some works, e.g. by Willaert et al. (2010), Cho et al. (2013), design controllers that depends on the estimate of the environment stiffness, however either they do not guarantee robust performance, or the achieved operating range is limited to low environment stiffness. Moreover, such works rely on accurate, unbiased, low noise and/or fast convergence of the estimated environment stiffness, requirements which in practice are difficult to meet simultaneously.

Another approach to address performance and stability, when the environment stiffness varies in a wide range, is the use of switching control. Some existing switching control methods suggest to switch between different operating points of the overall system, see, e.g., Liberzon (2003), Leith and Leithead (2000), though systems with uncertainty are not considered and/or smooth switching is not guaranteed. Multiple model adaptive control, which is also a switching based method,

has been used in teleoperation in Shahdi and Sirouspour (2005), however uncertainty in the operator is not included and there is no smooth switching between controllers.

We propose the use of a switching robust controller that accounts for uncertainty in the operator and environment dynamics as well as uncertainty and noise in the estimation of the environment stiffness k_e that is used for control scheduling. We use operator and environment models such that the uncertainty Δ in the bilateral teleoperation system is defined by the operator and environment stiffness parameters. The human operator's model structure is based on an operator's hand measurements. The proposed multi-controller structure consists of N_c LTI robust controllers, in which the i th controller has robust performance in an uncertainty region Δ_i , such that all regions combined cover the uncertainty set Δ . Moreover, such controllers are designed to share a common quadratic Lyapunov function, which ensures stable and smooth switching between them. Additionally, to be robust to uncertainty and noise in the estimated parameter that allows the scheduling of the robust controllers, we define a minimum overlapping between the regions Δ_i .

In this thesis it is the first time that experiments are presented using switching robust control in teleoperation, such that robust performance is guaranteed under time-varying uncertainty in the operator, the environment, and the estimation of the scheduling parameter k_e . The synthesis, simulations and experiments demonstrate the potential of the proposed method to improve the robust performance in teleoperation systems.

In Section 3.2 we describe the system's modelling and the framework for control design of the proposed switching robust controller for teleoperation systems. Synthesis, Simulations and experimental results are presented and discussed in Section 3.3. Finally, in Section 3.4 the conclusions are presented.

3.2 Switching robust control approach

3.2.1 LFR model of a teleoperation system

Similarly as in Chapter 2, we make use of a Linear Fractional Representation (LFR) of the bilateral teleoperation system. Deriving a LFR of a system amounts to isolating the uncertain parameters such that an interconnection structure as depicted in Fig. 3.1 is obtained. Let $\delta_i = [\underline{\delta}_i, \bar{\delta}_i]$, $i = 1, \dots, n_p$ be families of bounded parametric uncertainties with possibly different lower and upper bounds.

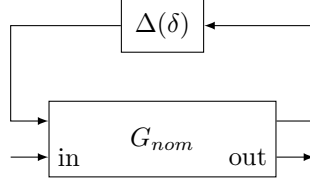


Figure 3.1: Linear Fractional Representation of a System.

Let $\delta_i(t) \in \delta_i, i = 1, \dots, n_p$ be parametric uncertainties and define the vector δ as the vector of all n_p parametric uncertainties, that is, $\delta = \text{col}(\delta_1, \dots, \delta_{n_p}) \in \mathbb{R}^{n_p}$. $\Delta(\delta)$ is the block diagonal mapping that acts on δ , i.e. $\Delta(\delta) = \text{diag}(\delta_1, \dots, \delta_{n_p})$. q and p are the signals interfacing with the uncertainty block in the sense that $p = \Delta(\delta)q$. In particular, at any time instant t this means that $p(t) = \Delta(\delta(t))q(t)$ is an ordinary matrix multiplication. To derive the LFR model of the teleoperation system, the uncertainty parameters δ are defined and then isolated and collected into the uncertainty block $\Delta(\delta)$. To this end, we first define the models of the different components of a teleoperation system. We apply our methods on a system using the particular mass-damper-spring models for master and slave devices, which interact with the operator and environment respectively as depicted in Fig. 3.2, where $m_m > 0, b_m \geq 0, k_m \geq 0$ are the fixed parameters of the master device; $m_s > 0, b_s \geq 0, k_s \geq 0$ are the fixed parameters of the slave device; f_m, f_s are the actuation forces to the master and slave devices respectively; f_h, f_e represent the total force exerted by the operator and environment respectively; and x_m, x_s are the positions of the master and slave devices respectively. By definition they also represent the positions of the operator and environment respectively.

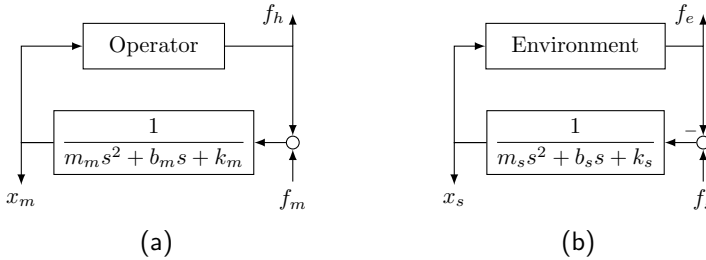


Figure 3.2: Diagram of (a) operator/master device and (b) environment/slave device.

Operator model

For the operator, we make use of a model with the same structure as presented in Chapter 2. In such a model the main source of uncertainty comes from the operator's arm-hand stiffness k_h , which allows to reduce the numerical control design complexity. This also implies that the human arm-hand mass m_h is considered fixed, and as shown in the results in Chapter 2, the control design for $m_h \approx 0.5$ kg delivered unstable controllers for when the master device is released, i.e. all the operator's mechanical properties are zero. In this chapter our focus is on increasing the system's performance given that the operator and environment models resemble the operating conditions sufficiently close. Therefore we consider specific operating conditions such that m_h is low. Obtaining models and the corresponding control design that account for a wider range of operating conditions is left as future work. In this work, such conditions of low operator mass are achieved when the system is manipulated only with the hand, resting the wrist on a rigid object as shown in Fig. 3.3. The experimental setup is further described in Appendix A.

Next, we identified experimentally the hand dynamics of an operator while the operator manipulated, in the way previously explained, the master-device of the experimental setup, which has built-in force and position sensors. The operator dynamics are inherently time-varying and to obtain a time-varying model can be a difficult task. Instead, we simply identify several LTI models and then we combine them into a time-varying model. This works under the assumption that the operator can behave as an LTI system if he/she tries to remain static. We presented seven virtual springs to the operator with stiffness values $k_e^V \in [0, 5000]$ N/m such that $f_m = -k_e^V x_m + f_m^{ID}$, in which f_m^{ID} will be used as a disturbance signal for system identification. In particular, we used a system's sampling rate of 2000 Hz and a frequency range of $[1, 60]$ Hz for the multi-sine. Initially we set $f_m^{ID} = 0$ N and then the operator was asked to move the master device in order to feel the virtual

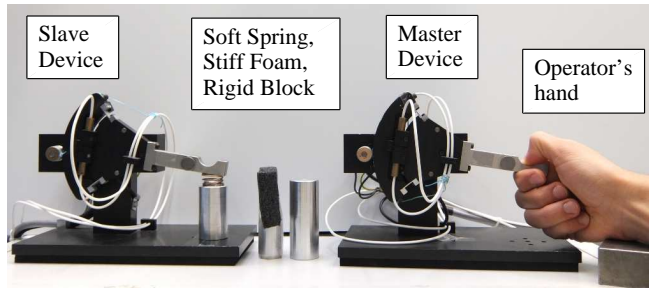


Figure 3.3: 1-DoF setup for bilateral teleoperation. The operator rests his wrist in a rigid block to bound his dynamics to those of the hand.

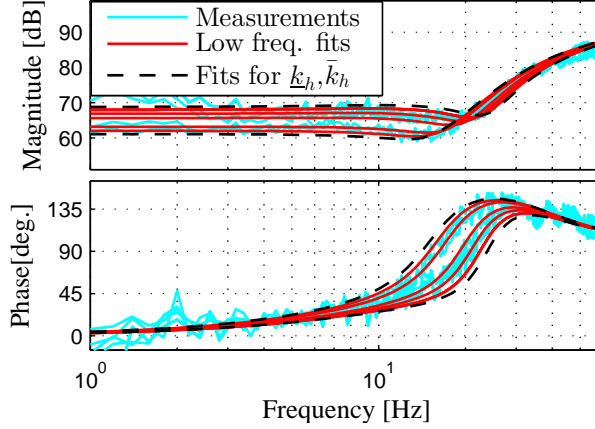


Figure 3.4: Hand frequency response measurements $Z_h^{\text{meas}}(i\omega)$ and low-frequency approximations $Z_h(i\omega)$.

spring. Subsequently, the operator was asked to stop in a position of his/her choice where he/she could still feel the virtual spring. The idea is that the operator exerts a force level such that he/she could feel that he/she has a correct haptic perception of the virtual environment. This is clearly subjective to the operator. Nevertheless, the aim of the experiment is that the operator changes intuitively his/her exerted force and grip for different virtual springs. Afterwards, a multi-sine signal was applied to the master device via f_m^{ID} while the operator tried to keep his/her hand static. Forces $f_h(t)$ and positions $x_m(t)$ were measured and then their Fourier transforms $F_h^{\text{meas}}(j\omega) = \mathcal{F}(f_h(t))(j\omega)$ and $X_m^{\text{meas}}(j\omega) = \mathcal{F}(x_m(t))(j\omega)$ were computed. Next, we obtained frequency response function (FRF) measurements of the operator's hand dynamics as $Z_h^{\text{meas}}(j\omega) = \frac{F_h^{\text{meas}}(j\omega)}{X_m^{\text{meas}}(j\omega)}$ in a frequency range of [1,60] Hz. The corresponding hand FRF measurements for all virtual springs are shown in Fig. 3.4.

Based on the measurements, for the hand dynamics $Z_h(s)$ we use the model structure given in (3.1), where m_h , b_h , k_h , are the mass, damping and stiffness of the human hand, ω_{zh} , z_{ph} and ω_{ph} are the parameters of the filter $Q_h(s)$ which characterizes the measured operator dynamics above 30 Hz .

$$Z_h(s) = \frac{F_h(s)}{X_m(s)} = (m_h s^2 + b_h s + k_h) Q_h(s), \quad (3.1)$$

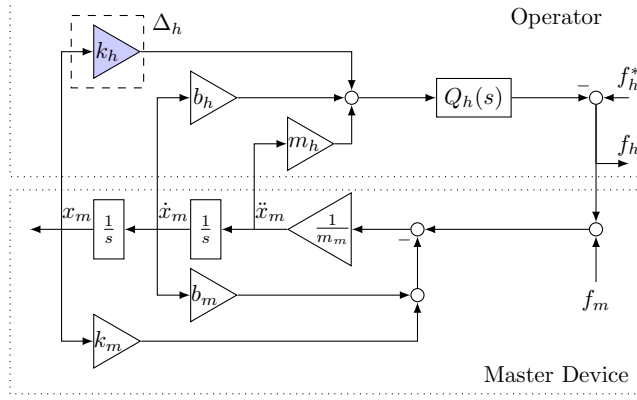


Figure 3.5: Block diagram representation of the operator/master device pair.

where

$$Q_h(s) = \frac{\frac{s}{\omega_{zh}} + 1}{\frac{s^2}{\omega_{ph}^2} + 2z_{ph}\frac{s}{\omega_{ph}} + 1}.$$

Then, we optimized the variables m_h , b_h , k_h , ω_{zh} , z_{ph} and ω_{ph} to fit each measurement to the model minimizing the cost function $W_{Z_h}(i\omega) = \|(Z_h(i\omega) - Z_h^{\text{meas}}(i\omega)) / |Z_h^{\text{meas}}(i\omega)|\|_2$ for $\omega \in 2\pi[1, 60]$ rad/s. The optimization is done using a constrained nonlinear optimization method provided by the command `fmincon` in Matlab®. In practice the optimization problem has several local minima, thus initial conditions and interval constraints must be provided to the solver. Those initial conditions and their respective constraints are estimated based on the measurements and are adjusted until a satisfactory match between $Z_h(i\omega)$ and $Z_h^{\text{meas}}(i\omega)$ is obtained. The resulting parameters were found to be within the following ranges; $m_h \in [0.112, 0.134]$ kg, $b_h \in [5.88, 8.94]$ N s/m, $k_h \in [1257, 2501]$ N/m, $\omega_{zh} \in [69.5, 102.5]$ rad/s, $z_{ph} \in [0.54, 0.70]$ and $\omega_{ph} \in [184.0, 239.8]$ rad/s. To reduce complexity of the model and control design, we have used a low-frequency approximation by allowing variation in k_h only and fixing all other parameters to their centered values in the corresponding intervals, thus $m_h = 0.123$ kg, $b_h = 7.41$ N s/m, $\omega_{zh} = 86$ rad/s, $z_{ph} = 0.62$ and $\omega_{ph} = 211.9$ rad/s. The corresponding fitted models are depicted in Fig. 3.4. Finally, to include possible extra variation in k_h , we enlarge the range of values of k_h by 20%, and we use $k_h \in [1131.3, 2751.1]$ N/m. The resulting $Z_h(s)$ fitted models for \underline{k}_h and \bar{k}_h are depicted with dashed lines in Fig. 3.4. One can see that the approximation fits well for low frequencies and, moreover, allows to reduce the number of uncertain parameters in the operator

model. Because only k_h is considered uncertain, using the model proposed here for control design has implications. Mainly, the system's performance could decrease for users with dynamic properties that differ largely from those considered here. It is possible to extend the number of uncertainty parameters in the operator's model at the cost of increasing the numerical complexity of the synthesis procedure. The operator identification was performed for a single operator. From the arm-hand models presented here and in Chapter 2, we can already conclude that the structure of Eq. 3.1 covers sufficiently well the dynamics of different arm-hand configurations, i.e. different arm-hand poses that result in the use of different groups of muscles. This is an indication that the operator's model-structure presented here could be valid for other users as well. Regarding the range of variation of the operator's model-parameters, it is clear that different arm-hand configurations result in different ranges of variation of parameters. This can be seen if we compare the parameters found here with those in Chapter 2. Furthermore, the parameters are expected to vary among different users. Nevertheless, less variation is expected if the arm-hand pose during experiments is similar among users. However, more subjects are needed to evaluate whether the structure of the operator's model and the proposed low frequency approximation are still valid.

Though the identification was performed via LTI techniques, in what follows below, we assume that during operation k_h is time-varying in the sense that $k_h(t) \in [\underline{k}_h, \bar{k}_h]$ for all $t > 0$.

Finally, combining the master device and operator models, we arrive at the model diagram for the operator/master device depicted in Fig. 3.5, where f_h^* is the active force generated by the operator and $\Delta_h = k_h$ defines the time-varying, bounded and uncertain parameter of the human hand dynamics model.

Environment model

Next, we consider environments with mass-damper-spring dynamics:

$$f_e = f_e^* + (m_e \ddot{x}_s + b_e \dot{x}_s + k_e x_s),$$

which model a significant class of applications of interest. Here, m_e , b_e and k_e are the non-negative mass, damping and stiffness coefficients of the environment respectively, and f_e^* is the active force from the environment, if present. We focus on the environment stiffness k_e as the main cause of the dynamic variation, hence m_e and b_e are assumed fixed and k_e is assumed to be bounded (though within a wide range), and in addition time-varying. This choice is suitable for applications in which the effect of k_e on f_e is dominant, e.g. in stiffness discrimination tasks like those in surgery. For other environment types the uncertainty structure and parameters can be redefined. One should keep in mind that because of

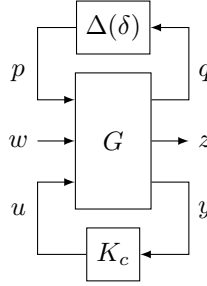


Figure 3.6: Generalized plant.

the intrinsic robust stability/performance trade-off, it is expected that the greater the uncertainty set, the lower the achievable performance. Subsequently, the coupled environment/slave-device system can be obtained in a similar way as for the operator/master-device system. The uncertainty block in the environment/slave-device model is given, then, by $\Delta_e = k_e$.

Generalized plant

Having the two models of environment/slave and operator/master, we set up an LFR model of the teleoperation system as a generalized plant G as in Fig. 3.6. The different elements of the diagram are defined in the same way as for the model presented in Chapter 2. They are described briefly here as follows: From the modeling we have that the uncertain parameters are $\delta_1 = k_h$, $\delta_2 = k_e$, thus $\delta = \text{col}(k_h, k_e)$. The uncertainty block is then defined as $\Delta(\delta(t)) = \begin{bmatrix} k_h(t) & 0 \\ 0 & k_e(t) \end{bmatrix}$, $\Delta \in \Delta$, where

$$\Delta = \left\{ \begin{bmatrix} k_h & 0 \\ 0 & k_e \end{bmatrix} : k_h \in [\underline{k}_h, \bar{k}_h], k_e \in [\underline{k}_e, \bar{k}_e] \right\}.$$

The vector q and p contain the signals interfacing the uncertainty, thus we can infer that $q = \text{col}(x_m, x_s)$, $p(t) = \Delta(\delta(t))q(t)$. One can see that the model can be easily adapted to the cases in which other parameters might also be assumed to be uncertain. The measured signals are included in the vector y , and we assume that we can measure the position and forces of the master and slave devices, possibly contaminated with measurement noise vector. Therefore, we have that $y = \text{col}(f_h, f_e, x_m, x_s) + y_n$, where $y_n = \text{col}(f_{hn}, f_{en}, x_{mn}, x_{sn})$ represents the noise in the measurements. The disturbance signals of the system are represented by the vector w . We treat the active forces from the operator and environment as disturbance signals. Including the noise channels y_n as disturbances explicitly increases

the robustness properties that would help to obtain a controller more suitable for the actual implementation. Thus, we define $w = \text{col}(f_h^*, f_e^*, f_{hn}, f_{en}, x_{mn}, x_{sn})$. Additionally, the actuation signal vector u contains the forces actuated from the motors of the master and the slave devices. Thus, $u = \text{col}(f_m, f_s)$. The performance vector z is defined as $z = \text{col}(f_h - f_e, x_m - x_s, f_m, f_s)$. Via the component, $f_h - f_e$, we enforce that the human operator should feel the same force applied by the environment. The second component, $x_m - x_s$, is the position error to obtain tracking between master and slave. The actuation variables are also included as channels to be penalized to avoid controllers with high gains. G is the LTI model that contains all the fixed model dynamics of the different components of the bilateral teleoperation system: the master device, the slave device, the fixed operator dynamics and the fixed environment dynamics if present. Finally, K_c is the to-be-designed controller that maps the measured signals y to the actuation signals u .

The control design problem is then to find a controller K_c that achieves robust stability and robust performance for all $\Delta \in \Delta$. At this point we still need to define what structure the controller K_c will have, which will be the subject of the next section.

3.2.2 Switching robust control design using a common quadratic Lyapunov function

In Chapter 2, using Linear Matrix Inequalities (LMI's) (Scherer and Weiland (2010)), we synthesized a single LTI robust controller with robust performance for bounded environment stiffness k_e in the range of low stiffness environments. Our research focus is on obtaining high performance teleoperated systems for a wider range of environment stiffness $k_e \in [\underline{k}_e, \bar{k}_e]$, covering not only soft stiffness environments. As it will be shown later, the achievable performance of controllers designed with the methodology presented in Chapter 2 degrades considerably as the maximal environment stiffness \bar{k}_e is increased. From a control point of view, one of the reasons for this performance degradation is the lack of flexibility of the controller to adapt to large changes in the uncertainty parameters of the system. Therefore, in this chapter we present control architecture in which we increase the flexibility of the controller architecture so we can achieve a better performance index and therefore reduce the performance degradation for large ranges of k_e .

We propose a switching robust control architecture. The main idea consists of scheduling different robust controllers according to the estimate \hat{k}_e of the actual value of k_e . Thus, we design a specific number N_c of LTI controllers, in which the i th controller has an uncertainty set Δ_i of robust performance, such that all

regions combined form a larger set such that $\Delta \subseteq \Delta_1 \cup \dots \cup \Delta_{N_c}$, where Δ describes the uncertainty region of the system.

To describe the partition, let $\delta_{(i)j} = [\underline{\delta}_{(i)j}, \bar{\delta}_{(i)j}]$, $i = 1, \dots, N_c$; $j = 1, \dots, n_p$ be families of bounded parametric uncertainties. Let $\delta_{(i)j}(t) \in \delta_{(i)j}$, $i = 1, \dots, N_c$; $j = 1, \dots, n_p$ be parametric uncertainties and define the vectors $\delta_{(i)} = \text{col}(\delta_{(i)1}, \dots, \delta_{(i)n_p}) \in \mathbb{R}^{n_p}$, $i = 1, \dots, N_c$. $\Delta_i(\delta_{(i)})$, $i = 1, \dots, N_c$ are the block diagonal mappings that acts on $\delta_{(i)}$, i.e. $\Delta_i(\delta_{(i)}) = \text{diag}(\delta_{(i)1}, \dots, \delta_{(i)n_p})$, $i = 1, \dots, N_c$. Then, each subregion Δ_i is described by $\Delta_i \in \Delta_i$, where the class Δ_i is defined as

$$\Delta_i = \left\{ \text{diag}(\delta_{(i)1}, \dots, \delta_{(i)n_p}) : \delta_{(i)1} \in [\underline{\delta}_{(i)1}, \bar{\delta}_{(i)1}], \dots, \delta_{(i)n_p} \in [\underline{\delta}_{(i)n_p}, \bar{\delta}_{(i)n_p}] \right\}$$

for $i = 1, \dots, N_c$, that $\Delta \subseteq \Delta_1 \cup \dots \cup \Delta_{N_c}$. In our specific case $n_p = 2$. Therefore each regions Δ_i , $i = 1, \dots, N_c$ is a ‘rectangle’ in the $k_h - k_e$ plane. The specific distribution of Δ_i , $i = 1, \dots, N_c$ will be given in Section 3.2.3.

Augmented plant model for control design

Before describing the control synthesis method, we need to augment the model shown in Fig. 3.6 in order to incorporate the uncertainty partitions Δ_i , $i = 1, \dots, N_c$ and a more suitable form that is usable for control design. To this end, consider the model diagram presented in Fig. 3.7 in which we have augmented and partitioned the model in Fig. 3.6 in N_c augmented generalized plants \tilde{G}_i . The different components of the augmented model are described as follows:

- V and W are weighting filters described with stable LTI systems. They allow to shape in frequency domain the desired system performance. These filters will be defined in detail in Section 3.2.5. Meanwhile they are assumed to be known.
- \tilde{w} and \tilde{z} are weighted copies of w and z via predefined filters V and W respectively. That is $w = V\tilde{w}$ and $\tilde{z} = Wz$.
- $\tilde{\delta}_{(i)}$, $i = 1, \dots, N_c$. are the vectors $\tilde{\delta}_{(i)} = \text{col}(\tilde{\delta}_{(i)1}, \dots, \tilde{\delta}_{(i)n_p})$ of the transformed uncertain parameters $\tilde{\delta}_{(i)j} \in \tilde{\delta}_{(i)j}$ such that $\tilde{\delta}_{(i)j} = [\tilde{\delta}_{(i)j}, \bar{\tilde{\delta}}_{(i)j}]$ and $0 \in \tilde{\delta}_{(i)j}$ for $i = 1, \dots, N_c$ and $j = 1, \dots, n_p$. The main idea is that the intervals $\delta_{(i)j}$ are mapped one to one to the intervals $\tilde{\delta}_{(i)j}$. The specific transformations from parameters $\delta_{(i)j}$ to $\tilde{\delta}_{(i)j}$ will be given in Section 3.2.3. Meanwhile they are assumed to be known.
- $\tilde{\Delta}_i(\tilde{\delta}_{(i)})$, $i = 1, \dots, N_c$ is the block diagonal concatenation of the parameters

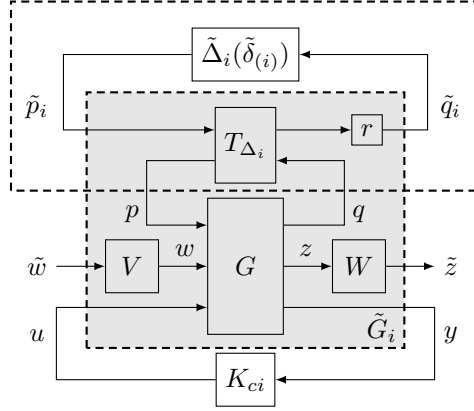


Figure 3.7: Set of generalized plants with weighting filters, uncertainty transformation and scaling. The dashed block in the upper part equals $\Delta_i(\delta)$ provided $r = 1$.

in $\delta_{(i)}$.

$$\tilde{\Delta}_i(\tilde{\delta}_i(t)) = \text{diag}(\tilde{\delta}_{(i)1}, \dots, \tilde{\delta}_{(i)n_p}), \quad \tilde{\Delta}_i \in \tilde{\mathbf{\Delta}}_i,$$

where

$$\tilde{\mathbf{\Delta}}_i = \left\{ \text{diag}(\tilde{\delta}_{(i)1}, \dots, \tilde{\delta}_{(i)n_p}) : \tilde{\delta}_{(i)1} \in [\underline{\tilde{\delta}}_{(i)1}, \bar{\tilde{\delta}}_{(i)1}], \dots, \tilde{\delta}_{(i)n_p} \in [\underline{\tilde{\delta}}_{(i)n_p}, \bar{\tilde{\delta}}_{(i)n_p}] \right\}$$

for $i = 1, \dots, N_c$.

- The vector \tilde{q} and \tilde{p} contain the signals interfacing the new uncertainty block $\tilde{\Delta}$. Thus $\tilde{p}(t) = \tilde{\Delta}(\tilde{\delta}(t))\tilde{q}(t)$.
- $r \in [0, 1]$: is a scaling factor that allows to scale down the uncertainty blocks $\tilde{\Delta}_i$. This allows to perform an iterative process during the control design in which one starts with the nominal case $r = 0$, i.e. no uncertainty, and finalizes with an unscaled uncertainty set for $r = 1$. We will refer to a nominal plant if $r = 0$. If $r = 1$ we have that $\Delta_i(\delta_i)$ equals the dashed block in the upper part of Fig. 3.7.
- $T_{\Delta_i} : \mathbb{R}^{2n_p \times 2n_p}, i = 1, \dots, N_c$ are constant matrices such that :

$$\begin{pmatrix} \tilde{q}_i \\ \tilde{p} \end{pmatrix} = \begin{pmatrix} r & 0 \\ 0 & 1 \end{pmatrix} T_{\Delta_i} \begin{pmatrix} \tilde{p}_i \\ q \end{pmatrix}, i = 1, \dots, N_c$$

T_{Δ_i} is used to map one to one the uncertain parameter set $\mathbf{\Delta}_i$ to the transformed uncertain parameter set $\tilde{\mathbf{\Delta}}_i$. The transformations T_{Δ_i} allows to

obtain a nominal values of $\Delta_i(\delta_{(i)}^{\text{Nom}}) \in \mathbf{\Delta}_i$ for $r = 0$. The specific transformations from matrices $T_{\Delta_i, i=1, \dots, N_c}$ will be given in Section 3.2.3. Meanwhile they are assumed to be known.

- $K_{ci}, i = 1, \dots, N_c$ are then the LTI controllers $K_{ci}(s) = C_{ci}(Is - A_{ci})^{-1}B_{ci} + D_{ci}$, which we will identify with its state space description by writing

$$K_{ci}(s) = \left[\begin{array}{c|c} A_{ci} & B_{ci} \\ \hline C_{ci} & D_{ci} \end{array} \right],$$

One can derive a model of the generalized plant \tilde{G}_i for $i = 1, \dots, N_c$. We denote its state space representation by the following equation:

$$\begin{pmatrix} \dot{x} \\ \tilde{q}_i \\ \tilde{z} \\ y \end{pmatrix} = \begin{pmatrix} A_i & B_{(i)1} & B_{(i)2} & B_i \\ rC_{(i)1} & rD_{(i)1} & rD_{(i)12} & rE_{(i)1} \\ C_{(i)2} & D_{(i)21} & D_{(i)2} & E_{(i)2} \\ C_i & F_{(i)1} & F_{(i)2} & 0 \end{pmatrix} \begin{pmatrix} x \\ \tilde{p}_i \\ \tilde{w} \\ u \end{pmatrix}, i = 1, \dots, N_c$$

Uncertainty and performance description

Similarly as in Chapter 2, we will use a specific class of Integral Quadratic Constraints (IQCs) (see Megretski and Rantzer (1997)) to model uncertainties $\tilde{\Delta}_i \in \mathbf{\tilde{\Delta}}_i$. Then consider \mathbf{P}_i as sets of symmetric matrices $P_i \in \mathbb{R}^{2n_p \times 2n_p}$ that satisfy the following IQC

$$\int_0^{T_0} \begin{pmatrix} \tilde{\Delta}_i(\tilde{\delta}_i) \tilde{q}_i(t) \\ \tilde{q}_i(t) \end{pmatrix}^T P_i \begin{pmatrix} \tilde{\Delta}_i(\tilde{\delta}_i) \tilde{q}_i(t) \\ \tilde{q}_i(t) \end{pmatrix} dt \geq 0 \quad (3.2)$$

for all $q \in \mathcal{L}_2[0, T_0]$, $T_0 \in \mathbb{R}_+$, $\tilde{\Delta}_i \in \mathbf{\tilde{\Delta}}_i$ and $i = 1, \dots, N_c$.

The matrix P_i for a specific i is a so called *multiplier*. It allows to describe mathematical properties of the uncertainty block $\tilde{\Delta}_i$. The set \mathbf{P}_i needs to be further classified in order to describe specific type of uncertainties. Because the class $\mathbf{\tilde{\Delta}}_i$ is convex, it can be expressed as a convex combination of generators $\tilde{\delta}_{(i)}^j, j = 1, \dots, 2^{n_p}$. Then, as shown in Chapter 2, we can describe $\mathbf{\tilde{\Delta}}_i$ by means of classifying the sets \mathbf{P}_i by the symmetric matrices P_i that satisfy the following finite number of inequalities

$$\begin{pmatrix} I \\ 0 \end{pmatrix}^T P_i \begin{pmatrix} I \\ 0 \end{pmatrix} \preceq 0 \quad (3.3)$$

$$\begin{pmatrix} \tilde{\Delta}_i(\tilde{\delta}_{(i)}^j) \\ I \end{pmatrix}^T P_i \begin{pmatrix} \tilde{\Delta}_i(\tilde{\delta}_{(i)}^j) \\ I \end{pmatrix} \succeq 0, \quad i = 1, \dots, N_c \quad j = 1, \dots, 2^{n_p} \quad (3.4)$$

In fact, (3.3) and (3.4) imply also (3.2), see Sections 1.3 and 2.2.2. In this case, matrices $P_i, i = 1, \dots, N_c$ are then constant full block multipliers describing bounded and time-varying real parametric uncertainties. Also notice that imposing structure and dynamics in the matrices P_i , other types of uncertainty can be described as shown in Polat and Scherer (2012), which can be exploited in future works. Once we characterize the uncertain sets Δ_i by \mathbf{P}_i , we will describe the performance criterion used here.

We have chosen the performance criterion based upon the \mathcal{L}_2 gain of the mapping from disturbance channels \tilde{w} to the performance channels \tilde{z} as is customary in model-based \mathcal{H}_∞ control, e.g., see Skogestad and Postlethwaite (2005). The \mathcal{L}_2 gain from \tilde{w} to \tilde{z} can be expressed as:

$$\sup_{0 \neq \tilde{w} \in \mathcal{L}_2} \frac{\|\tilde{z}\|_2}{\|\tilde{w}\|_2} < \gamma, \quad (3.5)$$

in which γ can be interpreted as a worst-case gain from the disturbances \tilde{w} to the performance signals \tilde{z} . Therefore, instantaneous responses that can be felt by the operator have a direct effect on the performance criterion. This makes the \mathcal{L}_2 gain a suitable performance criterion for teleoperation systems. The \mathcal{L}_2 gain can be expressed in a standard form as a quadratic performance criterion:

$$\int_0^\infty \begin{pmatrix} \tilde{w}(t) \\ \tilde{z}(t) \end{pmatrix}^T P_p \begin{pmatrix} \tilde{w}(t) \\ \tilde{z}(t) \end{pmatrix} dt < 0 \text{ for all } 0 \neq \tilde{w} \in \mathcal{L}_2, \quad (3.6)$$

with

$$P_p = \begin{pmatrix} -\gamma^2 I & 0 \\ 0 & I \end{pmatrix}$$

The standard form to describe performance in Eq. (3.6) allows the use of other quadratic performance criteria via P_p , see, e.g., Section 1.3 and Scherer and Weiland (2000). To keep the generality of the theory used here, we will use the symbol P_p to describe our specific performance criterion.

We proceed with the LMI-based switching robust controller design such that the closed loop is robustly stable and satisfies the performance specifications. The robust control synthesis concepts are adapted from Scherer and Weiland (2010).

Switching robust control synthesis using a common Lyapunov function

First, we describe a general framework to design switching robust controllers, then in Section 3.2.3 we provide a more specific framework of the control design applied to the bilateral teleoperation problem.

We introduce the shorthand notation for the closed loop matrices

$$\tilde{G}_i(s) \star K_{ci}(s) = \left[\begin{array}{c|cc} \mathcal{A}_i & \mathcal{B}_{(i)1} & \mathcal{B}_{(i)2} \\ \hline \mathcal{C}_{(i)1} & \mathcal{D}_{(i)11} & \mathcal{D}_{(i)12} \\ \mathcal{C}_{(i)2} & \mathcal{D}_{(i)21} & \mathcal{D}_{(i)22} \end{array} \right], i = 1, \dots, N_c \quad (3.7)$$

obtained by closing the loop in Fig. 3.7 with the controller K_{ci} , such that the obtained system has as inputs the vector $\text{col}(\tilde{p}_i, \tilde{w})$, and as outputs the vector $\text{col}(\tilde{q}_i, \tilde{z})$.

Initially, assume we have certain $K_{ci}(s)$ that achieves nominal stability for each Δ_i for $i = 1, \dots, N_c$. That is for when $r = 0$. Moreover, let $\mathbf{P}_i, i = 1, \dots, N_c$ be the sets of symmetric matrices P_i that satisfy conditions (3.3) and (3.4);

Theorem 3.1. *The closed loop systems $\tilde{G}_i(s) \star K_{ci}(s)$ with $r \in (0, 1]$ shown in Fig. 3.7 are robustly stable for all $\tilde{\Delta}_i \in r\tilde{\Delta}_i$ with robust quadratic performance characterized by P_p if there exist a symmetric matrix \mathcal{X} and matrices $P_i \in \mathbf{P}_i$ such that (3.3), (3.4),*

$$\mathcal{X} \succ 0 \quad (3.8)$$

and

$$\left(\star \right)^T \left(\begin{array}{cc|cc} 0 & \mathcal{X} & 0 & 0 \\ \mathcal{X} & 0 & 0 & 0 \\ \hline 0 & 0 & P_i & 0 \\ 0 & 0 & 0 & P_p \end{array} \right) \left(\begin{array}{ccc} I & 0 & 0 \\ \hline \mathcal{A}_i & \mathcal{B}_{(i)1} & \mathcal{B}_{(i)2} \\ 0 & I & 0 \\ \hline \mathcal{C}_{(i)1} & \mathcal{D}_{(i)11} & \mathcal{D}_{(i)12} \\ 0 & 0 & I \\ \hline \mathcal{C}_{(i)2} & \mathcal{D}_{(i)21} & \mathcal{D}_{(i)22} \end{array} \right) \prec 0 \quad (3.9)$$

holds for $i = 1, \dots, N_c$. Moreover robust stability and quadratic performance are also achieved for arbitrary fast switching between the uncertain closed loop systems $r\tilde{\Delta}_i \star \tilde{G}_i(s) \star K_{ci}(s)$ for $i = 1, \dots, N_c$.

Remark 3.2. *The point of Theorem 3.1 is that all closed loop systems $\tilde{G}_i(s) \star K_{ci}(s)$ share a common quadratic Lyapunov function $V(x) = x^T \mathcal{X} x$. This means that the overall switched system is globally stable under arbitrary fast switching between all N_c controllers (see Liberzon (2003)). Moreover, the resulting switching is smooth because there are not discontinuities in the obtained Lyapunov function. Thus, the design of the K_{ci} controllers can be linked to ensure robust stability and quadratic performance under switching of controllers and for all $\Delta \in \tilde{\Delta}$, assuming that each controller is active in its own uncertainty region of operation.*

Remark 3.3. *Theorem 3.1 allows to do analysis of robust performance of the system given the controllers $K_{ci}(s), i = 1, \dots, N_c$. Then all the involved conditions are LMIs. However, in the case of controller synthesis, there is an issue. In (3.9), the outer factors involving the state-space matrices of $K_{ci}(s)$ multiply the blocks of the multiplier P_i involving unknown variables rendering the constraint a BMI. However, by means of the transformations that have been given in Scherer*

and Weiland (2010); Masubuchi et al. (1998); Scherer. et al. (1997), it is possible to make (3.9) an LMI when either P_i or $(A_{ci}, B_{ci}, C_{ci}, D_{ci})$ are fixed. Moreover, $(A_{ci}, B_{ci}, C_{ci}, D_{ci})$ matrices also multiply each other, hence a linearization is needed. Fortunately, this can be avoided with a Schur complement argument. In Chapter 2 it is shown how to perform such linearization for one controller. This procedure can be expanded to the multi-controller case in a straightforward way.

Initially, we have neither a controller nor a multiplier by which the constraints are satisfied. Hence one typically starts with the nominal system $G_{nom} = \mathbf{0}_{\bar{p}_i \bar{q}_i} \star \tilde{G}_i, i = 1, \dots, N_c$ (which is an upper LFT and equivalent to removing the uncertainty channels). Then we design a nominally stabilizing controllers $K_{ci}(s), i = 1, \dots, N_c$ denoted by K_{cnom} with certain performance level, utilizing equations in Theorem 3.1 after removing the columns and rows corresponding to the uncertainty channels. As mentioned in remark 3.3, extra transformations are needed to arrive to LMI's that allow to design the controller parameters, mainly two steps are needed, first a congruence transformation is used to arrive to transformed parameters and subsequently a linearisation lemma is applied. The necessary procedure is illustrated in Chapter 2 (see also Scherer and Weiland (2010)) for one controller and can be expanded to the multi-controller case in a straightforward way. After having computed a nominal controller K_{cnom} , it is possible to search for feasible multipliers via Theorem 3.1. Obviously, we can not expect a robust stability certificate from the initial controller K_{cnom} since there is no constraint enforcing it. Thus, we need to first scale down the uncertainty size with small r to the level that K_{cnom} robustly stabilizes the system. Then by a line search over the feasible uncertainty size via the scaling factor $r \in (0, 1]$, we obtain feasible stability multipliers P_i .

Clearly, we assume the existence of a nominal controller that provides an initial condition for the first iteration that will not lead to a local minimum very close to $r = 0$, which in practice is actually the case. To summarize, we start with the design of a nominal controller. Then, we iterate the following steps:

- for fixed controllers K_{ci} , maximize r using the bisection algorithm and get the multipliers P_i , while minimizing γ , keeping $\gamma < \bar{\gamma}$, for a certain $\bar{\gamma}$.
- for fixed P_i matrices, maximize r using the bisection algorithm and get the controllers K_{ci} while minimizing γ , keeping $\gamma < \bar{\gamma}$, for a certain $\bar{\gamma}$.
- Once $r = 1$ is achieved, we iterate the two previous steps and on each the performance level γ is minimized until no further progress can be made.

The value $\bar{\gamma}$ is introduced such that at the initial steps of the iterative synthesis procedure we allow γ to be large, in order to avoid local minima around small values of the uncertainty scaling r , and then, after reaching $r = 1$, we minimize γ . Details on the iterative procedure are given in Appendix B, from which we have used the version II of the iterative procedure. As a final remark, we emphasize that the

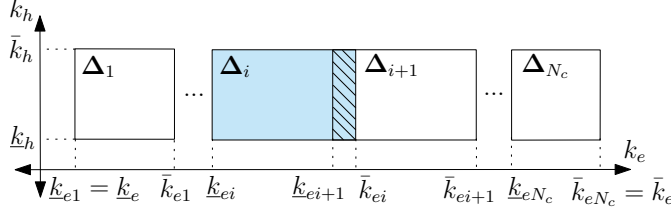


Figure 3.8: Uncertainty regions Δ_i of a switching robust controller.

resulting controllers obtained by this methodology do not have a specific internal structure. Thus, typically full matrices A_{ci} , B_{ci} , C_{ci} and D_{ci} , for $i = 1, \dots, N_c$ are obtained, which results in controllers that use all combinations of the measured inputs to compute the actuation outputs.

3.2.3 Tailor-made solution for bilateral teleoperation

In order to apply the procedure presented in Section 3.2.2 to our design case, we need first to select the partition of the uncertainty set $\Delta = \left\{ \begin{bmatrix} k_h & 0 \\ 0 & k_e \end{bmatrix} \mid k_h \in [\underline{k}_h, \bar{k}_h], k_e \in [\underline{k}_e, \bar{k}_e] \right\}$.

We consider adaptation of the controller to changes in k_e . This because we are interested in a large range of variation in k_e . Moreover, from the operator modeling we found that k_h varies in a more limited range. Next, define the uncertainty blocks Δ_i such that $\Delta_i = \left\{ \begin{bmatrix} k_h & 0 \\ 0 & k_{ei} \end{bmatrix} \right\}$ for $i = 1, \dots, N_c$ and $\Delta_i \in \Delta$, where the class $\Delta_i = \left\{ \begin{bmatrix} k_h & 0 \\ 0 & k_{ei} \end{bmatrix} : k_h \in [\underline{k}_h, \bar{k}_h], k_{ei} \in [\underline{k}_{ei}, \bar{k}_{ei}] \right\}$ and $\Delta \subseteq \Delta_1 \cup \dots \cup \Delta_{N_c}$. The distribution of regions Δ_i is illustrated in Fig. 3.8. In view to the nomenclature used in Section 3.2.2, we have that $\delta_{(i)} = \text{col}(k_h, k_{ei})$, $i = 1, \dots, N_c$. For a better illustration and readability, we will make use of the parameters k_h and k_{ei} , the corresponding vector $\delta_{(i)}$ can be constructed at the moment that the synthesis procedure is implemented.

Next, the overlapping between the regions will be exploited later to avoid chattering behavior and to guarantee robustness to uncertainty in the estimation of k_e . We assume that

$$\underline{k}_e = \underline{k}_{e1} < \underline{k}_{e2} < \bar{k}_{e1} < \underline{k}_{e3} < \bar{k}_{e2} < \dots < \bar{k}_{eN_c} = \bar{k}_e$$

Next, we still need to define all \underline{k}_{ei} and \bar{k}_{ei} . There is a lot of flexibility in this respect, here we present a distribution in which only N_c and \bar{k}_{e1} are tunable parameters, however other choices can be made.

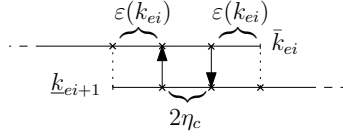


Figure 3.9: Overlapping of two adjacent uncertainty regions.

First, we define the ranges Δ_{k_h} and $\Delta_{k_{ei}}$ as the projection of the uncertainty regions Δ_i on the parameters k_h and k_e respectively. In this case $\Delta_{k_h} = \{k_h : k_h \in [\underline{k}_h, \bar{k}_h]\}$ and $\Delta_{k_{ei}} = \{k_{ei} : k_{ei} \in [\underline{k}_{ei}, \bar{k}_{ei}]\}$.

Next, we define the amount of overlapping between ranges $\Delta_{k_{ei}}$ sufficiently large to make the system robust to noise and uncertainty in the estimation of k_e . To illustrate this, consider that the estimate \hat{k}_e of k_e is given by:

$$\hat{k}_e = k_e \pm \varepsilon(k_e) + \eta(k_e) \quad (3.10)$$

where $\varepsilon(k_e)$ represents the magnitude of the uncertainty in \hat{k}_e and $\eta(k_e)$ represents the zero-mean noise signal in the estimation such that $|\eta(k_e)| < \eta_c$ for $k_e \in [\underline{k}_e, \bar{k}_e]$. Note that ε and η can possibly depend on k_e . Next, to guarantee robust performance of the whole switching system, consider the overlapping section in the k_e axes of two adjacent regions Δ_i , Δ_{i+1} as depicted in Fig. 3.9, where

$$\underline{k}_{ei+1} \leq \bar{k}_{ei} - 2\varepsilon(\bar{k}_{ei}) - 2\eta_c \quad (3.11)$$

and it is assumed that $\varepsilon(\bar{k}_{ei}) > \varepsilon(\underline{k}_{ei+1})$.

$\varepsilon(\bar{k}_{ei})$ accounts for the uncertainty in the estimation and the introduced hysteresis gap with size $2\eta_c$ avoids chattering behavior due to noise. Then, if the switching from region i to a higher indexed region is taken when $\hat{k}_e > \bar{k}_{ei} - \varepsilon(\bar{k}_{ei})$ and the switching from region $i+1$ to a lower indexed region is taken when $\hat{k}_e < \underline{k}_{ei+1} + \varepsilon(\bar{k}_{ei})$, considering that Eq. (3.10) holds, robustness against uncertainty and noise in \hat{k}_e is guaranteed.

Now, we need to apply a transformation to the parameters such that the scaling $r = 0$ correspond a the nominal case $\Delta_i(\delta_i^{\text{Nom}}) \in \Delta_i$. Therefore, the uncertain parameters k_h and k_{ei} are transformed to new uncertain parameters $\tilde{k}_h, \tilde{k}_{ei}$, thus the new uncertainty block is given by $\tilde{\Delta} = \begin{bmatrix} \tilde{k}_h & 0 \\ 0 & \tilde{k}_{ei} \end{bmatrix}$, for which the synthesis procedure is applied.

Such transformation needs to have linear representation so it can be incorporated into the augmented generalized plant via T_{Δ_i} . We consider a transformation from

k_{e1} to $\tilde{k}_{e1} \in [0, 1]$ as follows:

$$\tilde{k}_{e1} = \frac{k_{e1} - \underline{k}_e}{\bar{k}_{e1} - \underline{k}_e} \quad (3.12)$$

One can show that the nominal case $\tilde{k}_{e1} = 0$ correspond to $k_{e1}^N = \underline{k}_e$ and that $\tilde{k}_{e1} \in [0, 1]$ is mapped back to $\Delta_{k_{e1}} = \{k_{e1} : k_{e1} \in [\underline{k}_e, \bar{k}_{e1}]\}$, i.e. we fix $\bar{k}_{e1} = \underline{k}_e$. For k_h we use a similar transformation.

Now, for k_{ei} , $i > 1$ we use the transformation from k_{ei} to $\tilde{k}_{ei} \in [-1, 1]$:

$$\tilde{k}_{ei} = \frac{1}{r_d} \left(\frac{k_{ei}/k_{ei}^N - 1}{k_{ei}/k_{ei}^N + 1} \right) \quad (3.13)$$

where k_{ei}^N is the untransformed nominal value corresponding to $\tilde{k}_{ei} = 0$ and $0 < r_d < 1$ is a parameter. One can show that $\tilde{k}_{ei} \in [-1, 1]$ is mapped back to

$$\Delta_{k_{ei}} = \left\{ k_{ei} : k_{ei} \in \left[\frac{1 - r_d}{1 + r_d} k_{ei}^N, \frac{1 + r_d}{1 - r_d} k_{ei}^N \right] \right\} \quad (3.14)$$

We see that $\underline{k}_{ei}(r_d, k_{ei}^N)$ and $\bar{k}_{ei}(r_d, k_{ei}^N)$. Now, connecting Eq. (3.14), Eq. (3.11), the parameters of the environment $\underline{k}_e, \bar{k}_e$, specifications of the estimator $\varepsilon(k_e)$, η_c , and predefining \bar{k}_{e1} , N_c , it is possible to compute k_{ei}^N and r_d . Thus in the following we summarize the synthesis tuning procedure.

First, we set $\underline{k}_{e1} = \underline{k}_e$. Then, we specify \bar{k}_{e1} , which can be used as a tuning parameter. Next, using Eq. (3.11), we can compute $\underline{k}_{e2}(\underline{k}_e, \varepsilon, \eta_c)$, which can be replaced in Eq. (3.14) to find then for any $i > 1$: $k_{ei}^N(r_d, \underline{k}_e, \varepsilon, \eta_c)$, $\underline{k}_{ei}(r_d, \underline{k}_e, \varepsilon, \eta_c)$ and $\bar{k}_{ei}(r_d, \underline{k}_e, \varepsilon, \eta_c)$. Then, r_d can be computed if we define a priori the number of controllers N_c , given that $\bar{k}_{eN_c}(r_d, \underline{k}_e, \varepsilon, \eta_c) = \bar{k}_e$. This function is non-linear but can be numerically solved using for instance a bisection algorithm. Now, combining all transformations, then the corresponding transformation matrices are:

$$T_{\Delta_1} = \begin{pmatrix} 0 & \text{diag}(\bar{k}_h - \underline{k}_h, \bar{k}_{e1} - \underline{k}_{e1}) \\ I & \text{diag}(\underline{k}_h, \underline{k}_{e1}) \end{pmatrix}$$

and

$$T_{\Delta_i} = \begin{pmatrix} \text{diag}(0, k_{ei}^N) & \text{diag}(\bar{k}_h - \underline{k}_h, r_d) \\ \text{diag}(1, k_{ei}^N) & \text{diag}(\underline{k}_h, 2r_d) \end{pmatrix}, i = 2, \dots, N_c$$

Hence, all what is left, is to use the synthesis process described in Section 3.2.2 for the transformed uncertainty $\tilde{\Delta}$, which in turn will guarantee robust performance of the overall system for the whole uncertainty set $\Delta = \left\{ \begin{bmatrix} k_h & 0 \\ 0 & k_e \end{bmatrix} : k_e \in [\underline{k}_e, \bar{k}_e], k_h \in [\underline{k}_h, \bar{k}_h] \right\}$ and uncertainty and noise in the estimate \hat{k}_e .

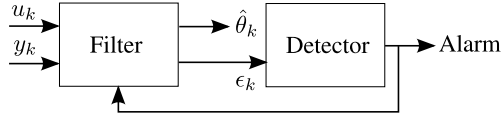


Figure 3.10: Estimator with Change Detection

As a final remark, we emphasize that transformation in Eq. (3.13) serves just as a way to distribute the regions when $N_c > 2$ with a reduced number of tuning parameters. However other choices can be explored, for example manually distributing the regions a priori and then using transformation in Eq. (3.12) for all parameters.

3.2.4 Environment estimation

To be able to implement the proposed switching robust control, we need a mechanism that tells the controller when to switch from $K_{cj}(s)$ to $K_{ci}(s)$ on the basis of changes (possibly rapid and sudden) in the environment stiffness k_e . In this thesis, we make use of an estimator that provides an estimate \hat{k}_e of k_e . Such estimate is used in the way illustrated in Section 3.2.3 to determine when to activate certain controller $K_{ci}(s)$.

Particularly, the estimator needs to be able to deal with abrupt changes of the environment stiffness in order to schedule the different controllers $K_{ci}(s)$, $i = 1, \dots, N_c$ correctly. To this end, we have chosen one estimator proposed in Gustafsson (2000) (see page 25), the structure of which is shown in Fig. 3.10. The working principle of this estimator is as follows: the *filter* block processes the discrete inputs u_k and outputs y_k of a system described by a *model* (in our case an environment model) to get an estimate $\hat{\theta}_k$ of certain parameters θ_k (the parameters of our environment model). Then, the signal ϵ_k is used to detect abrupt changes in the parameters and under certain criteria, the *detector* block sends an *alarm* to the filter to adapt quickly to the changes. Following the guidelines in Gustafsson (2000), the different blocks are described below.

Environment model as a linear regression model

The environment model selected here is given as

$$f_{me}(t) = k_e(t)x_s(t) + f_e^*(t) + f_{en}(t)$$

where f_{me} denotes the measured environment force. If we sample the previous model at discrete time instants denote by k , then the environment model equation can be incorporated into the discrete version of a standard linear regression model given by:

$$y_k = \varphi_k^T \theta_k + e_k$$

where $e_k = f_{en}(k)$, $y_k = f_{me}(k)$, the parameter vector is then $\theta_k = \text{col}(k_e(k), f_e^*(k))$ and the so called regression vector φ_k is given by $\varphi_k = \text{col}(u_k, 1)$ with $u_k = x_s(k)$.

The linear regression model can be interpreted as the measurement equation in a discrete state space model,

$$\begin{aligned}\theta_{k+1} &= \theta_k + v_k \\ y_k &= \varphi_k^T \theta_k + e_k\end{aligned}$$

where v_k is the parameter noise and $Q_k = \text{Cov}(v_k)$ and $R_k = \text{Cov}(e_k)$. Note that the variation in the parameter θ is embedded in the signal v_k , also known as the innovation signal.

Filter

Having such state model, we can utilize a Kalman filter to get an estimate $\hat{\theta}_k = \text{col}(\hat{k}_e(k), \hat{f}_e^*(k))$ of the parameter vector θ (see Gustafsson (2000), page 142). This results in a Kalman filter for linear regressions, which is implemented in its recursive form as follows:

$$\begin{aligned}\varphi_k &= \text{col}(u_k, 1) \\ K_k &= \frac{P_{k-1} \varphi_k}{R_k + \varphi_k^T P_{k-1} \varphi_k} \\ P_k &= P_{k-1} - \frac{P_{k-1} \varphi_k \varphi_k^T P_{k-1}}{R_k + \varphi_k^T P_{k-1} \varphi_k} + Q_k \\ \hat{\theta}_k &= \hat{\theta}_{k-1} + K_k (y_k - \varphi_k^T \hat{\theta}_{k-1}) \\ \epsilon_k &= y_k - \varphi_k^T \hat{\theta}_k\end{aligned}$$

where R_k is taken as 1 without loss of generality and Q_k is a design parameter that determines the speed of converge of the filter. Large values of Q_k make the filter to react faster but also the estimate will have more noise. The variable ϵ_k is the error between the actual measurement and the reconstructed measurement obtained with $\hat{\theta}_k$.

Detector

The detector block is defined as a threshold function in order to decide when to make the filter to react fast. Thus, when $|\epsilon_k| < L_{|\epsilon_k|}$, no alarm is generated and we use $Q_k = Q_{nom}$. When $|\epsilon_k| \geq L_{|\epsilon_k|}$, it means that \hat{y}_k has deviated too much from the true measurement and the filter must adapt rapidly to the new environment by setting $Q_k = Q_{fast}$.

Therefore, the estimator is tuned via $L_{|\epsilon_k|}$, Q_{nom} and Q_{fast} . This tuning is essential to be able to detect abrupt changes fast enough to schedule on time the controllers of the multi-controller structure. The next step in the design is then to translate the specifications via weighting filters W and V .

3.2.5 Weighting filter design

In robust control design it is customary to implement frequency dependent weights on the performance channels (see Fig. 3.7). The filters V and W are block diagonal transfer matrices emphasizing the frequency band in which we want the particular channel to be penalized. Thus $V = \text{diag}(V_{f_h^*}, V_{f_e^*}, V_{f_{hn}}, V_{f_{en}}, V_{x_{mn}}, V_{x_{sn}})$ and $W = \text{diag}(W_{f_h-f_e}, W_{x_m-x_s}, W_{f_m}, W_{f_s})$. Ideally, one wants to have $f_h - f_e = 0$ and $x_m - x_s = 0$. In this case we would get perfect transparency, but as is known, this type of design is unrealistic and has poor stability properties. Instead, it is desirable to relax such a strict requirement by appropriate choices of V and W .

Instead we are interested in forcing the force and position tracking errors such that in frequency domain $|F_h(\omega) - F_e(\omega)| < \gamma |F_w(\omega)|$ and $|X_m(\omega) - X_s(\omega)| < \gamma |X_w(\omega)|$, where $F_h(\omega), F_e(\omega), X_m(\omega), X_s(\omega)$ are the Fourier transform of f_h, f_e, x_m, x_s respectively, $F_w(\omega)$ and $X_w(\omega)$ represent the desired level of force and position tracking in the frequency band of interest and $\gamma > 0$ is as small as possible. We assume $|F_w(\omega)| > 0$ and $|X_w(\omega)| > 0$ sufficiently small at low frequencies to achieve force and position tracking for sufficiently slow varying forces and positions. This will lead to a desired level of performance in the frequency range in which the human operator performs movements. On the other hand, we need to have feasible control action with magnitude bounded forces f_m, f_s and a reduced amplification of disturbance w to z at high frequencies. This to avoid saturation and the excitation of high frequency dynamics. These requirements are translated into the filters W and V which are shaped accordingly. Thus we put more weight at frequencies where we want to lower the \mathcal{L}_2 -gain. We translate the performance specifications

by defining the following filters:

$$\begin{aligned}
 W_{f_h-f_e}(s) &= \left(c_{s1} \frac{\frac{s}{\omega_{bw}} + 1}{\frac{s}{\omega_{bw}} + c_{lf1}} \right)^2 \\
 W_{x_m-x_s}(s) &= c_{xs} c_{s2} \frac{\frac{s}{\omega_{bw}} + 1}{\frac{s}{\omega_{bw}} + c_{lf2}} \\
 W_{f_m}(s) &= W_{f_s}(s) = c_{s3} \frac{\frac{s}{\omega_{lp}} + 1}{\frac{s}{\omega_r} + 1} \\
 V_{f_h^*} &= V_{f_e^*} = c_{s4} \\
 V_{f_{hn}} &= V_{f_{en}} = c_{s5} \\
 V_{x_{mn}} &= V_{x_{sn}} = \frac{c_{s6}}{c_{xs}}
 \end{aligned}$$

Typical shapes of the magnitude-bode plots $|1/W_{x_m-x_s}(i\omega)|$ (which has a similar shape as $|1/W_{f_h-f_e}(i\omega)|$) and $|1/W_{f_m}(i\omega)|$ (which the same shape as $|1/W_{f_s}(i\omega)|$) are shown in Fig. 3.11.

ω_{bw} defines the desired closed-loop bandwidth, ω_{lp} defines the desired bandwidth of the actuation force signals. With the values c_{lf1} , c_{lf2} we put a limit to $W_{f_h-f_e}$ and $W_{x_m-x_s}$ at low frequencies. This also ensures the filters $W_{f_h-f_e}$ and $W_{x_m-x_s}$ to be stable. Stability of all filters is necessary to ensure that a stabilizing controller K_c exists for the guaranteed plant. A second order filter was selected for $W_{f_h-f_e}$ to increase the tracking performance obtained in practice. On the other hand for $W_{x_m-x_s}$ a first order filter was sufficient. To avoid non-causal W_{f_m} and W_{f_s} , we inserted high frequency poles at ω_r . Moreover, c_{xs} is used to scale penalties on positions with respect to penalties on forces. This makes the magnitude of positions and forces numerically comparable. To keep the tuning more intuitively, c_{xs} is designed independently and it is not integrated to c_{s2} in $W_{x_m-x_s}$. Finally, c_{s1}, \dots, c_{s6} are scaling constants that are used for further tuning.

3.3 Switching robust control applied to a 1-DoF academic setup

To demonstrate the potential of our approach, in this section we provide synthesis, simulations and experimental results of a teleoperation system using a switching

Table 3.1: Numerical parameters

$m'_m = 0.7 \times 10^{-3}$	$m'_s = 0.84 \times 10^{-3}$	kg m ² /rad
$b'_m = 1.44 \times 10^{-1}$	$b'_s = 1.17 \times 10^{-1}$	N m s/rad
$k'_m = 0.20$	$k'_s = 0.14$	N m/rad
$m_h = 0.123$	$m_e = 0$	kg
$b_h = 7.41$	$b_e = 0$	N s/m
$k_h \in [1131.3, 2751.1]$	$k_e \in [80, 20000]$	N/m
$\omega_{ph} = 211.9$	$\omega_{zh} = 86$	rad/s
$z_{ph} = 0.62$		—

robust controller. The procedure is applied to the experimental setup described in Appendix A. Using frequency response measurements, the parameters of second order models for the devices are identified. Those parameters are listed in Table 3.1. In the same table we show the parameters of operator and environment dynamics computed at the end-effector. We have selected $k_e \in [80, 20\,000]$ N/m because we aim to guarantee performance and stability for environment stiffness values in a wide range.

On the following subsections the tuning of synthesis procedure is illustrated, sub-

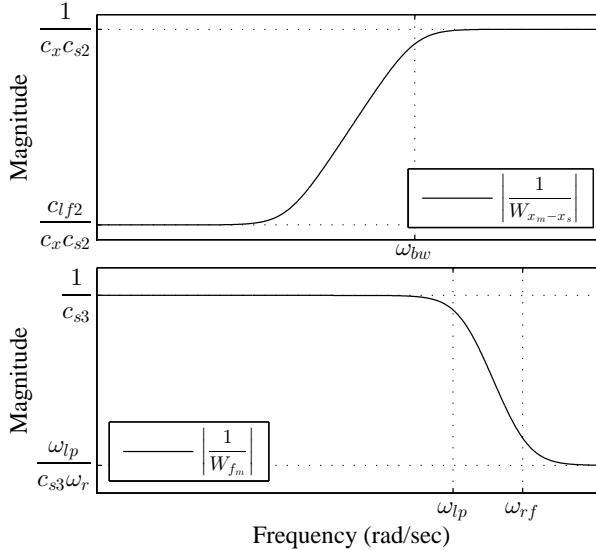

Figure 3.11: Magnitude bode plots of $1/W_{x_m-x_s}$ and $1/W_{f_m}$.

Table 3.2: Achieved \mathcal{L}_2 gain γ for different N_c and \bar{k}_{e1} . For $N_c = 1$, $\bar{k}_{e1} = \bar{k}_e = 20\,000\text{ N/m}$

\bar{k}_{e1}	$N_c = 1$	$N_c = 2$	$N_c = 3$
2000	37.6099	8.5254	10.7056
2500	37.6099	7.9688	7.0874
3000	37.6099	11.6333	14.4165
3500	37.6099	10.1025	24.5288
4000	37.6099	8.3862	17.6172
4500	37.6099	9.4531	29.2603
5000	37.6099	30.1880	17.1069

sequently simulations and experiments are carried out for different cases of fixed and time-varying environment stiffness.

3.3.1 Synthesis results

The first step is to select the numerical parameters of the weighting filters. The tuning procedure is an iterative process. Because this step was already performed in Chapter 2 for the 1-DoF academic setup utilized here, we use the same numerical parameters. Then, we set $\omega_{bw} = 2\pi \times 10\text{ rad/s}$ as the desired closed loop bandwidth. The actuation forces f_m, f_s were penalized from 60 Hz and beyond, hence $\omega_{lp} = 2\pi \times 60\text{ rad/s}$. We set $c_{lf1} = c_{lf2} = 10^{-2}$ and $\omega_r = 2\pi \times 500\text{ rad/s}$. For the rest of the scaling factor, we use $c_{xs} = 31.6$, $c_{s1} = 0.56$, $c_{s2} = 0.5$, $c_{s3} = 0.4$, $c_{s4} = 1$, $c_{s5} = 0.5$ and $c_{s6} = 0.25$. Next, the environment estimator parameters $\varepsilon(k_e)$ and η_c are selected to be $\varepsilon(k_e) = 0.1k_e$ and $\eta_c = 200\text{ N/m}$. This gave sufficient overlap between uncertainty regions during the experimental phase.

In order to explore the flexibility offered by the number of controllers N_c and maximal bound \bar{k}_{e1} of controller K_{c1} on the achieved performance index γ , we performed the synthesis procedure for different N_c and \bar{k}_{e1} . As described at the end of Section 3.2.3, for the synthesis of each set of controllers, at the initial steps of the iterative synthesis procedure we allow γ to be large. This is achieved with the condition $\gamma < \bar{\gamma}$, with $\bar{\gamma} = 100$, in order to avoid to some extent local minima around small values of the uncertainty scaling r . Then, after reaching $r = 1$, γ is minimized. The results for different N_c and \bar{k}_{e1} are illustrated in Table 3.2. Because we are interested in wide range of environments only, note that for $N_c = 1$, \bar{k}_{e1} is fixed to $\bar{k}_{e1} = \bar{k}_e = 20\,000\text{ N/m}$.

No hard conclusions can be made here because the synthesis procedure is non-

convex, therefore there is no guarantee to achieve the global optimum during the controller design. Nevertheless, the results shows that indeed the proposed switching architecture leads to improved performance during the synthesis in comparison to a single LTI robust controller. We see that adding one extra controller, i.e. $N_c = 2$ is enough to achieve a considerable increase of performance. $N_c = 3$ led to the best γ for $\bar{k}_{e1} = 2500 \text{ N/m}$. Nevertheless, for all the \bar{k}_{e1} tested, on average γ is better for $N_c = 2$ than for $N_c = 1$ and $N_c = 3$. The latter case can be due to the fact that an increase in the number of controllers increases the numerical complexity as well, thus it is more likely that the solver face numerical problems in some of the intermediate steps, for instance on finding a suitable gradient to find a sub-optimal.

3.3.2 Simulation results

For simulation purposes we compare the results from the LTI Robust Controller, hereafter referred as the RC, and a Switching Robust Controller, hereafter referred as SRC. We selected the SRC with the best achieved γ during the synthesis procedure, i.e. the one corresponding to $N_c = 3$ and $\bar{k}_{e1} = 2500 \text{ N/m}$ in Table 3.2, hereafter referred as SRCN3.

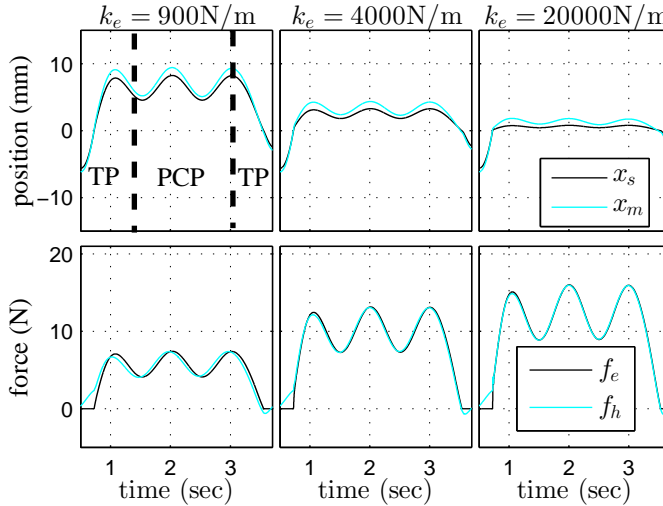


Figure 3.12: Time domain responses from simulations of interaction with different springs at $x_s > 0$, using a single Robust Controller (RC). Transient Parts (TP) and Permanent Contact Part (PCP) are illustrated.

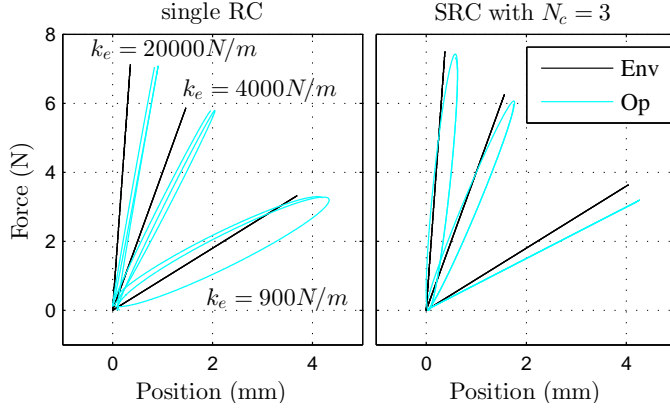


Figure 3.13: Force versus Position plots from simulations of interaction with different springs during the PCP using the RC and the SRCN3. The larger the slope the larger the stiffness.

In order to test the controllers, we simulate a scenario in which an operator manipulates the system with the slave device in free-air and then gets in contact with a spring located at $x_s > 0$. Then after some periodic movements the operator comes back again to the slave in the free-air situation. As an example of such scenario consider the top-left plot in Fig. 3.12,

where we used $f_h^* = 9(1 + \tanh((t - 1.5)/0.2)) + 4(\cos(2\pi t) - 1) - 9(1 + \tanh((t - 3.5)/0.2))$ N and $k_h = 1131.3$ N/m for the operator. The Transient Parts (TP) correspond to time slots where there is a transition between free air and contact with the spring or vice-versa. The Permanent Contact Part (PCP) is a time slot after the TP has passed and periodic movements are performed while being in permanent contact with the spring.

We then simulate the closed-loop system for three different springs $k_e = 900$ N/m, $k_e = 4000$ N/m and $k_e = 20000$ N/m. Initially we simulate the system using the RC, the corresponding time domain signals of positions and forces are presented in Fig. 3.12. From the TP one can see that the controller is robust to sudden changes in the environment. This is in accordance with the results in Chapter 2 in which a single RC was also designed. From the PCP, on one hand we observe that force tracking is achieved for all cases with slight decrease for the low stiff environment. On the other hand, the position tracking performance of the RC is noticeably degraded. The magnitude of x_m is larger than the one of x_s . As a consequence, the operator perceives a lower stiffness in comparison with the real environment stiffness. This can be observed from force versus position plots on the environment and operator sides as in the left plot of Fig. 3.13, where for illustrative

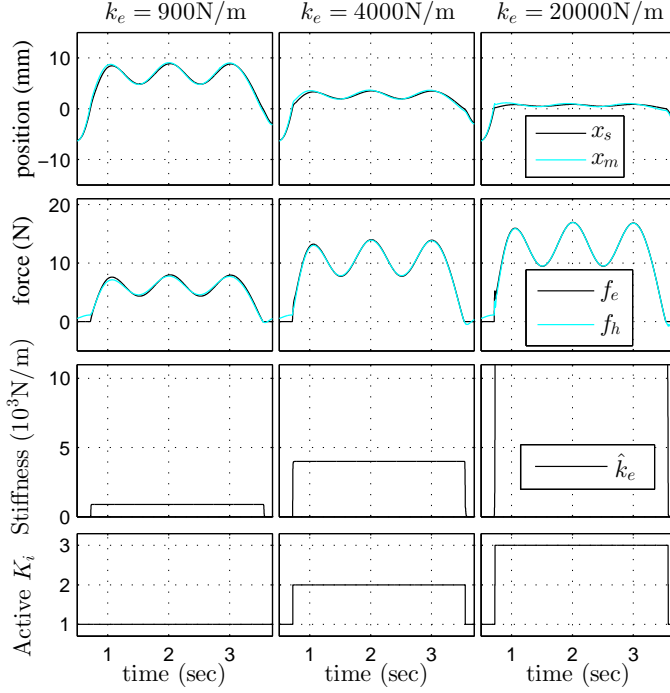


Figure 3.14: Time domain responses from simulations of interaction with different springs at $x_s > 0$, using a Switching Robust Controller (SRC) with $N_c = 3$. y -axis of the \hat{k}_e -plots are zoomed-in for illustration purposes.

purposes, the forces and positions plots are shifted such that all the plots had the $(0, 0)$ point in common. The slope of the f_e versus x_s plots represent the stiffness of environment and the slope of the f_h versus x_m plots represent the stiffness being felt by the operator.

Subsequently, the SRCN3 is simulated. The environment estimator described in Section 3.2.4 is implemented and tuned according to the guidelines in Gustafsson (2000). For simulation purposes we use the following parameters; $L_{|\epsilon_k|} = 0.2 \text{ N}$, $Q_{fast} = \text{diag}([10^7, 10])$ and $Q_{nom} = \text{diag}([1, 10^{-5}])$. The time domain responses of the whole system are depicted in Fig. 3.14, where the y -axis of the \hat{k}_e -plots are zoomed-in for illustration purposes.

First, we observe that the chosen environment estimator is indeed capable to follow rapid and sudden changes in the environment, which allows to schedule the correct controller. Next, from the TP we see that the switching takes place smoothly in all cases, because all controllers of the SRCN3 share a common Lyapunov function.

Table 3.3: Orthogonal linear regression analysis results to evaluate stiffness reflection in the simulations. k_r is the estimated stiffness and d_r is the mean distance of the estimated line. Between brackets the percentage of the environment stiffness that is reflected to the operator is shown.

Parameters	Units	Env.	Operator	
			RC	SRCN3
k_r	N/m	900	795 (88%)	746(83%)
$d_r \times 10^{-4}$	-	0	4.2	0.04
k_r	N/m	4000	2876 (72%)	3492(87%)
$d_r \times 10^{-4}$	-	0	0.58	0.96
k_r	N/m	20000	8153 (41%)	13930 (70%)
$d_r \times 10^{-4}$	-	0	0.35	0.98

Finally, from the PCP we can observe that both position and force tracking are improved with respect to the RC, especially noticeable in the position tracking. Force versus position plots are illustrated in the right plot of Fig. 3.13. When using the RC in an environment with low stiffness, from the figure one can observe a noticeable hysteresis-like effect in the perceived dynamics by the operator. Such effect can be seen as dynamics on top of a pure stiffness, which are expected to appear in the figure as straight lines as it is the case for the environment stiffness. Such dynamics can be caused by the damping injected by the controller, causing a phase difference between the position and force signals in the operator side. Thus, the less deviation from a straight line in the figure the closer is the resemblance with a pure stiffness. In that respect, for low stiffness the SRCN3 presents a great improvement. In order to make a better evaluation of the results in Fig. 3.13, we performed an orthonormal regression in order to fit straight lines to each of the force versus position plots presented in the figure. The orthonormal regression optimization uses the sum of the square of the distances of the points to the fitted line as a function cost. From the regression we can obtain the fitted line slope k_r and the mean distance d_r to the fitted line. k_r indicates the estimated stiffness and d_r gives a rough indication on the amount of dynamics on top of that stiffness. The results are shown in Table 3.3. For low stiffness, the RC presents a better reflected stiffness than the SRCN3, however, as indicated before, the hysteresis-like effect is much larger than with the SRCN3, which worsens the overall operator's perception of the soft spring. Regarding the results for the other two virtual springs, the SRCN3 has a better stiffness reflection than the RC. Though the amount of reflected dynamics are less with the RC. This discrepancy in the behaviour of the controllers is a result of the synthesis optimization, which aims to minimize the \mathcal{L}_2 gain from disturbance to performance variables (including tracking error) of the overall system under the presence of uncertainties. In this

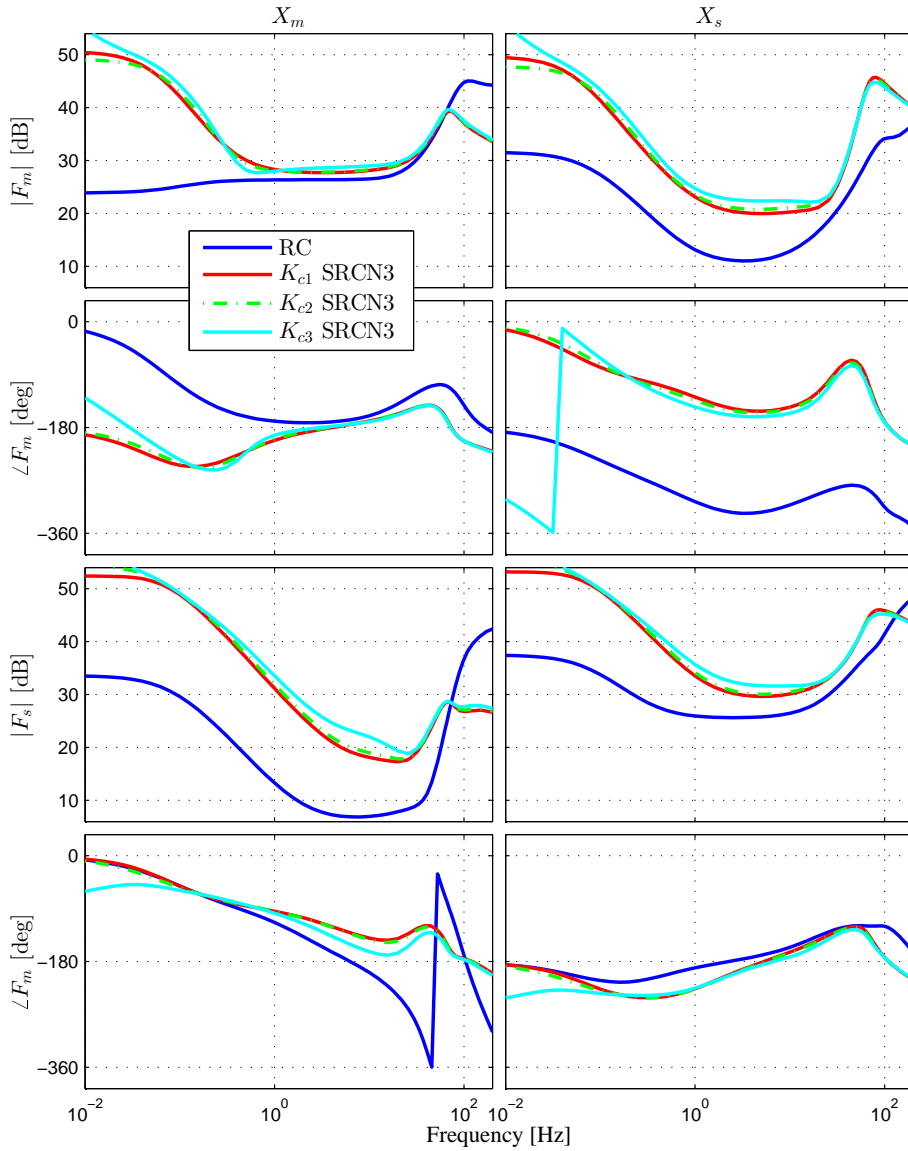


Figure 3.15: Bode plots from position inputs to actuation outputs of the RC and the three LTI controllers of the SRCN3.

particular case, the SRCN3 introduces higher phase difference between the force and position signals of the master and slave sides for higher values in k_e . This still resulted in a more optimal controller in terms of the γ value. In turn, from the simulations and the respective analysis, one can see that the improvement of the \mathcal{L}_2 gain of the system yielded better environment stiffness reflection.

As pointed out in Section 3.2.2, the obtained MIMO controllers and their corresponding SISO components do not have a specific structure like those of typical PID controllers. Instead, the obtained controllers are “full” controllers in the sense that they have components corresponding to all combinations of the available inputs and outputs. Because of this lack of structure, from the different controllers and their realizations it is not straightforward to determine specific parameters like proportional gains, damping, etc. Consider the bode plots of the RC and the LTI controllers of the SRCN3 depicted in Fig. 3.15. For illustration purposes, we have only used the position input channels. In general, one can see that the K_{ci} , $i = 1, \dots, 3$ of the SRCN3 present higher gains than the RC, which in general results in a better tracking performance. Interestingly, the SRCN3 controllers have a change in sign with respect to the RC in the channels involving f_m and x_m, x_s . Moreover, in the component from x_m to f_s of the RC, the phase decreases while the gain increases, which correspond to non-minimum phase behaviour of the corresponding component. These kind of designs are not intuitive and they are the result of the underlying numerical optimization. Finally, the difference among the K_{ci} , $i = 1, \dots, 3$ seems not to be too large. This suggests that it could be possible to find a single controller using a similar strategy as the one used to find the SRC. For instance, in future works one can explore the use of a single controller but still partitioning the uncertainty region during the synthesis procedure.

3.3.3 Experiments

In this section, we validate the simulation results with experiments on a physical setup. We test three different environments shown in Fig. 3.3; a soft spring with stiffness $k_e \approx 850$ N/m, one stiff foam with $k_e \approx 6000$ N/m and a metallic rigid block to test hard contacts. They were placed below the end-effector of the slave device as shown in Fig. 3.3.

Next, the environment estimator is re-tuned experimentally. This process can be done without the SRC, for instance using a classical controller scheme like position-position architecture. Using the guidelines of Section 3.2.4 we finally use with the following parameters; $L_{|\epsilon_k|} = 0.9$ N/m, $Q_{fast} = \text{diag}([10^8, 10^3])$ and $Q_{nom} = 0.5 \times \text{diag}([10^3, 10^{-2}])$.

Next, for implementation of the switching architecture we tested several SRCs.

During the experimental phase we noticed that the output of the environment estimator worsens for high values of stiffness, e.g. $k_e > 5000$ N/m, having high noise and uncertainty. This can be due to noise in the signals, for example because of quantization. Thus, we recommend to use switching boundaries within $k_e < 5000$ N/m. This made it difficult to differentiate between the uncertainty areas in that range, thus making the switching structure to fail. However, for stiffness values in the low and medium range, the environment estimator showed satisfactory results. Moreover, note that accuracy is needed only around overlapping regions, thus the SRC offers an advantage in that respect. On the other hand, some of the controllers appear to excite un-modelled high-frequency resonance dynamics, causing high frequency vibrations, which rendered these controllers useless. Based on those findings, we have selected the SRC corresponding to $N_c = 2$ and $\bar{k}_{e1} = 2000$ N/m in Table 3.2, hereafter referred as SRCN2, which still have an largely improved performance in comparison with the RC.

For the experiments, we drove the system under similar operating conditions as to the simulation part, i.e. Transient Parts and Permanent Contact Part. The time domain response of the closed-loop system is shown in Fig. 3.16, where the y -axis of the \hat{k}_e -plots are zoomed-in for illustration purposes. The environment estimator works fast and with low noise for environment stiffness up to $k_e \approx 5000$ N/m. The discrepancy for high stiffness values will be explained later on this section together with the analysis of force versus position plots. By analysing the data of the time-responses, one can compare the time when the slave enters into contact with the environment and the time when the estimator switches to a fast convergence mode. For the first two environment stiffness this time was approximately 60 ms and for the hard contact this time was less than 10 ms. For all cases, after the fast mode was active, the convergence time was less than 10 ms. In fact, for the hard contact, the switch of controller took place within 15 ms after the slave device entered in contact with the metal block.

From the estimator structure in Section 3.2.4 one can see that the estimates of the environment stiffness \hat{k}_e and the exogenous environment force \hat{f}_e^* are simultaneously computed. In general, the accuracy and convergence of the parameters of an estimator depend not only on the tuning but also on having a correct model. Thus, the proposed estimator works well only for environments where stiffness is the dominant phenomenon. In the experimental results, we can see that $\hat{k}_e(k)$ stays around an average value despite continuous movements. This is an indication that the parameters have reached convergence. Moreover, the estimations accuracy was enough to distinguish between the different test springs, which is the main goal of the use of the estimator in the multi-controller structure. A correct tuning of the proposed estimator is important, this because a fast detection in the changes allows to schedule the controllers on time. We emphasize that accuracy is only needed to estimate which region of stiffness is active.

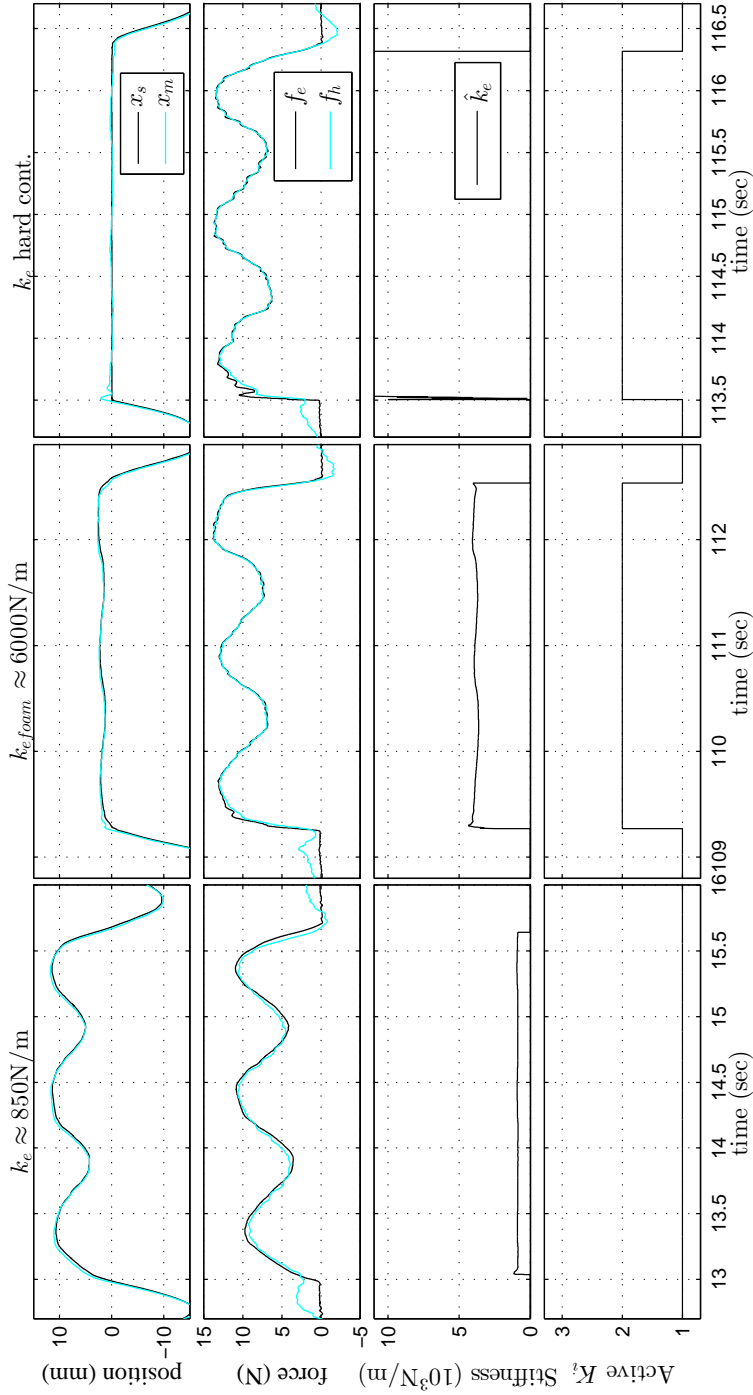


Figure 3.16: Time domain responses from experiments during interaction with different springs, using a Switching Robust Controller (SRC) with $N_c = 2$. y -axis of the \hat{k}_e -plots are zoomed-in for illustration purposes.

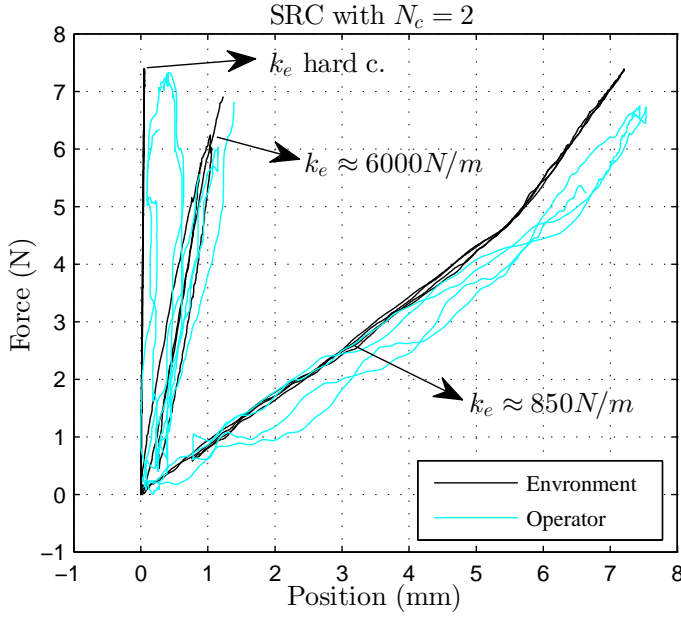


Figure 3.17: Force versus Position plots from experiments of interaction with different springs during the PCP using the SRCN2. The larger the slope the larger the stiffness.

During the TP, most of the transitions are made in a stable and smooth fashion despite that the environment changes rapidly and the switching between controllers. These results are in accordance with the obtained simulations results. Although theoretically the controller is designed for k_e up to 20000 N/m, the system remained stable during the transition from free-air to the hard contact, showing only a small overshoot. Moreover, the depicted response of the hard contact corresponds to a soft hand's grip of the end effector, for medium-hard grips transitions with less overshoot were achieved.

Next, regarding the PCP, force and position tracking results are very similar to those of simulations, despite that we implemented a controller with a slightly increased γ . The results of the PCP are further analysed by plotting the forces versus the positions at both master and slave sides as shown in Fig. 3.17. At first sight, the stiffness reflected to the operator appears to be close to the real environment stiffness for all test springs. The results are similar to those of the SRCN3 shown in the right plot of Fig. 3.13. The main difference is that for the soft environment, during the experiments of the SRCN2 the resemblance of a pure stiffness on the operator side is less than in simulations of the SRCN3. This

Table 3.4: Orthogonal linear regression analysis results to evaluate stiffness reflection from the experiment results. k_r is the estimated stiffness and d_r is the mean distance of the estimated line. Between brackets the percentage of the environment stiffness that is reflected to the operator is shown.

Parameters	Units	Env.	Operator
			SRCN2
k_r	N/m	835	743(88%)
$d_k \times 10^{-4}$	-	0.51	2.96
k_r	N/m	6370	5641(88%)
$d_k \times 10^{-4}$	-	0.76	0.81
k_r	N/m	141110	54458 (39%)
$d_k \times 10^{-4}$	-	0.02	1.34

is also the case in simulations using the SRCN2 (not shown here). For a pure environment stiffness, the discrepancy on the operator side is a result of a phase difference between the force and position signals reflected to the operator. Such phase difference is not directly minimized during the control synthesis. Instead, the magnitude of the force and position tracking error is minimized. Thus, two controllers can result in a similar system's performance level γ but different phase behavior between the force and position signals reflected to the operator. During the experiments with the SRCN2, those added dynamics were slightly noticed, being the stiffness still the main phenomenon felt by the operator. To quantify the results in Fig. 3.17, a similar analysis as with the simulation results is done. We performed an analysis of the experimental force versus position plots of the PCP by fitting straight lines to them using an orthonormal regression. The results of the analysis are displayed in Table 3.4. Because the stiffness of the soft spring changes at $x_e > 5$ mm, for that specific case we restricted the data to $x_e < 5$ mm. One can see from the table that a high percentage of the environment stiffness is reflected to the operator for the soft spring and the stiff foam. Moreover these percentages are also similar to those obtained in simulations of the SRCN3 (see Table 3.3), which has a similar γ . For the hard contact, it seems that the reflected stiffness is poor with only 39% of the original stiffness. However, the reflected stiffness $k_r = 55\,000$ N/m is high enough to give the operator a realistic feeling of a hard wall. Interestingly, for the stiff-foam and the hard contact, the environment stiffness values in Table 3.4 are higher than those estimated by the environment estimator, see Fig. 3.16. The reason is that high stiffness values result in lines with high slopes. The environment estimator uses a least squares optimization, which penalizes the deviation points to a line only in the force signal, making it more sensitive to sensor noise for high values of stiffness. Thus, the stiffness estimator accuracy is compromised for high stiffness values. Instead, the results in

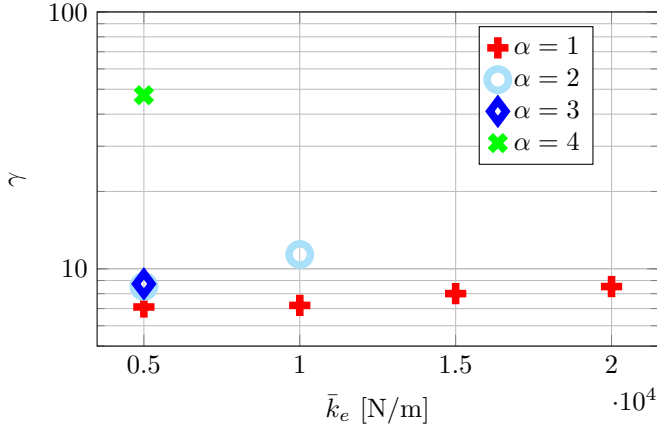


Figure 3.18: Weighted \mathcal{L}_2 -gain performance analysis of the SRC2 for different operator masses $m_h = \alpha m_h^N$ with $m_h^N = 0.123$ kg.

Table 3.4 were obtained with an orthonormal regression which uses the distance of the points to the fitted line, which makes this technique more accurate. Accuracy for all environment stiffness values in the range of interest is not required in the proposed multi-controller structure, being this property one of its main advantages. An adequate estimation \hat{k}_e is only needed in the overlapping region between the uncertainty sets Δ_1 and Δ_2 . Thus, the recursive least squares method used by the environment estimator still provides a good solution.

Now, the focus on this work was on improving the performance given that the uncertainty description matches the experimental conditions. Thus, because the modelling assumes a low operator mass, the former experiments were performed trying to use only the operator's hand as shown in Fig. 3.3. As soon as this operating conditions are kept, we drove the system in different ways but we could not destabilize it. However, we experimented with other operator configurations in which more muscles and therefore more mass is used. For those cases we observed that the system presented unstable behaviour for transition to stiff environments. The methodologies based on model, like the one here used, guarantee the required performance under the explicitly modelled dynamics of the system. Thus for conditions outside those considered during the synthesis process no a priori conclusion can be made. Nevertheless, we can make an analysis on how the robust performance of the system is affected as a function of the operator mass.

Consider Fig. 3.18 in which we make an analysis of the performance of the closed loop system in Fig. 3.7, i.e. including weighting filters, as a function of \bar{k}_e , i.e. the

maximal environment stiffness. The different plots correspond to different operator masses $m_h = \alpha m_h^N$ as a function of the nominal operator mass $m_h^N = 0.123$ kg found in Section 3.2.1, the rest of the parameters remain unchanged. For the case $\alpha = 1$, as expected the system is robustly stable for all $\bar{k}_e \leq 2.0$ kN/m. For $\alpha = 2$, no γ value was found for $\bar{k}_e \geq 1.5$ kN/m, which means that robust performance is not guaranteed in that region. Moreover for $\bar{k}_e \leq 1.0$ kN/m a degradation in performance is already noticeable. For $\alpha = 3$ and $\alpha = 4$, γ values were only found for $\bar{k}_e \leq 5.0$ kN/m and a trend in degradation of performance can be noticed as the operator mass increases.

Finally, we give some indications on how the uncertainty description can be improved to account a priori also for larger ranges of operator's mass. It is desirable to include the operator parameters ranging from zero up to the maximum of their variation. This ranges from the case when the operator releases the device, up to the case when a tight grip is performed under different arm-hand configurations. However, there are two main challenges while doing so. On one hand, when the parameters become zero, notice that the system becomes uncontrollable in terms of performance because the controller has no more effect on f_h . On the other hand, the constant multipliers utilized here for uncertainty description takes into account arbitrary fast time-varying parameters, thus it introduces too much conservatism if also the operator's mass is made uncertain. The first issue could be addressed by separating conditions for robust stability and for robust performance, thus having two different uncertain parameter ranges for each of them. Reduction of the conservatism in the second issue is possible via frequency-dependent, i.e., dynamic multipliers (Megretski and Rantzer (1997)), with which is possible to imposed bounds on the rate of variation of the operator's parameters. These issues will be topic of future research.

3.4 Conclusions

In this chapter we proposed a new approach towards control design for bilateral teleoperation. We used a multi-controller structure in which several robust controllers are scheduled according to an estimate \hat{k}_e of the environment stiffness. The synthesis results demonstrated that with the proposed Switching Robust Controller (SRC) we were able to improve the achieved performance in comparison with the case when only a single LTI robust controller is used. Simulations and experiments validated the synthesis results, the designed SRC achieved robust performance for all the uncertainty region it was designed for, i.e. low mass operator with time-varying stiffness and time-varying environment stiffness within a wide range. Moreover, the switching among robust controllers was made in a stable and smooth way, because they all share a common Lyapunov function.

In the next chapter, we propose a similar multi-controller structure, in which stable switching among controllers is achieved without the requirement of a common Lyapunov function.

Chapter 4

Switching Robust Control via Dwell Time Conditions

IN switching robust control, stable and smooth switching among controllers will be guaranteed by the existence of a common Lyapunov function. In this chapter, we propose a method to further reduce conservatism in the achievable performance of switching robust control synthesis for teleoperation systems. In this approach multiple Lyapunov functions with a special structure are introduced, which are linked by conditions of minimum average dwell time switching among controllers. We show the advantage of the proposed method by means of a control design synthesis for a 1-DoF teleoperation system, and by means of simulations of the corresponding closed loop system.

4.1 Introduction

Teleoperation systems are used to manipulate a remote environment by means of a master and a slave device. Moreover, the use of haptic feedback can provide a feeling of tele-presence to the operator. It is desirable that the system presents high performance, e.g. the operator feels as if he/she is manipulating the environment directly, in a stable fashion. Nevertheless, the inherent trade-

This chapter is based on the following manuscript: López Martínez, C. A., Molengraft, R. v. d., and Steinbuch, M. (2014d). Switching robust control synthesis for teleoperation via dwell time conditions. In *9th International Conference, EuroHaptics 2014*, Versailles, France. Springer. To appear online

off between performance and (robust) stability represents a challenging problem in designing controllers that meet an appropriate balance (Hokayem and Spong (2006), Passenberg et al. (2010)). During many years the focus of the control design was only on stability. Therefore, passivity (Niemeyer and Slotine (1991)) based methods have been widely used to design controllers that guarantee stability but performance is often not taken into account. Moreover, some of these techniques are only applicable to Linear Time Invariant (LTI) systems, while, in practice operator/environment dynamics are inherently time-varying and partially bounded. Some works have explicitly addressed performance and stability while incorporating those properties. For instance, Vander Poorten (2007) used virtual shunt dynamics to put bounds on the maximum operator impedance. In Chapter 2 we have used a parametric model to include time variation and boundedness of the operator and the environment dynamics. This allowed us to balance transparency and stability during the control design process. We achieved a limited robustness range of environment stiffness, not fully covering realistic conditions in applications such as minimally invasive surgery, needle insertion, etc., in which environment stiffness can vary from $83N/m$ for fat, up to $6902N/m$ for the ribcage bone, see Bankman et al. (1990). Furthermore, hard contacts might be present for example during collision between instruments. Therefore, it is desirable to further increase the range of environment-related parameters for which performance and stability can be guaranteed in order to cover the requirements of real-life surgical conditions.

To increase the region of performance, one can think about estimating the environment stiffness and use such estimation to design a controller that adapts accordingly. Willaert et al. (2010) and Cho and Lee (2009) use environment estimation for bilateral teleoperation control. However they do not provide quantitative information on the environment stiffness range in which robust performance is achieved, or the achieved operating range is limited to soft environment stiffness. Moreover, these works rely on unbiased, low noise and fast convergence of the estimated environment stiffness, requirements which in practice are difficult to meet simultaneously.

In Chapter 3 we proposed the use of switching robust control. We accounted for uncertainty in the operator and environment dynamics as well as uncertainty and noise in the estimation of the environment stiffness that is used for control scheduling. The controllers were designed such that they share a common quadratic Lyapunov function, which ensures stability under arbitrary fast switching between them. This in fact adds conservatism since it is expected that consecutive switching between controllers does not happen infinitely fast. Therefore, to decrease such conservatism, an average switching dwell time concept (Hespanha and Morse (1999)) can be used. Its application to control synthesis poses a challenging problem due to non-linearity of the resulting conditions. Such a concept has been

already used in Kruszewski et al. (2012) for robustness against time-varying delays, and also in Lu et al. (2006) for LPV control of an aircraft. Based on the latter work we propose an extension to the methods in Chapter 3, such that the requirement of a common Lyapunov function is relaxed and we find conditions for control synthesis that reduce the conservatism in the achievable performance. This is the first time that conditions of average dwell time are used to synthesize controllers in switching robust control for teleoperation systems. We validate the proposed method by means of a control design synthesis for a 1-DoF teleoperation system and we present simulations showing transition and contact with different environments.

In Section 4.2 we briefly discuss the model of the 1-DoF teleoperation system and we describe the framework for control synthesis of the proposed method. Simulations are presented and discussed in Section 4.3. Finally, in Section 4.4 the conclusions are presented.

4.2 Adding control design flexibility via dwell time conditions

4.2.1 Model of the teleoperation system for switching robust control

Generalized plant

We use the same model as in Chapter 2 which is briefly discussed here. The model consists of two subsystems, an operator/master-device pair and an environment/slave-device pair. We consider master, slave devices and environments with mass-damper-spring dynamics. For the operator's arm model, we used the same model as the one that is identified in Chapter 2. The model is described by an impedance $Z_h(s)$, which consists of a mass-damper-spring system and a filter $Q_h(s)$ modeling the operator's arm-hand dynamics above 10 Hz. In such a model only the operator stiffness k_h is considered to be uncertain and time-varying. Therefore, $\Delta_e = k_h$ represents the uncertainty block of the operator/master-device dynamics. Similarly, only the environment stiffness k_e is considered uncertain. Therefore, $\Delta_h = k_e$ represents the uncertainty block of the environment/slave-device pair dynamics.

Subsequently, all different components are gathered and the teleoperation is modeled using a so called generalized plant structure. The system model's structure is shown in Fig. 4.1, where q and p are the signals interfacing the uncertainty

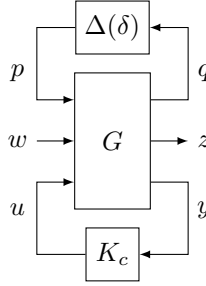


Figure 4.1: Generalized plant.

block Δ , w the disturbances of the system, y the measured signals, u the actuation signals, and z the performance signals. G contains all fixed parameters of operator, master and slave devices. The controller K_c in this case represents the controller to be designed. In the model, the operator stiffness k_h and the environment stiffness k_e are assumed to be uncertain, bounded and they are also considered time-varying to account for more realistic behavior. Thus, the number of uncertain parameters of the system is $n_p = 2$ and the vector of uncertain parameters is $\delta = \text{col}(\delta_1, \delta_2)$ with $\delta_1 = k_h$, $\delta_2 = k_e$. The uncertainty block is then defined as $\Delta(\delta(t)) = \begin{bmatrix} k_h(t) & 0 \\ 0 & k_e(t) \end{bmatrix}$, $\Delta \in \mathbf{\Delta}$, where

$$\mathbf{\Delta} = \left\{ \begin{bmatrix} k_h & 0 \\ 0 & k_e \end{bmatrix} : k_h \in [\underline{k}_h, \bar{k}_h], k_e \in [\underline{k}_e, \bar{k}_e] \right\}.$$

Please see Section 2.2.1 for details.

Augmented plant model for control design

Before introducing the model used for control design, first we discuss the main idea of switching robust control for bilateral teleoperation presented in Chapter 3. It consists of designing a specific number N_c of LTI controllers, in which the controller K_i , $i = 1, \dots, N_c$ has an uncertainty region $\mathbf{\Delta}_i$ of robust performance, such that $\mathbf{\Delta} \subseteq \mathbf{\Delta}_1 \cup \dots \cup \mathbf{\Delta}_{N_c}$. Each K_i is then activated in its corresponding region $\mathbf{\Delta}_i$ based on an estimate \hat{k}_e of k_e with possibly uncertainty and noise.

Thus, the uncertainty region $\mathbf{\Delta}$ is partitioned in N_c sub regions

$$\mathbf{\Delta}_i = \left\{ \begin{bmatrix} k_h & 0 \\ 0 & k_{ei} \end{bmatrix} : k_h \in [\underline{k}_h, \bar{k}_h], k_{ei} \in [\underline{k}_{ei}, \bar{k}_{ei}] \right\}$$

such that $\mathbf{\Delta} \subseteq \mathbf{\Delta}_1 \cup \dots \cup \mathbf{\Delta}_{N_c}$, for $i = 1, \dots, N_c$ as illustrated in Fig. 4.2. Based on the figure, we define uncertainty vectors $\delta_{(i)} = \text{col}(k_h, k_{ei})$, $i = 1, \dots, N_c$. Define

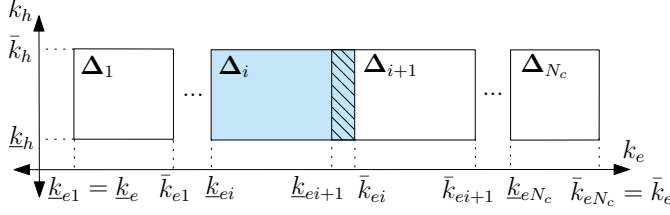


Figure 4.2: Uncertainty regions Δ_i of a switching robust controller.

also the uncertainty blocks $\Delta_i(\delta_{(i)}) = \begin{bmatrix} k_h & 0 \\ 0 & k_{ei} \end{bmatrix}$ for $i = 1, \dots, N_c$ such that $\Delta_i \in \Delta_i$. Note that although k_e is estimated, it is still considered as an uncertainty on each sub-region Δ_i . There is overlap between the regions to avoid incorrect scheduling of controllers due to uncertainty and noise in the estimation of k_e , e.g. when a controller is activated in a region Δ_i that does not correspond to it. We consider that the estimate \hat{k}_e of k_e is given by $\hat{k}_e = k_e \pm \varepsilon(k_e) + \eta(k_e)$ where $\varepsilon(k_e)$ represents the magnitude of the uncertainty in \hat{k}_e and $\eta(k_e)$ represents a zero-mean noise signal in the estimation whose magnitude is bounded, i.e. $|\eta(k_e)| < \eta_c$ for $k_e \in [\underline{k}_e, \bar{k}_e]$. The distribution of the regions is similar as in Chapter 3 and is specified in more detail in Section 3.2.3.

Next, we need to augment the model shown in Fig. 4.1 in order to incorporate the uncertainty partitions $\Delta_i, i = 1, \dots, N_c$ and a more suitable form that is usable for control design. Consider the model diagram presented in Fig. 4.3 in which we have augmented and partitioned the model in Fig. 4.1 in N_c augmented generalized plants \tilde{G}_i . The different components of the augmented model are described in the same way as in Section 3.2.2. We summarize the description as follows:

The blocks V and W are weighting filters described with stable LTI systems. They allow to shape in frequency domain the desired system performance. See Section 3.2.5 for details. \tilde{w} and \tilde{z} are weighted copies of w and z via predefined filters V and W respectively. That is $w = V\tilde{w}$ and $\tilde{z} = Wz$. $\tilde{\delta}_{(i)} = \text{col}(\tilde{k}_h, \tilde{k}_{ei}), i = 1, \dots, N_c$, are the transformed version of the parameters vectors $\delta_{(i)}$. The specific transformation is given in Section 3.2.3. $\tilde{\Delta}_i(\tilde{\delta}_{(i)}), i = 1, \dots, N_c$ is the block diagonal concatenation of the parameters in $\tilde{\delta}_{(i)}$. The vector \tilde{q} and \tilde{p} contain the signals interfacing the new uncertainty block $\tilde{\Delta}$. Thus $\tilde{p}(t) = \tilde{\Delta}(\tilde{\delta}(t))\tilde{q}(t)$. The variable $r \in [0, 1]$ is a scaling factor that allows to scale down the uncertainty blocks $\tilde{\Delta}_i$. This allows to perform an iterative process during the control design in which one starts with the nominal case $r = 0$, i.e. no uncertainty, and finalizes with an unscaled uncertainty set for $r = 1$. We will refer to a nominal plant if $r = 0$. If $r = 1$ we have that $\Delta_i(\delta_{(i)})$ equals the dashed block in the upper part of Fig. 4.3. $T_{\Delta_i} : \mathbb{R}^{2n_p \times 2n_p}, i = 1, \dots, N_c$ are constant matrices that allow

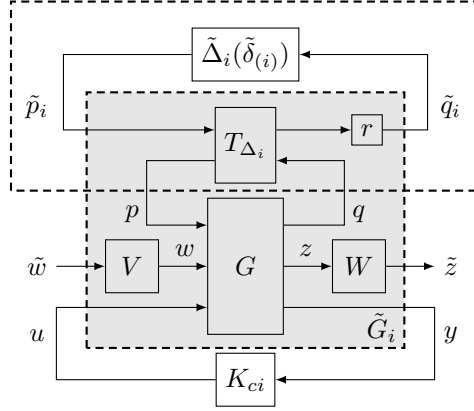


Figure 4.3: Set of generalized plants with weighting filters, uncertainty transformation and scaling. The dashed block in the upper part equals $\tilde{\Delta}_i(\delta)$ provided $r = 1$.

to map one to one the uncertain parameter set Δ_i to the transformed uncertain parameter set $\tilde{\Delta}_i$. The transformations T_{Δ_i} allows to obtain nominal values of $\Delta_i(\delta_{(i)}^{\text{Nom}}) \in \Delta_i$ for $r = 0$. The specific transformations from matrices $T_{\Delta_i, i=1, \dots, N_c}$ are given in Section 3.2.3. The blocks $K_{ci}, i = 1, \dots, N_c$ are then the LTI controllers $K_{ci}(s) = C_{ci}(Is - A_{ci})^{-1}B_{ci} + D_{ci}$, which we will identify by their state space description by writing

$$K_{ci}(s) = \left[\begin{array}{c|c} A_{ci} & B_{ci} \\ \hline C_{ci} & D_{ci} \end{array} \right], \quad i = 1, \dots, N_c. \quad (4.1)$$

One can derive a model of the generalized plant \tilde{G}_i for $i = 1, \dots, N_c$. We denote its state space representation by the following equation:

$$\begin{pmatrix} \dot{x}_p \\ \dot{\tilde{q}}_i \\ \dot{\tilde{z}} \\ \dot{y} \end{pmatrix} = \begin{pmatrix} A_i & B_{(i)1} & B_{(i)2} & B_i \\ rC_{(i)1} & rD_{(i)1} & rD_{(i)12} & rE_{(i)1} \\ C_{(i)2} & D_{(i)21} & D_{(i)2} & E_{(i)2} \\ C_i & F_{(i)1} & F_{(i)2} & 0 \end{pmatrix} \begin{pmatrix} x_p \\ \tilde{p}_i \\ \tilde{w} \\ u \end{pmatrix}, \quad i = 1, \dots, N_c$$

Uncertainty and performance description

Similarly as in Chapter 2, we will use a specific class of Integral Quadratic Constraints (IQCs) (see Megretski and Rantzer (1997)) to model uncertainties $\tilde{\Delta}_i \in \tilde{\Delta}_i$. Then consider \mathbf{P}_i as sets of symmetric matrices $P_i \in \mathbb{R}^{2n_p \times 2n_p}$ that satisfy

the following IQC

$$\int_0^{T_0} \begin{pmatrix} \tilde{\Delta}_i(\tilde{\delta}_i)\tilde{q}_i(t) \\ \tilde{q}_i(t) \end{pmatrix}^T P_i \begin{pmatrix} \tilde{\Delta}_i(\tilde{\delta}_i)\tilde{q}_i(t) \\ \tilde{q}_i(t) \end{pmatrix} dt \geq 0 \quad (4.2)$$

for all $q \in \mathcal{L}_2[0, T_0]$, $T_0 \in \mathbb{R}_+$, $\tilde{\Delta}_i \in \tilde{\Delta}_{\mathbf{i}}$ and $i = 1, \dots, N_c$. The matrix P_i is a so called *multiplier*. To describe bounded and time-varying real parametric uncertainties we used the same matrix families $\mathbf{P}_i, i = 1, \dots, N_c$ described in Sections 1.3 and 2.2.2.

We have chosen the performance criterion based upon the \mathcal{L}_2 gain of the mapping from disturbance channels \tilde{w} to the performance channels \tilde{z} as is customary in model-based \mathcal{H}_∞ control, e.g., see Skogestad and Postlethwaite (2005). The \mathcal{L}_2 gain from \tilde{w} to \tilde{z} can be expressed in a standard form as a quadratic performance criterion:

$$\int_0^\infty \begin{pmatrix} \tilde{w}(t) \\ \tilde{z}(t) \end{pmatrix}^T P_p \begin{pmatrix} \tilde{w}(t) \\ \tilde{z}(t) \end{pmatrix} dt < 0 \text{ for all } 0 \neq \tilde{w} \in \mathcal{L}_2, \quad (4.3)$$

with

$$P_p = \begin{pmatrix} -\gamma^2 I & 0 \\ 0 & I \end{pmatrix}$$

The standard form to describe performance in Eq. (4.3) allows the use of other quadratic performance criteria via P_p , see, e.g., Section 1.3 and Scherer and Weiland (2000). To keep the generality of the theory used here, we will use the symbol P_p to describe our specific performance criterion.

4.2.2 Switching robust control design using multiple quadratic Lyapunov functions

In Chapter 3, we designed a switching robust controller for the 1-Dof teleoperation system described in Appendix A. It consists of $N_c = 2$ controllers sharing a common quadratic Lyapunov function $V(x) = x^T \mathcal{X} x$, with x representing the state vector of the closed loop system. This makes the overall switched system globally stable in case of arbitrary fast switching between the N_c controllers (Liberzon (2003)). In this way, the design of the different $K_{ci}(s)$ controllers is linked to ensure robust performance under switching of controllers and for $\Delta \in \tilde{\Delta}$, given that each controller K_i is active in its corresponding region of operation $\tilde{\Delta}_i$. With this methodology, in Chapter 3 it was shown that it is possible to improve robust performance, as compared with the case when using a single controller. However, the requirement of a common Lyapunov function might limit the potential of the proposed multi-controller structure. To add additional flexibility other than having more than one controller, we propose the use of multiple Lyapunov functions.

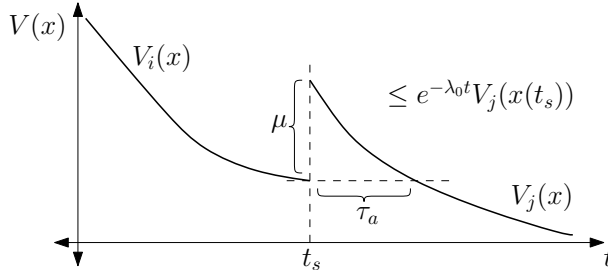


Figure 4.4: Interpretation of dwell time conditions

The disadvantage of the requirement of a common Lyapunov function is that it adds unnecessary conservatism. In real applications such as minimally invasive surgery, the slave devices might encounter sudden changes in the environment, however consecutive switching of environment is not expected to take place infinitely fast. Therefore, we might relax the requirement of a common Lyapunov function and allow a different one per controller, given that we guarantee specific conditions on how much they differ. In order to achieve this, we make use of the average dwell time concept in switching systems by Hespanha and Morse (1999). It basically states that a switched system has average dwell time τ_a if the average time between consecutive switches in the system is at least τ_a .

Such concept has been applied for stability analysis of switched systems, see Liberzon (2003). Consider a switched system with N_c subsystems. Consider a switching signal $\sigma(t) \in \{1, \dots, N_c\}$ that determines which subsystem is active at time t . Then consider that each subsystem of the switched system has a Lyapunov function $V_i(x)$ for $i = 1, \dots, N_c$ such that

$$V_j(x) \leq \mu V_i(x), \quad i, j = 1, \dots, N_c \quad (4.4)$$

for some $\mu > 1$. It is proven that (see Liberzon (2003), Section 3.2.2), if

$$\frac{\partial V_i}{\partial x} \dot{x} \leq -\lambda_0 V_i(x), \quad i = 1, \dots, N_c \quad (4.5)$$

for some $\lambda_0 > 0$, then the switched system is stable for every switching signal σ with average dwell time

$$\tau_a > \frac{\ln(\mu)}{\lambda_0}.$$

Eq. (4.5) guarantees a minimal exponential decay constant λ_0 of the Lyapunov functions $V_i(x), i = 1, \dots, N_c$. To interpret those results, consider Fig. 4.4, in which there is a switching from system i to system j at the time instant t_s . The value of the Lyapunov function after switching has a bound given by Eq. (4.4).

Thus, because of the minimal exponential decay rate guaranteed by Eq. (4.5), after τ_a seconds it is guaranteed that $V_j(x) \leq V_i(x)$ and it would be safe to switch to another controller again.

Now, this same concept is applied to the robust control design for bilateral teleoperation systems. We know that conditions on Theorem 2.1 and 3.1 come from the theory of dissipative systems (see Section 1.3), in which basically we have that

$$\frac{\partial V}{\partial x} \dot{x} \leq s(w, z) \quad (4.6)$$

where $s(w, z) \geq 0$ is a so called supplied function which is specified by the used performance criterion, see also Scherer and Weiland (2000). Thus, we simply have to extend (4.6) (applied to each closed loop i of Fig. 4.3) with the right hand side of Eq. (4.5) to obtain

$$\frac{\partial V_i}{\partial x} \dot{x} - s(w, z) \leq -\lambda_0 V_i(x), \quad \lambda_0 > 0, \quad i = 1, \dots, N_c, \quad (4.7)$$

which implies (4.5) if the external input $w = 0$. Consequently, a guaranteed exponential decay rate of the function $t \mapsto V(x(t))$ with decay rate λ_0 is obtained. Then using also (4.4) and quadratic Lyapunov functions of the form $V_i(x) = x^T \mathcal{X}_i x, i = 1, \dots, N_c$ we arrived to the following result:

Initially, assume we have certain $K_{ci}(s)$ that achieves nominal stability for each Δ_i for $i = 1, \dots, N_c$. That is for when $r = 0$. Moreover, let $\mathbf{P}_i, i = 1, \dots, N_c$ be the sets of symmetric matrices P_i that satisfy conditions (3.3) and (3.4). Then:

Theorem 4.1. *Given constants $\mu > 1, \lambda_0 > 0$, the closed loop systems $\tilde{G}_i(s) \star K_{ci}(s)$ with $r \in (0, 1]$ shown in Fig. 4.3 are robustly stable for all $\tilde{\Delta}_i \in r\tilde{\mathbf{\Delta}}_i$ with robust quadratic performance characterized by P_p if there exist symmetric matrices \mathcal{X}_i , and symmetric matrices $P_i \in \mathbf{P}_i$ such that*

$$\mathcal{X}_i \succ 0 \quad (4.8)$$

$$\mathcal{X}_i \preceq \mu \mathcal{X}_j \quad (4.9)$$

$$(\star)^T \left(\begin{array}{ccc|ccc} 0 & \mathcal{X}_i & 0 & 0 & 0 & 0 \\ \mathcal{X}_i & 0 & 0 & 0 & 0 & 0 \\ 0 & 0 & \lambda_0 \mathcal{X}_i & 0 & 0 & 0 \\ \hline 0 & 0 & 0 & P_i & 0 & 0 \\ 0 & 0 & 0 & 0 & P_p & 0 \end{array} \right) \left(\begin{array}{ccc} I & 0 & 0 \\ \mathcal{A}_i & \mathcal{B}_{(i)1} & \mathcal{B}_{(i)2} \\ I & 0 & 0 \\ \hline 0 & I & 0 \\ \mathcal{C}_{(i)1} & \mathcal{D}_{(i)11} & \mathcal{D}_{(i)12} \\ 0 & 0 & I \\ \hline \mathcal{C}_{(i)2} & \mathcal{D}_{(i)21} & \mathcal{D}_{(i)22} \end{array} \right) \prec 0 \quad (4.10)$$

holds for $i, j = 1, \dots, N_c$. Moreover, robust stability is achieved for switching between the uncertain closed loop systems $r\tilde{\Delta}_i \star \tilde{G}_i(s) \star K_{ci}(s)$, $i = 1, \dots, N_c$ if the average dwell time

$$\tau_a > \frac{\ln(\mu)}{\lambda_0} \quad (4.11)$$

The matrices $\mathcal{A}_i, \mathcal{B}_{(i)m}, \mathcal{C}_{(i)n}, \mathcal{D}_{(i)mn}$ $i = 1, \dots, N_c$, $m, n = 1, 2$ are given in (3.7) and correspond to the state space realizations of the systems obtained by closing the loop in Fig. 4.3 with the controller K_{ci} , such that the obtained system has as inputs the vector $\text{col}(\tilde{p}_i, \tilde{w})$, and as outputs the vector $\text{col}(\tilde{q}_i, \tilde{z})$. Therefore, the controller matrices $A_{ci}, B_{ci}, C_{ci}, D_{ci}$, are incorporated in the matrices in in (3.7).

Now, our goal is to find conditions that could lead us to reduce conservatism of the control synthesis procedure requiring a common Lyapunov function. However a new problem arises when translating conditions in Eq. (4.9) to synthesis conditions. To illustrate this, we describe first how a standard controller synthesis procedure works.

Similar as in Chapters 2 and 3, Eq. (4.10) is actually not a LMI when K_{ci}, \mathcal{X}_i and P_i are unknown. It is still possible to obtain controllers via an iterative synthesis procedure. If we iterate between a controller step to find controllers K_{ci} and an analysis step to find uncertainty multipliers P_i , it is possible to make Eq. (4.10) an LMI as follows. When the controllers K_{ci} are known, Eq. (4.10) becomes already a LMI, i.e. linear in the unknown parameters \mathcal{X}_i and P_i . However, in the case when P_i is known, two additional steps are needed to transform Eq. (4.10) into a LMI. The details of these steps are found in the work of Scherer and Weiland (2000). Here we will describe part of the first step, which is key to understand the control synthesis method proposed here. It consists of the congruence transformation of the Lyapunov functions $V_i(x) = x^T \mathcal{X}_i x$. Consider the next partition of the matrices \mathcal{X}_i ,

$$\mathcal{X}_i = \begin{pmatrix} X_i & U_i \\ U_i^T & * \end{pmatrix} \text{ and } \mathcal{X}_i^{-1} = \begin{pmatrix} Y_i & V_i \\ V_i^T & * \end{pmatrix} \quad (4.12)$$

with U_i, V_i arbitrary invertible matrices that satisfy $X_i Y_i + U_i V_i^T = I$. Next, if we apply a congruence transformation to Eq. (4.8) with matrix

$$\mathcal{Y}_{Ai} = \begin{pmatrix} Y_i & I \\ V_i^T & 0 \end{pmatrix} \quad (4.13)$$

it is transformed to

$$\mathbf{X}_i = \begin{pmatrix} Y_i & I \\ I & X_i \end{pmatrix} \succ 0. \quad (4.14)$$

In a similar way Eq. (4.10) is transformed with matrix

$$\mathcal{Y}_{Bi} = \text{diag}(\mathcal{Y}_{Ai}, I, I) \quad (4.15)$$

to an equation that depends on the collected matrix variables $v_i = \{X_i, Y_i, K_i, L_i, M_i, N_i\}$, where K_i, L_i, M_i, N_i are transformed variables that represent the controller. By an additional step such equation can be made affine in its unknowns, see Section 2.2.2 for a similar procedure applied to the synthesis of a single robust controller. The resulting transformed equations are given here for completeness:

Define

$$\begin{aligned} \mathbf{A}_i(v_i) &= \begin{pmatrix} A_i Y_i + B_i M_i & A_i + B_i N_i C_i \\ K_i & A_i X_i + L_i C_i \end{pmatrix} \\ \mathbf{B}_{(i)n}(v_i) &= \begin{pmatrix} B_{(i)n} + B_i N_i F_{(i)n} \\ X_i B_{(i)n} + L_i F_{(i)n} \end{pmatrix} \\ \mathbf{C}_{(i)m}(r, v_i) &= \begin{pmatrix} r_m(C_{(i)m} Y_i + E_{(i)m} M_i) & r_m(C_{(i)m} + E_{(i)m} N_i C_i) \end{pmatrix} \\ \mathbf{D}_{(i)mn}(r, v_i) &= \begin{pmatrix} r_m(D_{(i)mn} + E_{(i)m} N_i F_{(i)n}) \end{pmatrix} \end{aligned}$$

for $m, n = 1, 2$. $i = 1, \dots, N_c$. $r_1 = r$ and $r_2 = 1$. Define also

$$\begin{aligned} B_{(i)l}(v) &= \begin{pmatrix} \mathbf{A}_i(v) & \mathbf{B}_{(i)1}(v) & \mathbf{B}_{(i)2}(v) \\ \mathbf{C}_{(i)1}(v) & \mathbf{D}_{(i)11}(v) & \mathbf{D}_{(i)12}(v) \\ \mathbf{C}_{(i)2}(v) & \mathbf{D}_{(i)21}(v) & \mathbf{D}_{(i)22}(v) \end{pmatrix} \\ A_l &= \text{col}(I, (I \ 0 \ 0)); \\ Q_{(i)l} &= \text{diag}(0, Q_i, Q_p, \lambda_0 \mathbf{X}_i) \\ S_{(i)l} &= \text{col}(\text{diag}(I, S_i, S_p), 0) \\ U_{(i)l} &= \text{diag}(I, R_i^{-1}, R_p^{-1}) \\ T_l &= \text{diag}(0, I, I) \end{aligned}$$

for $i = 1, \dots, N_c$. Then Eq. (4.10) is equivalent to

$$\begin{pmatrix} A_l^T Q_{(i)l} A_l + A_l^T S_{(i)l} B_{(i)l}(v) + B_{(i)l}(v)^T S_{(i)l}^T A_l & B_{(i)l}(v)^T T_l \\ T_l^T B_{(i)l}(v) & -U_{(i)l} \end{pmatrix} \prec 0, \quad i = 1, \dots, N_c \quad (4.16)$$

Now, the main inconvenience with Theorem 4.1 to arrive at synthesis conditions comes from the fact that we can not apply a congruence transformation with \mathcal{Y}_{Ai} to Eq. (4.9) because it involves different indexes i, j . One can think of treating *only* equation (4.9) without transformation. Thus, from (4.12) we get the following equation for \mathcal{X}_i :

$$\mathcal{X}_i = \begin{pmatrix} X_i & U_i \\ U_i^T & -U_i^T Y_i V_i^{-T} \end{pmatrix} \quad (4.17)$$

The non-linear lower-right term in Eq. (4.17) poses an issue to make the synthesis process solvable with LMIs. To solve this issue, we use the same trick applied by Lu et al. (2006), which is described in the following paragraphs.

First, one can select $V_i = Y_i$ and therefore $U_i = Y_i^{-1} - X_i$, thus \mathcal{X}_i in Eq. (4.17) becomes

$$\mathcal{X}_i = \begin{pmatrix} X_i & Y_i^{-1} - X_i \\ Y_i^{-1} - X_i & X_i - Y_i^{-1} \end{pmatrix} \quad (4.18)$$

which can be written as

$$\mathcal{X}_i = \begin{pmatrix} I & -I \\ 0 & I \end{pmatrix} \begin{pmatrix} Y_i^{-1} & 0 \\ 0 & X_i - Y_i^{-1} \end{pmatrix} \begin{pmatrix} I & -I \\ 0 & I \end{pmatrix}^T.$$

Therefore, partitioning the closed loop state vector as $x = \text{col}(x_p, x_c)$, where x_p and x_c are the state vectors of the plant and controller respectively, the quadratic Lyapunov functions $V_i(x)$ becomes:

$$V_i(x) = x_p^T Y_i^{-1} x_p + (x_c - x_p)^T (X_i - Y_i^{-1}) (x_c - x_p) \quad (4.19)$$

In this partition x_p and x_c have the same dimension. This is indeed the case when the nominal controller is designed with the same methods proposed here.

Now, note that conditions in Eq. (4.4) are only necessary at the moment of switching. Therefore, if at the switching moments the controller state vector is reset to $x_c = x_p$, the Lyapunov function at the switching instant becomes

$$V_i([x_p, x_p]^T) = x_p^T Y_i^{-1} x_p \quad (4.20)$$

Next, if (4.14) holds, from partition in (4.12) we can conclude that $Y_i \succ 0$ and therefore $Y_i^{-1} \succ 0$, which can be substituted in condition (4.9) to obtain

$$Y_i^{-1} \preceq \mu Y_j^{-1}, \quad i, j = 1, \dots, N_c.$$

Finally, we can also conclude that

$$Y_i \preceq \mu Y_j, \quad i, j = 1, \dots, N_c, \quad (4.21)$$

which are conditions affine in (Y_i, Y_j) that can be used together with conditions in (4.14) and (4.16) to synthesize controllers K_{ci} , given that P_i is known and that the controller state is reset to $x_c = x_p$ at the switching instants.

We formalize the result by the following synthesis theorem.

Theorem 4.2. *For given $P_i \in \mathbf{P}_i$ and given constants $\mu > 1$, $\lambda_0 > 0$. There exist controllers $K_{ci}(s)$ and Lyapunov certificates \mathcal{X}_i as in (4.18) such that the closed loop systems $\tilde{G}_i(s) \star K_{ci}(s)$ are robustly stable for all $\tilde{\Delta}_i \in r\tilde{\Delta}_i$ with $r \in (0, 1]$ and with robust quadratic performance characterized by P_p if there exist variables $v_i = (X_i, Y_i, K_i, L_i, M_i, N_i)$ such that (4.14), (4.21) and (4.16) hold for $i, j = 1, \dots, N_c$. Moreover, robust stability is achieved for switching between the uncertain closed loop systems $r\tilde{\Delta}_i \star \tilde{G}_i(s) \star K_{ci}(s)$, $i = 1, \dots, N_c$ if the average dwell time*

$$\tau_a > \frac{\ln(\mu)}{\lambda_0}$$

provided that the controller is reset to $x_c = x_p$ when a switching occurs.

The matrices of the state space representation of each $K_{ci}(s)$ are then computed using the following equation

$$\begin{pmatrix} A_{ci} & B_{ci} \\ C_{ci} & D_{ci} \end{pmatrix} = \begin{pmatrix} U_i & X_i B_i \\ 0 & I \end{pmatrix}^{-1} \begin{pmatrix} K_i - X_i A_i Y_i & L_i \\ M_i & N_i \end{pmatrix} \begin{pmatrix} V_i^T & 0 \\ C_i Y_i & I \end{pmatrix}^{-1} \quad (4.22)$$

with $V_i = Y_i$ and $U_i = Y_i^{-1} - X_i$.

Before summarizing the iterative synthesis procedure, for the robust analysis steps we need Lyapunov certificates \mathcal{X}_i compatible with those obtained with Theorem 4.2, i.e. \mathcal{X}_i with structure as in (4.18). Therefore, to obtain P_i when K_i is known, we use the following theorem.

Theorem 4.3. *Given given constants $\mu > 1$, $\lambda_0 > 0$ and controllers $K_{ci}(s)$, the closed loop systems $\tilde{G}_i(s) \star K_{ci}(s)$ with $r \in (0, 1]$ shown in Fig. 4.3 are robustly stable for all $\tilde{\Delta}_i \in r\tilde{\Delta}_i$ with robust quadratic performance characterized by P_p if there exist symmetric matrices $X_i \succ 0$, $Y_{Ii} = Y_i^{-1} \succ 0$, and symmetric matrices $P_i \in \mathbf{P}_i$ such that*

$$\mathcal{X}_i = \begin{pmatrix} X_i & Y_{Ii} - X_i \\ Y_{Ii} - X_i & X_i - Y_{Ii} \end{pmatrix} \succ 0 \quad (4.23)$$

$$Y_{Ii} \preceq \mu Y_{Ij} \quad (4.24)$$

and (4.10) hold for $i, j = 1, \dots, N_c$. Moreover, robust stability is achieved for switching between the uncertain closed loop systems $r\tilde{\Delta}_i \star \tilde{G}_i(s) \star K_{ci}(s)$, $i = 1, \dots, N_c$ if the average dwell time

$$\tau_a > \frac{\ln(\mu)}{\lambda_0}$$

provided that the state of the controller is reset to $x_c = x_p$ when a switching occurs.

We finally summarize the synthesis procedure as follows. We define each region Δ_i , transform it and scale in the same way as in the methods in Chapter 3. Then, without loss of generality, the uncertainty parameters can be transformed into new parameters $\tilde{k}_h \in [0, 1]$, $\tilde{k}_{ei} \in [0, 1]$ such that transformed uncertainty becomes $\tilde{\Delta}_i = \begin{bmatrix} \tilde{k}_h & 0 \\ 0 & \tilde{k}_{ei} \end{bmatrix}$. Then, we design first a nominal controller for $r = 0$, by using Theorem 4.2 after removing the uncertainty channels. Then, we iterate the following steps:

- for fixed K_i , maximize r using the bisection algorithm and get the corresponding matrices P_i by using Theorem 4.3 while minimizing γ , keeping $\gamma < \bar{\gamma}$, for a certain $\bar{\gamma}$.
- for fixed P_i , maximize r using the bisection algorithm and get the corresponding controllers K_{ci} by using Theorem 4.2 while minimizing γ , keeping $\gamma < \bar{\gamma}$, for a certain $\bar{\gamma}$.
- Once $r = 1$ is achieved, we iterate the two previous steps and on each the performance level γ is minimized until no further progress can be made.

The value $\bar{\gamma}$ is introduced such that at the initial steps of the iterative synthesis procedure we allow γ to be large. This allows to avoid local minima around small values of the uncertainty scaling r . Then, after reaching $r = 1$ we minimize γ . Details on the iterative procedure are given in Appendix B, from which we have used the version II of the iterative procedure.

Now, the reset conditions introduced here helped to relax the requirement of a common Lyapunov function. However, the actual implementation of such reset poses two issues. Firstly, it requires the implementation of an observer that could follow abrupt changes accurately and in a robustly stable fashion. Secondly, even if we implement such observer, sudden high frequency peaks might be introduced when resetting the controller state, which in theory does not represent an issue for stability since the total Lyapunov function remains decreasing, however unmodeled dynamics can be excited in practice leading to instability. In fact such peaks were observed in simulation. A solution to avoid those issues is not to perform the controller state reset at the moment of switching. All we have to do is to perform a final analysis using Theorem 4.1, take $r = 1$ and minimize γ . In fact even less conservative results are obtained in the analysis since we do not have to enforce a particularly structure in \mathcal{X}_i . Thus, the reset conditions are only used to be able to have a synthesis procedure based on LMI's that relax the requirement of a common Lyapunov function.

4.3 Simulation results

To show the advantage of the proposed method with respect to that in Chapter 2 and Chapter 3. In this chapter we use the model parameters from Chapter 2 of the following subsystems: weighting filters, operator, master and slave parameters. The uncertainty partition is done in the same way as in Chapter 3. The rest of the parameters are set to: $N_c = 2$, $k_e \in [80, 20000]N/m$ to include soft and stiff environments, $\bar{k}_{e1} = 3900N/m$, $\bar{\gamma} = 40$, $\mu = 1.2$, $\lambda_0 = 0.3$, $|\epsilon(k_e)| < 0.15k_e$ and $\eta_c < 50N/m$. The remainder parameters are then computed: $\tau_a = 0.608sec$, $\underline{k}_{e1} = 80N/m$, $\underline{k}_{e2} = 2350N/m$ and $\bar{k}_{e2} = 20000N/m$.

The LMIs involved in the controller synthesis procedure were solved using the solver Sedumi by Sturm (1999). We performed the synthesis procedure for three cases: a single controller, two controllers with a common Lyapunov function and two controllers with different Lyapunov functions with average dwell time conditions. For the first and second case we obtained $\gamma = 24.7$ and $\gamma = 19.64$ respectively, for the third case we obtained $\gamma = 14.95$ using Theorem 4.3, and after performing analysis without controller state reset using Theorem 4.1 we obtained $\gamma = 12.98$.

To further asses the performance of the different controllers, we simulate the system in time domain. For the operator stiffness we used the nominal stiffness $k_h = 776.7N/m$. For the environment, we used different virtual springs such that when the slave position changes from free air at $x_s < 0$ to $x_s \geq 0$, we test three different stiffness values consecutively on each transition to $x_s \geq 0$: $k_e = 800N/m$, $k_e = 4000N/m$ and $k_e = 20000N/m$. To simulate the desired task we used the human active force $f_h^* = (0.2 - 0.6\cos(\pi t))N$. Moreover, because the implementation of the environment estimator is not on the focus of this work, we constructed manually the estimate \hat{k}_e by taking $\epsilon(k_e) = 0.14k_eN/m$ and $\eta_c = 49N/m$.

The time domain responses of master and slave device's positions and operator and environment forces are depicted in Fig. 4.5 for all three cases from left to right. For the last two cases there is a switch of controllers so that the corresponding controller K_2 is active when in contact with the springs $k_e = 4000N/m$ and $k_e = 20000N/m$. At first sight, all cases achieve position and force tracking. The differences between the test cases can be better seen in the error signals, which are further illustrated in Fig. 4.6. From the position error signals, one can see that the position tracking is better with the first case compare to the second one, however improvement can be noticed in the force tracking of the second case with respect to the first. In fact we obtained a better γ for the second case. The weighting filters scaling could be such that slightly more relevance is given to force tracking. The weighting filters tuning can be evaluated when the system is tested experimentally.

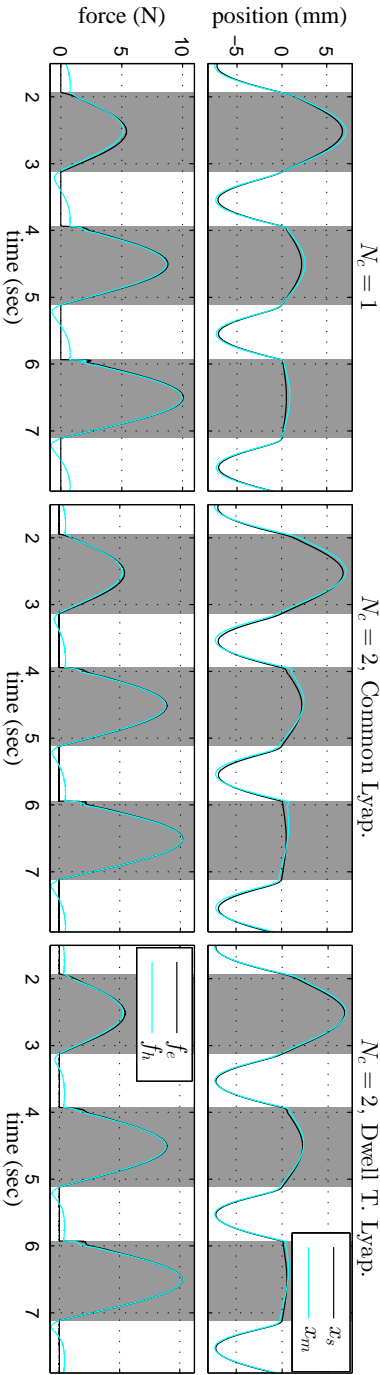


Figure 4.5: Time domain responses of positions and operator forces when using different control synthesis methods. Three environment stiffness are tested, the gray areas show when the slave is in contact with the environment.

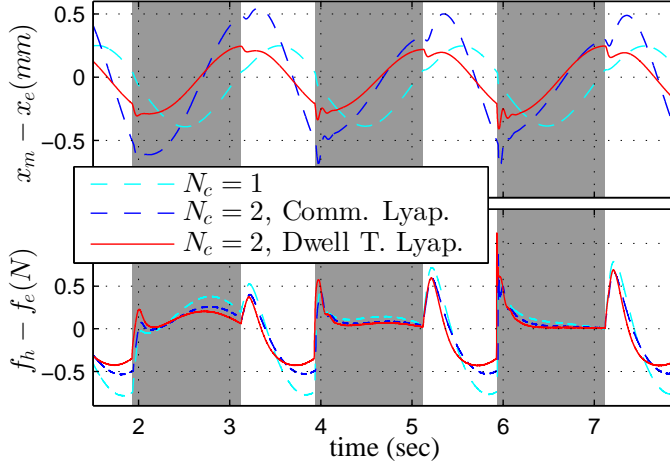


Figure 4.6: Force and position error responses. Gray areas indicate contact with environment.

Now, using the controller synthesized with the method proposed here, one can see that in general both position and force tracking are improved with respect to the other two cases. The improvement is especially noticeable in the force tracking signals after the peak response following the controller switching. However, an increase in the peak force right after contact with the different environments is observed for the controller proposed here.

When the slave device is in free air, the smaller the magnitude of the force felt by the operator, the better is the haptic feeling of free air, and it is improved by the last two controllers in comparison with the case where a single controller is used. Moreover, one can see that all the controllers can handle the transition from $k_e = 0\text{N/m}$ to $k_e = 20000\text{N/m}$, representing a hard contact.

As a last remark, the controller here designed guarantees robust stability given that the switching sequence satisfies the minimum average dwell time. Under the specific testing scenarios presented here, simulations showed that the transitions are stable. However, one can wonder whether there is any guarantee that the system will always present stable transitions and satisfy the average dwell time. In theory, the theorems presented here do not guarantee that explicitly because smoothness during the switching is not guaranteed. For instance, large value of μ gives more freedom during the control design which can improve the performance level γ . However, for large values of μ , the procedure would get close to the case of having independent Lyapunov functions, for which a direct switch among controllers would cause oscillatory behavior that may compromised the

stability. Therefore, there is a trade-off between a smooth transition guaranteed by a common Lyapunov function and an improved performance level γ obtained via multiple and independent Lyapunov functions. Moreover, a large value of λ_0 results in an increased rate of decay of the Lyapunov functions V_i , which can be beneficial to rapidly reject transient responses after controller switching. However, there might not exist a controller that results in a large value of λ_0 and also meets the requirements imposed on the actuation signals via the weighting filters.

In fact, initial exploratory experiments were performed with the controller proposed here. For some tests, the increased peak forces in the system's response, after contact with the environment, made the operator to react in such a way that the average dwell time was not satisfied. Hence, it would be interesting to study in depth the effect of the design variables μ and λ_0 not only on γ , but also on the time-domain response (in simulations and experiments) during the transition after controller switching.

4.4 Conclusions

In this chapter, we have proposed a new methodology for control synthesis of a switching robust controller for bilateral teleoperation. It is not required to have a common Lyapunov function among its controllers but instead the controllers are linked with a condition based on average dwell time switching. The synthesis results showed already that we can achieve a lower \mathcal{L}_2 gain γ using the new relaxed conditions. Moreover, simulations confirmed the expected improvement in position and force tracking with respect to the case where a single controller and two controllers with a shared Lyapunov function are used. Thus the results demonstrated the potential of the approach towards increasing performance of the system.

In the next chapter, we will introduce a multi-controller structure that allows for independent performance optimization of its different robust controllers.

Chapter 5

Bumpless Transfer of Robust Controllers for Teleoperation

IN THIS CHAPTER we propose a controller scheme with multiple robust controllers in which every controller is performance-optimized separately. The switching among them is based on bumpless transfer and they are scheduled using an environment stiffness estimator. Limited accuracy and noise of such estimator is also taken into account during control design. We show the applicability of the approach by experiments on a 1-DOF teleoperated system.

5.1 Introduction

Bilateral teleoperation systems are intended to provide a feeling of tele-presence using force feedback while an operator manipulates a remote environment by means of a master and a slave device. It is desirable that the system presents high performance, e.g. the operator feels as if he/she is manipulating the environment directly, in a stable fashion. However, the inherent trade-off between performance and (robust) stability represents a challenging problem in designing controllers that meet an appropriate balance, see, e.g., Hokayem and Spong (2006), Passenberg et al. (2010). Passivity (Niemeyer and Slotine (1991)) based methods have been widely used to design controllers that guarantee stability but performance

This chapter is based on the following manuscript: López Martínez, C. A., Molengraft, R. v. d., and Steinbuch, M. (2014a). High performance teleoperation by bumpless transfer of robust controllers. In *IEEE Haptics Symposium 2014*, pages 209–214, Houston, TX, U.S.A

is not taken into account. On the other hand, operator/environment dynamics are inherently time-varying, operator dynamics are bounded and in many applications environment parameters such as mass, damping and stiffness are bounded as well. Such properties are often not taken into account explicitly. Some works have addressed performance and stability while incorporating knowledge on operator/environment bounded dynamics. For instance, in Vander Poorten (2007) the author used virtual shunt dynamics to put bounds on the maximum operator impedance. In the methods presented in Chapter 2, we included such properties during the control design process to balance transparency and stability. We also experimentally validated the design of a robust Linear Time Invariant (LTI) controller, which yields a high performance for time-varying environment stiffness in a limited range. However, for applications such as minimally invasive surgery, needle insertion, etc., environment stiffness can vary from $83N/m$ for fat, up to $2483N/m$ for bone (see Gerovich et al. (2004)) and even up to $6902N/m$ for the ribcage (see Bankman et al. (1990)). Furthermore hard contacts might be present for example by collision between instruments. Therefore, it is desirable to further increase the range in which performance and stability is achieved in order to cover the requirements of real-life surgical conditions.

In many cases there is no guarantee that a single LTI controller exists that ensures both high performance and stability for a wide range of environment stiffness values. In case such controller exists, finding it involves a non-convex optimization process, see, e.g., Vander Poorten (2007) and Chapter 2, which might lead to a local optimum. To increase the region of performance, one can think about estimating the environment stiffness and use such estimation to design a controller that adapts accordingly. Some works, e.g. Willaert et al. (2010), Cho and Lee (2009), use environment estimation for bilateral teleoperation control. However they do not provide quantitative information on the environment stiffness range in which robust performance is achieved, or the achieved operating range is limited to soft environment stiffness below $500N/m$. Moreover, these works rely on unbiased, low noise and fast convergence of the estimated environment stiffness, requirements which in practice are difficult to meet simultaneously.

Switching control could provide a solution to the problem into consideration. Some existing switching control methods suggest to switch between different operating points of the overall system, see, e.g., Leith and Leithead (2000), Liberzon (2003), but uncertainty in the parameters is not taken into account or stable switching is not guaranteed. Multiple model adaptive control, which is also a switching based method, has been used in teleoperation in Shahdi and Sirouspour (2005). However performance is not guaranteed and the results exhibit undesired high frequency responses. We have already explored switching robust control techniques in Chapters 3 and 4. We designed switching robust controllers that account for uncertainty in the operator and environment dynamics, as well as uncertainty

and noise in the estimation of the environment stiffness that is used for control scheduling. In Chapter 3, the controllers were designed such that they share a common quadratic Lyapunov function, which ensures stable and smooth switching among them. In Chapter 4, the requirement of a common quadratic Lyapunov function was relaxed. Instead, different Lyapunov functions are used that are linked using conditions from a minimum average dwell time requirement.

Therefore in this chapter we propose a controller scheme similar as in Chapters 3 and 4, with the main difference that every controller is designed separately and the switching among them is based on bumpless transfer (see Zaccarian and Teel (2005)). In this way we avoid the conservatism added by requiring conditions linking the different Lyapunov functions, yet achieving stable switching. This allows to optimize the performance of each controller in its respective range of operation. Moreover, we implemented the whole scheme experimentally, including the bumpless compensator and an environment estimator capable of following rapid changes in the environment stiffness. This is the first time that experiments are presented in teleoperation using switching of robust controllers by bumpless transfer. In such a way, robust performance is guaranteed while interacting with different types of environments, either with soft or with stiff environments. Furthermore, when the environment changes from one type to the other, the switch between the underlying controllers is done such that high frequency peaks in the system's response are avoided.

In Section 5.2 we describe the framework for control design and implementation of the proposed controller scheme. Experiments are presented and discussed in Section 5.3. Finally, in Section 5.4 the conclusions are presented.

5.2 Bumpless transfer in bilateral teleoperation

5.2.1 Linear fractional representation of a teleoperation system

To formulate the synthesis problem of our switching controller, we first describe the teleoperation system model. It was already presented in Chapter 2 and it is briefly discussed here. The model consists of two subsystems, operator/master-device pair and environment/slave-device pair. We consider master, slave devices and environments with mass-damper-spring dynamics. For the operator's arm model, we used the same model identified in Chapter 2. The model is described by an impedance $Z_h(s)$, which consists of a mass-damper-spring system and a filter $Q_h(s)$ modeling the operator's arm-hand dynamics above 10 Hz. In such a model only the operator stiffness k_h is considered to be uncertain and time-varying.

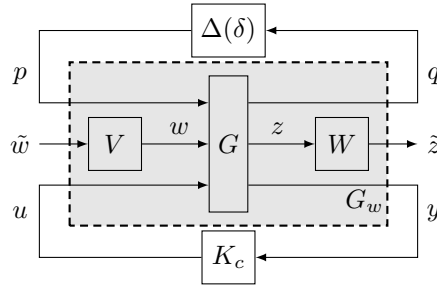


Figure 5.1: Generalized plant with weighting filters.

Therefore, $\Delta_h = k_h$ represents the uncertainty block of the operator/master-device dynamics. Similarly, only the environment stiffness k_e is considered uncertain. Therefore, $\Delta_h = k_e$ represents the uncertainty block of the environment/slave-device pair dynamics.

Subsequently, all different components are gathered and the teleoperation is modeled using a so called generalized plant structure. The system model's structure is shown in Fig. 5.1, where q and p are the signals interfacing the uncertainty block Δ , w the disturbances of the system, y the measured signals, u the actuation signals, and z the performance signals. G contains all fixed parameters of operator, master and slave devices. The controller K_c in this case represents the controller to be designed. In the model, the operator stiffness k_h and the environment stiffness k_e are assumed to be uncertain, bounded and they are also considered time-varying to account for more realistic behavior. Thus, the number of uncertain parameters of the system is $n_p = 2$ and the vector of uncertain parameters is $\delta = \text{col}(\delta_1, \delta_2)$ with $\delta_1 = k_h$, $\delta_2 = k_e$. The uncertainty block is then defined as $\Delta(\delta(t)) = \begin{bmatrix} k_h(t) & 0 \\ 0 & k_e(t) \end{bmatrix}$, $\Delta \in \mathbf{\Delta}$, where

$$\Delta = \left\{ \begin{bmatrix} k_h & 0 \\ 0 & k_e \end{bmatrix} : k_h \in [\underline{k}_h, \bar{k}_h], k_e \in [\underline{k}_e, \bar{k}_e] \right\}.$$

V and W are weighting filters described with stable LTI systems. They allow to shape in frequency domain the desired system performance. See Section 3.2.5 for details. \tilde{w} and \tilde{z} are weighted copies of w and z via predefined filters V and W respectively. That is $w = V\tilde{w}$ and $\tilde{z} = Wz$.

Finally, for the actual implementation of the synthesis procedure, a transformation of the parameters and a scaling are used. Please see Section 2.2.1 for details.

5.2.2 Uncertainty region distribution and robust control design

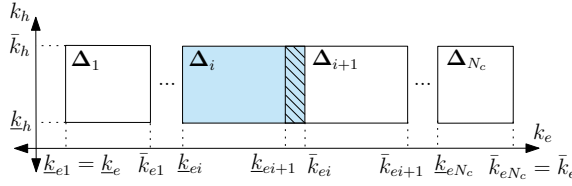
In Chapter 2, using Linear Matrix Inequalities (LMI's) (Scherer and Weiland (2010)), we synthesized a single LTI robust controller with robust performance operation for environment stiffness k_e up to $\approx 3000N/m$. In order to increase the operational range of environment stiffness and being able to deal with stiff environments, we propose the use of a multi robust-controller structure that schedules different robust controllers according to the estimate \hat{k}_e of k_e . The idea is to design certain number N_c of LTI robust controllers, in which the i th controller has an uncertainty region Δ_i of robust performance, such that all regions combined covers the desired region Δ .

A similar framework has been presented in Chapters 3 and 4. The method presented here differs in two main points. Firstly, the switching strategy in Chapter 3 is based on the existence of a common Lyapunov function, which might not exist or in order to find it we might have to sacrifice performance. In Chapter 4 the Lyapunov functions involved in the control synthesis are linked using dwell time conditions, which could still introduce conservatism in the achievable performance. The switching here is based on bumpless transfer (see Zaccarian and Teel (2005) and references therein) and does not require conditions linking the involved Lyapunov functions. This allows for independent performance optimization of each controller. Secondly, in the methods in Chapters 3 and 4 the partition of the whole uncertainty has to be made prior to the controller synthesis, increasing the number of variables to be defined beforehand. Here instead, only the whole desired uncertainty region and a desired level of performance need to be defined, because the synthesis algorithm proposed here finds automatically a distribution of the regions.

The methodology consists on designing a certain number N_c of robust controllers, which will be determined by the synthesis algorithm itself. In order to divide the uncertainty region Δ into sub-regions $\Delta_i, i = 1, \dots, N_c$, we define N_c uncertainty blocks Δ_i such that $\Delta_i = \begin{bmatrix} k_h & 0 \\ 0 & k_{ei} \end{bmatrix}$ for $i = 1, \dots, N_c$ and $\Delta_i \in \Delta$, where the class $\Delta_i = \left\{ \begin{bmatrix} k_h & 0 \\ 0 & k_{ei} \end{bmatrix} : k_h \in [\underline{k}_h, \bar{k}_h] \wedge k_{ei} \in [\underline{k}_{ei}, \bar{k}_{ei}] \right\}$ and $\Delta \subseteq \Delta_1 \cup \dots \cup \Delta_{N_c}$. Such partition is depicted in Fig. 5.2. There is overlap between the regions to avoid chattering behavior due to noise and to avoid wrong scheduling of controllers due to uncertainty and noise in the estimation of k_e . To illustrate this, consider that the estimate \hat{k}_e of k_e is given by:

$$\hat{k}_e = k_e \pm \varepsilon(k_e) + \eta(k_e) \quad (5.1)$$

where $\varepsilon(k_e)$ represents the magnitude of the uncertainty in \hat{k}_e and $\eta(k_e)$ represents the zero-mean noise signal in the estimation such that $|\eta(k_e)| < \eta_c$ for $k_e \in [\underline{k}_e, \bar{k}_e]$.


 Figure 5.2: Uncertainty regions Δ_i of a switching robust controller.

Next, consider the overlapping section in the k_e axes of two adjacent regions Δ_i , Δ_{i+1} as depicted in Fig. 5.3, where

$$\underline{k}_{ei+1} \leq \bar{k}_{ei} - 2\varepsilon(\bar{k}_{ei}) - 2\eta_c \quad (5.2)$$

and it is assumed that $\varepsilon(\bar{k}_{ei}) > \varepsilon(\underline{k}_{ei+1})$. $\varepsilon(\bar{k}_{ei})$ accounts for the uncertainty in the estimation and the introduced hysteresis gap with size $2\eta_c$ avoids possible chattering behavior due to noise, i.e. that there are rapid and repeated switching between two controllers. Then, if the switching from the indexed region i to a higher indexed region is taken when $\hat{k}_e > \bar{k}_{ei} - \varepsilon(\bar{k}_{ei})$ and the switching from the indexed region $i + 1$ to a lower indexed region is taken when $\hat{k}_e < \underline{k}_{ei+1} + \varepsilon(\bar{k}_{ei})$, considering that Eq. (5.1) holds, false switching between regions due to uncertainty and chattering due to noise in \hat{k}_e is avoided. This methodology assumes that the uncertainty is uniformly bounded with sufficient small bound, which in practice might not be hold at all times, however if the estimator detects the new environment fast enough, stability is not compromised as will be shown in the experimental results.

Next, assume that the bounds of the region Δ_i is known. Then we are interested in designing a controller $K_{ci}(s)$ with a state space representation denoted by

$$K_{ci}(s) = \left[\begin{array}{c|c} A_{ci} & B_{ci} \\ \hline C_{ci} & D_{ci} \end{array} \right], \quad i = 1, \dots, N_c, \quad (5.3)$$

that achieves robust performance for all $\Delta_i \in \Delta_i$. Following the methodology in previous chapters, we use a performance criterion based on the \mathcal{L}_2 gain (Skogestad and Postlethwaite (2005)) between disturbance variables \tilde{w} and performance

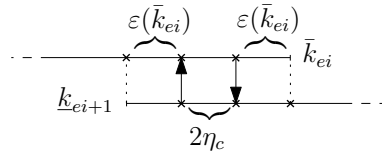


Figure 5.3: Overlap of two adjacent uncertainty regions.

variables \tilde{z} . This gain is denoted by γ . Furthermore, it is desirable to obtain a maximum gain $\bar{\gamma}$ that defines the minimum performance level that we want to achieve for each closed loop of the multi robust-controller structure. To this end, we can apply the synthesis process described in Chapter 2 and further detailed in Appendix B (see version I of the procedure).

Finally, in order to fully determine the regions Δ_i , we propose a sequential procedure. We start by the synthesis of the first controller $K_{c1}(s)$. We define $\underline{k}_{e1} = \underline{k}_e$ and we maximize \bar{k}_{e1} using a bisection algorithm while keeping the performance gain of the first controller $\gamma_1 \leq \bar{\gamma}$. Once that is done, we continue with the controller design of $K_{c2}(s)$. By using the minimum amount of overlap as in Eq. (5.2), we define $\underline{k}_{e2} = \bar{k}_{e1} - 2\varepsilon(\bar{k}_{e1}) - 2\eta_c$ and maximize \bar{k}_{e2} using bisection again keeping the performance gain of the second controller $\gamma_2 \leq \bar{\gamma}$. The procedure is repeated until we achieve $\bar{k}_{ei} = \bar{k}_e$, thus we have covered the whole uncertainty region Δ .

Now, the controllers $K_{ci}(s)$ guarantee robust performance for each region Δ_i separately. In order to couple the regions, we switch between the controllers as needed by using bumpless transfer.

5.2.3 Bumpless transfer between robust controllers

There are no a priori conditions that guarantee a stable switching between the controllers $K_{ci}(s)$. Therefore a suitable strategy must be used. If a direct switch of controllers is done, the initial condition of the state of the new controller might cause discontinuities and large peaks in the control signal. This can generate high frequency peaks in the system's response at the moment of switching. To decrease such behavior, we use the same idea as in bumpless transfer in Zaccarian and Teel (2005). Basically, the idea is to keep the off-line controllers virtually in the loop by means of simulation. Each off-line controller put in a virtual loop with an internal model, and such loop is perturbed using signals of the real system. The result is that at the moment the switching occurs, the state of the new on-line controller is compatible with the new environment, allowing that undesirable high frequency peaks in the system's response are decreased. In Zaccarian and Teel (2005) they used the concept for non uncertain plants. In our case, the plant presents large uncertainty, however the controllers designed here can deal with rapid changes in the plant within certain region. This motivated us to implement the bumpless transfer as depicted in Fig. 5.4, in which K_{ci} represents the controller currently on-line and K_{cj} any of all the other controllers that remain off-line. The bumpless compensator for K_{cj} consists then by a plant out of the corresponding group of plants for which the controller is robust to. Therefore, we use the same model G as in Fig. 5.1 and we select a single element $\Delta = \Delta_j^B = \begin{bmatrix} k_h^B & 0 \\ 0 & k_{ej}^B \end{bmatrix}$ from the

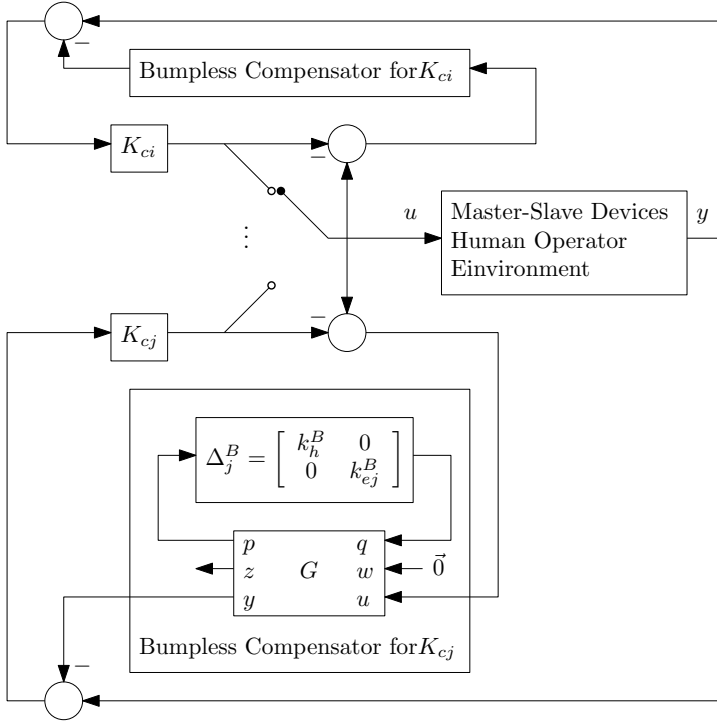


Figure 5.4: Bumpless transfer scheme for teleoperation control

corresponding region Δ_j . In this way the off-line controller is virtually kept on-line and since we used $\Delta_j^B \in \Delta_j$, its stability, while off-line, is guaranteed. Now, at the moment of switching, the new selected controller has been interacting with a plant model compatible with the new environment. This in the sense that both belong to the region of robustness of the controller that will enter on-line. This intuitive idea makes the state of the new selected controller compatible with the new environment and the current state of the master and slave devices. As it will be shown in the experimental results, this way of switching makes it possible to avoid large peaks at high frequencies in the system's response in comparison with a direct switching. In turn, this results in a stable switching among the controllers as the experimental results will show.

5.2.4 Environment estimation

In order to schedule the different controllers, we need an estimator that is able to deal with possibly rapid and sudden changes of the environment stiffness k_e . We

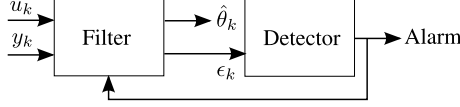


Figure 5.5: Estimator with Change Detection

make use of the same estimator as in Chapter 3, which is an estimator proposed in Gustafsson (2000). The structure of the estimator is shown in Fig. 5.5. The working principle of this estimator is as follows: the *filter* block processes the discrete inputs u_k and outputs y_k of a system described by a *model* (in our case an environment model) to get an estimate $\hat{\theta}_k$ of certain parameters θ_k (the parameters of our environment model). Then, the signal ϵ_k is used to detect abrupt changes in the parameters and under certain criteria, the *detector* block sends an *alarm* to the filter to adapt quickly to the changes. Following the guidelines in Gustafsson (2000), the different blocks are described below.

Environment model as a linear regression model

We write our environment model in the following form

$$y_k = \varphi_k^T \theta_k + e_k$$

where k denotes sampled time instants, y_k is the measured environment force, e_k is the corresponding noise, the environment parameters vector is $\theta_k = \text{col}(k_e(k), f_e^*(k))$ with $f_e^*(k)$ being the active component of the environment force, and the so called regression vector φ_k is given by $\varphi_k = \text{col}(u_k, 1)$ with $u_k = x_s(k)$ being the position of the slave device.

Filter

For the filter block we utilize a Kalman filter for linear regressions, which is implemented in its recursive form as follows:

$$\begin{aligned} \varphi_k &= \text{col}(u_k, 1) \\ K_k &= \frac{P_{k-1} \varphi_k}{R_k + \varphi_k^T P_{k-1} \varphi_k} \\ P_k &= P_{k-1} - \frac{P_{k-1} \varphi_k \varphi_k^T P_{k-1}}{R_k + \varphi_k^T P_{k-1} \varphi_k} + Q_k \\ \hat{\theta}_k &= \hat{\theta}_{k-1} + K_k (y_k - \varphi_k^T \hat{\theta}_{k-1}) \\ \epsilon_k &= y_k - \varphi_k^T \hat{\theta}_k \end{aligned}$$

where $\hat{\theta}_k$ is the estimated vector of the environment model parameters, R_k is taken as 1 without loss of generality and Q_k is a design parameter that determines the speed of converge of the filter. Large values of Q_k make the filter to react faster but also the estimate will have more noise. The variable ϵ_k is the error between the actual measurement and the reconstructed measurement obtained with $\hat{\theta}_k$.

Detector

The detector block is defined as a threshold function in order to decide when to make the filter to react fast. Thus, when $|\epsilon_k| < L_{|\epsilon_k|}$, no alarm is generated and we use $Q_k = Q_{nom}$. When $|\epsilon_k| \geq L_{|\epsilon_k|}$, it means that \hat{y}_k has deviated too much from the true measurement and the filter must adapt rapidly to the new environment by setting $Q_k = Q_{fast}$.

Therefore, the estimator is tuned via $L_{|\epsilon_k|}$, Q_{nom} and Q_{fast} . This tuning is essential to be able to detect abrupt changes fast enough to schedule on time the controllers of the multi-controller structure.

5.3 Experimental results on a 1-DoF academic setup

Experiments were carried out on the setup described in Appendix A. For the master-slave devices, the operator and the weighting filters we have used the same parameters as in Chapter 2. The environment estimator parameters were experimentally determined, we used $Q_{nom} = \text{diag}(1, 0.01)$, $Q_{fast} = \text{diag}(10^7, 1)$, $L_{|\epsilon_k|} = 1.0 \text{ N}$, $|\varepsilon(k_e)| \leq 0.15k_e$ and $\eta_c = 50 \text{ N/m}$ which gave us good results in practice. We used a desired range for $k_e \in [80, 40000] \text{ N/m}$ to include both soft and stiff environments as in hard contacts. Finally, we selected $\bar{\gamma} = 5$.

The LMIs involved in the controller synthesis procedure were solved using the solver Sedumi (see Sturm (1999)). Because variation in m_h is not considered, making the design for its nominal value $m_h^N = 0.53 \text{ kg}$ can cause instability when the master device is in free air (see Chapter 2). One possible solution to that problem is to make the design for a reduced mass $m_h = r_m m_h^N$, $r_m \in [0, 1]$. The side effect is that there will be a decrease in performance due to the bandwidth reduction. We proceed the design with $m_h = 0.3m_h^N$ which gave us stability in free air. Then, after applying the complete synthesis procedure we obtained in total two controllers with $\gamma_1 = 4.45$, $\underline{k}_{e1} = 80 \text{ N/m}$, $\bar{k}_{e1} = 3897 \text{ N/m}$, $\gamma_2 = 4.46$, $\underline{k}_{e2} = 2630 \text{ N/m}$ and $\bar{k}_{e2} = 40000 \text{ N/m}$.

For implementation, all controllers were discretized using the tustin method with

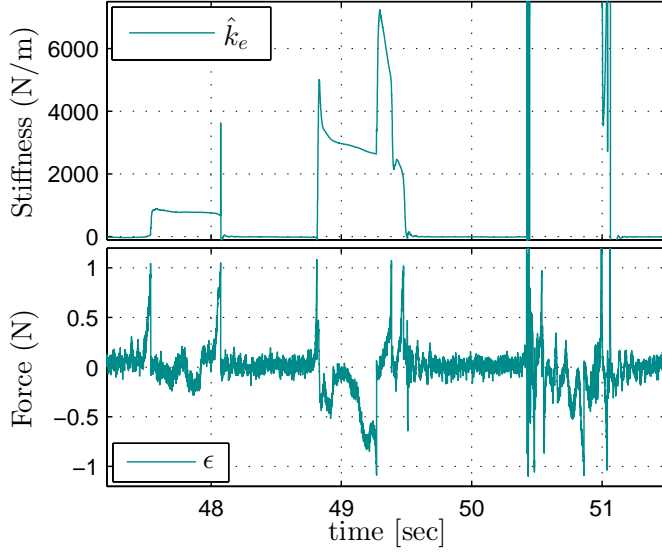


Figure 5.6: Environment estimator responses to different materials

a sample period $T_s = 5 \times 10^{-4} \text{ sec.}$. For the bumpless compensators we selected $k_h^B = 776.7 \text{ N/m}$, $k_{e1}^B = 80 \text{ N/m}$ and $k_{e2}^B = 4000 \text{ N/m}$, which are arbitrary choices. To perform the experiments, different materials are located such that the slave device enters in contact with them as shown in Fig. A.1. Initially the operator moves the master such that the slave device is in free air, then it comes initially in contact with a soft spring. The procedure is consecutively repeated for a stiff foam and for a piece of metal.

First, we analyze the response of the environment estimator shown in Fig. 5.6. One can see that indeed the environment estimator adapts rapidly to the new environment, confirming the suitability of the selected estimator structure. At the moments in which the environment changes, one can also notice that $|\epsilon| \geq 1.0$ and immediately after the filter is reset, it follows a fast convergence transient and therefore a decrease in ϵ . However, some peaks in \hat{k}_e are seen before convergence which are not present if the system is simulated. More insight is required to understand that phenomenon and will be study in the future.

Next, the time domain results of positions and forces of the system are illustrated in Fig. 5.7. The bottom plot shows the index of the current on-line controller. Regarding the performance after transitions and while in contact with the different environments, we see indeed that force and position tracking is achieved for all cases. This indicates that the operator feels a stiffness close to the real environment stiffness. In fact, the performance of a single robust controller while in contact with

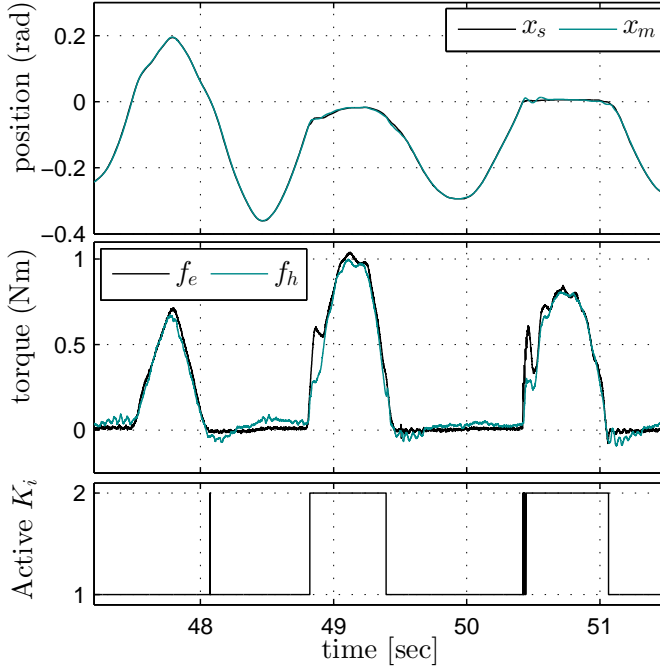


Figure 5.7: Response of the proposed controller to transitions from free air to different environments

different environments has been already analysed in Chapter 2. The experiments here performed focuses more on the transition phase, therefore sustained contact is hold shortly. At the switching moments between the two controllers, the transition is specially noticeable in some oscillations and an overshoot in the response of f_e , which is specially more noticeable for stiffer environments. However, such oscillation is not of high frequency, thus avoiding the excitation of un-modeled dynamics and it is rapidly damped after 0.2 seconds. Moreover, there is a small oscillation in x_m present only after rigid contact. One can also see that some rapid consecutive switches occur around 48 sec and 50.5 sec due to the peaks in \hat{k}_e , however stability was not compromised in none of the cases.

Next, to make a fair comparison, we repeated the same experiments for the case when bumpless transfer is not applied but a direct switching. We zoom-in in the responses of the switching instants from free air to the stiff foam and back to free air. The actuation torques and the torque responses for both type of switching are shown in Fig. 5.8. When the direct switching is applied, the actuation torques present discontinuity at the switching instants causing high frequency response in

f_h and f_e as well. In fact, in the transition back to free air the system becomes unstable and the experiment stops around 29.3 sec. On the contrary, bumpless transfer can cope with both transitions and discontinuities in the actuation forces are barely noticeable avoiding high frequency response.

Regarding stability of the whole teleoperation system with bumpless transfer, each robust controller guarantees robust performance within each uncertainty region Δ_i . Now at the switching moments the bumpless transfer reduces the high frequency peaks, however stability for fast consecutive switches is not fully guaranteed. The decisive factors are in fact the environment estimation and the switching transient response. For the first, the estimator needs to be accurate enough around the values where switching takes place. Regarding the transient response, from the experimental results we can say that if no switching takes place within the transient behavior, the system will remain stable thanks to the robustness of the on-line controller. After the oscillations are damped out, i.e. approximately 0.2 sec. for our test case, a new switching could take place safely. Such transient behavior is still undesirable and will be felt by the operator, however, we have seen that it is more noticeable for stiffer environments, therefore the operator could perceive the transient as part of the change to a stiff environment and in that case the proposed scheme will still offer a realistic feeling of such hard contacts. Thus the methodology presents a high potential to be used in practice, provided that a proper stability analysis will support our hypothesis on stability. As a possible direction for stability analysis of the proposed scheme, one can start by assuming that we know the current plant within the current active region Δ_i , and by assuming that we also know the plant to which we are going to switch to within the

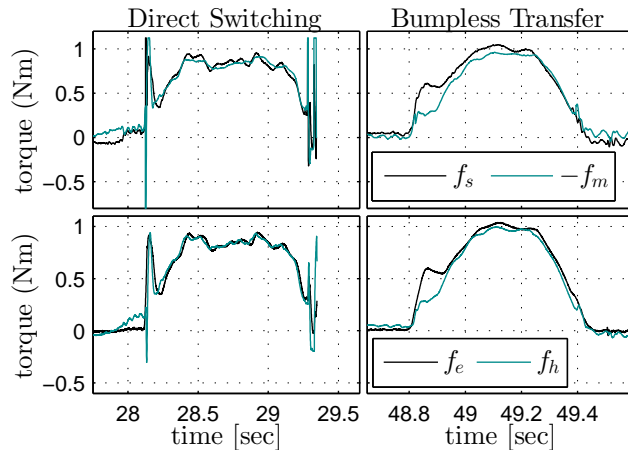


Figure 5.8: Transitions of direct switching and bumpless transfer

future active region Δ_j . Then one can model the teleoperation system as a hybrid system and try to find a common Lyapunov function or dwell time conditions (see Leith and Leithead (2000)) on the switching between the respective closed loop plants. The procedure can be then repeated for different plants among Δ_i and Δ_j . This will be subject of future research.

Finally, is important to mention that the computational requirements of the proposed scheme can increase considerably. Define O_P and O_W as the order of the plant P_0 and of the weighting filters respectively. In a normal switching scheme only one controller is computationally active a time, then only one controller K_{ci} of order $O_P + O_W$ is computed at all instants. In the proposed scheme all the N_c controllers are computationally active and moreover plant models are also active, therefore it is needed to compute a system of order $(O_P + O_W)N_c + O_P(N_c - 1)$. In our example we have that $O_P = 10$, $O_w = 5$ and $N_c = 2$, therefore we went from a computation of a system of order 15 to one of order 40.

5.4 Conclusions

In this chapter, we have presented an experimental approach to obtain high performance teleoperation in both soft and stiff environments by means of the separate synthesis of robust controllers for different environment stiffness regions. We showed that it is possible to avoid high frequency peak responses when switching between robust controllers by means of bumpless transfer. It has the advantage that each controller can be designed separately to achieve a minimum level of desired performance. As a result we obtained one controller for low and medium stiffness values and another for stiff environments. Moreover, we showed that the scheduling between the controllers can be made properly even in the case of sudden changes of environment thanks to the implementation of a stiffness estimator with change detection. As a disadvantage, some transient behavior might be felt by the operator in the switching moments, however during the experiments stability was not compromised by it and after the transition the system presents high performance. Hence, the potential of switching by bumpless transfer of robust controllers in bilateral teleoperation is clear.

In the next chapter we will applied the robust control methods presented in Chapter 2 and this chapter in a surgical robot, which present non-ideal properties, e.g. different dynamics of master and slave devices, structural resonances, and no force sensor on the master side among others.

Chapter 6

Model-Based Robust Control for a Non-Ideal Teleoperator

D*ESIGN specifications in real-life applications of bilateral teleoperation, e.g. minimally invasive surgery, can impose a series of properties on the master and slave devices, such as heavy weights, high friction, structural resonances and lack of force sensors, resulting in non-ideal teleoperators. When high quality force feedback is desired for those systems, the design and implementation of a bilateral controller becomes very challenging. In this chapter, two recently developed control methodologies, which provide high performance and robustness under time-varying dynamics of operator and environment, are implemented in a surgical setup designed for robotic assisted surgery. The experimental results demonstrate that using a model based robust control methodology, high performance for free-air and soft environments is achieved, despite the limitations of the system. Moreover, a stable and realistic interaction with stiff environments is obtained.*

6.1 Introduction

A teleoperator, which consists of a master device, a slave device and a bilateral controller, is used to provide a feeling of tele-presence using force feedback while

This chapter is based on the following manuscript: López Martínez, C. A., Molengraft, R. v. d., and Steinbuch, M. (2014b). Model based robust control for bilateral teleoperation: Applied to a non-ideal teleoperator. *In preparation for journal publication*

an operator manipulates a remote environment. Such systems have been used in different applications, e.g. remote handling of hazardous materials (e.g. Wei and Kui (2004)), teleoperation of aerial robots (e.g. Mersha et al. (2014)) and minimally invasive surgery (MIS). In the latter, robotic devices enter the body through a trocar. This means that only small incisions on the patient are needed, which results in less trauma and faster recovery times. However, the complexity for the surgeon increases as compared to open surgery, which can deteriorate his/her performance. Robot assisted MIS has been proposed as a solution for this complication, moreover it introduces the possibility of scaling the operator's movements, tremor filtering and increased positioning accuracy of the robotic instrument. As a disadvantage, there is a lack of force feedback which was naturally provided by the mechanical instruments in conventional MIS. Force feedback is highly desirable as it helps the surgeons to improve diagnosis by palpation of tissues (Tholey et al. (2005)) and it could reduce the completion time of the surgical procedure (Richards et al. (2000)). Perfect force and position tracking between the master/operator and the slave/environment sides would give the operator a feeling as if he/she is manipulating the environment directly. However, stability becomes an issue under such scenario, see Lawrence (1993a). Nevertheless, it is desirable to achieve certain force and position tracking performance that would give the operator at least a very similar perception of the real environment. Hence, when we refer to the performance of the teleoperation system, we refer to the performance with respect to force and position tracking between the master/operator and slave/environment sides.

In practice, the implementation of force feedback in teleoperators can be very challenging. The main reason is that both master and slave device are typically non-ideal, e.g. due to mechanical, geometric and economic constraints. Examples of often inevitable imperfections are friction, finite stiffness of the construction and lack of force sensors, limitations that are not present in academic setups that are commonly used on the literature to test bilateral controllers. Therefore, commercially available surgical systems do not have force feedback, e.g. the Da Vinci system (Guthart and Salisbury Jr (2000)), for which achieving force feedback is difficult due to the high mass of the slave (Shimachi et al. (2008)).

In the last decades different methods have been proposed for the design of bilateral controllers for teleoperators, and one of the greatest challenges is to deal with the inherent trade-off between performance and (robust) stability of bilateral teleoperation, see, e.g., Hokayem and Spong (2006), Passenberg et al. (2010). Control design tools based on passivity theory, e.g. Niemeyer and Slotine (1991), Ryu (2007), have been widely used to ensure stability of the system. Other works, e.g. Kim et al. (2013), Vander Poorten (2007) Willaert et al. (2014) consider performance in the design. However, the chosen modelling approach introduces much conservatism. Other techniques use estimation of the environment stiffness

to improve the performance of the system, see e.g. Beelen et al. (2013), Willaert et al. (2010), Cho et al. (2013). However, they rely on unbiased, low noise and fast convergence of the estimated environment stiffness, requirements which in practice are difficult to meet simultaneously. High performance controllers have been already reported in the literature, for example in Willaert et al. (2014), however the technique is limited to master and slave devices with identical mass damper spring dynamics. Additionally, most of the aforementioned techniques has been implemented only on academic setups.

As a solution to those issues, we have proposed in Chapter 2 a model based methodology to design robust controllers against bounded and time-varying dynamics of the operator and environment. Moreover, we also proposed multi-controller structures in Chapter 3 and Chapter 5 that improve performance on teleoperation systems. These techniques have been successfully implemented in an academic setup, where the results were promising, however a proof of concept in a non-ideal teleoperator is needed.

In this chapter, we focus on the practical implementation of the control methodologies proposed in Chapter 2 and in Chapter 5 on a non-ideal teleoperator surgical setup named SOFIE developed by van den Bedem et al. (2010), which was designed for minimally invasive surgery. The main limitations of the setup are: heavy weight, non-backdrivability and high levels of friction in the slave device, and, structural resonances and no force sensors in the master device. All this together makes the bilateral controller design and its implementation for such a system a difficult task to accomplish.

In Section 6.2.1 we describe the surgical setup, and in Section 6.2.2 we present the utilized modelling approach to be able to do control synthesis. In Sections 6.2.3 to 6.2.5 we recapitulate the robust control methodologies. Next, in Section 6.3 we present the synthesis, simulation and experimental results, followed by a discussion on them. Finally, in Section 6.4, the conclusions are given and potential future improvements are proposed.

6.2 Model based robust control applied to SOFIE robot

6.2.1 Experimental setup

The tele-surgical system shown in Fig. 6.1 is utilized to evaluate the potential of model based robust control for bilateral teleoperation. The master device, designed

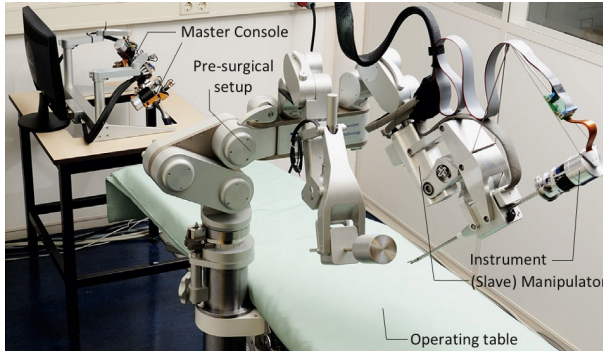


Figure 6.1: Medical Robot SOFIE designed by van den Bedem et al. (2010) (picture by Bart van Overbeeke/Bart van Overbeeke Fotografie)

by Hendrix et al. (2011), can be considered as a low friction and light device. Moreover it does not have a force sensor and has structural resonances.

The slave device (van den Bedem et al. (2010)), on the other hand, is heavy and it has high friction. The slave robotic system consists of a pre-surgical base, with two manipulators as shown in Fig. 6.1, an endoscope and two instruments. The pre-surgical base provides the initial orientation of the manipulators. It consists of a five-DoF platform-adjustment connected to the operating table, a platform and three five-DoF manipulator-adjustments, each carrying a four-DoF instrument-manipulator. Each instrument-manipulator provides three rotations and one translation of an instrument-tube to manipulate the tip. The relation between these DoFs and the nine moving bodies of an instrument-manipulator is illustrated in Fig. 6.2; here ϕ and ψ are rotations in the plane tangent to the abdominal wall of the patient, which are kinematically fixed at the trocar point P. The symbol θ represents the angle of rotation aligned with the center line of an instrument-tube and z represents the displacement along this same center line. The manipulator is schematically drawn in its nominal orientation, i.e. $\phi = \psi = \theta = 0$ rad and $z = 0.19$ m. The angles $\phi(t)$, $\psi(t)$, $\theta(t)$ and the translation $z(t)$ (in lower case) are the signals evaluated in the time domain and they represent the displacements in the DoFs Φ , Ψ , Θ and Z (in upper case), respectively.

All DoFs Φ , Ψ , Θ and Z of the slave-manipulator are compatible with Φ , Ψ , Θ and Z of the master-device and can thus be coupled in joint-space.

In this work, only the Ψ is chosen for controller design and experiments, since it exhibits the most imperfections. For instance, in Fig. 6.2, in body 7, a brake-encoder-actuator-gearbox combination provides the movement, with a varying transmission ratio, see Table 6.1. Furthermore, this Ψ transmission is

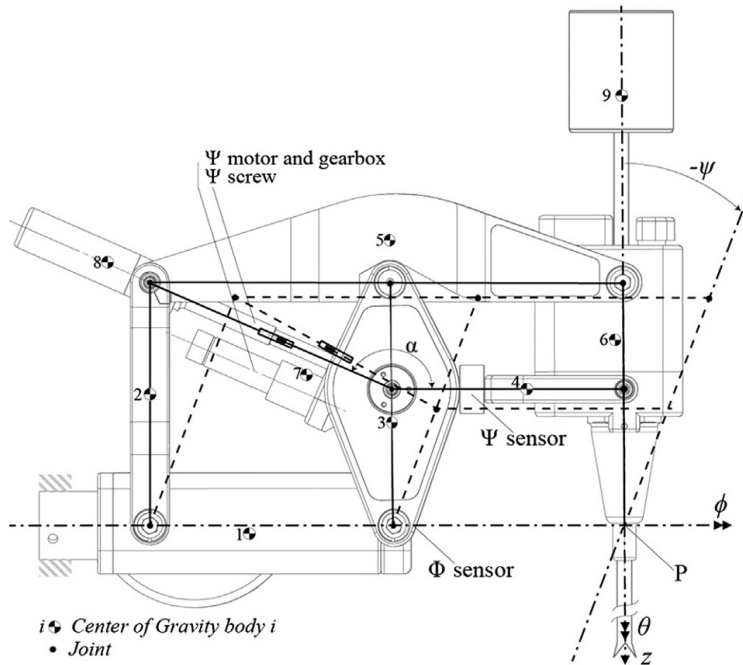


Figure 6.2: Schematic Surgical Robot Sofie: joints and moving bodies. See van den Bedem et al. (2010)

non-backdrivable, i.e. that it can only be moved from its actuation input. More relevant information and parameters of the instrument-manipulator are provided in Table 6.1. A real-time data acquisition (DAQ) system is used to couple the

Table 6.1: Tele-surgical system hardware parameters (van den Bedem et al. (2010)).

Friction Slave	$< 2.2 \text{ N m}$
Gearbox ratio slave- Ψ	1100 – 1700 (varying)
Force sensor Ψ :range	4 N m (20 N at the tip ^a)
Force sensor Ψ :noise level	$< 6 \text{ mN m}$ ($< 0.03 \text{ N}$ at the tip ^a)
Friction master	$< 0.03 \text{ N m}$
Maximum master torque f_m	0.51 N m
Sampling frequency	4 kHz
^a At nominal insertion depth $z = 0.19 \text{ m}$	

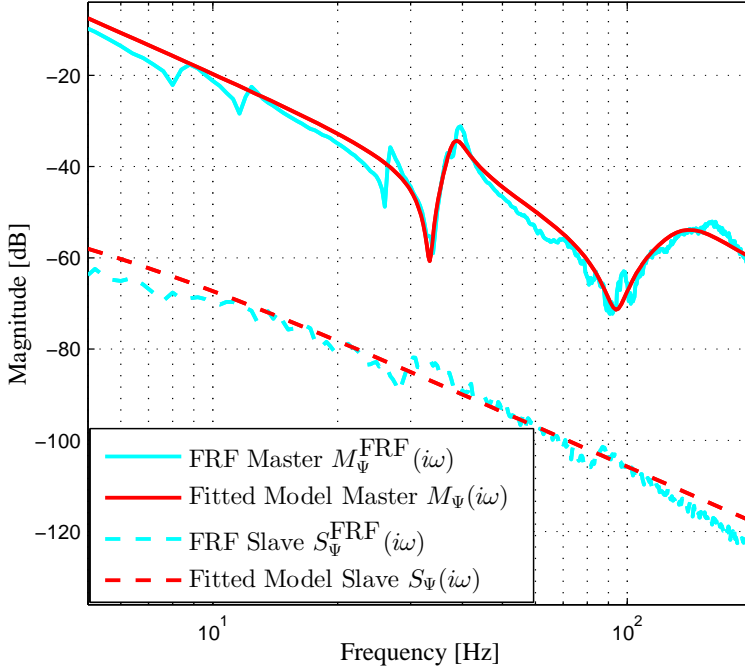


Figure 6.3: Magnitude of the Frequency Response Function (FRF) measurements and magnitude bode diagram of the corresponding fitted models of Master and Slave Devices in Ψ DoF.

master and the slave robot. It consists of a dSPACE rack, running a Matlab-Simulink-generated real-time application with a sampling frequency of 4 kHz.

The magnitude of the Frequency Response Function (FRF) measurements from input torque (in N m) to output rotation (in rad) of the Ψ DoF is shown in Fig 6.3. In the same figure the respective magnitude bode diagram of the fitted models $M_{\Psi}(i\omega)$ and $S_{\Psi}(i\omega)$ for both master and slave devices are shown. During all experiments in this work, all the other DoFs are kept at their nominal values. Hereafter, we assume the slave device interacts with the environment at the instrument's tip at a distance of $L_{SE} = 19\text{cm}$ from the trocar point P. In a similar way, we assume that the operator interacts at a distance of $L_{MO} = 20\text{cm}$ from the rotation axes of Ψ in the master device. Therefore, for notational convenience, if not specified otherwise, when we use units of force, distance, mass, etc., we refer to those parameters computed on the interaction points previously described. Moreover, when we use units of torque, rotation, inertia, etc., we refer to those parameters computed either with respect to the trocar point P or to the master-

Table 6.2: Modelling Numerical parameters

$m_m = 2.4 \times 10^{-3}$	$m_s = 0.5$	$\text{kg m}^2/\text{rad}$
$b_m = 12.8 \times 10^{-3}$	$b_s = 20.04$	$\text{N m s}/\text{rad}$
$k_m = 12.0 \times 10^{-3}$	$k_s = 0.0$	$\text{N m}/\text{rad}$
$m_h = 0.53$	$m_e = 0$	kg
$b_h = 46$	$b_e = 0$	$\text{N s}/\text{m}$
$k_h \in [731, 1200]$	$k_e \in [80, 10000]$	N/m
$\omega_{ph} = 219.9$	$\omega_{zh} = 69.9$	rad/s
$z_{ph} = 1.7$		—

device's rotation axes in Ψ accordingly.

6.2.2 Modelling of the teleoperation surgical system for control synthesis

Similarly as already presented in previous chapters, we make use of a Linear Fractional Representation (LFR) of the bilateral teleoperation system. Deriving a LFR of a system amounts to isolating the uncertain parameters such that an interconnection structure as depicted in Fig. 6.4 is obtained.

$\Delta(\delta)$ is the block diagonal concatenation of the vector of uncertain real parameters δ . To this end, we first define the models of the different components of the teleoperation system under consideration. The master and slave devices interact with the operator and environment respectively as depicted in Fig. 6.5, where m_m, b_m, k_m and m_s, b_s, k_s are fixed parameters of the master and slave devices respectively which are computed from the fitted models in Fig. 6.3 and shown in Table 6.2; M_{HFD} represents the high frequency dynamics of the master device, thus

$$M_{\Psi}(s) = \frac{1}{m_m s^2 + b_m s + k_m} M_{\text{HFD}}(s);$$

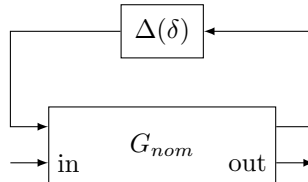


Figure 6.4: Linear Fractional Representation of a System.

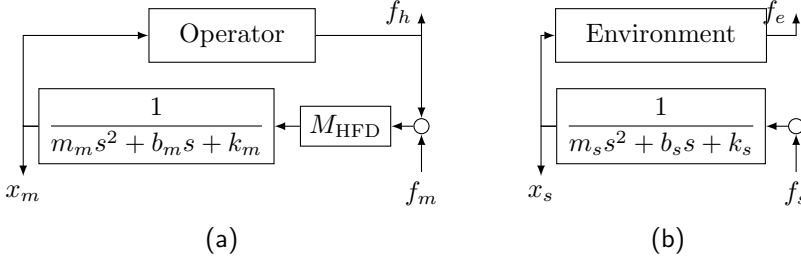


Figure 6.5: Diagram of (a) operator/master device and (b) environment/slave device.

f_m, f_s are the actuation forces to the master and slave devices respectively; f_h, f_e represent the total force exerted by the operator and environment respectively; and x_m, x_s are the positions of the master and slave devices respectively, by definition they also represent the positions of the operator and environment respectively. Two main aspects of this application make the modelling different to the classical teleoperation's system modelling presented in literature. First, one can see that the dynamics of the master device have been split in a mass-damper-spring system and high frequency dynamics. Such separation will be used to obtain the final LFR of the system. Second, the environment force is not fed-back to the slave device. This is a simplified model of the non-backdrivability property of the slave device. In practice, high loads on the instrument will lead to an increased friction on the slave device, which could be modelled and then friction compensation could be used, however, the focus is on testing the robust control technique under those non-ideal properties. The next step is to define models for both operator and environment.

Operator Model

For the operator, we make use of the model structure presented in Chapter 2 and shown in Eq. (6.2.2), in which it is assumed that the main source of uncertainty comes from the operator's arm-hand stiffness k_h , which allows to reduce the control design complexity.

$$Z_h(s) = \frac{F_h(s)}{X_m(s)} = (m_h s^2 + b_h s + k_h) Q_h(s),$$

where

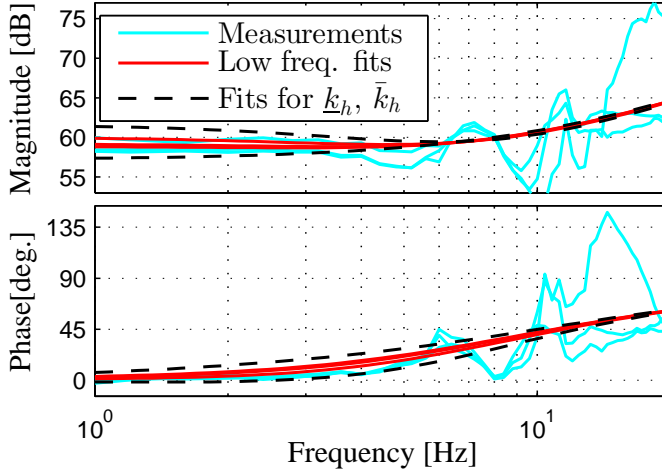
$$Q_h(s) = \frac{\frac{s}{\omega_{zh}} + 1}{\frac{s^2}{\omega_{ph}^2} + 2z_{ph}\frac{s}{\omega_{ph}} + 1}.$$

We followed a similar procedure as proposed in Chapter 2. We performed different experiments to get FRF measurements $Z_h^{\text{meas}}(j\omega)$ of $Z_h(s)$. Because the master device does not have a force sensor, $Z_h^{\text{meas}}(j\omega)$ is reconstructed using two FRF measurements. First we obtained an FRF from the closed loop from f_m to x_m shown in Fig 6.5.(a), i.e. the closed loop between the master device and the operator's hand. Then, $M_\Psi^{\text{FRF}}(i\omega)$ in Fig 6.3 is used to compute the operator's hand FRF $Z_h^{\text{meas}}(j\omega)$.

We did three experiments in which we presented three virtual springs to the operator with stiffness values in the range $k_e^V \in [0, 5000]$ N/m such that $f_m = -k_e^V x_m + f_m^{ID}$, in which f_m^{ID} will be used as a disturbance signal for system identification. In particular, we used a system's sampling rate of 4000 Hz and a frequency range of $[1, 40]$ Hz for the multi-sine. Initially we set $f_m^{ID} = 0$ N and then the operator was asked to move the master device in order to feel the virtual spring. Subsequently, the operator was asked to stop in a position of his/her choice where he/she could still feel the virtual spring. The idea is that the operator exerts a force level such that he/she could feel that he/she has a correct haptic perception of the virtual environment. This is clearly subjective to the operator. Nevertheless, the aim of the experiment is that the operator changes intuitively his/her exerted force and grip for different virtual springs. Afterwards, a multi-sine signal was applied to the master device via f_m^{ID} while the operator tried to remain static. Actuation forces $f_m(t)$ and positions $x_m(t)$ were measured and then their Fourier transforms $F_m^{\text{meas}}(j\omega) = \mathcal{F}(f_m(t))(j\omega)$ and $X_m^{\text{meas}}(j\omega) = \mathcal{F}(x_m(t))(j\omega)$ were computed. Then, the frequency response function (FRF) measurements of the operator's arm-hand dynamics $Z_h^{\text{meas}}(j\omega)$ is computed in a frequency range of $[1, 20]$ Hz, the results of which are depicted in Fig. 6.6.

We observed that the quality of the obtained measurements is low especially above 10 Hz. Nevertheless, the frequency content of the operator's movement is assumed to be dominant in frequencies below that. Moreover, with the measurements we are interested mainly in obtaining a rough estimation on how the operator changes his arm stiffness. As it will be shown on the experimental results, a model based on this measurements is sufficient to obtain satisfactory results.

To reduce the complexity on the optimization process to fit the model parameters, we use the mass value m_h found in Chapter 2 since it is assumed that the operator uses a similar posture to manipulate the master device, i.e. with the elbow rested on a table, thus we use $m_h = 0.53$ kg. Then, we optimized the variables b_h, k_h, ω_{zh} ,

Figure 6.6: Arm FRF Measurements in Ψ DoF.

z_{ph} and ω_{ph} to fit each measurement to the model minimizing the cost function $W_{Z_h}(i\omega) = \|(Z_h(i\omega) - Z_h^{\text{meas}}(i\omega))\|_2$ for $\omega \in 2\pi[1, 20]$ rad/s. The optimization is done using a constrained nonlinear optimization method provided by the command `fmincon` in Matlab[®]. Then, to reduce complexity of the model and the control design, we have used a low-frequency approximation by allowing variation in k_h only and fixing all other parameters to their centred values of the corresponding intervals found in the optimization. Such fitted models are depicted in Fig. 6.6, where we used $m_h = 0.53$ kg, $b_h = 46$ Ns/m, $\omega_{zh} = 69.9$ rad/s, $z_{ph} = 1.7$ and $\omega_{ph} = 219.9$ rad/s and $k_h = [877, 1000]$ N/m.

Finally, we include possible extra variation in k_h to increase the robustness of the system. Hence, we enlarge the range of values of k_h by 20% resulting in the range $k_h \in [731, 1200]$ N/m. The resulting $Z_h(s)$ fitted models for $\underline{k}_h = 731$ N/m and $\bar{k}_h = 1200$ N/m are shown with dashed lines in Fig. 6.6. All the operator's parameters are summarized in Table 6.2. Though the identification was performed via LTI techniques, in what follows below, we assume that during operation k_h is time-varying within $k_h(t) \in [\underline{k}_h, \bar{k}_h]$ for all $t > 0$.

Combining the master device and operator models, we arrive at the model diagram for the operator/master device depicted in the two upper blocks in Fig. 6.7, where f_h^* is the active force generated by the operator and $\Delta_h = k_h$ defines the time-varying, bounded and uncertain parameter of the human hand dynamics model. One can see that the master device model separation in a mass-damper-spring system and high frequency dynamics allows for a representation such that a state

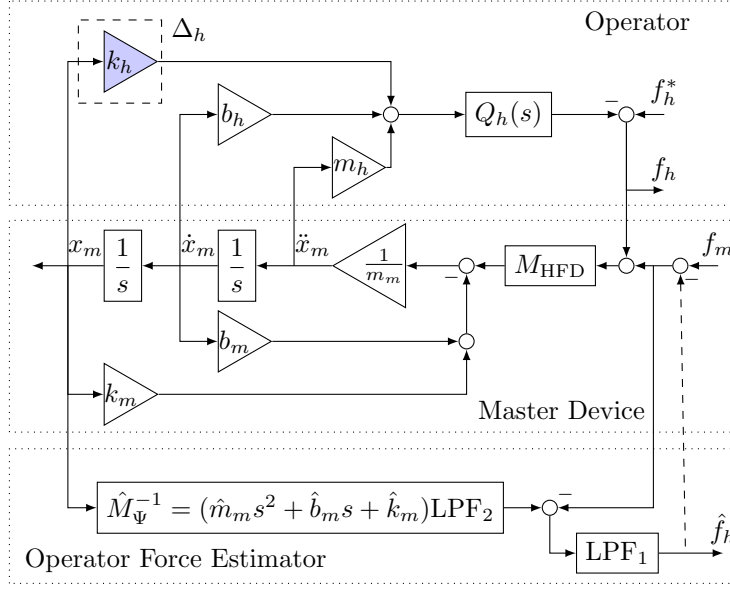


Figure 6.7: Block diagram representation of the operator/master device pair, and operator force estimator.

space model can be easily extracted, which is necessary for control synthesis.

Operator's force estimator

Next, for control synthesis it is desirable to have information about forces and positions in both operator and environment sides. However, in real-life applications, the master device usually does not have a force sensor, as in the case here. To estimate the operator's force, in this work we implement a disturbance observer see, e.g., Schrijver and Van Dijk (2002), the structure of which is shown in the lower part of Fig. 6.7, where \hat{M}_Ψ represents a model of the master device, LPF_1 and LPF_2 are low pass filters of first and second order respectively. In a standard implementation of a disturbance observer, an accurate model \hat{M} is highly desirable. Moreover, the dashed interconnection in the lower part of Fig. 6.7 is used in a standard observer to increase robustness of the estimated force accuracy against model uncertainty. This results in the following mapping from the signals x_m and f_m to the estimate \hat{f}_h in a standard disturbance observer:

$$\hat{f}_h = (1 - \text{LPF}_1)^{-1} \text{LPF}_1 (\hat{M}_\Psi^{-1} x_m - f_m)$$

We made two main modifications with respect to a standard disturbance observer. First, because we are interested in the operator's force estimation only for low frequencies, and to decrease the order of the overall system model, in \hat{M}_Ψ^{-1} we use only the low frequency part of the master device model, i.e. a mass-damper-spring model structure, in which \hat{m}_m , \hat{b}_m and \hat{k}_m are estimates of the mass, damper and stiffness of the master device, and in this case they only serve for illustrative purposes since we do not know the real values, therefore we set them equal to those of the model from Fig 6.3. LPF₂ is especially used to avoid a non-proper transfer function, which does not have a state space representation, and also to avoid excessive amplification of high frequency noise. Second, the dashed interconnection in the lower part of Fig. 6.7 is usually used to increase the robustness properties of the estimator as previously mentioned. However, there is no guarantee that the observer will be stable under such unitary feedback. Moreover, it can be seen as a local force feed-back which will have effect on the haptic perception on the operator side when combined with a controller, which will provide an additional loop from \hat{f}_h to f_m . Thus, to avoid those issues, we do not use the dashed interconnection. This results in the following mapping from the signals x_m and f_m to the estimate \hat{f}_h :

$$\hat{f}_h = \text{LPF}_1(\hat{M}_\Psi^{-1}x_m - f_m)$$

The loop from \hat{f}_h to f_m is closed only via the controller, which will provide robust performance of the overall system and guarantee stability properties of the force observer as will be shown in the results.

Environment model

Continuing with the system modelling, we consider environments with dominant spring dynamics:

$$f_e = f_e^* + k_e x_s \quad (6.1)$$

Here, $k_e \geq 0$ is the stiffness coefficient of the environment, and f_e^* is the active force from the environment, if present. We focus on the environment stiffness k_e as the main cause of the environment dynamic variation, hence k_e is assumed to be bounded (though within a wide range), and time-varying, i.e. $k_e(t) \in [\underline{k}_e, \bar{k}_e]$ for all $t > 0$. This choice is suitable for applications in which the effect of k_e on f_e is dominant, e.g. in stiffness discrimination tasks like those in surgery. For other environment types the uncertainty structure and parameters can be redefined.

In contrast to the master device, the slave device does have a force sensor which provides information on the environment force f_e . Thus, the coupled environment/slave-device system can be obtained based on Eq. (6.1) and Fig. 6.5.(b). The uncertainty block in the environment/slave-device model is given, then, by $\Delta_e = k_e$.

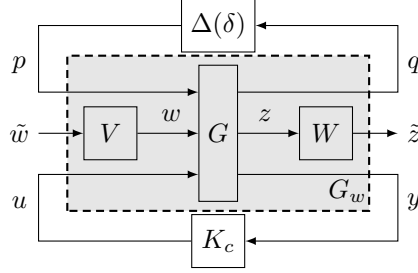


Figure 6.8: Generalized plant with weighting filters.

Weighted generalized plant

Having the two models of environment/slave and operator/master, we set up an LFR model of the teleoperation system as a generalized plant G_w as in Fig. 6.8, such that

$$\begin{pmatrix} \dot{x} \\ q \\ \tilde{z} \\ y \end{pmatrix} = \begin{pmatrix} A & B_1 & B_2 & B \\ C_1 & D_1 & D_{12} & E_1 \\ C_2 & D_{21} & D_2 & E_2 \\ C & F_1 & F_2 & 0 \end{pmatrix} \begin{pmatrix} x \\ p \\ \tilde{w} \\ u \end{pmatrix}$$

is a state space representation of G_w . In G we embed the non-uncertain part of the operator/master-device/force-observer and environment/slave-device models.

The uncertainty block is then defined as $\Delta(\delta(t)) = \begin{bmatrix} k_h(t) & 0 \\ 0 & k_e(t) \end{bmatrix}$ $\Delta \in \mathbf{\Delta}$, where

$$\mathbf{\Delta} = \left\{ \begin{bmatrix} k_h & 0 \\ 0 & k_e \end{bmatrix} : k_h \in [\underline{k}_h, \bar{k}_h], k_e \in [\underline{k}_e, \bar{k}_e] \right\}.$$

The vector q and p contain the signals interfacing the uncertainty, thus we define $q = \text{col}(x_m, x_s)$ and $p(t) = \Delta(\delta(t))q(t)$. One can see that the model can be easily adapted to the cases in which other parameters might also be assumed to be uncertain. We assume that we can measure the environment force and position of the master and slave devices, possibly contaminated with measurement noise vector $y_n = \text{col}(f_{en}, x_{mn}, x_{sn})$. The measured signals are included in the vector y as well as the estimated operator force \hat{f}_h , thus $y = \text{col}(\hat{f}_h, f_e, x_m, x_s) + \text{col}(0, y_n)$. The disturbance signals of the system are represented by the vector w . We treat the active forces from the operator and environment as disturbance signals. We include the noise channels y_n as disturbances. This allows to increase the robustness against noise, which helps to obtain a controller more suitable for implementation.

Thus, we define $w = \text{col}(f_h^*, f_e^*, f_{en}, x_{mn}, x_{sn})$. Additionally, the actuation signal vector u is defined as $u = \text{col}(f_m, f_s)$. Finally, the performance vector z is defined as $z = \text{col}(f_h - f_e, x_m - x_s, f_m, f_s)$. Via the component $f_h - f_e$, we enforce that the human operator should feel the same force applied by the environment. The second component, $x_m - x_s$, is the position error to obtain tracking between master and slave. The actuation variables are also included as channels to be penalized to avoid controllers with high gains. Finally, \tilde{w} and \tilde{z} are weighted copies of w and z via predefined filters V and W respectively, which allow to shape the desired system performance.

The chosen performance criterion is defined as the \mathcal{L}_2 gain, γ , of the mapping from disturbance channels \tilde{w} to the performance channels \tilde{z} , as is customary in model-based \mathcal{H}_∞ control, e.g., see Skogestad and Postlethwaite (2005). The \mathcal{L}_2 gain from \tilde{w} to \tilde{z} can be expressed as:

$$\sup_{0 \neq \tilde{w} \in \mathcal{L}_2} \frac{\|\tilde{z}\|_2}{\|\tilde{w}\|_2} < \gamma, \quad (6.2)$$

in which γ can be interpreted as a worst-case gain from the disturbances \tilde{w} to the performance signals \tilde{z} . Therefore, instantaneous responses that can be felt by the operator have a direct effect on the performance criterion. This makes the \mathcal{L}_2 gain a suitable performance criterion for teleoperation systems.

Finally, K_c represents the to-be-designed controller. The aim of the controller design is then to find a controller K_c that has robust performance for all $\Delta \in \mathbf{\Delta}$. In the coming sections we will shortly describe the robust control methods to be evaluated in the surgical setup.

6.2.3 Robust control under time-varying uncertainties

One of the main objectives in this chapter is the evaluation of the model based control method for teleoperation proposed in Chapter 2. Such method allows to synthesize a controller K_c such that the closed loop system in Fig. 6.8 has robust performance under arbitrary fast and bounded parametric uncertainty given by $\Delta \in \mathbf{\Delta}$. For the details on the exact control synthesis procedure, the reader is referred to Chapter 2.

Such control design method has been satisfactorily tested in a one-DoF academic setup with force and position sensors in both master and slave devices. In order to apply it to our specific application, all what we need is the model of our system, which was already obtained in Section 6.2.2, and the specification of the weighting filters W and V on the performance channels in Fig. 6.8, as it is customary in robust control design. With these filters we specify a desired level of

force and position tracking in frequency domain. We use the same filter structure as in Chapter 2, with the main modification that in our application we do not have force sensor at the master side. The filters V and W are block diagonal transfer matrices emphasizing the frequency band in which we want the particular channel to be penalized. Thus $V = \text{diag}(V_{f_h}^*, V_{f_e}^*, V_{f_{en}}, V_{x_{mn}}, V_{x_{sn}})$ and $W = \text{diag}(W_{f_h-f_e}, W_{x_m-x_s}, W_{f_m}, W_{f_s})$. Ideally, one wants to have $f_h - f_e = 0$ and $x_m - x_s = 0$. In this case we would get perfect transparency, but as is known, this type of design is unrealistic (Lawrence (1993b)) and has poor stability properties.

Instead, it is desirable to relax such strict requirement, we are interested in forcing the force and position tracking errors such that in frequency domain $|F_h(\omega) - F_e(\omega)| < |F_w(\omega)|$ and $|X_m(\omega) - X_s(\omega)| < |X_w(\omega)|$ where $F_w(\omega)$ and $X_w(\omega)$ represent the desired level of force and position tracking in the frequency band of interest. We use $|F_w(\omega)| > 0$ and $|X_w(\omega)| > 0$ sufficiently small at low frequencies to achieve force and position tracking, which will lead to a desired level of performance in the frequency range in which the human operator performs movements. On the other hand, we need to have feasible control action that is magnitude bounded forces f_m , f_s and a reduced amplification at high frequencies, to avoid saturation and the excitation of high frequency dynamics. Those requirements are translated into the filters W and V shaped accordingly. Thus we put more weight at frequencies where we want to lower the \mathcal{L}_2 -gain.

After the filters have been defined, it is possible then to design a controller for a specific range of bounded operator and environment stiffness.

6.2.4 Switching robust control via bumpless transfer of robust controllers

The methods in Section 6.2.3 can provide high robust performance for bounded environment stiffness k_e in the range of low stiffness environments. However, in real-life applications it might be desired to guarantee stability of the teleoperation system for a wide range of environment stiffness $k_e \in [\underline{k}_e, \bar{k}_e]$, covering also stiff environments. In Chapter 3 it is shown that for those cases a single LTI controller might not be sufficient to achieve desired levels of robust performance of the teleoperation system, therefore the authors proposed a multi-controller structure, which will be tested in our non-ideal teleoperator. The main idea consists of scheduling different robust controllers according to the estimate \hat{k}_e of the actual value of k_e . Thus, a specific number N_c of LTI controllers are designed, in which the i th controller $K_{ci}(s)$ has an uncertainty set Δ_i of robust performance, such that all regions combined form a larger set such that $\Delta \subseteq \Delta_1 \cup \dots \cup \Delta_{N_c}$, where Δ describes the uncertainty set of the system. Such uncertainty distribution is de-

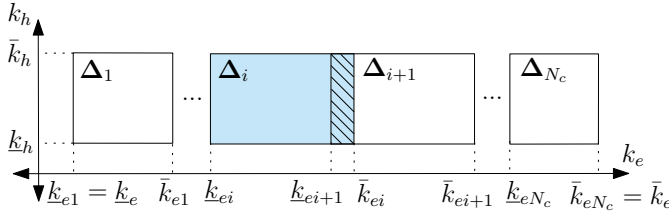


Figure 6.9: Uncertainty regions Δ_i of a switching robust controller.

picted in Fig. 6.9. The overlap between regions can be used to guarantee stability under bounded uncertainty in the estimation signal \hat{k}_e .

Next, in order to switch between controllers in a stable way, in Chapter 5 we used bumpless transfer of robust controllers, which is an extension of the bumpless transfer technique by Zaccarian and Teel (2005). The main idea is to keep all controllers online, either with the real plant, or with a virtual model. This idea is illustrated in Fig. 6.10, where K_{ci} represents the controller that is currently active, and K_{cj} one of all the other $N_c - 1$ controllers that remain disconnected

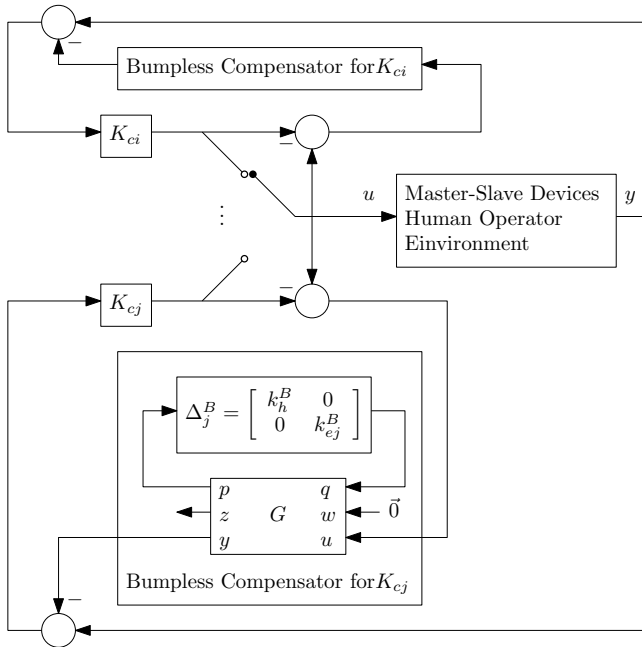


Figure 6.10: Bumpless Transfer Scheme for Teleoperation Control

from the real system. The bumpless compensator for K_{ej} consists then by a plant out of the corresponding group of plants for which the controller is robust to. Therefore we used the same model G as in Fig. 6.8 but we select a single element $\Delta = \Delta_j^B = \begin{bmatrix} k_h^B & 0 \\ 0 & k_{ej}^B \end{bmatrix}$ from the corresponding region Δ_j . In this way the off-line controller is virtually kept on-line and since we used $\Delta_j^B \in \Delta_j$, its stability, while off-line, is guaranteed.

This technique has been experimentally tested in a one-DoF setup in Chapter 5, and will be evaluated in our surgical system.

6.2.5 Environment estimation

To be able to implement the multi-controller structure, we need an estimator that is able to deal with abrupt changes of the environment stiffness k_e . We make use of the same estimator as in Chapter 3, which is an estimator proposed in Gustafsson (2000). The structure of the estimator is shown in Fig. 6.11. The working principle of this estimator is as follows: the *filter* block processes the discrete inputs u_k and outputs y_k of a system described by a *model* (in our case an environment model) to get an estimate $\hat{\theta}_k$ of certain parameters θ_k (the parameters of our environment model). Then, the signal ϵ_k is used to detect abrupt changes in the parameters and under certain criteria, the *detector* block sends an *alarm* to the filter to adapt quickly to the changes. Following the guidelines in Gustafsson (2000), the different blocks are described below.

Environment model as a linear regression model

We write our environment model in the following form

$$y_k = \varphi_k^T \theta_k + e_k$$

where k denotes sampled time instants, y_k is the measured environment force, e_k is the corresponding noise, the environment parameters vector is $\theta_k = \text{col}(k_e(k), f_e^*(k))$ with $f_e^*(k)$ being the active component of the environment force, and the so called

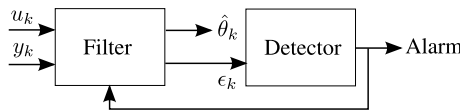


Figure 6.11: Estimator with Change Detection

regression vector φ_k is given by $\varphi_k = \text{col}(u_k, 1)$ with $u_k = x_s(k)$ being the position of the slave device.

Filter

For the filter block we utilize a Kalman filter for linear regressions, which is implemented in its recursive form as follows:

$$\begin{aligned}\varphi_k &= \text{col}(u_k, 1) \\ K_k &= \frac{P_{k-1}\varphi_k}{R_k + \varphi_k^T P_{k-1} \varphi_k} \\ P_k &= P_{k-1} - \frac{P_{k-1}\varphi_k \varphi_k^T P_{k-1}}{R_k + \varphi_k^T P_{k-1} \varphi_k} + Q_k \\ \hat{\theta}_k &= \hat{\theta}_{k-1} + K_k(y_k - \varphi_k^T \hat{\theta}_{k-1}) \\ \epsilon_k &= y_k - \varphi_k^T \hat{\theta}_k\end{aligned}$$

where $\hat{\theta}_k$ is the estimated vector of the environment model parameters, R_k is taken as 1 without loss of generality and Q_k is a design parameter that determines the speed of converge of the filter. Large values of Q_k make the filter to react faster but also the estimate will have more noise. The variable ϵ_k is the error between the actual measurement and the reconstructed measurement obtained with $\hat{\theta}_k$.

Detector

The detector block is defined as a threshold function in order to decide when to make the filter to react fast. Thus, when $|\epsilon_k| < L_{|\epsilon_k|}$, no alarm is generated and we use $Q_k = Q_{nom}$. When $|\epsilon_k| \geq L_{|\epsilon_k|}$, it means that \hat{y}_k has deviated too much from the true measurement and the filter must adapt rapidly to the new environment by setting $Q_k = Q_{fast}$.

Therefore, the estimator is tuned via $L_{|\epsilon_k|}$, Q_{nom} and Q_{fast} . This tuning is essential to be able to detect abrupt changes fast enough to schedule on time the controllers of the multi-controller structure.

6.3 Results of robust control applied on SOFIE robot

In this section we provide synthesis, simulations and experimental results. Initially one robust controller designed with the method mentioned on Section 6.2.3 is

evaluated on the surgical system. Then, a multi-controller structure as described in Section 6.2.4 is also implemented and experimentally tested.

6.3.1 Controller synthesis results

For the controller synthesis we tune the weighting filters such that force and position tracking is achieved for frequencies below $f_{bw} = 10$ Hz, and the actuation forces f_m, f_s are penalized from 60 Hz and beyond. The reader is referred to Chapter 2 for more details on the weights structure and fine tuning procedure. Moreover, the cut-off frequency of the low pass filters LPF_1 and LPF_2 in the force estimator is set to 20 Hz, which suppress noise above the frequencies of interest.

For the first controller to be evaluated, we select a desired environment range as $k_e \in [80, 3000]$ N/m, which covers the range of stiffness present in soft tissue environments (see Gerovich et al. (2004)).

Then, using the model found in Section 6.2.2, we apply the control synthesis procedure of Chapter 2. We get a controller $K_c(s)$ covering the uncertainty region of interest and with a performance index $\gamma = 10.7$. The resulting order of the controller $O_{K_c} = 21$, which is equal to the order of the generalized plant G_w , i.e. including the weighting filters. We make the remark that in comparison to classical controller schemes like position-position error, position-force, etc., the obtained controller does not have a defined structure, other than its number of inputs and outputs. In that sense the controller uses all available combinations from inputs to outputs, as opposed to most classical controller architectures in which some input-output combinations are not used. Hereafter, the obtained Robust Controller (RC) will be referred as the RC.

Next, for illustrative purposes, we evaluate the properties of the force estimator when used in combination with the RC. We added uncertainty in the model used in the estimator by setting its parameters to $\hat{m}_m = c_p m_m$, $\hat{b}_m = c_p b_m$ and $\hat{k}_m = c_p k_m$ for $c_p \in [0.8, 1.2]$. Then, we computed the transfer functions from f_h to \hat{f}_h . We compare two cases, in the first one, we used the standard dashed interconnection in Fig. 6.7, in the second one, instead, we used the control element from \hat{f}_h to f_m of the RC previously designed. The magnitude bode diagrams of the resulting transfer functions from f_h to \hat{f}_h are depicted in Fig. 6.12. As reported in the literature, the standard feedback provides robust and accurate estimations in the frequency region of interest. However, from the figure one can see resonance peaks that can have undesirable effects on the haptic feedback to the operator. On top of that, the estimator is not to be stable for $c_p \in [0.8, 0.9]$. On the other hand, the estimator using the feedback via $K_c(s)$ presents better stability robustness properties because all transfer functions were stable. Moreover resonance peaks

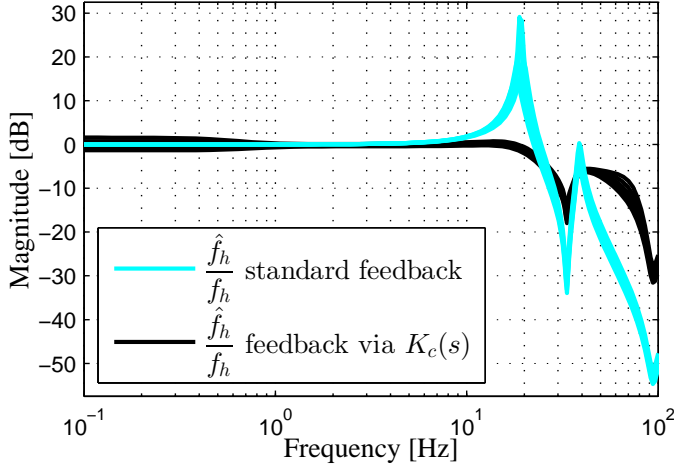


Figure 6.12: Magnitude Bode Diagram of the transfer functions from f_h to \hat{f}_h under model uncertainty; using a standard feedback loop and a feedback via the robust controller $K_c(s)$

are not present which is beneficial for our application. As a trade-off, robustness of the estimation accuracy is slightly degraded for very low frequencies, which did not have a significant influence on the simulation and experimental phase as will be shown later.

Next, we also evaluate a multi-controller based on bumpless transfer of robust controllers. The controller designed based on this structure is hereafter referred as the Bumpless Transfer Controller (BTC). For this controller, we select a wider range of environment stiffness $k_e \in [80, 10000]$ N/m. We divide the total uncertainty region in two partitions, therefore $N_c = 2$. We select the first region equal to the previous synthesis case covering soft tissue environments, i.e. $\Delta_1 = \left\{ \begin{bmatrix} k_h & 0 \\ 0 & k_{e1} \end{bmatrix} : k_h \in [731, 1200], k_{e1} \in [80, 3000] \text{ N/m} \right\}$. Thus we can use the controller $K_c(s)$ as $K_{c1}(s)$. For the second region we select $\Delta_2 = \left\{ \begin{bmatrix} k_h & 0 \\ 0 & k_{e2} \end{bmatrix} : k_h \in [731, 1200], k_{e2} \in [2500, 10000] \text{ N/m} \right\}$. After applying the synthesis procedure in Chapter 2, we get a controller $K_{c2}(s)$ with a performance index $\gamma = 9.2$. Both controllers $K_{c1}(s)$ and $K_{c2}(s)$ have an order of $O_{K_{c1}} = O_{K_{c2}} = 21$.

In order to improve the operator's haptic perception when the slave device is in "free air", i.e. no contact with any environment, we implemented a PID controller (with a weak integrator and additional low-pass filters) that tracks the position of the master device in the slave device. The idea is that this controller is only active when the environment force is lower than a small threshold $f_e < 0.05$ N m. Thus, the operator will only feel the dynamics of the light master device. We defined

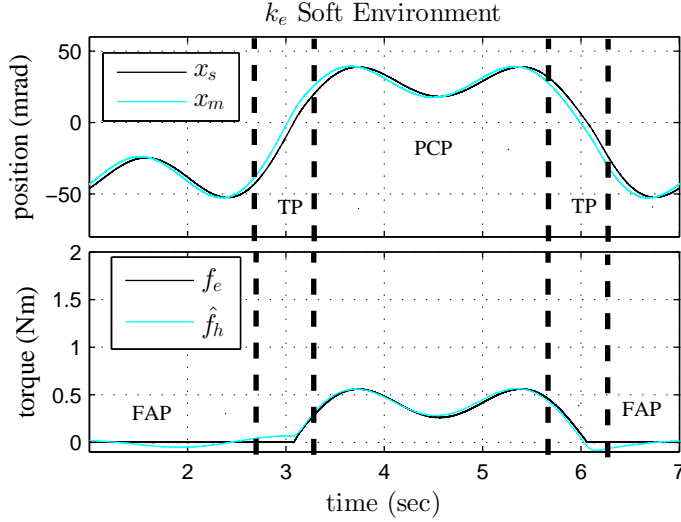


Figure 6.13: Simulated time domain response of one robust controller when interacting with a soft environment

the position tracking controller as $K_{c0}(s)$, the order of which is $O_{K_{c0}} = 3$. This controller was manually tuned. The aim is to obtain a similar position tracking performance as the one of the controller $K_{c1}(s)$. This improves in practice the transient behavior transition between controllers $K_{c0}(s)$ and $K_{c1}(s)$.

Next, in order to implement the bumpless transfer structure, we need to define the elements $\Delta_j^B \in \Delta_j$ to compute the bumpless compensators for controllers $K_{c0}(s)$, $K_{c1}(s)$ and $K_{c2}(s)$ respectively. The component k_h^B is selected as $k_h^B = (\bar{k}_h - \underline{k}_h)/2$. The components k_{ej}^B are selected arbitrarily, thus we use the next three elements:

$$\Delta_0^B = \begin{bmatrix} 1016.7 & 0 \\ 0 & 0 \end{bmatrix}, \quad \Delta_1^B = \begin{bmatrix} 1016.7 & 0 \\ 0 & 500 \end{bmatrix}, \quad \Delta_2^B = \begin{bmatrix} 1016.7 & 0 \\ 0 & 5000 \end{bmatrix} \text{ N/m.}$$

The order of each bumpless compensator is $O_C = 16$. Thus, the total order of BTC is then $O_{BTC} = O_{K_{c0}} + O_{K_{c1}} + O_{K_{c2}} + 3O_C = 93$. This is one of the disadvantages of this technique, which demands high computational capabilities. Finally, all the controllers, the bumpless compensators and the force estimator blocks are discretized with the ‘tustin’ method with a sample frequency of 4000 Hz.

6.3.2 Simulation results

To test the controllers, we simulate a scenario in which an operator manipulates the system with the slave device in free-air and then gets in contact with a spring located at $x_s > 0$. Then after some periodic movements the operator comes back again to the slave in the free-air situation. As an example of such scenario see Fig. 6.13. The Free Air Parts (FAP) correspond to time slots when there is no contact with the environment. The Transient Parts (TP) correspond to time slots where there is a transition between the FAP and contact with the spring or vice-versa. The Permanent Contact Part (PCP) is a time slot after the TP has passed and periodic movements are performed while being in permanent contact with the spring. For the operator we have used $f_h^* = (2 \cos(1/3\pi t) + \cos(\pi t))\text{N m}$ and $k_h = 1016.7\text{N/m}$. In the simulations, both signals \hat{f}_h and f_h have unnoticeable differences in the plots, therefore we only plot the signal \hat{f}_h when we illustrate the operator force, this to be consistent with the experiments in which the real operator force is not available.

First, we test the Robust Controller (RC). We simulate the closed-loop system interacting with a spring with $k_e = 400\text{N/m}$, which represents a soft environment. The corresponding time domain response of the position and force signals are presented in Fig. 6.13. One can see stable responses during the Transient Parts (TP), which is ensured from the synthesis of the RC. Moreover we observe that in the Permanent Contact Part (PCP) there is force and position tracking of the simulated teleoperated system. On the other hand, the force tracking degrades during the Free Air Parts (FAP) and some forces are noticeable in the operator side, These forces can degrade the haptic rendering of a free-air environment provided by the teleoperator.

Next, we test the Bumpless Transfer Controller (BTC) by simulating the closed-loop system with springs with $k_e = 400\text{N/m}$ and $k_e = 10\,000\text{N/m}$ representing soft and stiff materials respectively. For simulation purposes we assume we can know perfectly the environment stiffness, thus we set $\hat{k}_e = k_e$. The time domain results are depicted in Fig. 6.14, on the left for the soft spring, and on the right for the stiff environment.

One can see that the response in the FAPs is improved because now \hat{f}_h is close to zero in those time slots. For the soft spring, we can see that during the TP, the transient response is smooth and barely noticeable, despite the fact that there is a switch between $K_{c0}(s)$ and $K_{c1}(s)$. Next, regarding the interaction with the stiff spring, the response presents some overshoot behavior during the TP, yet that overshoot in positions and forces is rapidly damped out. During the PCP, for the soft spring force and position tracking is obtained as expected from the RC results. For the stiff spring, we can see that the position tracking degrades slightly,

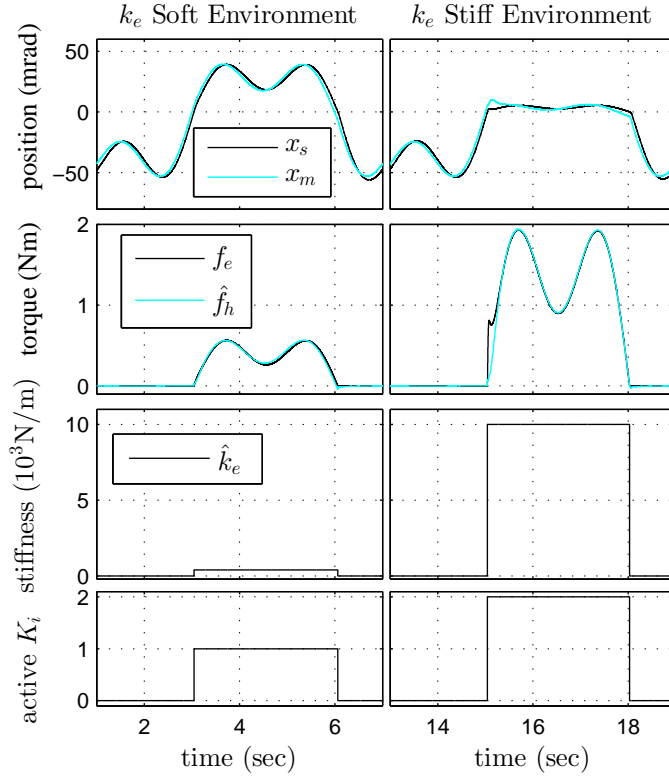


Figure 6.14: Simulated time domain response of bumpless transfer controller when interacting with an environment with stiffness $k_e = 400 \text{ N/m}$ (left) and $k_e = 10000 \text{ N/m}$ (right).

however the operator still would perceive a correct haptic perception of the stiff environment as it will be shown later.

We also analyse the performance of the system by means of force versus position plots on the environment and operator sides as shown in Fig. 6.15. The slope of f_e versus x_s plots represent the stiffness of environment and the slope of the \hat{f}_h versus x_m plots represent the stiffness being felt by the operator. We can see that in the PCP both controllers $K_{c1}(s)$ and $K_{c2}(s)$ provide to the operator a haptic perception close to that of the environment, which is desirable in our application. Moreover, during the FAP the estimated operator's force is very small, which is desirable when there is not environment in contact with the slave device. These simulations results confirms that the controller design through the proposed methods leads to promising results. In the next section we present results

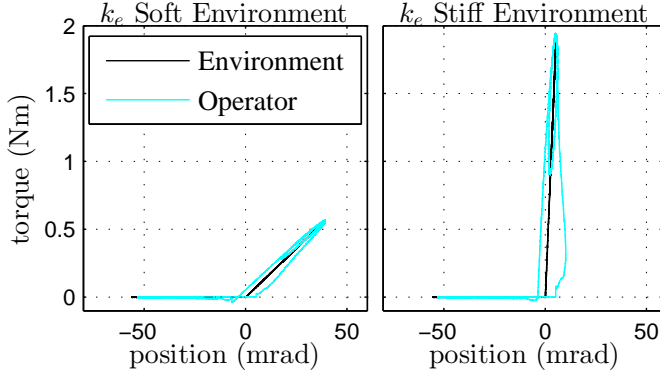


Figure 6.15: Simulated time domain response of one robust controller when interacting with an environment with stiffness $k_e = 400\text{N/m}$ (left) and $k_e = 10000\text{N/m}$ (right).

of both controllers, the RC and the BTC, that validate experimentally the used control design methodology.

6.3.3 Experiments

In this section, we validate the RC and the BTC with experiments on the surgical setup described in Section 6.2.1.

We test two different environments: a soft foam with stiffness $k_e \approx 400\text{N/m}$, and a stiff foam with $k_e \approx 10000\text{N/m}$. For the experiments, we drove the system under similar operating conditions as to the simulation part, i.e. Free-Air Parts

Initially we test the RC controller, the time domain responses for the interaction with both type of environments are depicted in Fig. 6.16. Regarding the interaction with the soft foam, the response during the TPs is completely smooth, i.e. there are neither oscillations nor overshoots, which verifies the robustness properties of the RC controller. During the PCP, the tracking performance is less than that of the simulations results, which can be mainly due to the high friction present in the slave device. However, if we analyse the results by means of force versus position plots as depicted in Fig. 6.17, one can see that in the PCP the operator perceives a similar stiffness as that of the environment, which validates the potential of the control approach. Next, the interaction of the RC with a stiff environment resulted in an unstable behaviour as can be seen from the oscillations in Fig. 6.16, result which could be already expected from the controller synthesis, because robust

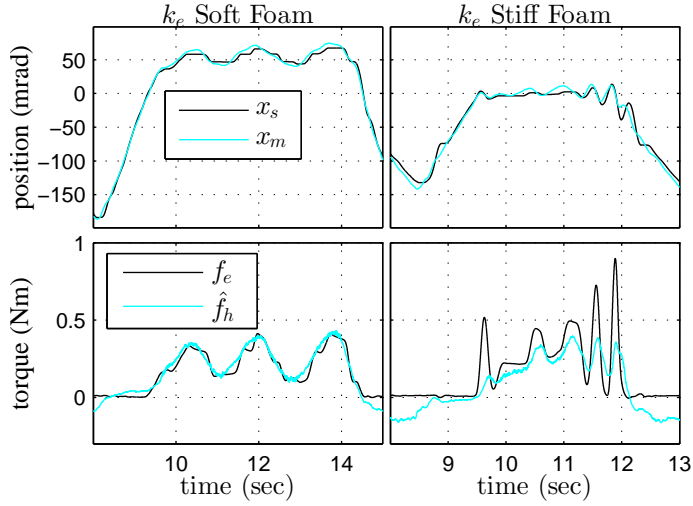


Figure 6.16: Time domain response of one robust controller when interacting with different environments

performance is not guaranteed for stiff environments. (FAP), Transient Parts (TP) and Permanent Contact Part (PCP).

Regarding the FAPs one can see some noticeable forces on the operator side which

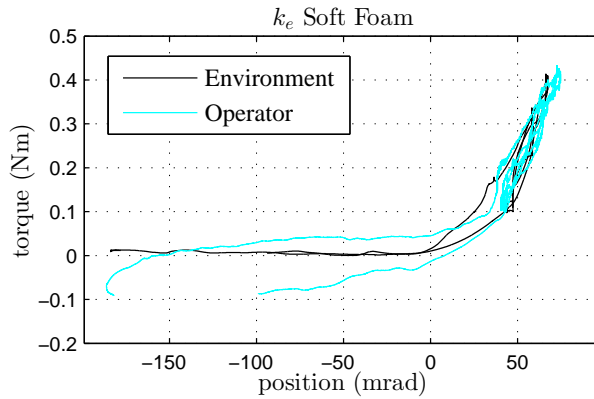


Figure 6.17: Force versus Position plots from experiments of a robust controller when there is interaction with a soft foam.

were perceived as a damping action, this in fact degraded the operator's haptic feeling of a free-air environment. Such dynamics can be also seen in the force versus position plots in Fig. 6.17. Next, to be able to implement the BTC, we tuned the environment estimator experimentally. This process can be done without the BTC being active, for instance using only the tracking controller $K_{c0}(s)$. We gathered data from tests in which we interacted with different environments. The data were then processed off-line to tune the estimator parameters using the guidelines of Section 6.2.5. We arrived to the following parameters: $L_{|\epsilon_k|} = 0.2\text{ N}$, $Q_{fast} = \text{diag}([10^6, 10^3])$ and $Q_{nom} = 0.5 \times \text{diag}([10^2, 1])$.

The time domain response of the closed-loop system is shown in Fig. 6.18. The environment estimator works fast and accurate enough to be able to distinguish

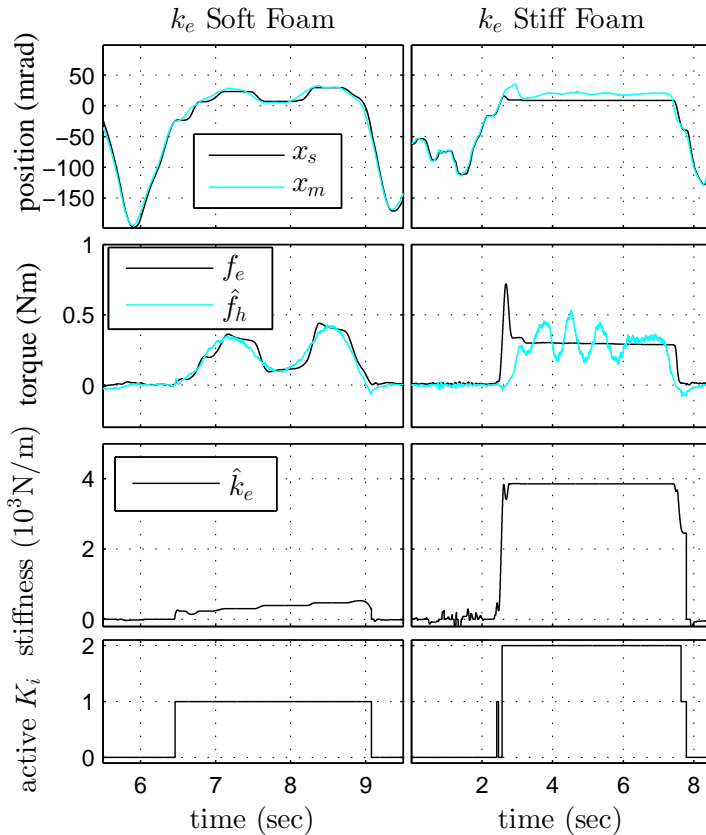


Figure 6.18: Time domain response of the bumpless transfer controller when interacting with different environments.

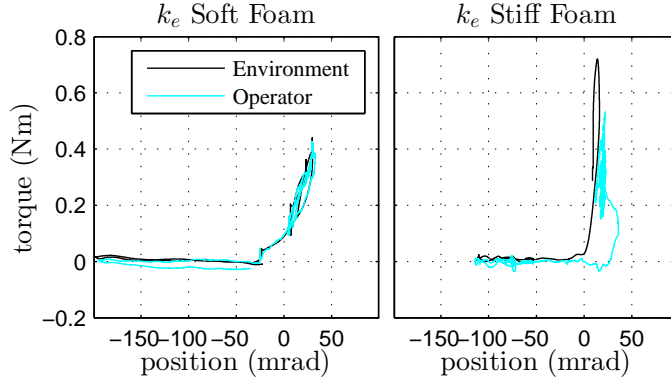


Figure 6.19: Time domain response of the switching robust controller when interacting with different environments

between the two types of environments. We make emphasis that a correct tuning of the estimator is important, this because a fast detection in the changes allows to schedule the controllers on time, accuracy is only important to determine the region in which the stiffness environment lies and not its exact value.

Next, when interacting with the soft spring, the responses in the TPs are free of overshoots and oscillations and the results are very similar as those in the simulations. Moreover, the FAP is improved with respect to the RC. In fact in this scheme the operator does not feel additional dynamics other than those of the master device, and because it is light, the haptic perception of having a free-air environment on the slave side is realistic. To have a different picture of the results, forces versus position plots for this test are presented in the left part of Fig. 6.19. One can see that the BTC provides a very similar stiffness of the environment at the operator side at all times. The response during the TP when getting into contact with a stiff environment presents some overshoot, however the stability was not compromised during the experiments. Subsequently, during the PCP, the operator performs periodic movements, however the slave does not move during this time slot. The cause for the lack of movement of the slave device in stiff environments comes from two combined facts: first the slave device is non-backdrivable, which in principle means that the device only moves when it actuated from the actuation signals f_s , second, the slave device has high friction, thus, the actuation signals from the controller need to be sufficiently large to move the slave device. Yet with this phenomenon, the operator was able to perceive a high stiffness on the master side as can be in Fig. 6.19.

6.3.4 Discussion

The simulation and experimental results for the RC confirmed the results obtained in Chapter 2. The description of the operator and environment as explicitly time-varying is suitable for the controller synthesis in bilateral teleoperation, especially because of the sudden changes in the environment. Moreover, because we used a model based control synthesis, there are no restrictions on matches in the mechanical properties of the master and slave devices to apply the method, contrary to for instance in Willaert et al. (2014). The main challenge in this chapter was to apply the synthesis methods in an non-ideal teleoperator with properties like the non-backdrivability of the slave device and not having a force sensor in the master device. The latter aspect was challenging in order to get a model for the operator. Nonetheless, it was enough to get a rough estimation of the operator's model parameters in order to obtain good experimental results, which shows that even under those limitations the synthesis method can be applied.

Moreover, the fact that we included the force estimator in the system's model, was essential to obtain good experimental results. The standard disturbance observer can have poor stability robustness properties as found before. In our case, the loop from \hat{f}_h to f_m was designed only by the control synthesis procedure, thus it was guaranteed that a stable force estimator is obtained. Moreover its stability robustness properties against model uncertainty were improved.

Next, regarding the multi-controller structure, the results showed that multiple controllers, which were designed to have a good performance in their respective regions of interest of environment stiffness, were successfully combined by means of the bumpless transfer technique proposed in Chapter 5. Thus the operator could have a good feeling when the slave is in free air, plus a good stiffness reflection when discriminating soft tissues and, additionally, a feeling of a high stiffness for stiff environments, all this combined while having a stable interaction. In fact, the switching between the controller $K_{c0}(s)$ and $K_{c1}(s)$ is made in a stable and smooth way, which makes the BTC very promising in applications where it is expected that the slave device is mainly either on free-air or in contact with soft tissue. The switch to controller $K_{c2}(s)$ presents some overshoot behavior but stability was not compromised during the experiments. The subsequent force and position tracking was degraded but still a high stiffness is provided to the operator. However, if force tracking under stiff environments is relevant, for instance for cutting bone, then such an issue needs improvement. This may be achieved by implementing friction compensation on the slave device.

Finally, during the experimental phase we noticed that the accuracy of the environment estimator degrades for high values of stiffness, e.g. $k_e > 4000 \text{ N/m}$, the estimated values did not increased much despite the stiff environment. One of

the reasons we found is that the slave device barely moves right after getting in contact with the stiff environment due to the non-backdrivability and high friction of the slave device. In terms of the parameter estimation it means that no new information is available to update further the estimations. This behaviour would be problematic for techniques that rely on an accurate environment estimator, e.g. Willaert et al. (2010), Cho et al. (2013). In the BTC structure estimator accuracy is needed only around the overlapping region between Δ_1 and Δ_2 , which is used to determine whether to use $K_{c1}(s)$ or $K_{c2}(s)$. Thus, the BTC offers an advantage in that respect with other techniques that use environment estimation parameters in their control laws, and rely more on parameter estimation accuracy in a wide range of environment stiffness.

6.4 Conclusions

In this chapter we have implemented two type of controllers in a tele-surgical setup: one with a single LTI controller, and one with a multiple-controller structure. Both types were designed with model based robust control techniques. Because there is no sensor at the master device, rough estimates of the operator's model parameters were computed. Even with this limitation, the obtained experimental results matched with the theory and simulations. Moreover, due to the lack of force sensor in the master device, a disturbance observer was implemented to obtain an estimate of the operator's force. Despite the possible mismatch between the model of the master device and the real device, analysis showed that the proposed implementation of the operator's force estimator delivers accurate and robust estimates. Such result was obtained because the disturbance observer model was included in the system's model, improving the stability properties of the estimator after the control synthesis. Additionally, the results showed that it is possible to combine multiple robust controllers to reflect to the operator, in a stable way, a stiffness similar to that of the environment. Moreover, satisfactory results were obtained for different types of environment, ranging from free air and soft to stiff environments, despite non ideal properties of the surgical setup, like non-backdrivability, high mass and high friction in the slave device, and lack of force sensor on the master device. All this demonstrates the suitability and potential of the utilized control methods to be implemented in real-life engineering practice.

Chapter 7

Conclusions and Recommendations

7.1 Conclusions

In this thesis, we have presented a systematic approach towards control design for bilateral teleoperation. The approach involves modelling of the teleoperation system, in which we use models of the operator derived from experiments, and we use pre-defined models of the environment motivated by the type of the applications considered. In this way, the set of uncertain dynamics of the bilateral teleoperation system can be narrowed down to those present in a particular application, thus already reducing the conservatism in the modelling phase. Moreover, the proposed model describes the uncertain dynamics by means of parametric uncertainties. This allowed us to handle the uncertain parameters of the bilateral system in a systematic way. Therefore, it was possible to take explicitly into account properties like boundedness and time-variation of the operator and environment model parameters during control design.

Based on this modelling, we used synthesis tools that allowed us to systematically and simultaneously address stability and performance, in contrast with conventional methods in which both are treated separately. Throughout this thesis, the analysis, simulation and experimental results of the cases at hand were consistent with each other, showing that the assumptions we made during modelling and synthesis were appropriate, thus demonstrating the potential of the design methodology here presented. In this thesis we used a performance criterion based on force and position tracking. The synthesis tools allow for other performance

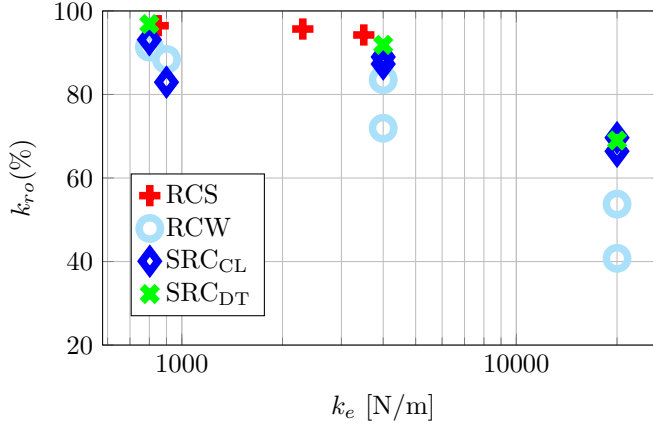


Figure 7.1: Orthogonal linear regression analysis results to evaluate stiffness reflection in the simulations. $k_{ro}(\%)$ is the percentage of the environment stiffness that is reflected to the operator is shown. RCS: Robust Controller for Soft environment stiffness (Chapter 2). RCW: Robust Controller for Wide range of environment stiffness (Chapters 3 and 4). SRC_{CL}: Switching Robust Controller with Common Lyapunov Function (Chapters 3 and 4). SRC_{DT}: Switching Robust Controller with Dwell Time conditions (Chapter 4).

criteria as long as they can be represented as linear matrix inequalities.

In order to quantify and compare the results obtained with the different techniques proposed in this thesis, we performed an analysis to determine the percentage k_{ro} of environment stiffness that is reflected to the operator. The analysis is the same as the one performed in Chapter 3. We took the responses in time domain of the system and extracted the data from the time slots in which there is a permanent contact with the environment. Then, for each set of data of forces versus positions values, an orthogonal regression is applied in order to fit a straight line. The slope of such a line is an estimation of the stiffness value corresponding to the respective set of points of force versus position values. The orthogonal regression uses the sum of the squares of the distance of the data points to the fitted line as optimization cost. This procedure is applied to both the operator and the environment sides. The ratio between both yields the percentage k_{ro} of environment stiffness that is reflected to the operator. The analysis is performed for all controllers that were designed for the 1-DoF setup utilized in this thesis. The results of the analysis for all the simulations is presented in Fig. 7.1 and the results of the analysis for all the experiments is illustrated in Fig. 7.2.

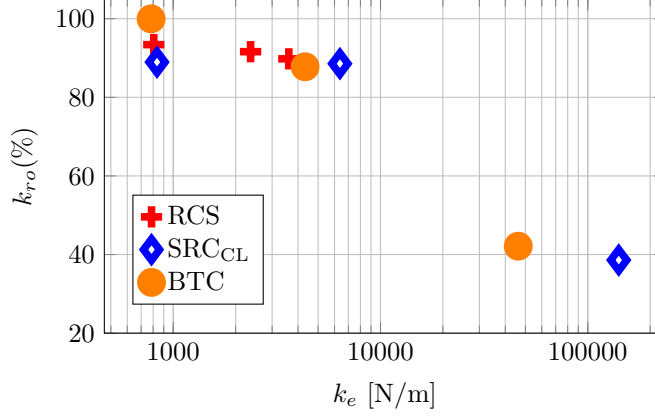


Figure 7.2: Orthogonal linear regression analysis results to evaluate stiffness reflection in the experiments. $k_{ro}(\%)$ is the percentage of the environment stiffness that is reflected to the operator is shown. RCS: Robust Controller for Soft environment stiffness (Chapter 2). SRC_{CL}: Switching Robust Controller with Common Lyapunov Function (Chapter 3). BTC: Bumpless Transfer Controller (Chapter 5).

Regarding the specific design case when a single robust controller is used, from Figures 7.1 and 7.2 one can see that k_{ro} is always greater than 90%. Hence, the simulation and experimental results demonstrated that the proposed methods allowed to obtain high performance and stability simultaneously in the range of soft environments, not only during continued contact, but also for sudden changes of the environment as observed in the time domains plots. This confirms that by treating explicitly the operator and environment model parameters as time-varying, the bilateral teleoperation system is described more realistically. From Fig. 7.1 one can see that if a single robust controller is designed for a wide range of values of environment stiffness, the overall factor k_{ro} decreases, which is an example of the robust stability and performance trade-off in bilateral teleoperation systems.

In order to improve the performance of the system and to extend the usable range of values of environment stiffness, in this thesis we have also proposed a multi-controller structure. The main idea is that several robust controllers are scheduled according to an estimate \hat{k}_e of the actual environment stiffness. The main challenge of this type of control is to achieve a stable and preferably smooth transition between the different controllers, especially because in bilateral teleoperation large overshoots and oscillatory behavior responses can degrade the haptic perception of the operator. To this end, we explored three different methods for controller switching, one based on the existence of a common lyapunov function, one based on dwell time conditions, and one based on bumpless transfer.

Even under the requirement on the existence of a common lyapunov function, the synthesis results showed that it is possible to improve the performance of the teleoperated system using the multi-controller structure, in comparison with the case when only a single LTI robust controller is used. Analysis results of k_{ro} in Fig. 7.1 confirm such overall improvement of performance. Moreover, the simulations and experiments validated the synthesis results and also demonstrated that indeed a smooth and stable switching among controllers is achieved because they all share a common lyapunov function.

In the case in which the controller synthesis was based on dwell time conditions, the theoretical results demonstrated that the flexibility added on the relation between the lyapunov functions corresponding to the different controllers indeed resulted in improved performance. This is confirmed by a better overall k_{ro} with respect to the other controllers evaluated in Fig. 7.1. Although the simulation showed that switching is made in a stable way, stability is only guaranteed under the condition that the dwell times are respected. However, smoothness during switching is not fully guaranteed, for instance, if a large dwell time is used during synthesis, the results would be equivalent to having all the controllers designed independently, for which a direct switch would cause oscillatory dynamics and large overshoots which compromises the system's stability. Hence, more insight is needed in the restrictions on the usable average dwell times that can work on practice.

Interestingly, even if the controllers are designed independently, experimental results showed that stable switching among the controllers can still be achieved using the proposed bumpless transfer scheme. The main advantage of this scheme is that each controller can be separately optimized for performance in its corresponding region of uncertainty dynamics. The analysis results in Fig. 7.2 shows that an overall improved k_{ro} is achieved with the proposed scheme. In conclusion, it was possible to successfully combine one controller optimized for low and medium stiffness values and another optimized for stiff environments, thus improving the overall performance of the system.

The stability of the multi-controller schemes depends on the fast convergence of the environment estimator. However we point out that the accuracy is needed only to determine to which region the environment stiffness belongs to. Thus the estimator can be optimized for this purpose. In fact, we showed that it is possible to implement an estimator that has a fast response to sudden and rapid changes in the environment. The corresponding response time was small enough to perform stable switching among the LTI controllers of the multi-controller schemes. However, more insight is needed to know what is the maximum allowable estimator response time to guarantee stability of the closed loop system. On the other hand, a parameter estimator is not per se needed to determine which controller should be active, because it is only needed to know to which region the environment

currently belongs. Alternative approaches are suggested in the next section.

Throughout this thesis we proposed different control design methodologies, systematically increasing the performance of the bilateral teleoperation system as confirmed by the analysis of the simulation and experimental results in Figures 7.1 and 7.2 respectively. Comparing the multi-controller structures, one can see the improvement was mainly noticeable for low environment stiffness, which is the region of environment stiffness of major interest in many medical applications.

The model-based robust control approach was implemented in a real telesurgical setup. Because there was no force sensor at the master device, we made use of a disturbance observer to obtain an estimate of the operator's force. A key aspect to a successful implementation was the fact that the disturbance estimator was included in the model together with the master device and operator dynamics. In this way, the controller synthesis guaranteed the stability of the whole system including the estimator. Moreover, analysis results showed that the proposed implementation of the operator's force estimator delivers robust estimations. The experimental results demonstrated that the model-based robust control is also suitable for non-ideal teleoperators, with characteristics such as a heavy, non-backdrivable slave and a master device with structural resonances and no force sensor. This shows the suitability and potential of the utilized control methods to be implemented in real-life engineering practice.

Regarding numerical complexity of the different methods, there are two aspects to look at, the synthesis complexity and the implementation complexity. In terms of synthesis complexity, for the single robust controller case, the number of variables to be solved by the LMI depends directly on the order of the models and the number of uncertain parameters of the system. In the multi-controller case, the synthesis complexity increases proportionally with the number of LTI controllers to be used because all the controllers have to be designed simultaneously. In contrast, the bumpless transfer scheme allows for independent controller design, which allows to split the synthesis complexity in parts. On the other hand, in terms of implementation complexity, the bumpless transfer exhibits the worse case because all the controllers need to be active either in the loop with the real plant or in a virtual loop with a plant model, which is the main disadvantage of this scheme. The other schemes require less computational power since only one controller is active at a time.

7.2 Recommendations for future research

The methods and results presented in this thesis are just a preamble to show the potential of the proposed approach, and it opens a new research line on modelling and control design for bilateral teleoperation systems. There are still several open challenges in order to develop further the methodologies here presented. Thus, in this section we indicate the main points for improvement and give future directions to continue this research in different areas.

Modelling

In this thesis, the human arm models were derived from experiments conducted on one operator and for specific types of posture, while he/she grabbed the master devices. Thus, it is desirable to broaden the model to cover different postures and operators. It is expected that the group of muscles that an operator uses while manipulating the master device will change for different postures. Thus, we foresee this will increase the range of variation of parameters like mass and damping of the model found in Chapter 2, thus more parameters would need to be considered uncertain as well. This will increase the set of dynamics covered, however, the utilized methods in this thesis describe arbitrary fast time-varying parametric uncertainty, which might be too conservative, limiting the achievable performance. Therefore, increasing the number of uncertain parameters should be complemented by a better description of the parameters, for instance, including bounds on the rate of variation of the operator's arm model parameters. In fact, Polat (2014) showed that including bounds on the rate of variation of the parameters of an operator's model reduces conservatism on the achievable performance.

Moreover, during normal operation, many mechanical properties of the operator's arm depend on the forces he/she is exerting. A model including such information could reduce the conservatism on the set of dynamics covered by the model, which combined with the appropriate control methods could increase even further the achievable performance.

Control Synthesis

All the proposed methods provided robust performance for the uncertainty region taken into account during synthesis. However, outside that region, the robust stability properties are not known a-priori. For instance, when the common lyapunov function technique was used to synthesize a multi-controller, its robustness properties degraded rapidly for increased operator's hand mass. Thus, it is desirable to increase the region of uncertainty for which robust stability can be guaranteed. On the other hand, one can imagine that the uncertainty region for which robust performance is desirable does not have to be the region for which robust stability is needed. For instance, performance is desirable while the master device is grabbed but it may not be required when the master device is released or grabbed

with a light grip. This could be addressed in two ways. First, two different uncertainty sets could be defined, one for stability and one for performance. Because the controller parameters depend on the nominal augmented generalized plant in Fig. 2.8, i.e. when $r = 0$, nominal \tilde{G} must be the same for both regions, the one for performance and the one for stability. Second, one could define a performance measure depending on the operator parameters or even on the operator's force. Thus when the master device is released, the performance requirements can be made less tight.

Environment estimation for switching control

In the multi-controller structure, we used an environment stiffness estimator to determine which controller needs to be active. However, we emphasize that we do not need to know per se the value of the environment stiffness but only the range it currently belongs to. Another methodology to achieve this, could be the use of a multi-estimator scheme, see, e.g., Yamamoto et al. (2008). The main idea is that several environment models are evaluated and then according to a selection criterion, one model is selected, which contains the parameters we are looking for. One can imagine that to cover a sufficiently large range of parameter values, many of such environment models would be needed. However, we would be only interested in the overlapping between the partitions of the whole uncertainty region (see Fig. 3.8 and Fig. 3.9). Therefore we could use environment models covering only the regions of overlapping to discriminate between the different partitions.

Improving switching control

The results showed that the multi-controller with bumpless transfer technique presents a high potential to improve the performance of the bilateral teleoperation system. However, its high computational power requirement is a big disadvantage. Especially if the technique would be used in multi-DoF systems. To solve this, another way to achieve stable switching among controllers is to perform a correct reset of the states of the controller at the instant it becomes active. Many researchers have already studied that problem in other fields. For instance, Pour Safaei et al. (2012) propose a reset map to initialize the controller after switching. Similar concepts could be applied to our bilateral control problem. Usually such reset maps require to know the states of the plant, which in our case means that we would need to implement a robust state observer, which is luckily a convex problem to solve (see Scherer and Weiland (2000)). If this technique would succeed, then the complexity of the bumpless transfer controller would be greatly reduced since instead of having a bumpless compensator for each controller, we would only need an estimator and a reset map for all controllers.

In principle, the bumpless transfer controller allows for independent controller design. However, one would expect that if we want to switch between two controllers that have a big difference in performance, for instance in position tracking, large actuation signals are more likely to appear. Thus more insight is needed

to know how the difference in performance between the controllers will affect the transient behavior after the switch.

General recommendations

Finally, all the results presented in this thesis were tested in 1-DoF systems. In order to move to a multi-DoF implementation there are a number of challenges involved. The operator model needs to be extended to several DoF and it must be evaluated whether it would be necessary to consider coupling between its different DoF. In case of the multi-controller structure, a particularly difficult situation would be, for instance, the end effector sliding over a surface, such that one DoF is perpendicular to the surface and the other DoF is tangent to the same surface. Particularly, the DoF tangent to the surface would experience some dynamics that depend on the forces between the other DoF and the object. Thus, those dynamics does not correspond entirely to being in contact nor in free air, which complicates the selection of the controller in the multi-controller structure. Such scenarios will definitely need to be studied in future work.

References

- Abbink, D. A., Mulder, M., and Boer, E. R. (2012). Haptic shared control: smoothly shifting control authority? *Cognition, Technology & Work*, 14(1):19–28.
- Aliaga, I., Rubio, A., and Sanchez, E. (2004). Experimental quantitative comparison of different control architectures for master-slave teleoperation. *IEEE Transactions on Control Systems Technology*, 12(1):2–11.
- Anderson, R. and Spong, M. W. (1989). Bilateral control of teleoperators with time delay. *Automatic Control, IEEE Transactions on*, 34(5):494–501.
- Bankman, I. N., Gruben, K. G., Halperin, H. R., Popel, A. S., Guerci, A. D., and Tsitlik, J. E. (1990). Identification of dynamic mechanical parameters of the human chest during manual cardiopulmonary resuscitation. *IEEE Transactions on Biomedical Engineering*, 37(2):211–217.
- Beelen, M. J., Naus, G. J., van de Molengraft, M. R. J., and Steinbuch, M. (2013). Force feedback control design for nonideal teleoperators. *Control Engineering Practice*, 21(12):1694–1705.
- Cavusoglu, M., Sherman, a., and Tendick, F. (2002). Design of bilateral teleoperation controllers for haptic exploration and telemanipulation of soft environments. *IEEE Transactions on Robotics and Automation*, 18(4):641–647.
- Cho, Ho, J., Son, H. I., Lee, D. G., Bhattacharjee, T., and Lee, D. Y. (2013). Gain-scheduling control of teleoperation systems interacting with soft tissues. *IEEE Transactions on Industrial Electronics*, 60(3):946–957.
- Cho, J. H. and Lee, D. Y. (2009). Gain-scheduling control of a teleoperation system. *IEEE International Conference on Systems Man and Cybernetics*, pages 1489–1495.

- Colgate, J. E. and Brown, J. M. (1994). Factors affecting the z-width of a haptic display. In *Robotics and Automation, 1994. Proceedings., 1994 IEEE International Conference on*, pages 3205–3210. IEEE.
- Cyberneticzoo (2010). Early teleoperators, exoskeletons and industrial robots. <http://cyberneticzoo.com/?p=4152>.
- dimension, F. (2010). Omega.3. <http://www.forcedimension.com/products>.
- Dyck, M., Jazayeri, A., and Tavakoli, M. (2013). Is the human operator in a teleoperation system passive? In *World Haptics Conference (WHC), 2013*, pages 683–688. IEEE.
- Franken, M., Stramigioli, S., Reilink, R., Secchi, C., and Macchelli, A. (2009). Bridging the gap between passivity and transparency. In *Proceedings of Robotics: Science and Systems*, pages 36–41.
- Fu, M. J. and Cavusoglu, M. C. (2012). Human-arm-and-hand-dynamic model with variability analyses for a stylus-based haptic interface. *Systems, Man, and Cybernetics, Part B: Cybernetics, IEEE Transactions on*, 42(6):1633–1644.
- Gerovich, O., Marayong, P., and Okamura, A. M. (2004). The effect of visual and haptic feedback on computer-assisted needle insertion. *Computer aided surgery official journal of the International Society for Computer Aided Surgery*, 9(6):243–249.
- Goertz, R. C. (1953). Remote-control manipulator. US Patent 2,632,574.
- Goertz, R. C. and Thompson, W. M. (1954). Electronically controlled manipulator. *Nucleonics (US) Ceased publication*, 12.
- Gustafsson, F. (2000). *Change Detection Adaptive Filtering and Change Detection*. Wiley.
- Guthart, G. and Salisbury Jr, J. K. (2000). The intuitivetm telesurgery system: Overview and application. In *Proceedings of the IEEE international conference on robotics and automation*, pages 618–621.
- Hace, A., Franc, M., and Jezernik, K. (2011). Sliding mode control for scaled bilateral teleoperation. *IECON 2011 37th Annual Conference of the IEEE Industrial Electronics Society*, pages 3430–3435.
- Haddadi, A. and Hashtrudi-Zaad, K. (2010). Bounded-impedance absolute stability of bilateral teleoperation control systems. *IEEE Transactions on Haptics*, 3(1):15–27.

-
- Hannaford, B. (1989). Stability and performance tradeoffs in bi-lateral telemanipulation. *Robotics and Automation 1989 Proceedings 1989 IEEE International Conference on*, 3:1764–1767.
- Hannaford, B. (2002). Time-domain passivity control of haptic interfaces. *IEEE Transactions on Robotics and Automation*, 18(1):1–10.
- Hashtrudi-Zaad, K. and Salcudean, S. E. (1996). Adaptive transparent impedance reflecting teleoperation. In *Robotics and Automation, 1996. Proceedings., 1996 IEEE International Conference on*, volume 2, pages 1369–1374. IEEE.
- Hendrix, R. (2011). *Robotically assisted eye surgery: A haptic master console*. PhD thesis, Department of Mechanical Engineering, Eindhoven University of Technology.
- Hendrix, R., Rosielle, P. C. J. N., Nijmeijer, H., and Steinbuch, M. (2011). *Robotically assisted eye surgery: A haptic master console*. PhD thesis, Eindhoven University of Technology, Eindhoven.
- Hespanha, J. P. and Morse, A. S. (1999). Stability of switched systems with average dwell-time. In *Decision and Control, 1999. Proceedings of the 38th IEEE Conference on*, volume 3, pages 2655–2660. IEEE.
- Hokayem, P. and Spong, M. (2006). Bilateral teleoperation: An historical survey. *Automatica*, 42(12):2035–2057.
- Hu, Z., Salcudean, S., and Loewen, P. (1995). Robust controller design for teleoperation systems. In *Systems, Man and Cybernetics, 1995. Intelligent Systems for the 21st Century., IEEE International Conference on*, volume 3, pages 2127–2132. IEEE.
- Khan, S., Sabanovic, A., and Nergiz, A. O. (2009). Scaled bilateral teleoperation using discrete-time sliding-mode controller. *IEEE Transactions on Industrial Electronics*, 56(9):3609–3618.
- Kim, J., Chang, P. H., and Park, H.-S. (2013). Two-channel transparency-optimized control architectures in bilateral teleoperation with time delay. *IEEE Transactions on Control Systems Technology*, 21(1):40–51.
- Kim, K. and Çavusoglu, M. C. (2007). Quantitative comparison of bilateral teleoperation systems using γ -synthesis. *IEEE Transactions on Robotics*, 23(4):776–789.
- Kruszewski et al., A. (2012). A switched system approach to exponential stabilization through communication network. *IEEE Transactions on Control Systems Technology*, 20(4):887–900.

- Lawrence, D. (1993a). Stability and transparency in bilateral teleoperation. *IEEE Transactions on Robotics and Automation*, 9(5):624–637.
- Lawrence, D. A. (1993b). Stability and transparency in bilateral teleoperation. *IEEE Trans. Robot. Autom.*, 9(5):624–637.
- Leith, D. J. and Leithead, W. E. (2000). Survey of gain-scheduling analysis and design. *International Journal of Control*, 73(11):1001–1025.
- Liberzon, D. (2003). *Switching in Systems and Control*. Birkhuser.
- Llewellyn, F. (1952). Some fundamental properties of transmission systems. *Proc. IRE*, 40:271–283.
- López Martínez, C. A., Molengraft, R. v. d., and Steinbuch, M. (2014a). High performance teleoperation by bumpless transfer of robust controllers. In *IEEE Haptics Symposium 2014*, pages 209–214, Houston, TX, U.S.A.
- López Martínez, C. A., Molengraft, R. v. d., and Steinbuch, M. (2014b). Model based robust control for bilateral teleoperation: Applied to a non-ideal teleoperator. *In preparation for journal publication*.
- López Martínez, C. A., Molengraft, R. v. d., and Steinbuch, M. (2014c). Switching robust control for bilateral teleoperation. *Under review for journal publication*.
- López Martínez, C. A., Molengraft, R. v. d., and Steinbuch, M. (2014d). Switching robust control synthesis for teleoperation via dwell time conditions. In *9th International Conference, EuroHaptics 2014*, Versailles, France. Springer. *To appear online*.
- López Martínez, C. A., Polat, İ., Molengraft, R. v. d., and Steinbuch, M. (2014e). Robust high performance bilateral teleoperation under bounded time-varying dynamics. *IEEE Transactions on Control Systems Technology*. *Accepted for journal publication*.
- Love, L. J. and Book, W. J. (2004). Force reflecting teleoperation with adaptive impedance control. *Systems, Man, and Cybernetics, Part B: Cybernetics, IEEE Transactions on*, 34(1):159–165.
- Lu, B., Wu, F., and Kim, S. (2006). Switching lpv control of an f-16 aircraft via controller state reset. *Control Systems Technology, IEEE Transactions on*, 14(2):267–277.
- Masubuchi, I., Ohara, A., and Suda, N. (1998). LMI-based controller synthesis: A unified formulation and solution. *International Journal of Robust and Nonlinear Control*, 8(8):669–686.

- Megretski, A. and Rantzer, A. (1997). System analysis via integral quadratic constraints. *Automatic Control, IEEE Transactions on*, 42(6):819–830.
- Mersha, A. Y., Stramigioli, S., and Carloni, R. (2014). On bilateral teleoperation of aerial robots. *IEEE Transactions on Robotics*, 30(1):258–274.
- Mitra, P. and Niemeyer, G. (2008). Model-mediated telemanipulation. *The International Journal of Robotics Research*, 27(2):253–262.
- Namerikawa, T., Ito, S., and Kawada, H. (2005). Robust control of master-slave robot system considering environmental uncertainties. *Proceedings of SPIE, Optomechatronic Systems Control*, (5):60520F–60520F–12.
- Niemeyer, G. and Slotine, J.-J. (1991). Stable adaptive teleoperation. *IEEE Journal of Oceanic Engineering*, 16(1):152–162.
- Nuño, E., Basañez, L., and Ortega, R. (2011). Passivity-based control for bilateral teleoperation: A tutorial. *Automatica*, 47(3):485–495.
- Passenberg, C., Peer, A., and Buss, M. (2010). A survey of environment-, operator-, and task-adapted controllers for teleoperation systems. *Mechatronics*, 20(7):787–801.
- Payne, J. J. (1949). Remote-control manipulator. US Patent 2,476,249.
- Polat, I. (2011). Stability analysis of bilateral teleoperation systems with time-varying environments. In *American Control Conference*, pages 1139–1144, San Francisco, CA, USA.
- Polat, İ. (2014). *Robustness Analysis and Controller Synthesis for Bilateral Teleoperation Systems via IQCs*. PhD thesis, Eindhoven University of Technology, Eindhoven.
- Polat, İ. and Scherer, C. W. (2012). Stability analysis for bilateral teleoperation: An IQC formulation. *IEEE Transactions on Robotics*, 28(6):1294–1308.
- Polushin, I. G., Liu, X. P., and Lung, C.-H. (2012). Stability of bilateral teleoperators with generalized projection-based force reflection algorithms. *Automatica*, 48(6):1005–1016.
- Pour Safaei, F. R., Hespanha, J. P., and Stewart, G. (2012). On controller initialization in multivariable switching systems. *Automatica*, 48(12):3157–3165.
- Raju, G. J., Verghese, G. C., and Sheridan, T. B. (1989). Design issues in 2-port network models of bilateral remote manipulation. In *Robotics and Automation, 1989. Proceedings., 1989 IEEE International Conference on*, pages 1316–1321. IEEE.

- Richards, C., Rosen, J., Hannaford, B., Pellegrini, C., and Sinanan, M. (2000). Skills evaluation in minimally invasive surgery using force/torque signatures. *Surgical Endoscopy*, 14(9):791–798.
- Ryu, J.-H. (2007). Bilateral Control with Time Domain Passivity Approach Under Time-varying Communication Delay. *RO-MAN 2007 - The 16th IEEE International Symposium on Robot and Human Interactive Communication*, pages 986–991.
- Ryu, J.-H., Kwon, D.-S., and Hannaford, B. (2004). Stable Teleoperation With Time-Domain Passivity Control. *IEEE Transactions on Robotics and Automation*, 20(2):365–373.
- Scherer, C. and Weiland, S. (2000). Lecture notes disc course on linear matrix inequalities in control.
- Scherer., C. W., Gahinet, P., and Chilali, M. (1997). Multiobjective output-feedback control via lmi optimization. *IEEE Transactions on Automatic Control*, 42(7):896–911.
- Scherer, C. W. and Weiland, S. (2010). Linear matrix inequalities in control. Technical Report 2010-56, SimTech Cluster of Excellence, 70569 Stuttgart.
- Schrijver, E. and Van Dijk, J. (2002). Disturbance observers for rigid mechanical systems: equivalence, stability, and design. *Journal of Dynamic Systems, Measurement, and Control*, 124(4):539–548.
- Shahdi, S. A. and Sirouspour, S. (2005). Multiple model control for teleoperation in unknown environments. *Proceedings of the 2005 IEEE International Conference on Robotics and Automation*, (April):703–708.
- Shimachi, S., Hirunyanitiwatna, S., Fujiwara, Y., Hashimoto, A., and Hakozaiki, Y. (2008). Adapter for contact force sensing of the da vinci® robot. *The International Journal of Medical Robotics and Computer Assisted Surgery*, 4(2):121–130.
- Skogestad, C. and Postlethwaite, I. (2005). *Multivariable feedback control analysis and design*. John Wiley.
- Sontag, E. D. (2008). Input to state stability: Basic concepts and results. In *Nonlinear and optimal control theory*, pages 163–220. Springer.
- Speich, J. E., Shao, L., and Goldfarb, M. (2005). Modeling the human hand as it interacts with a telemanipulation system. *Mechatronics*, 15(9):1127–1142.
- Sturm, J. F. (1999). Using sedumi 1.02, a matlab toolbox for optimization over symmetric cones. *Optimization Methods and Software*, 11(1):625–653.

-
- Tee, K. P., Burdet, E., Chew, C.-M., and Milner, T. E. (2004). A model of force and impedance in human arm movements. *Biological cybernetics*, 90(5):368–375.
- Tholey, G., Desai, J. P., and Castellanos, A. E. (2005). Force feedback plays a significant role in minimally invasive surgery: results and analysis. *Annals of surgery*, 241(1):102.
- van den Bedem, L. J. M., Steinbuch, M., Broeders, I. A. M. J., and Rosielle, P. C. J. N. (2010). *Realization of a demonstrator slave for robotic minimally invasive surgery*. PhD thesis, Eindhoven University of Technology, Eindhoven.
- Vander Poorten, E. (2007). *Improving haptic fidelity for intuitive manipulation in scaled teleoperation and virtual environment*. PhD thesis, Department of Mechanical Engineering, University of Kyoto.
- Wei, W. and Kui, Y. (2004). Teleoperated manipulator for leak detection of sealed radioactive sources. In *Robotics and Automation, 2004. Proceedings. ICRA'04. 2004 IEEE International Conference on*, volume 2, pages 1682–1687. IEEE.
- Willaert, B., Corteville, B., Reynaerts, D., Van Brussel, H., and Vander Poorten, E. (2009). Bounded environment passivity of the classical Position-Force teleoperation controller. *2009 IEEE/RSJ International Conference on Intelligent Robots and Systems*, pages 4622–4628.
- Willaert, B., Goethals, P., Reynaerts, D., Van Brussel, H., and Vander Poorten, E. (2010). Transparent and shaped stiffness reflection for telesurgery. in: *Advances in haptics*.
- Willaert, B., Reynaerts, D., van Brussel, H., and Poorten, E. B. V. (2014). Bilateral teleoperation: Quantifying the requirements for and restrictions of ideal transparency. *IEEE Transactions on Control Systems Technology*, 22(1):387–395.
- Yamamoto, T., Bernhardt, M., Peer, A., Buss, M., and Okamura, A. M. (2008). Techniques for environment parameter estimation during telemanipulation. *2008 2nd IEEE RAS & EMBS International Conference on Biomedical Robotics and Biomechatronics*, pages 217–223.
- Zaccarian, L. and Teel, A. R. (2005). The \mathcal{L}_2 (l_2) bumpless transfer problem for linear plants: Its definition and solution. *Automatica*, 41(7):1273 – 1280.

Appendix A

1-DoF Academic Setup

The setup is shown in Fig. A.1. It consists of two similar devices, each with one rotational degree of freedom, that are used as master and slave. A schematic view of one of the devices is shown in Fig. A.2. The device is actuated by an electrical motor ① which provides the actuation force. Each device has two main segments, the first segment ③ is attached to the motor via a capstan drive ②, the second segment ④, in which the end-effector ⑦ is fixed, is attached to the first segment through two elastic but stiff elements ⑥. The difference in movement between the two segments, which is in order of $100\mu\text{m}$, provides information about the interaction forces f_h and f_e . Such difference is measured via inductive sensors ⑤ that are connected to a voltage amplifier and a 16-bit Analog to Digital Converter. At the end-effector, a force-measurement range of $\pm 15\text{N}$ with a resolution of approximately 7mN is achieved. The position of the motor is measured by means of incremental encoders with a resolution of 7500 pulses/revolution. The system's

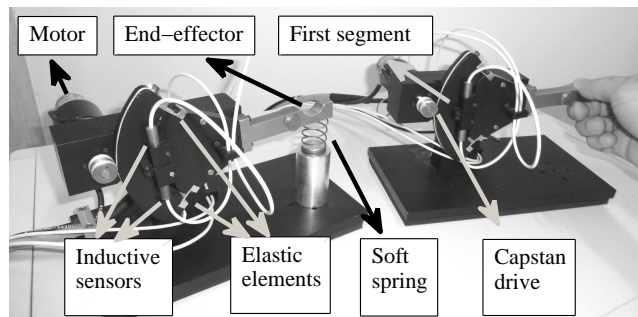


Figure A.1: 1-DoF setup for bilateral teleoperation.

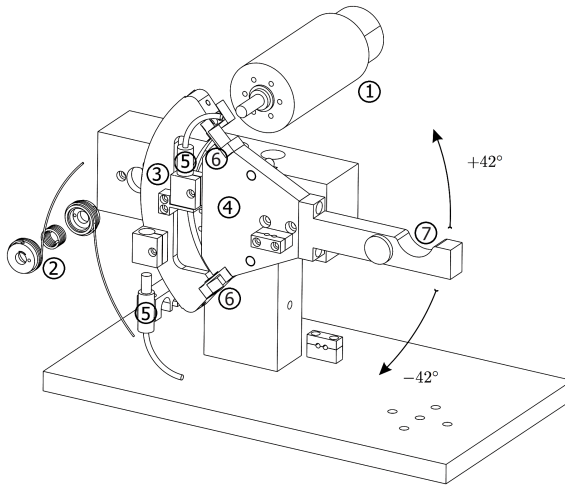


Figure A.2: Schematic of one 1-DoF device for bilateral teleoperation Hendrix (2011)

sampling rate is 2000 Hz. During the tests, the end effector point is in contact with the operator's hand in the master device and with springs in the slave device as depicted in Fig. A.1. The end effector is located at 7.5 cm from the device's rotational axis.

Appendix B

Controller-Multiplier Synthesis Procedure

In the following we will describe the controller-multiplier synthesis procedures used in this thesis. There are two versions of the iterative synthesis procedure, both of them explained in Sections B.2 and B.3 respectively.

The aim of the algorithm is to synthesize a multi-controller consisting of N_c LTI robustly stabilizing controllers $K_{ci}(s), i = 1, \dots, N_c$ of the form

$$K_{ci}(s) = \left[\begin{array}{c|c} A_{ci} & B_{ci} \\ \hline C_{ci} & D_{ci} \end{array} \right].$$

given the weighted generalized plants with transformed and scaled uncertainties.

$$\tilde{G}_i(s) = \left[\begin{array}{c|ccc} A_i & B_{(i)1} & B_{(i)2} & B_i \\ \hline rC_{(i)1} & rD_{(i)1} & rD_{(i)12} & rE_{(i)1} \\ C_{(i)2} & D_{(i)21} & D_{(i)2} & E_{(i)2} \\ C_i & F_{(i)1} & F_{(i)2} & 0 \end{array} \right], i = 1, \dots, N_c$$

Notice that for designing a single robust controller one can use $N_c = 1$.

B.1 Definitions of variables and set of LMIs

The set of variables and Linear Matrix Inequalities (LMIs) varies depending on the specific control synthesis method used. We first give the common definitions and then the definitions specific to each control synthesis method.

B.1.1 Definitions common to all control synthesis methods

- r : scaling of the uncertainty channels, $r \in [0, 1]$.
- $\tilde{\delta}_{(i)}^j, i = 1, \dots, N_c, j = 1, \dots, N_{\text{pg}}$: are the N_{pg} generators of the convex hull $\tilde{\delta}_{(i)} = \text{co}(\tilde{\delta}_{(i)}^1, \dots, \tilde{\delta}_{(i)}^{N_{\text{pg}}})$ describing the region $\tilde{\delta}_{(i)}$ of variation of the vector $\tilde{\delta}_{(i)}$ of transformed parametric uncertainties. It is assumed that $0 \in \tilde{\delta}_{(i)}$.
- $\tilde{\Delta}_{ij}(\tilde{\delta}_{(i)}^j), i = 1, \dots, N_c, j = 1, \dots, N_{\text{pg}}$: matrix diagonal concatenation of the elements of $\tilde{\delta}_{(i)}^j$. i.e. $\tilde{\Delta}_{ij}(\tilde{\delta}_{(i)}^j) = \text{diag}(\tilde{\delta}_{(i)1}^j, \dots, \tilde{\delta}_{(i)N_p}^j)$, where N_p is the number of uncertain parameters of the system.
- $P_i, i = 1, \dots, N_c$: Matrix variables corresponding to the multipliers describing the uncertainty regions $\tilde{\delta}_{(i)}, i = 1, \dots, N_c$. Assume $P_i = P_i^T$ and define the partition

$$P_i = \begin{pmatrix} Q_i & S_i \\ S_i^T & R_i \end{pmatrix}$$

See Section 1.3 for a discussion on uncertainty description via multipliers.

- $\gamma_{\text{sq}} = \gamma^2$: is the square of γ .
- $\underline{\gamma}_{\text{sq}}, \bar{\gamma}_{\text{sq}}$: minimum and maximum value allowed for γ^2 at a certain iteration.
- P_p : matrix corresponding to the performance criterion

$$P_p = \begin{pmatrix} Q_p & S_p \\ S_p^T & R_p \end{pmatrix} = \begin{pmatrix} -\gamma_{\text{sq}} I & 0 \\ 0 & I \end{pmatrix}$$

See Section 1.3 for a discussion on performance description via quadratic performance criterion.

- $v_i = \{X_i, Y_i, K_i, L_i, M_i, N_i\}, i = 1, \dots, N_c$: collected matrix variables used as decision variables for the controller synthesis step.
- Define the next matrices

$$\begin{aligned}
\mathbf{A}_i(v_i) &= \begin{pmatrix} A_i Y_i + B_i M_i & A_i + B_i N_i C_i \\ K_i & A_i X_i + L_i C_i \end{pmatrix} \\
\mathbf{B}_{(i)n}(v_i) &= \begin{pmatrix} B_{(i)n} + B_i N_i F_{(i)n} \\ X_i B_{(i)n} + L_i F_{(i)n} \end{pmatrix} \\
\mathbf{C}_{(i)m}(r, v_i) &= \begin{pmatrix} r_m(C_{(i)m} Y_i + E_{(i)m} M_i) & r_m(C_{(i)m} + E_{(i)m} N_i C_i) \end{pmatrix} \\
\mathbf{D}_{(i)mn}(r, v_i) &= \begin{pmatrix} r_m(D_{(i)mn} + E_{(i)m} N_i F_{(i)n}) \end{pmatrix} \\
\mathbf{X}_i(v_i) &= \begin{pmatrix} Y_i & I \\ I & X_i \end{pmatrix}
\end{aligned}$$

for $m, n = 1, 2$. $i = 1, \dots, N_c$. $r_1 = r$ and $r_2 = 1$.

- Equation to compute controller matrices:

$$\begin{aligned}
&\begin{pmatrix} A_{ci} & B_{ci} \\ C_{ci} & D_{ci} \end{pmatrix} \\
&= \begin{pmatrix} U_i & X_i B_i \\ 0 & I \end{pmatrix}^{-1} \begin{pmatrix} K_i - X_i A_i Y_i & L_i \\ M_i & N_i \end{pmatrix} \begin{pmatrix} V_i^T & 0 \\ C_i Y_i & I \end{pmatrix}^{-1} \quad (\text{B.1})
\end{aligned}$$

where U_i and V_i are invertible matrices satisfying $I - X_i Y_i = U_i V_i^T$. See coming sections to see which U_i and V_i matrices are used.

- Given controllers $K_{ci}(s)$, $i = 1, \dots, N_c$, define the following closed loop systems matrices

$$\tilde{G}_i(s) \star K_{ci}(s) = \left[\begin{array}{c|cc} \mathcal{A}_i & \mathcal{B}_{(i)1} & \mathcal{B}_{(i)2} \\ \hline \mathcal{C}_{(i)1} & \mathcal{D}_{(i)11} & \mathcal{D}_{(i)12} \\ \mathcal{C}_{(i)2} & \mathcal{D}_{(i)21} & \mathcal{D}_{(i)22} \end{array} \right], i = 1, \dots, N_c.$$

B.1.2 Definitions for the synthesis method using a common Lyapunov function and for the bumpless transfer method

- *Only* for the case that a common Lyapunov function $V(x) = x^T \mathcal{X} x$ is used, define:

$$\mathcal{X} = \mathcal{X}_1 = \mathcal{X}_2 = \dots = \mathcal{X}_{N_c}$$

$$Y = Y_1 = Y_2 = \dots = Y_{N_c}$$

$$X = X_1 = X_2 = \dots = X_{N_c}$$

- $\text{LMI}_{\text{ana}}(\gamma_{\text{sq}}, \mathcal{X}_i, P_i)$: Set of linear matrix inequality conditions for the robust performance analysis step. The variables between brackets are the decision variables used in these LMIs.

$\text{LMI}_{\text{ana}}(\gamma_{\text{sq}}, \mathcal{X}_i, P_i)$ is defined as:

$$\begin{aligned} & \begin{pmatrix} I \\ 0 \end{pmatrix}^T P_i \begin{pmatrix} I \\ 0 \end{pmatrix} \prec 0, \quad i = 1, \dots, N_c. \\ & \begin{pmatrix} \tilde{\Delta}_i(\tilde{\delta}_{(i)}^j) \\ I \end{pmatrix}^T P_i \begin{pmatrix} \tilde{\Delta}_i(\tilde{\delta}_{(i)}^j) \\ I \end{pmatrix} \succeq 0, \quad i = 1, \dots, N_c, \quad j = 1, \dots, N_{\text{pg}} \\ & \mathcal{X}_i \succ 0, \quad i = 1, \dots, N_c. \\ & \left(\star \right)^T \left(\begin{array}{cc|cc} 0 & \mathcal{X}_i & 0 & 0 \\ \mathcal{X}_i & 0 & 0 & 0 \\ \hline 0 & 0 & P_i & 0 \\ 0 & 0 & 0 & P_p \end{array} \right) \begin{pmatrix} I & 0 & 0 \\ \mathcal{A}_i & \mathcal{B}_{(i)1} & \mathcal{B}_{(i)2} \\ \hline 0 & I & 0 \\ \mathcal{C}_{(i)1} & \mathcal{D}_{(i)11} & \mathcal{D}_{(i)12} \\ \hline 0 & 0 & I \\ \mathcal{C}_{(i)2} & \mathcal{D}_{(i)21} & \mathcal{D}_{(i)22} \end{pmatrix} \prec 0, \quad i = 1, \dots, N_c \end{aligned}$$

Note that $\text{LMI}_{\text{ana}}(\gamma_{\text{sq}}, \mathcal{X}_i, P_i)$ indeed defines a linear constraint on the decision variables.

- $\text{LMI}_{\text{syn}}(\gamma_{\text{sq}}, v_i)$: Set of linear matrix inequality conditions for the robust performance controller synthesis step. v_i is defined in Section B.1.1. The variables between brackets are the the decision variables used in these LMIs. Define

$$\begin{aligned} B_{(i)l}(v) &= \begin{pmatrix} \mathbf{A}_i(v) & \mathbf{B}_{(i)1}(v) & \mathbf{B}_{(i)2}(v) \\ \mathbf{C}_{(i)1}(v) & \mathbf{D}_{(i)11}(v) & \mathbf{D}_{(i)12}(v) \\ \mathbf{C}_{(i)2}(v) & \mathbf{D}_{(i)21}(v) & \mathbf{D}_{(i)22}(v) \end{pmatrix} \\ Q_{(i)l} &= \text{diag}(0, Q_i, Q_p) \\ S_{(i)l} &= \text{diag}(I, S_i, S_p) \\ U_{(i)l} &= \text{diag}(I, R_i^{-1}, R_p^{-1}) \\ T_l &= \text{diag}(0, I, I) \end{aligned}$$

for $i = 1, \dots, N_c$. Then $\text{LMI}_{\text{syn}}(\gamma_{\text{sq}}, v_i)$ is defined as

$$\begin{aligned} & \begin{pmatrix} Y_i & I \\ I & X_i \end{pmatrix} \succ 0, \quad i = 1, \dots, N_c, \\ & \begin{pmatrix} Q_{(i)l} + S_{(i)l} B_{(i)l}(v) + B_{(i)l}(v)^T S_{(i)l}^T & B_{(i)l}(v)^T T_l \\ T_l^T B_{(i)l}(v) & -U_{(i)l} \end{pmatrix} \prec 0, \quad i = 1, \dots, N_c \end{aligned}$$

- $\text{LMI}_{\text{syn}}^{\text{nom}}(\gamma_{\text{sq}}, v_i)$: Set of linear matrix inequality conditions for the initialization controller synthesis step, i.e. for the nominal plant. The variables between brackets are the decision variables used in these LMIs. They are obtained by removing the uncertainty channels from the $\text{LMI}_{\text{syn}}(\gamma_{\text{sq}}, v_i)$.

Define the following matrices:

$$\begin{aligned} B_{(i)l}(v) &= \begin{pmatrix} \mathbf{A}_i(v) & \mathbf{B}_{(i)2}(v) \\ \mathbf{C}_{(i)2}(v) & \mathbf{D}_{(i)22}(v) \end{pmatrix} \\ Q_{(i)l} &= \text{diag}(0, Q_p) \\ S_{(i)l} &= \text{diag}(I, S_p) \\ U_{(i)l} &= \text{diag}(I, R_p^{-1}) \\ T_l &= \text{diag}(0, I) \end{aligned}$$

for $i = 1, \dots, N_c$. Then, Specifically, $\text{LMI}_{\text{syn}}^{\text{nom}}(\gamma_{\text{sq}}, v_i)$ is defined as

$$\begin{pmatrix} Y_i & I \\ I & X_i \end{pmatrix} \succ 0, \quad i = 1, \dots, N_c,$$

$$\begin{pmatrix} Q_{(i)l} + S_{(i)l}B_{(i)l}(v) + B_{(i)l}(v)^T S_{(i)l}^T & B_{(i)l}(v)^T T_l \\ T_l^T B_{(i)l}(v) & -U_{(i)l} \end{pmatrix} \prec 0, \quad i = 1, \dots, N_c.$$

- For given v_i we compute the controller matrices $\{A_{ci}, B_{ci}, C_{ci}, D_{ci}\}$ of $K_{ci}(s)$, $i = 1, \dots, N_c$ in Eq.(B.1) with $U_i = X_i$ and $V_i = X_i^{-1} - Y_i$. This is a particular decomposition to achieve that $I - X_i Y_i = U_i V_i^T$.

B.1.3 Definitions for the synthesis method using dwell time conditions

- $\mu > 1$: real number that determined a bound on the discrepancy between Lyapunov functions represented by \mathcal{X}_i .
- $\lambda_0 > 0$: minimal exponential decay constant of the Lyapunov functions represented by \mathcal{X}_i
- τ_a : represents the average dwell time of the switched system representing the bilateral teleoperation system and it is given by:

$$\tau_a > \frac{\ln(\mu)}{\lambda_0}.$$

See Section 4.2.2 for details.

- Y_{Ii} : matrix variables that denotes Y^{-1} . It is used in the analysis step.
- \mathcal{X}_i : The Lyapunov function must have the following structure.

$$\mathcal{X}_i = \begin{pmatrix} X_i & Y_{Ii} - X_i \\ Y_{Ii} - X_i & X_i - Y_{Ii} \end{pmatrix} \succ 0, \quad i = 1, \dots, N_c$$

See Section 4.2.2 for details.

- $\text{LMI}_{\text{ana}}(\gamma_{\text{sq}}, \mathcal{X}_i, P_i)$: Set of linear matrix inequality conditions for the robust performance analysis step. The variables between brackets are the decision variables used in these LMIs.

$\text{LMI}_{\text{ana}}(\gamma_{\text{sq}}, \mathcal{X}_i, P_i)$ is defined as:

$$\begin{aligned} \begin{pmatrix} I \\ 0 \end{pmatrix}^T P_i \begin{pmatrix} I \\ 0 \end{pmatrix} &< 0, \quad i = 1, \dots, N_c. \\ \begin{pmatrix} \tilde{\Delta}_i(\tilde{\delta}_{(i)}^j) \\ I \end{pmatrix}^T P_i \begin{pmatrix} \tilde{\Delta}_i(\tilde{\delta}_{(i)}^j) \\ I \end{pmatrix} &\succeq 0, \quad i = 1, \dots, N_c. \quad j = 1, \dots, N_{\text{pg}} \\ \mathcal{X}_i &\succ 0, \quad i = 1, \dots, N_c. \end{aligned}$$

$$\frac{1}{\mu} Y_{Ij} \preceq Y_{Ii} \preceq \mu Y_{Ij}, \quad i, j = 1, \dots, N_c$$

$$(\star)^T \left(\begin{array}{ccc|ccc} 0 & \mathcal{X}_i & 0 & 0 & 0 & 0 \\ \mathcal{X}_i & 0 & 0 & 0 & 0 & 0 \\ 0 & 0 & \lambda_0 \mathcal{X}_i & 0 & 0 & 0 \\ \hline 0 & 0 & 0 & P_i & 0 & 0 \\ 0 & 0 & 0 & 0 & P_p & 0 \end{array} \right) \left(\begin{array}{ccc} I & 0 & 0 \\ \mathcal{A}_i & \mathcal{B}_{(i)1} & \mathcal{B}_{(i)2} \\ I & 0 & 0 \\ \hline 0 & I & 0 \\ \mathcal{C}_{(i)1} & \mathcal{D}_{(i)11} & \mathcal{D}_{(i)12} \\ 0 & 0 & I \\ \hline \mathcal{C}_{(i)2} & \mathcal{D}_{(i)21} & \mathcal{D}_{(i)22} \end{array} \right) < 0, \\ i, j = 1, \dots, N_c$$

Note that $\text{LMI}_{\text{ana}}(\gamma_{\text{sq}}, \mathcal{X}_i, P_i)$ indeed defines a linear constraint on the decision variables.

- $\text{LMI}_{\text{syn}}(\gamma_{\text{sq}}, v_i)$: Set of linear matrix inequality conditions for the robust performance controller synthesis step. v_i is defined in Section B.1.1. The variables between brackets are the the decision variables used in these LMIs.

Define

$$\begin{aligned}
 B_{(i)l}(v) &= \begin{pmatrix} \mathbf{A}_i(v) & \mathbf{B}_{(i)1}(v) & \mathbf{B}_{(i)2}(v) \\ \mathbf{C}_{(i)1}(v) & \mathbf{D}_{(i)11}(v) & \mathbf{D}_{(i)12}(v) \\ \mathbf{C}_{(i)2}(v) & \mathbf{D}_{(i)21}(v) & \mathbf{D}_{(i)22}(v) \end{pmatrix} \\
 A_l &= \text{col}(I, (I \ 0 \ 0)); \\
 Q_{(i)l} &= \text{diag}(0, Q_i, Q_p, \lambda_0 \mathbf{X}_i(v_i)) \\
 S_{(i)l} &= \text{col}(\text{diag}(I, S_i, S_p), 0) \\
 U_{(i)l} &= \text{diag}(I, R_i^{-1}, R_p^{-1}) \\
 T_l &= \text{diag}(0, I, I)
 \end{aligned}$$

for $i = 1, \dots, N_c$. Then $\text{LMI}_{\text{syn}}(\gamma_{\text{sq}}, v_i)$ is defined as

$$\begin{pmatrix} Y_i & I \\ I & X_i \end{pmatrix} \succ 0, \quad i = 1, \dots, N_c,$$

$$Y_i \preceq \mu Y_j, \quad i, j = 1, \dots, N_c$$

$$\begin{pmatrix} A_l^T Q_{(i)l} A_l + A_l^T S_{(i)l} B_{(i)l}(v) + B_{(i)l}(v)^T S_{(i)l}^T A_l & B_{(i)l}(v)^T T_l \\ T_l^T B_{(i)l}(v) & -U_{(i)l} \end{pmatrix} \prec 0, \\
 i = 1, \dots, N_c$$

- $\text{LMI}_{\text{syn}}^{\text{nom}}(\gamma_{\text{sq}}, v_i)$: Set of linear matrix inequality conditions for the initialization controller synthesis step, i.e. for the nominal plant. The variables between brackets are the decision variables used in these LMIs. They are obtained by removing the uncertainty channels from the $\text{LMI}_{\text{syn}}(\gamma_{\text{sq}}, v_i)$.

Define the following matrices:

$$\begin{aligned}
 B_{(i)l}(v) &= \begin{pmatrix} \mathbf{A}_i(v) & \mathbf{B}_{(i)2}(v) \\ \mathbf{C}_{(i)2}(v) & \mathbf{D}_{(i)22}(v) \end{pmatrix} \\
 A_l &= \text{col}(I, (I \ 0)); \\
 Q_{(i)l} &= \text{diag}(0, Q_p, \lambda_0 \mathbf{X}_i(v_i)) \\
 S_{(i)l} &= \text{col}(\text{diag}(I, S_p), 0) \\
 U_{(i)l} &= \text{diag}(I, R_p^{-1}) \\
 T_l &= \text{diag}(0, I)
 \end{aligned}$$

for $i = 1, \dots, N_c$. Then, Specifically. $\text{LMI}_{\text{syn}}^{\text{nom}}(\gamma_{\text{sq}}, v_i)$ is defined as

$$\begin{pmatrix} Y_i & I \\ I & X_i \end{pmatrix} \succ 0, \quad i = 1, \dots, N_c,$$

$$Y_i \preceq \mu Y_j, \quad i, j = 1, \dots, N_c$$

$$\begin{pmatrix} A_l^T Q_{(i)l} A_l + A_l^T S_{(i)l} B_{(i)l}(v) + B_{(i)l}(v)^T S_{(i)l}^T A_l & B_{(i)l}(v)^T T_l \\ T_l^T B_{(i)l}(v) & -U_{(i)l} \end{pmatrix} \prec 0, \\ i = 1, \dots, N_c$$

- For given v_i we compute the controller matrices $\{A_{ci}, B_{ci}, C_{ci}, D_{ci}\}$ of $K_{ci}(s)$, $i = 1, \dots, N_c$ in Eq.(B.1) with $V_i = Y_i$ and therefore $U_i = Y_i^{-1} - X_i$. This particular decomposition is needed so the theorems involving the dwell time conditions are valid. See Chapter 4.

B.2 Synthesis procedure: version I

Given the generalized plant $\tilde{G}_i, i = 1, \dots, N_c$, we aim to iteratively find robust controllers K_i that renders the sets $\text{LMI}_{\text{syn}}(\gamma_{\text{sq}}, v_i)$ and $\text{LMI}_{\text{ana}}(\gamma_{\text{sq}}, \mathcal{X}_i, P_i)$ feasible for different values of $(r, \gamma) \in [0, 1] \times [0, \infty]$. The main idea in this procedure is to gradually let γ increase between the iterations. This will result in a gradual increase of r until $r = 1$ is reached. This algorithm gives higher priority to performance than to robust stability.

Step 0. Initialization: controller for nominal plant

- 1: Set iteration counter $i_s = 0$ and scaling $r = 0$.
- 2: Solve set $\text{LMI}_{\text{syn}}^{\text{nom}}(\gamma_{\text{sq}}, v_i)$ while minimizing γ_{sq} .
- 3: Compute the controller matrices of $K_{ci}(s), i = 1, \dots, N_c$ using Eq. (B.1) and save the obtained value $\gamma_{\text{sq}(0)} = \gamma_{\text{sq}}$.

Step 1. Robust performance analysis: multiplier step

- 1: Increase iteration counter $i_s = i_s + 1$.
- 2: Set $\bar{\gamma}_{\text{sq}} = \rho^2 \gamma_{\text{sq}(i_s-1)}$ for some $1 < \rho < 2$. The idea is to gradually let γ increase in order to allow r to increase.
- 3: Start a bisection algorithm on r that maximizes r in the interval $[0, 1]$. To this end, initialize $\underline{r} = r_{i_s-1}$ and $\bar{r} = 1$ and start with a test value for $r \in [\underline{r}, \bar{r}]$, e.g. $r = (\underline{r} + \bar{r})/2$.
- 4: **repeat**
- 5: Use $K_{ci}(s), i = 1, \dots, N_c$ from previous controller step and solve the set $\text{LMI}_{\text{ana}}(\gamma_{\text{sq}}, \mathcal{X}_i, P_i)$ for minimal $\gamma_{\text{sq}} \in [0, \bar{\gamma}_{\text{sq}}]$.

```

6:   if  $\text{LMI}_{\text{ana}}(\gamma_{\text{sq}}, \mathcal{X}_i, P_i)$  is feasible then
7:       save current values of  $P_i$ . Set  $r_{i_s} = r$  and  $\gamma_{\text{sq}(i_s)} = \gamma_{\text{sq}}$  (to eventually
       be used in Step 2). Redefine the bounds  $\underline{r} = r$ , then try a larger value
        $r = (\underline{r} + \bar{r})/2$ .
8:   else
9:       make  $\bar{r} = r$  and try a smaller value  $r = (\underline{r} + \bar{r})/2$ .
10:  end if
11: until  $(\bar{r} - \underline{r}) < \epsilon_r$  for some small  $\epsilon_r > 0$ 
12: if  $r_{i_s} = 1$  then
13:     finish
14: else
15:     continue with Step 2.
16: end if

```

Step 2. Robust Performance synthesis: controller step

```

1: Increase iteration counter  $i_s = i_s + 1$ .
2: Set  $\bar{\gamma}_{\text{sq}} = \rho^2 \gamma_{\text{sq}(i_s-1)}$  for some  $1 < \rho < 2$ . The idea is to gradually let  $\gamma$  increase
   in order to allow  $r$  to increase.
3: Start a bisection algorithm on  $r$  that maximizes  $r$  in the interval  $[0, 1]$ . To this
   end, initialize  $\underline{r} = r_{i_s-1}$  and  $\bar{r} = 1$  and start with a test value for  $r \in [\underline{r}, \bar{r}]$ ,
   e.g.  $r = (\underline{r} + \bar{r})/2$ .
4: repeat
5:     Use  $P_i, i = 1, \dots, N_c$  from previous multiplier step and solve the set
        $\text{LMI}_{\text{syn}}(\gamma_{\text{sq}}, v_i)$  for minimal  $\gamma_{\text{sq}} \in [0, \bar{\gamma}_{\text{sq}}]$ .
6:     if  $\text{LMI}_{\text{syn}}(\gamma_{\text{sq}}, v_i)$  is feasible then
7:         save current values of  $v_i, r_{i_s} = r$  and  $\gamma_{\text{sq}(i_s)} = \gamma_{\text{sq}}$  (to eventually be
         used in Step 1), set  $\underline{r} = r$ , then try a larger value  $r = (\underline{r} + \bar{r})/2$ .
8:     else
9:         make  $\bar{r} = r$  and try a smaller value  $r = (\underline{r} + \bar{r})/2$ .
10:    end if
11: until  $(\bar{r} - \underline{r}) < \epsilon_r$  for some small  $\epsilon_r > 0$ 
12: if  $r_{i_s} = 1$  then
13:     finish
14: else
15:     continue with Step 1.
16: end if

```

B.3 Synthesis procedure: version II

The main idea in this procedure is to initially let γ take a large value. This will result in a fast convergence of r to $r = 1$, however with a poor performance because of the large γ . Then, γ is gradually minimized over the multiplier-controller iteration. This algorithm gives initially higher priority to robust stability than to performance.

Step 0. Initialization: controller for nominal plant

- 1: Set iteration counter $i_s = 0$ and scaling $r = 0$. Moreover set $\gamma_{sq} = \gamma_{Lsq}$, with large γ_{Lsq} , say $\gamma_{Lsq} = 100^2$.
- 2: Solve set $\text{LMI}_{\text{syn}}^{\text{nom}}(v_i)$ for fixed γ_{sq} .
- 3: Compute the controller matrices of $K_{ci}(s), i = 1, \dots, N_c$ using Eq. (B.1). Set $\underline{\gamma}_{sq} = 0$ and $\bar{\gamma}_{sq} = \gamma_{Lsq}$.

Step 1. Robust performance analysis: multiplier step

- 1: Increase iteration counter $i_s = i_s + 1$.
- 2: **if** $r_{i_s-1} = 1$ **then**
- 3: set $\underline{\gamma}_{sq} = \rho^2 \gamma_{sq(i_s-1)}$ for some $0.5 < \rho < 1$. The idea is to gradually let γ decrease.
- 4: **else**
- 5: keep current $\underline{\gamma}_{sq}$ and proceed.
- 6: **end if**
- 7: Start a bisection algorithm on r that maximizes r in the interval $[0, 1]$. To this end, initialize $\underline{r} = r_{i_s-1}$ and $\bar{r} = 1$ and start with a test value for $r \in [\underline{r}, \bar{r}]$, e.g. $r = (\underline{r} + \bar{r})/2$.
- 8: **repeat**
- 9: Use $K_{ci}(s), i = 1, \dots, N_c$ from previous controller step and solve the set $\text{LMI}_{\text{ana}}(\gamma_{sq}, \mathcal{X}_i, P_i)$ for minimal $\gamma_{sq} \in [\underline{\gamma}_{sq}, \bar{\gamma}_{sq}]$.
- 10: **if** $\text{LMI}_{\text{ana}}(\gamma_{sq}, \mathcal{X}_i, P_i)$ is feasible **then**
- 11: save current values of P_i , set $r_{i_s} = r$ and $\gamma_{sq(i_s)} = \gamma_{sq}$ (to eventually be used in Step 2), set $\underline{r} = r$, then try a larger value $r = (\underline{r} + \bar{r})/2$.
- 12: **else**
- 13: set $\bar{r} = r$ and try a smaller value $r = (\underline{r} + \bar{r})/2$.
- 14: **end if**
- 15: **until** $(\bar{r} - \underline{r}) < \epsilon_r$ for some small $\epsilon_r > 0$.
- 16: **if** $r_{i_s} = 1$ and $(\gamma_{sq(i_s)} - \gamma_{sq(i_s-1)}) < \epsilon_\gamma$ for some small $\epsilon_\gamma > 0$ **then**
- 17: finish
- 18: **else**

19: continue with Step 2.
 20: **end if**

Step 2. Robust Performance synthesis: controller step

1: Increase iteration counter $i_s = i_s + 1$.
 2: **if** $r_{i_s-1} = 1$ **then**
 3: set $\underline{\gamma}_{\text{sq}} = \rho^2 \gamma_{\text{sq}(i_s-1)}$ for some $0.5 < \rho < 1$.
 The idea is to gradually let γ decrease.
 4: **else**
 5: keep current $\underline{\gamma}_{\text{sq}}$ and proceed.
 6: **end if**
 7: Start a bisection algorithm on r that maximizes r in the interval $[0, 1]$. To this end, initialize $\underline{r} = r_{i_s-1}$ and $\bar{r} = 1$ and start with a test value for $r \in [\underline{r}, \bar{r}]$, e.g. $r = (\underline{r} + \bar{r})/2$.
 8: **repeat**
 9: Use $P_i, i = 1, \dots, N_c$ from previous multiplier step and solve the set $\text{LMI}_{\text{syn}}(\gamma_{\text{sq}}, v_i)$ for minimal $\gamma_{\text{sq}} \in [\underline{\gamma}_{\text{sq}}, \bar{\gamma}_{\text{sq}}]$.
 10: **if** $\text{LMI}_{\text{syn}}(\gamma_{\text{sq}}, v_i)$ is feasible **then**
 11: save current values of v_i , set $r_{i_s} = r$ and $\gamma_{\text{sq}(i_s)} = \gamma_{\text{sq}}$ (to eventually be used in Step 1), set $\underline{r} = r$, then try a larger value $r = (\underline{r} + \bar{r})/2$.
 12: **else**
 13: set $\bar{r} = r$ and try a smaller value $r = (\underline{r} + \bar{r})/2$.
 14: **end if**
 15: **until** $(\bar{r} - \underline{r}) < \epsilon_r$ for some small $\epsilon_r > 0$.
 16: Compute the controller matrices of $K_{ci}(s), i = 1, \dots, N_c$ using Eq. (B.1).
 17: **if** $r_{i_s} = 1$ and $(\gamma_{\text{sq}(i_s)} - \gamma_{\text{sq}(i_s-1)}) < \epsilon_\gamma$ for some small $\epsilon_\gamma > 0$ **then**
 18: finish
 19: **else**
 20: continue with Step 1.
 21: **end if**

Acknowledgments / Dankwoord / Agradecimientos

When I started writing these lines, I had to think of all people that in a way made this PhD dissertation possible, which led me to a long list. Especially because this achievement in my life did not start four years ago, but way before. This is a perfect opportunity to look back and to show them how much I value their support.

Todo se remonta desde que la vida en mi familia tuvo un cambio grande y tuvimos que tomar rumbos distintos. Gracias tía Ana por haberme recibido en tu casa en esos tiempos difíciles para Papá y Mamá. Al tío Benja le agradezco el apoyo que nos brindó a mí y a mi familia para mudarnos a Medellín, ese año sirvió como puente para iniciar mi carrera profesional y para adquirir una experiencia de vida invaluable. Quiero agradecerle inmensamente a tía Ana, tía Inés y a abuela Kika por su apoyo no solo económico sino también moral durante mi tiempo en la universidad en Medellín, sin ustedes este logro no hubiese sido posible. A todos los parceros de la U por aquellos tiempos invaluable, y a muchos de ustedes que vinieron a Esuroa así como yo a perseguir sus sueños por los viajes y experiencias que compartimos. Por supuesto a los parceros de microE por su gran amistad y a los profes por darme apoyo para dar el gran paso de mudarse y estudiar en el exterior. Principalmete a mi familia! Papá, Mamá, Pipe, Juanchito, Marthica, sobrinos por todos los buenos momentos que hemos pasado y el apoyo que me han brindado, ustedes son gran parte de mi motivación día a día. También a toda mi familia morrocroyera! la cabeza de la familia abuela Kika, a todos los tíos, tías, primos, primas, por los momentos inolvidables cada vez que nos vemos, así sea poco pero si que los sabemos aprovechar.

Thanks to all the international friends I met during my master's. You made the beginning of this life journey to the Netherlands very pleasant with amazing parties

and experiences. We all shared the same feelings about adapting to a new culture, which made a connection between all of us.

A la comunidad Latino Americana y Colombiana, aparte de acercarnos más a nuestras raíces, nuestras distintas actividades (sancochos, frijoladas, buñueladas, fiestas, etc.) fueron y siguen siendo una fuente de diversión muy importante en todos estos años. A Felipe que me dió la primera mano en este viaje que empecé hace seis años y por su amistad durante este tiempo. A Carolina y a Sebastián, gracias por ofrecirme su amistad y su casa, Sebas parcerero gracias por introducirme al mundo del whisky (sé que Felipe también te lo agradece) y por esas noches de vallenatos y reggae.

To my promotor Maarten Steinbuch, thanks for giving me the opportunity to start this PhD within your group and for your supervision during these years. Thanks for giving me the flexibility to shape my PhD. Thanks to that, my PhD became also a very diverse and even more enjoyable job. I could participate in robotic contests and travel around the world having enriching experiences. René, I thank you for your supervision and support. Your critical view and feedback was very valuable to follow the right track during these years. Siep, despite the fact that you were my promotor only during the last months of my PhD, your feedback and discussions helped to greatly improve this thesis.

I would like to thank to the committe members Daniela Constantinescu, Emmanuel Vander Poorten, Stefano Stramigioli and Henk Nijmeijer for the time you have spent reading this thesis and for providing your valuable feedback. Thanks to Jules, Kirsten, John, Luca, Rolf and all other members of the PITON project, for the pleasure of working together.

Thanks to all members of the Tech United team. I have had amazing experiences, enjoyed our weekly meetings, our victories and suffered the defeats. You were the best company in our travels around the world, both during the hard work and the relaxation time.

Thanks to Dennis and Ilhan for all the deep discussions about haptics control design. They helped me to shape my opinion in the field. Thank you Gerrit, Maarten Beelen, Geert-Jan, Harm and all participants of the happy Happy Haptics meetings, they were very useful to share our knowledge. Thanks also to all the master and bachelor students that I have supervised, your work was very helpful, especially within the PITON project.

Aan alle kantoorgenoten waarmee ik het kantoor gedeeld heb. Dank jullie wel voor de gezellige sfeer. Jeroen, ik zal de nuttige zinnen nooit vergeten die je me geleerd hebt. Rob dankjewel voor je nuttige Matlab tools. Ik ben nog steeds erg onder de indruk van je kat-master-vermogen. Joost, dank je voor alle foto fotomontages

die ons flink aan het lachen gemaakt hebben (Robazrael, dj C-LO, etc.). Eelco, je bent onze kantoor zoon, een eerstejaars PhD omringd door drukke vierdejaars PhDs, alsjeblieft zorg dat Schnautzie een goed leven heeft.

To all PhD colleagues, thanks for all the nice lunches, beers, coffees, events at Hora Est and outside the university. Thank you for the great times and experiences during conferences, we have built lots of nice stories.

These acknowledgments would not be complete without thanking my squash rival Menno Lauret, who finally won against me in an epic match during the CST D&C 24h-meeting. You have trained hard and you deserved it, just do not forget the big picture, the score is 'a lot'-1 and at the time I wrote this, I have yet to see the promised party and home-made belgian fries.

And, to finalize, to you Nina, mijn schatje. You came to my life in a very important moment. Thank you for supporting me during the end of this PhD, you brought me love and happiness.

Curriculum Vitae



César A. López M. was born on June 12, 1983 in Aguachica, Colombia. He did most of his basic education in a military school in Bucaramanga. In 1999, he finished high school in his birthplace at the public school “Jose María Campo Serrano”. He moved to Medellín, Colombia, where he worked as an operator of injection molding machines during one year. Then he started his bachelor studies in Electronic Engineering at the “Universidad de Antioquia”, focused mainly on digital systems design. In 2006, he went abroad to Tampa, Florida, U.S.A, for an internship on wireless sensor networks at the University of South Florida. The same year, he obtained his bachelor’s degree as the best student of his class. Then, he worked as a researcher and lecturer at his bachelor university and lecturing some courses at undergraduate educational institutions. Following his passion for applied mathematics, in 2008, he moved to the Netherlands to study the master program in Systems and Control at the Eindhoven University of Technology. He did his master’s internship within the department of Electrical Engineering implementing a mathematical model of a magnetic levitation device. Then he did his master’s project at ASML. He worked on the control design for improving the performance in vibration isolation systems. In 2010, he received his master’s degree with the honor “With great appreciation”. The same year he started his PhD within the Control Systems Technology group of the Eindhoven University of Technology. The result of his research was a model-based robust-control design methodology for teleoperation systems with force feedback, which is reported in this thesis. During his PhD he completed the educational program of the graduate school DISC. Additional to his PhD, he also participated in a multidisciplinary project together with people from academia and industry to develop a robotic steerable needle. Since 2011 he has been member of the Tech United RoboCup team from Eindhoven University of Technology. The team has won the RoboCup tournament in the robot soccer category twice. His main function in the team is to develop the pass strategy. César will continue his career in the high tech industry.

